



UNIVERSITÀ DEGLI STUDI DI PADOVA

DIPARTIMENTO DI SCIENZE CHIMICHE
CORSO DI LAUREA MAGISTRALE IN CHIMICA

TESI DI LAUREA MAGISTRALE

**TOWARD A SUBSTRATE INDEPENDENT
METHODOLOGY FOR CHIROPTICAL SENSING OF
CHIRAL AMIDES**

Relatore: Prof. CRISTIANO ZONTA

Controrelatore: Prof.ssa ELISABETTA COLLINI

Laureando: LORENZO CRACCO

ANNO ACCADEMICO: 2022/2023

SUMMARY

1. INTRODUCTION	1
1.1. RELEVANCE OF CHIRALITY: UNCOVERING ABSOLUTE CONFIGURATION AND ENANTIOMERIC EXCESS	1
1.2. ELECTRONIC CIRCULAR DICHROISM AND SUPRAMOLECULAR CHIROPTICAL SENSORS	4
1.3. CHIRALITY SENSING USING STEREODYNAMIC SYSTEMS AND ELECTRONIC CIRCULAR DICHROISM SPECTROSCOPY	10
1.3.1. Bridged biaryls	11
1.3.2. Imine foldamers	14
1.3.3. Trityl propellers	16
1.3.4. Metalloporphyrins	18
1.3.5. Stereodynamic metal complexes	20
2. AIM OF THE THESIS	27
3. RESULTS AND DISCUSSION	29
3.1. DESIGN AND SYNTHESIS OF THE LIBRARY OF CHIRAL AMIDES	29
3.2. ELECTRONIC CIRCULAR DICHROISM ANALYSIS	38
3.3. DEVELOPMENT OF A PREDICTIVE MULTIVARIATE MODEL	44
4. CONCLUSIONS	57
5. EXPERIMENTAL SECTION	59
5.1. GENERAL METHODS	59
5.2. ABBREVIATIONS	60
5.3. SYNTHESIS OF (<i>R</i>)- <i>N</i> -(1-PHENYLETHYL)ACETAMIDE (<i>R</i>)-14	61
5.4. SYNTHESIS OF (<i>R</i>)- <i>N</i> -(1-PHENYLETHYL)PROPIONAMIDE (<i>R</i>)-15	62
5.5. SYNTHESIS OF (<i>R</i>)- <i>N</i> -(1-PHENYLETHYL)ISOBUTYRAMIDE (<i>R</i>)-16	63
5.6. SYNTHESIS OF (<i>R</i>)- <i>N</i> -(1-PHENYLETHYL)PIVALAMIDE (<i>R</i>)-17	64
5.7. SYNTHESIS OF (<i>R</i>)- <i>N</i> -(1-PHENYLETHYL)BENZAMIDE (<i>R</i>)-18	65
5.8. SYNTHESIS OF (<i>R</i>)-2-PHENYL- <i>N</i> -(1-PHENYLETHYL)ACETAMIDE (<i>R</i>)-19	66
5.9. SYNTHESIS OF (<i>R</i>)- <i>N</i> -[1-(4-METHOXYPHENYL)ETHYL]ACETAMIDE (<i>R</i>)-21	67
5.10. SYNTHESIS OF (<i>R</i>)- <i>N</i> -[1-(4-METHOXYPHENYL)ETHYL]PROPIONAMIDE (<i>R</i>)-22	68
5.11. SYNTHESIS OF <i>N</i> -[(1 <i>R</i>)-1-(4-METHOXYPHENYL)ETHYL]THIOPHENE-2-CARBOXAMIDE (<i>R</i>)-23	69
5.12. SYNTHESIS OF (<i>S</i>)- <i>N</i> -[1-(1-NAPHTHYL)ETHYL]ACETAMIDE (<i>S</i>)-25	70
5.13. SYNTHESIS OF (<i>S</i>)- <i>N</i> -[1-(1-NAPHTHYL)ETHYL]PROPIONAMIDE (<i>S</i>)-26	71
5.14. SYNTHESIS OF (<i>S</i>)-3,3-DIMETHYL- <i>N</i> -[1-(1-NAPHTHYL)ETHYL]BUTYRAMIDE (<i>S</i>)-27	72
5.15. SYNTHESIS OF <i>N</i> -[(1 <i>S</i>)-1-(1-NAPHTHYL)ETHYL]THIOPHENE-2-CARBOXAMIDE (<i>S</i>)-28	73
5.16. SYNTHESIS OF (<i>S</i>)- <i>N</i> -[1-(2-NAPHTHYL)ETHYL]ACETAMIDE (<i>S</i>)-30	74
5.17. SYNTHESIS OF (<i>R</i>)- <i>N</i> -[1-(2-NAPHTHYL)ETHYL]ISOBUTYRAMIDE (<i>R</i>)-31	75
5.18. SYNTHESIS OF (<i>R</i>)- <i>N</i> -[1-(2-NAPHTHYL)ETHYL]BENZAMIDE (<i>R</i>)-32	76
5.19. SYNTHESIS OF (<i>R</i>)- <i>N</i> -(1-PHENYLPROPYL)ACETAMIDE (<i>R</i>)-34	77
5.20. SYNTHESIS OF (<i>R</i>)- <i>N</i> -(1-PHENYLPROPYL)PIVALAMIDE (<i>R</i>)-35	78
5.21. SYNTHESIS OF (<i>R</i>)-2-PHENYL- <i>N</i> -(1-PHENYLPROPYL)ACETAMIDE (<i>R</i>)-36	79
5.22. SYNTHESIS OF (<i>S</i>)- <i>N</i> -(INDAN-1-YL)ACETAMIDE (<i>S</i>)-38	80
5.23. SYNTHESIS OF (<i>S</i>)-3,3-DIMETHYL- <i>N</i> -(INDAN-1-YL)BUTYRAMIDE (<i>S</i>)-39	81
5.24. SYNTHESIS OF (<i>S</i>)- <i>N</i> -(1-CYCLOHEXYLETHYL)ACETAMIDE (<i>S</i>)-41	82
5.25. SYNTHESIS OF (<i>S</i>)- <i>N</i> -(1-CYCLOHEXYLETHYL)ISOBUTYRAMIDE (<i>S</i>)-42	83
5.26. SYNTHESIS OF (<i>S</i>)-3,3-DIMETHYL- <i>N</i> -(1-CYCLOHEXYLETHYL)BUTYRAMIDE (<i>S</i>)-43	84
5.27. SYNTHESIS OF (<i>S</i>)-2-PHENYL- <i>N</i> -(1-CYCLOHEXYLETHYL)ACETAMIDE (<i>S</i>)-44	85
5.28. SYNTHESIS OF <i>N</i> -[(2 <i>S</i>)-1-METHOXYPROPAN-2-YL]PIVALAMIDE (<i>S</i>)-46	86

5.29.	SYNTHESIS OF (<i>R</i>)- <i>N</i> -(1,2-DIMETHYLPROPYL)PROPIONAMIDE (<i>R</i>)-48	87
5.30.	SYNTHESIS OF <i>N</i> -[(1 <i>R</i>)-1,2-DIMETHYLPROPYL]THIOPHENE-2 CARBOXAMIDE (<i>R</i>)-49	88
5.31.	SYNTHESIS OF (<i>S</i>)-3,3-DIMETHYL- <i>N</i> -(3,3-DIMETHYL-2-BUTYL)BUTYRAMIDE (<i>S</i>)-51.....	89
5.32.	SYNTHESIS OF (<i>S</i>)-2-PHENYL- <i>N</i> -(3,3-DIMETHYL-2-BUTYL)ACETAMIDE (<i>S</i>)-52.....	90
5.33.	CD MEASUREMENTS AND <i>g</i> -FACTOR SPECTRA.....	91
5.34.	DFT CALCULATIONS	97
5.35.	¹ H NMR, ¹³ C NMR, AND ESI-MS CHARACTERIZATIONS.....	98
5.36.	COORDINATES OF OPTIMIZED STRUCTURES OF THE MOST STABLE CONFORMER FOUND FOR EACH AMIDE	143
6.	REFERENCES	155
7.	ACKNOWLEDGEMENTS	160

1. INTRODUCTION

1.1. RELEVANCE OF CHIRALITY: UNCOVERING ABSOLUTE CONFIGURATION AND ENANTIOMERIC EXCESS

Chirality is a pervasive property found at all scales in matter, from small molecules to spiral galaxies, from plant tendrils to architecture. Human beings themselves are chiral as a whole and they are made of chiral bioactive molecules, such as proteins, carbohydrates, lipids, and nucleic acids.^[1] Hence, chiral compounds play an extensive role in different aspects of synthetic chemistry, food chemistry, materials development, medical sciences, cosmetic preparations, and life sciences.

In the extended field of organic chemistry, one deeply researched topic concerns the incessant identification and improvement of new asymmetric synthetic pathways, whose goal is to achieve enantioselective processes. These aim to obtain preferentially one enantiomer over the other, most of the time through the use of chiral catalysts or auxiliary species.^[2] Since the continuous growth of the number of chiral molecules such as pharmaceuticals, fragrances, and agrochemicals, advantages brought by asymmetric synthesis are essential to their development. Developing new asymmetric reactions, or improving existing ones, requires a continuous work of optimisation of the catalytic systems (*e.g.* catalyst, auxiliary, reaction time, temperature, solvent, pH, concentration *etc.*), which demands a lot of time and effort to establish the optimal reaction conditions.^[3] To speed-up the process, high-throughput methodologies have been developed recently, such as parallel synthesis and combinatorial chemistry,^[4,5] computational molecular catalyst design^[6] and “Design of Experiments” (DoE) optimisation.^[7,8] In particular, both parallel synthesis and combinatorial chemistry allow to carry out experimentally the same iterative optimisation realized by traditional methods, but with the considerable advantage of being conducted on a larger ensemble of reaction conditions (Figure 2).^[9] These kind of synthetic approaches define a class of methodologies known as high-throughput screening (HTS) techniques.^[10,11]

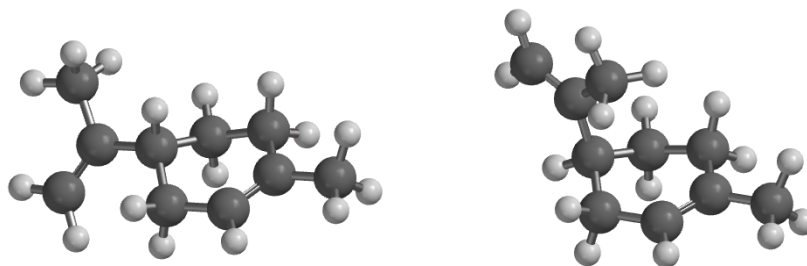


Figure 1. *D*-Limonene (orange essence, left) and *L*-limonene (turpentine essence, right) are respectively the (*R*)- and (*S*)-enantiomer of the chiral molecule limonene. Enantiomers are a pair of molecules that are not superimposable mirror images of each other.

Chirality configuration assessment and determination of enantiomeric excess are two features of crucial importance in asymmetric synthesis.^[12] Enantiomeric excess (*ee*) is defined by eqn (1)^[13] and it refers to the imbalance between the two enantiomers of a sample of chiral molecules, therefore it can be seen as a quantification of the purity of a chiral compound or, from a synthetic point of view, as an evaluation of the efficiency achieved by the asymmetric process. This parameter is defined in a range going from -100% to +100%, depending on which enantiomer is found in major amount (eqn (1)), but it is usually reported as absolute value, specifying the absolute configuration of the stereogenic centre/unit.

$$ee = \left(\frac{[R] - [S]}{[R] + [S]} \right) \cdot 100 \quad (1)$$

Enantiomers have to be isolated, separated or discriminated in order to determine enantiomeric excess, and this is achievable through diastereomeric interactions (not equivalent by symmetry), thus a chiral environment is needed for this purpose.^[14]

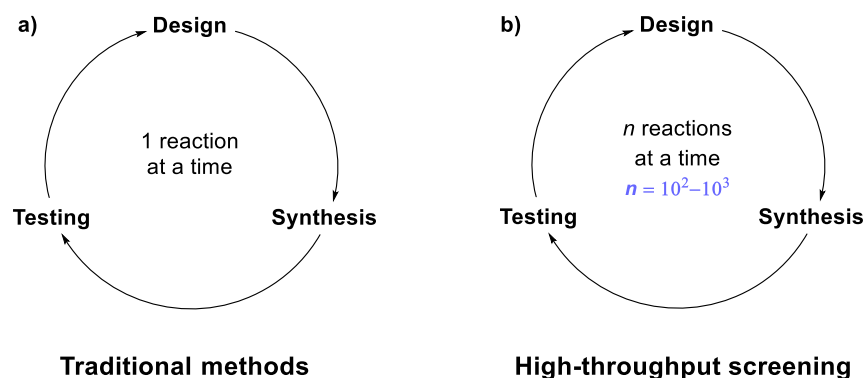


Figure 2. Differences in the screening of catalysts/auxiliaries in asymmetric synthesis by (a) traditional methods and (b) HTS techniques.

Nevertheless, while simultaneously running a high number of asymmetric syntheses is feasible, analysing the enantiomeric excess of reaction outcomes relies on methods that are still not sufficiently mature to keep up with such workflow. Since the

traditional means of analysis are too sluggish to process hundreds or even thousands of samples, this causes a bottleneck in the workflow. For this reason, chemists and biologists have to restrict the number of simultaneous reactions, trying to diminish the amount of needed analysis. Obviously, this is not the solution: the approximative ideal target number of processable samples per day is many thousands for a truly high-throughput analysis (HTA) approach, as estimated by Reetz almost 25 years ago.^[4] To recover the absolute configuration or to quantify enantiomeric excess different analytical techniques are currently used and/or still being developed. This includes nematic and cholesteric liquid crystals,^[15,16] IR thermography,^[17,18] NMR spectroscopy,^[19,20] mass spectrometry,^[21,22] X-rays,^[23] enzymatic and antibody methods,^[24,25] and chiral chromatography.^[26,27] Notably, the latter is the one that has been most intensively employed for decades for the determination of the enantiomeric excess. However, the time required to develop the methodology, to run the experiments, the cost of chiral columns, and instruments are pushing forward the research to develop cheaper, and time-efficient analytical tools for high-throughput chirality screening.

Within this context, chiroptical spectroscopies have received a particular attention from the scientific community as a solution to this challenge.^[13] These methods, which take advantage from the interaction between electromagnetic radiation and matter, are fast (*i.e.* a full spectrum is achievable in less than a minute) which is the prerequisite for the development of HTA methodologies. In typical chiroptical spectroscopies, chiral samples can be irradiated by linearly, circularly or elliptically polarized light. These lights are defined depending on the direction of the components of both electric and magnetic field (which together generate the electromagnetic radiation) along the propagation direction, and the detector measures the absorbed or emitted light.^[28] Information on the sample of interest are gathered due to the presence of at least one strong chromophore on the chiral analyte, which is a part of the molecule responsible for the generation of an absorption band after an electronic transition. However, chiral molecules often have weak chromophores and none, or just negligible, Cotton effects are observed (Figure 4a-b) in the UV-vis region. To improve signals in this region, one solution arose from chiral sensors which are molecules able to bind chiral molecules and to amplify chiroptically the chiral information.^[29]

1.2. ELECTRONIC CIRCULAR DICHROISM AND SUPRAMOLECULAR CHIROPTICAL SENSORS

Electronic circular dichroism (ECD) spectroscopy, called also just circular dichroism (CD), has become one of the most powerful techniques in the assessment of the absolute configuration of chiral molecules and in the enantiomeric excess determination of a non-racemic mixture of two enantiomers. Furthermore, it has found broad use also in the interpretation of structural aspects in chiral chromophoric species, especially in the characterization of the helical structure of DNA and RNA,^[30] and in the discernment of secondary structures of polypeptides and proteins.^[31] CD measures the difference in absorption between laevorotatory and dextrorotatory circularly polarized (LCP and RCP) light, which can be seen as the two components of linearly polarized light rotating, respectively, anti-clockwise and clockwise^[32]: when an absorbing optically active species is irradiated with light, the two circularly polarized components travel through it at different velocity ($v_L \neq v_R$) and they are differently absorbed ($\epsilon_L \neq \epsilon_R$).^[33] This spectroscopy works in the UV-vis range of the electromagnetic spectrum, where electronic transitions take place.

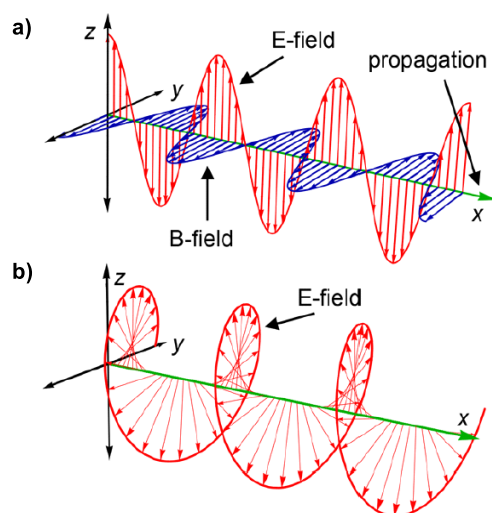


Figure 3. a) Linearly polarized light with electric (red) and magnetic (blue) field specified. b) Electric field of dextrorotatory circularly polarized light (magnetic field has been omitted for simplicity). Adapted from ref. ^[34].

For linearly polarized light (Figure 3a), the electric and magnetic field are in phase, therefore the electric field vector is always parallel to \hat{z} and it propagates along \hat{x} in time; for circularly polarized light (Figure 3b), the electric and magnetic field are out-of-phase by a $\pi/2$ factor, therefore the electric field vector is not always parallel to \hat{z} anymore, but it rotates around \hat{x} and it still propagates in time along \hat{x} , giving rise to a helical path. In this last case the magnitude of the electric field vector is constant.

CD experiments are carried out with a sample of a chiral compound solubilized in a proper solvent, which is alternatively irradiated with LCP and RCP light. The wavelength-dependent difference in absorption between these two components of the light is what generates the final CD spectrum of that substance (Figure 4c). Since enantiomers have equal but opposite interactions with LCP and RCP light, they display mirror-image CD spectra.^[13] Indeed, the CD spectrum obtained may be positive or negative, depending on whether LCP light is absorbed less than RCP light (negative CD signal) or more (positive CD signal) (eqn (3)).

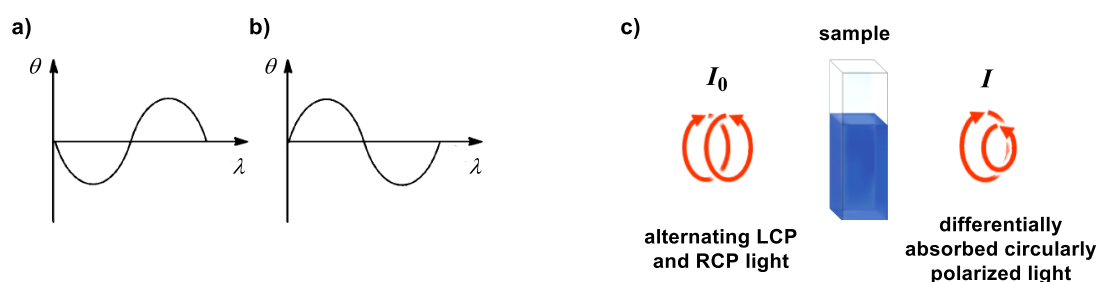


Figure 4. a) Positive Cotton effect and b) negative Cotton effect. c) General operation of CD spectroscopy, where the direction of the light beam is from I_0 (initial intensity) to I (intensity after sample absorption).

As already mentioned, the interactions that take place between LCP/RCP light and any chiral non-racemic sample are diastereomeric, thus different and consequently circular dichroism is defined as:

$$CD = A^l - A^r \quad (2)$$

where A^l and A^r are respectively the absorption of LCP and RCP lights and they are adimensional values. Eqn (2) gives a fundamental requirement to observe a dichroic peak (named also Cotton effect, Figure 4a-b), namely its correspondence to absorption bands. The output of CD spectrophotometers is typically given in units of observed ellipticity angle θ , linked to the CD effect through the relation^[34]:

$$\theta(mdeg) = 32982 \cdot CD \quad (3)$$

Since the CD signal follows the Lambert-Beer law, it is also possible to define the molar quantity:

$$\Delta\varepsilon = \varepsilon^l - \varepsilon^r = \frac{CD}{b \cdot C} \quad (4)$$

where $\Delta\varepsilon$ represents the molar circular dichroism expressed in $L \cdot mol^{-1} \cdot cm^{-1}$, ε^l and ε^r are respectively the molar absorption coefficient of LCP and RCP light expressed in

$\text{L}\cdot\text{mol}^{-1}\cdot\text{cm}^{-1}$, b is the optical path of the cuvette in cm and C is the concentration of the sample in $\text{mol}\cdot\text{L}^{-1}$. Since $\varepsilon^l \propto A^l$ and the same is true for RCP, from eqn (4) it is now possible to understand also mathematically why a CD spectrum may be positive or negative, and that depends precisely on which component of the light beam is mainly absorbed.

A quantitative descriptor of the chiroptical feedback of enantiomers is the Kuhn g -factor, sometimes also called anisotropy or dissymmetry factor, which is expressed by:

$$g = \frac{\Delta\varepsilon}{\varepsilon} = \frac{\varepsilon^l - \varepsilon^r}{\left(\frac{\varepsilon^l + \varepsilon^r}{2}\right)} = \frac{A^l - A^r}{A} \quad (5)$$

where ε represents the global molar extinction coefficient expressed in $\text{L}\cdot\text{mol}^{-1}\cdot\text{cm}^{-1}$ and A is the conventional absorbance of non-polarized light, which corresponds to the average between A^l and A^r . As reported in eqn (5), the crucial peculiarity of this physical quantity is its independence from the concentration of the sample and from the optical path of the cuvette.^[35] This is true when there is only one species in solution absorbing in the considered spectral window. Since g -factor depends on wavelength and on absorption parameters, it exhibits as well two features possessed also by CD and already cited, namely its existence only in correspondence to absorption bands ($\varepsilon \neq 0$) and as a signed property ($\Delta\varepsilon$ dependence). Therefore, when an optically active chiral non-racemic and non-enantiopure sample is analysed by means of CD spectroscopy, an imbalance in the absorption of the two circularly polarized components of the light beam is generated. In the presence of a wavelength region where only that analyte absorbs, from the resulting g -factor spectrum it is possible to extract information about the enantiomeric excess of the analysed species, only if a calibration curve is available. This is a remarkable result, because this spectroscopic measurement is simple, fast, and there is no need to separate the two enantiomers.

Nonetheless, as briefly introduced in paragraph 1.1, often some requirements of the chiral analyte are not met, in particular the presence of a strong chromophore, and in these cases a chiral-sensor is required for CD analysis (Figure 5-6). Sensors are supramolecular species able to bind chiral analytes and to amplify the chiral information, providing strong absorption bands that allow the assignment of absolute configuration and the quantification of enantiomeric excess.

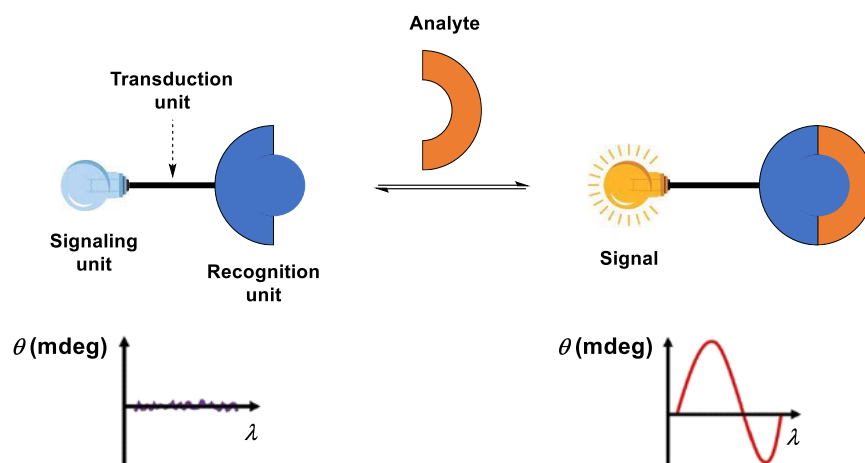


Figure 5. Top: schematic representation of the functioning of a general molecular sensor with guest complexation. Bottom: illustration of the type of enhanced CD response expected.

Chiroptical sensors based on non-covalent molecular recognition have been particularly studied in the last years due to their rapid equilibrium kinetic with guest molecules and their possibility to be recycled.^[36] Following the molecular recognition event, two possible diastereomers are usually formed (Figure 6). The enantiomeric excess of the chiral analyte, together with the different thermodynamic stability of the two newly formed species, determine an unbalance on the CD absorption. The higher the capability of the sensor to differentiate the enantiomers, the stronger the output in the CD.

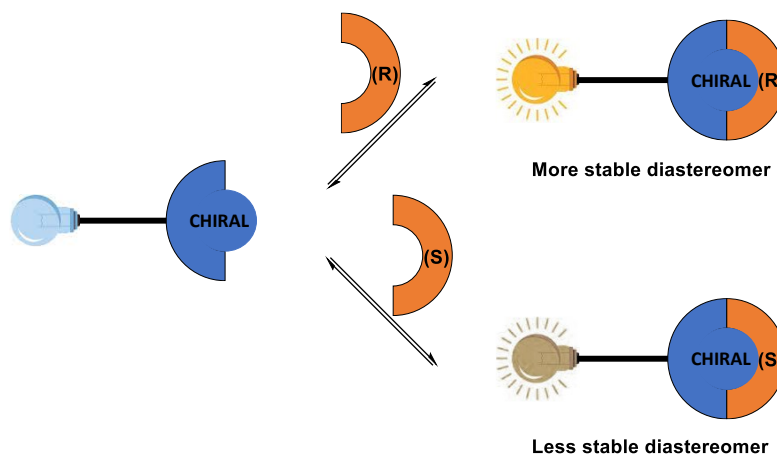


Figure 6. General operating principle of chiral molecular sensors to discriminate enantiomers of a guest.

A chromogenic or fluorogenic unit is frequently incorporated into both chiroptical sensor and analyte, or into just one of them, in close proximity to the binding site in order to achieve an induced dichroic signal upon binding. The chromophoric unit is usually integrated into the host rather than into the chiral substrate. The most frequent mechanism to cause the variation of the spectroscopic signal is the exciton coupling,

where chirality of the analyte induces a chiral orientation of dipole moments of at least two chromophores of the host.^[37]

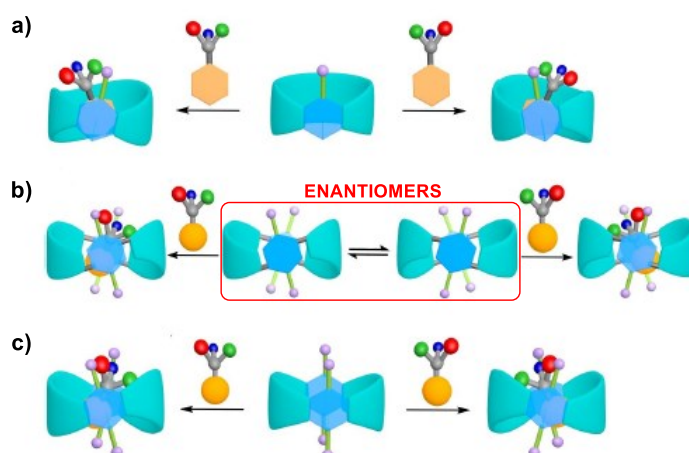


Figure 7. Illustration of three classes of supramolecular hosts, exhibiting different structural features, capable to cause a spectroscopical change upon binding of chiral substrates. Adapted from ref. ^[29].

Supramolecular chemists have implemented several host scaffolds, such as crown-ethers, calixarenes, cyclodextrins, cucurbiturils, pillararenes, resorcinarenes *etc.* These structures are often modified in order to incorporate a chromophore and to enhance discrimination of enantiomers. Three examples of supramolecular hosts used for this purpose are generally reported. The first is related to an achiral chiroptical sensor and a chiral analyte, which display both a chromophore (Figure 7a). Upon binding, the chiral environment of the guest molecule induces a change in the electronic structure of the chromophore host which give raise to a strong induced CD output. In this case, the Cotton effect (Figure 4a-b) is linked to the spatial orientation of the two chromophoric groups, thus assignment of absolute configuration of the analyte might be feasible.^[37] In the second example (Figure 7b), the guest may not possess chromophores, whereas the host presents more than one. In this case, the chiroptical sensor is chiral and racemic, but its two enantiomeric forms are linked through a dynamic equilibrium in solution. In this case, the chiral analyte dictates the preference to form one diastereomer (Figure 6).^[38] The imbalance between the two diastereomers depends on the different stabilities of the diastereomeric adducts. In the last case (Figure 7c), an achiral chiroptical sensor with two or more chromophores is used and, as a consequence of molecular recognition, a chiral conformation of the host is preferred. In this situation, the methodology is also suitable for chiral guests without chromophoric groups. For the second and third examples, the dichroic peaks are found at similar wavelengths for independently chiral guests, thus a portable instrument

performing in a narrow region of the UV-vis range could be designed and built, achieving a striking advantage of a ubiquitous and fast measurement capability.^[29]

The second reported example (Figure 7b) is particularly considered by supramolecular chemists, especially in the last few years.^[39] Chiroptical sensors of this kind are known also as stereodynamic probes, due to the dynamic equilibrium that interconverts between the two enantiomers of the host. Indeed, chiroptical sensing with stereodynamic systems based on different chiroptical spectroscopies, such as circular dichroism, vibrational circular dichroism (VCD),^[40] fluorescence-detected circular dichroism (FD CD),^[41] circular polarised luminescence (CPL)^[42] *etc.* are being studied as fast and sensitive methods for chirality recognition of small chiral substrates, therefore displaying a huge step forward for chirality analysis in HTA methodologies.

1.3. CHIRALITY SENSING USING STEREODYNAMIC SYSTEMS AND ELECTRONIC CIRCULAR DICHROISM SPECTROSCOPY

The strong dichroic output induced through non-covalent molecular recognition between stereodynamic molecular sensors and small chiral molecules has encouraged researchers to synthesise novel sensors with the final aim of earning accurate information about absolute configuration and enantiomeric excess of various chiral substrates. The success of CD analysis coupled with the use of stereodynamic probes are due to some features:^[39]

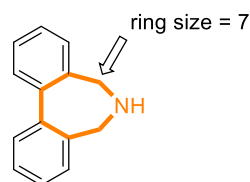
- The prompt availability of the probe, its efficiency in stoichiometric amounts and possibly in a fair range of environmental conditions, retrievable and reusable, and useful for a broad assortment of chiral analytes. Nonetheless, these chiroptical probes must be produced on purpose.
- The molecular recognition process and the asymmetric induction step should be instantaneous and furnish a time-efficient CD measurement. The explanation for this mechanism is the diverse binding affinities of the chiral substrate for the two enantiomeric forms of the sensor, leading to a magnitude of the dichroic signal dependent on the imbalance between the two generated diastereomers.
- The probe should generate an intense Cotton effect at high wavelengths (lower-energy radiation) in order to diminish interferences related to optically active impurities that could be found inside the final reaction mixture of asymmetric synthesis.
- To quantify accurately the enantiomeric excess of a sample, a strong dichroic signal is recommended, both to reduce the error in the determination and to diminish the amount of probe and analyte required.
- Reliable information about the absolute configuration of a wide range of analytes should be obtained, with molecular recognition based on distinct host-guest interactions and persistent chiral induction mechanism.

The enormous advancements achieved in the last decades in the field of supramolecular chemistry have encouraged many research groups to study potential stereodynamic systems applicable for chirality sensing. A vast landscape of small chiral substrates has been investigated, such as chiral carboxylic acids, amines, amides, alcohols *etc.*, with interesting and encouraging results. Notably, supramolecular

architectures, such as metal complexes which are able to rapidly accommodate a chiral ligand in their inner coordination sphere, chiral bridged aromatic frameworks, and propeller-like architectures are quite recursive in literature, probably due to their peculiar stereochemical diversity and the affordability and facility of accessibility and manipulation of recognizable chiral substrates. In the following, examples of some different classes of stereodynamic systems will be presented.

1.3.1. Bridged biaryls

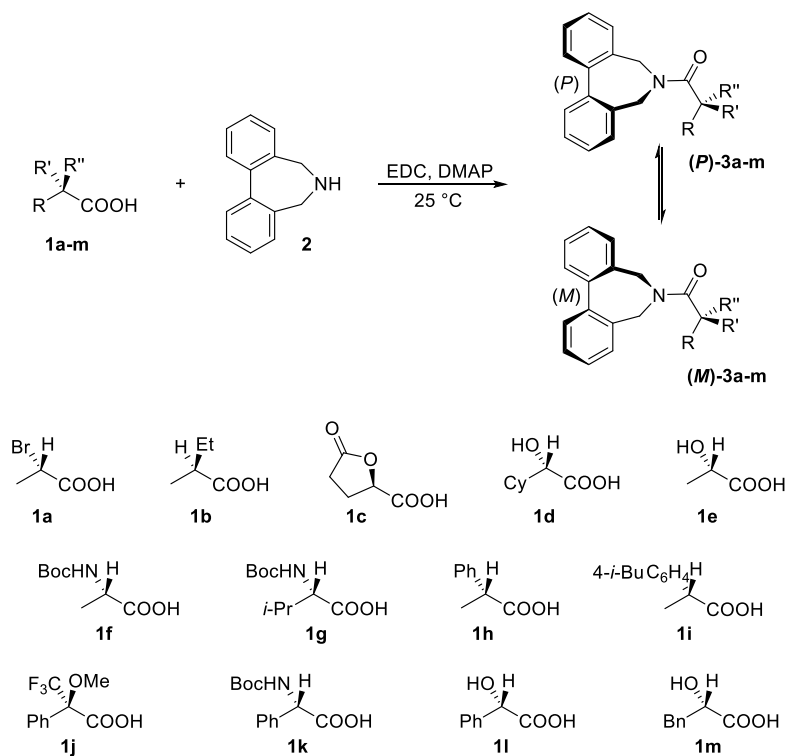
Bridged biaryls have been one of the first examples of stereodynamic probes. The energy barrier for the rotation of the C-C bond connecting the two aryls depends especially on steric effects, but sometimes even electronic effects can play a relevant role. The conformational stability of 2,2'-disubstituted biphenyls depends substantially on the ring size (Figure 8). Usually, even if in the other two *ortho*-positions are present bulky groups, biaryls with one bridging atom are not stable to rotation at room temperature; whereas, increasing the bridge length, the torsion angle between the two aromatic rings is increased, hence incrementing the CD output and the rotational energy barrier to racemization, until adequately seven-membered or larger rings (the central aryl-aryl bond is incorporated) are reached.



2,2'-disubstituted biphenyl

Figure 8. Structure of 2,2'-disubstituted biphenyl **2** reported by Rosini and coworkers. In this specific example, the considered ring is a seven-membered ring.

Rosini *et al.* synthesized a biphenyl-derived azepine probe able to recognize chiral carboxylic acids, which can be used to detect their absolute configuration.^[43] They observed that the reaction between a chiral α -substituted carboxylic acid **1** and amine **2** with addition of 1-ethyl-3-(3-dimethylaminopropyl)carbodiimide (EDC) and 4-dimethylaminopyridine (DMAP) overnight generates a diastereomeric mixture of amides **3** (Scheme 1) with yields ranging between 50% and 80%.



Scheme 1. Coupling reaction between the chiroptical sensor **2** and various chiral α -substituted carboxylic acids.

This procedure was carried out with different chiral α -substituted carboxylic acids **1a-m** and the purified products of coupling were analysed by means of CD and UV spectroscopy. The experimental observations proved that the sign of the resulting spectra is related to the structure of the chiral carboxylic acid employed. Indeed, the chirality transfer arises from the structural modification induced on **2** by the carboxylic acids. This is favoured by two main characteristics of this system: the close proximity of the stereogenic carbon centre of the analyte to the stereogenic bridged biphenyl unit and the rigidity of the resulting diastereomeric amides **3a-m**. Indeed, the partially planar nature of the peptide bond induces a rising of the energy barrier for the atropisomeric rotation around the aryl-aryl bond. The relative thermodynamic stability of the atropisomers **3a-m** depends on the intramolecular interactions existing between the chiroptical sensor **2** and the groups bound to the stereogenic centre of **1a-m**. The Cotton effect at approximately 250 nm depends by this induced imbalance toward the *M* or *P* atropisomer of the sensor, and the sign of this structure-dependent CD output is correlated to the absolute configuration of the analyte used. This dependence on the structure of chiral α -substituted carboxylic acids has been studied by crystallography, computations and NMR experiments, displaying two possible

conformations for **3a-m** and a dependent-preference for one of the two on the aromatic or aliphatic nature of the α -substituent.

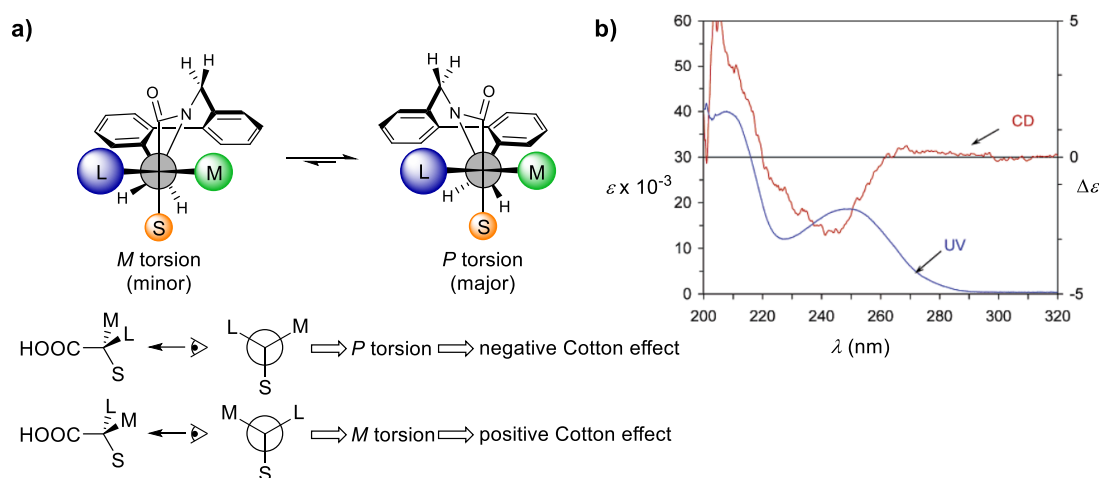


Figure 9. a) Schematic representation of the chiral induction model in biphenyl amides **3** due to α -alkyl-substituted carboxylic acids binding. b) CD and UV spectrum of **3a** ($\sim 1 \times 10^{-3}$ M in THF). [b] is adapted from ref. [43].

For α -alkyl-substituted carboxylic acids **1a-g** and **1m**, two conformations are possible and both direct the small group (S) in the plane defined by the peptide bond and in-between two benzylic protons of the azepine moiety (Figure 9). This conformational equilibrium is usually settled by steric effects, principally repulsion between the large group (L) and the biphenyl system, with the favoured conformer presenting the phenyl moiety proximal to L arranged “in parallel” to it. Depending on the enantiomer of the analyte employed, the preferential torsion in the biphenyl probe originates a signed CD signal: positive Cotton effect for *M* stereoisomer or negative Cotton effect for *P* stereoisomer. This leads to the possibility to derive the absolute configuration of the α -alkyl-substituted carboxylic acid studied from the sign of the CD output observed.

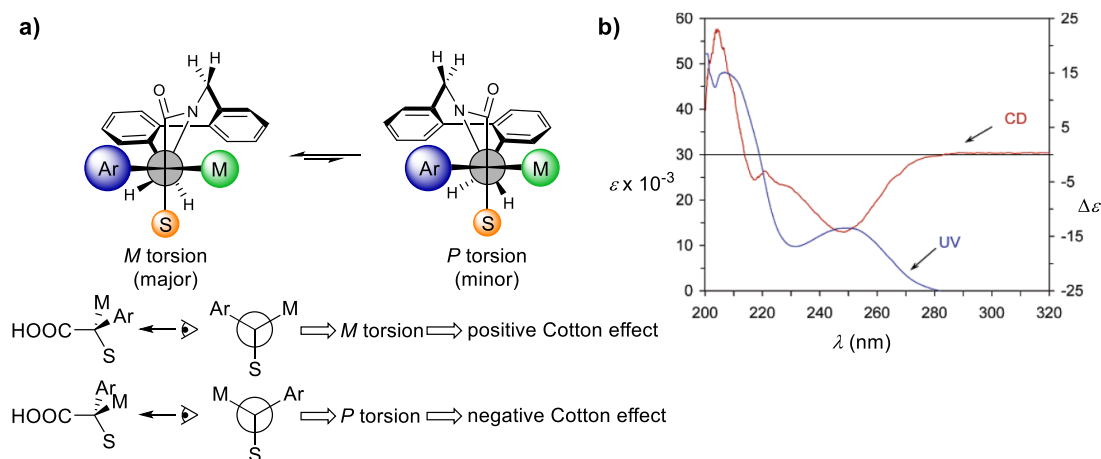
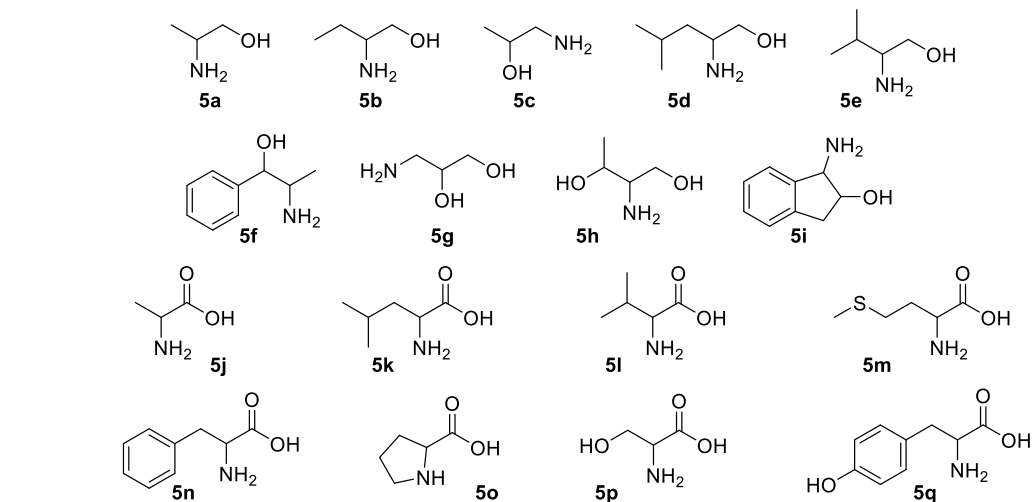
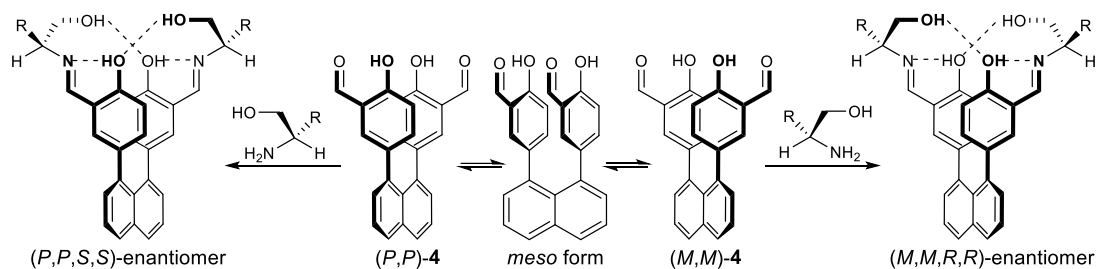


Figure 10. a) Schematic representation of the chiral induction model in biphenyl amides **3** due to α -aryl-substituted carboxylic acids binding ($Ar = L$). b) CD and UV spectrum of **3h** ($\sim 1 \times 10^{-3}$ M in THF). [b] is adapted from ref. [43].

The opposite verifies in the case of α -aryl-substituted carboxylic acids **1h-l**, where the electronic effects are much more important, and the favoured conformer presents the phenyl moiety proximal to Ar arranged “perpendicularly” to it, hence exploiting the stabilizing face-to-edge interactions (Figure 10).

1.3.2. Imine foldamers

There is a quite broad class of stereodynamic sensors able to form imines in presence of amines, amino alcohols and amino acids, which exhibit also a marked Cotton effect after binding the guest. The reported example is by Wolf and co-workers, who developed a triaryl chiroptical sensor **4** exhibiting two co-facial salicylaldehyde rings linked to the peri-positions of a naphthalene.^[44,45] This probe exists as a CD silent racemic mixture of rapidly interconverting enantiomers *via* a less stable *meso* form (Scheme 2). Notably, the condensation reaction between the aldehyde units of the chiroptical sensor and chiral amino alcohols or amino acids **5a-q** is rapid and quantitative (< 5 min at room temperature), due to the presence of the neighbouring phenol group. This allows the formation of homochiral salicylideneimine adducts in 2:1 ratio between chiral substrate and stereodynamic probe, with the genesis of a peculiar UV absorption band above 400 nm and a strong CD output (Figure 11). Crystallography, NMR experiments and mass spectrometry unveiled that the diimine formation with (*S*)-amino alcohols is linked through asymmetric transformation of the sensor toward the (*P,P*)-conformer, whereas with (*R*)-amino alcohol analytes is obtained the (*M,M*)-conformer. This chirality induction is controlled by an intramolecular pattern of hydrogen bonds that blocks the probe into a single conformation and at the same time lessens steric repulsions between the substrate residues and the stereodynamic probe scaffold. The strong CD signal gained can be associated to exciton coupling of the two salicylideneimine chromophores, and the corresponding dichroic peak is found at rather high λ values, which would bring the advantage of minimizing interferences if chiral impurities were present in the analysed sample. To ensure this relevance of the two linked co-facial salicylaldehyde rings, they measured the CD spectrum of a sample prepared mixing free salicylaldehyde and a chiral amino alcohol, demonstrating as a matter of fact that this mixture does not give rise to a CD signal (Figure 11a).



Scheme 2. Top: chirality induction with triaryl probe **4** and amino alcohols. Bottom: structures of chiral amino alcohols **5a-i** and chiral amino acids **5j-q** with the important feature of inducing strong CD outputs after binding to sensor **4**.

The chiroptical sensor **4** has been employed to accurately assess absolute configuration and to determine enantiomeric excess of a broad ensemble of amino alcohols and amino acids at low concentration. For each chiral substrate tested (**5a-q**), a linear correlation between the CD signal and the enantiomeric excess of the analyte was found, and the measurements were carried out without purification.

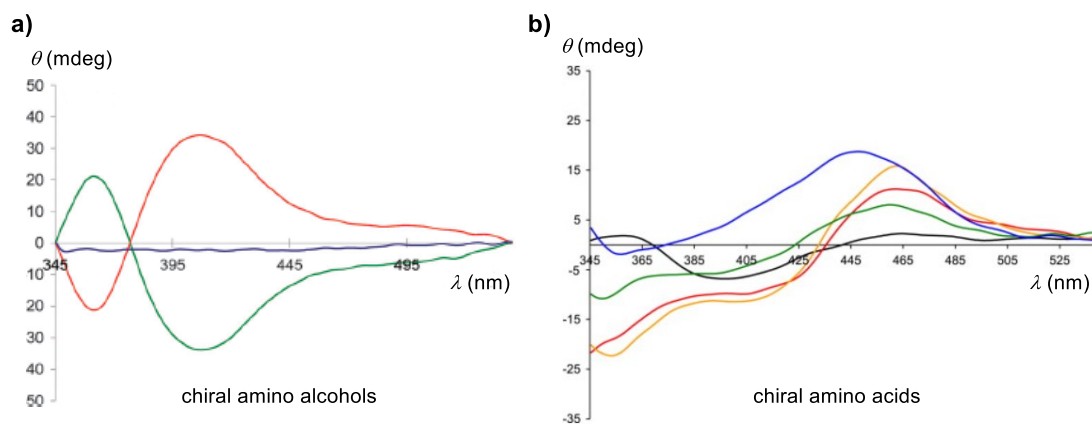
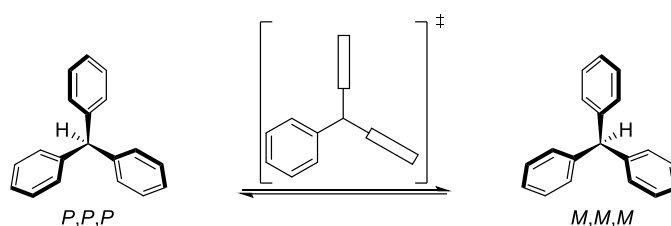


Figure 11. a) CD spectra of the diimines derived from binding between **4** and (R) -**5a** (green) and (S) -**5a** (red) (5.0×10^{-4} M in CHCl_3). The imine obtained from free salicylaldehyde and (R) -**5a** (blue) does not exhibit a CD signal neither at 5.0×10^{-3} M in CHCl_3 . Adapted from ref. [44]. b) CD spectra of the diimines derived from binding between **4** and (R) -**5j** (black), (R) -**5k** (red), (R) -**5l** (yellow), (R) -**5m** (green) and (R) -**5n** (blue) (2.5×10^{-4} M in CHCl_3). Adapted from ref. [45].

1.3.3. Trityl propellers

In classic organic chemistry, the trityl group (triphenylmethyl group) is commonly used as protecting groups for heteroatoms in amines, alcohols and thiols, and it is also acknowledged to display propeller chirality. The three phenyl rings are not on the same plane, but they are twisted and assume clockwise or counterclockwise arrangements, which engender three-dimensional helical conformations. Since each phenyl ring suffers from steric hindrance due to the other adjacent phenyl rings, molecular propellers exhibit gearing effects and the propeller blades go through energetically favoured correlated rotations. The interconversion between the stereoisomers of the trityl moiety happens rapidly at room temperature, but the mechanism is still not confirmed, even if it is largely believed to be a two-ring flipping mechanism where two phenyl experience conrotatory rotation through the propeller plane and the third non-flipping phenyl rotates in the opposite direction (Scheme 3).



Scheme 3. Interconversion between the enantiomeric conformations of Ph_3CH via two-rings flipping mechanism.

Gawronski, Rosini and others saw in this structure a possibility to study chirality of some analytes.^[46,47] In particular, they discovered that binding chiral alcohols or amines to the trityl moiety bothers the local C_3 -symmetry of Ph_3CH (Figure 12). Trityl ethers **6a-I** derivatives of reaction between trityl chloride and a chiral secondary alcohol were prepared and analysed with CD spectroscopy, and molecular modelling was also performed. All collected data displayed that P,M,P -conformer is the predominant species when the secondary alcohol has (R)-configuration, and vice versa for (S)-alcohol (Figure 12a).

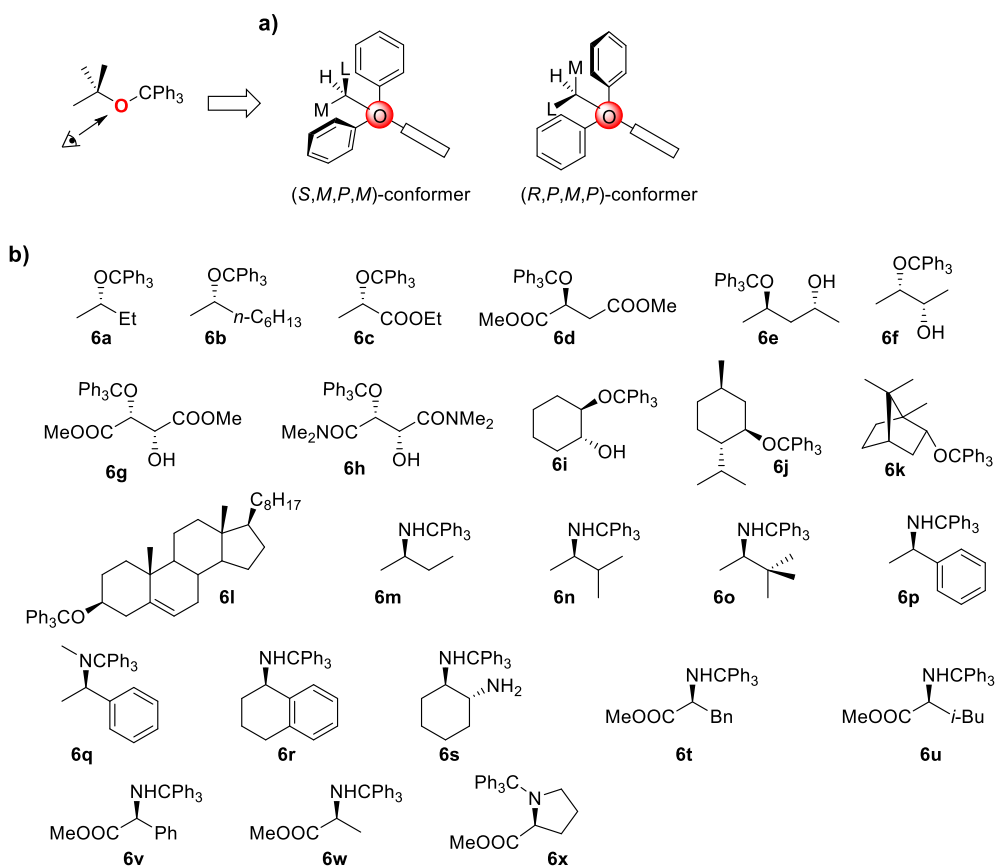


Figure 12. a) Favoured residual *M,P,M*- and *P,M,P*-conformations of chiral trityl ethers. The Newman projection shows the view of the stereoisomers along the ether *O-CPh₃* bond seen with the oxygen atom over the plane (red). b) Structures of the chiral substrates tested.

The CD output obtained is characteristic of this type of structures, therefore the C_1 -symmetry induced by chiral alcohols provides suitable characteristics to the trityl group to be employed as stereodynamic sensor to assign absolute configuration in the alcohol analyte. Trityl ethers exhibiting (*R*)-alcohol moiety reveal a positive Cotton effect between 200 and 225 nm, whereas (*S*)-alcohols present an opposite Cotton effect in the same wavelengths range (Figure 13). The same hypothesis and general observations apply also to *N*-tritylamines **6m-x**, even though they present more sophisticated equilibria due to stereogenic nitrogen fast inversion, which affects the propeller helicity of the probe and eventually the sign of the CD readout.

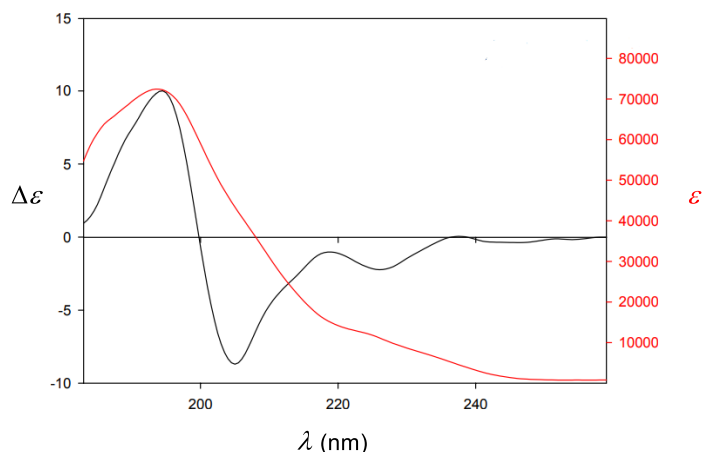


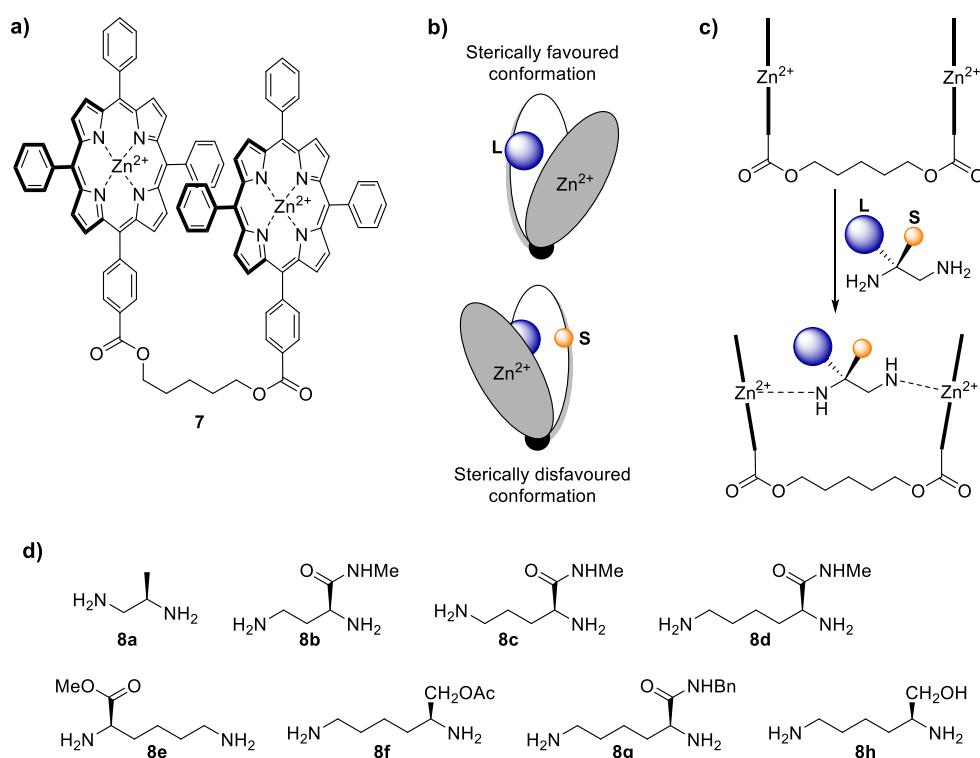
Figure 13. CD (black) and UV (red) spectrum of dimethyl (*S*)-malate trityl ether (**6d**, 3.14×10^{-4} M in MeCN). Adapted from ref. [46].

1.3.4. Metalloporphyrins

In the past decades, metalloporphyrins have received attention for their capability to perform exciton-coupled chiroptical sensing of the absolute configuration of a broad variety of substrates.^[48] 5,10,15,20-tetraarylporphyrins show an intense Soret band positioned above 400 nm ($4 \times 10^5 < \epsilon > 8 \times 10^5$): this peculiar strong absorption of tweezers-like metalloporphyrins grants CD spectra measurements with μM concentrations of both probe and chiral substrate. The location of this band at relatively high wavelengths is an advantage, because it allows to avoid interferences of dichroic peaks arising by other chromophoric compounds or impurities. Porphyrins are pretty easily metalated or modified, thus it is possible to obtain a wide class of metalloporphyrins exhibiting different properties depending on the metal, such as absorbance intensity and position, solubility, and Lewis acidity. Nevertheless, the necessity to develop new tweezer-like porphyrin architectures came up, since in most cases it was required a covalent binding of the chiral analyte to the porphyrin ring, and often the observed Cotton effects were quite poorly intense.

Nakanishi, Berova *et al.* prepared a tweezer **7** linking two zinc porphyrin units *via* a 1,5-pentadiol chain (Scheme 4).^[49,50] This probe is able to bind chiral substrates of diverse sizes, such as mono- and diamines, amino acids, and amino alcohols, thanks to the flexibility and length of the aliphatic linker. For example, diamine substrates **8a-h** are accommodated between the two porphyrin moieties due to coordination to the zinc centres, with the two porphyrins twisting to minimize steric repulsions with

the large group L on the stereogenic centre of the chiral diamine, hence achieving a chiral conformation.



Scheme 4. a) Structure of tweezer 7. b) Schematic representation of the two possible conformers of 7 after binding a chiral diamine. c) Illustration of the coordination of a chiral diamine to the Zn(II) centres in 7. d) Structures of the chiral diamine substrates tested.

This overall species generates an intense Cotton effect, which is related to the preferentially populated porphyrin twist that arranges L group far away from the two porphyrin rings, therefore this tweezer can be used as chiroptical sensor to uncover the absolute configuration of the cited chiral substrates (Figure 14). The tweezer can be recycled, since the chiral molecule is not covalently bound to the chiroptical sensor.

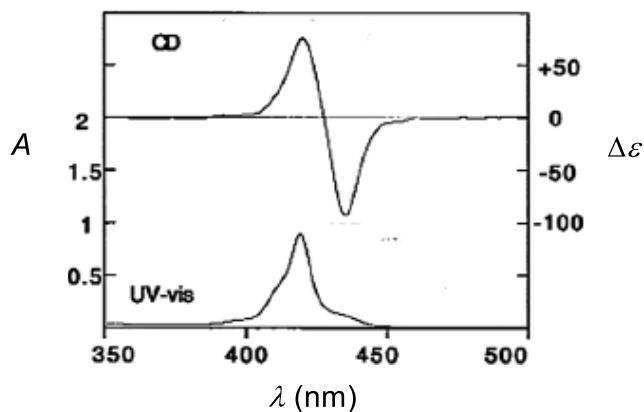


Figure 14. CD and UV-vis spectrum measured for the adduct generated upon coordination of 8a to 7 in hexane. Adapted from ref. [49].

1.3.5. Stereodynamic metal complexes

This class of stereodynamic sensors is probably the most populated and widely used approach, and it relies on the application of metal complexes of tetradentate ligands, which adopt two enantiomeric propeller-like conformations around the metal centre (*M* or *P* configuration) controlled by the coordination of a chiral substrate.

An example was reported by Canary, Anslyn *et al.*, who proposed *N,N*-bis[(2-quinolyl)methyl]-1-(2-pyridyl)methylamine copper(II) complex **9** (Figure 15a) as a chiroptical sensor to analyse chiral carboxylic acids and amino acids.^[51,52]

The equilibrium of this probe is perturbed through substitution of the apical solvent molecule by chiral substrates **10a-f** (Figure 15c). Data obtained from crystallography state that **9** shows a square pyramidal coordination sphere with one nitrogen of a quinolyl ring tending toward the apical position, but it is bended by the coordinated water molecule, so the overall geometry is distorted toward a trigonal bipyramidal structure. Upon binding of chiral analytes **10a-f**, a very intense CD signal is generated around 240 nm, with its sign depending on the enantiomer of the recognized substrate (Figure 15b): negative Cotton effect for (*R*)-analytes and *P* helicity of the probe, whereas positive Cotton effect for the (*S*)-enantiomer and *M* propeller twist. This stereodynamic probe has found application in the assignment of absolute configuration and quantification of enantiomeric excess of **10b**, **10d**, **10e**, providing results within 1.8-4.1% error for enantiomeric excess.

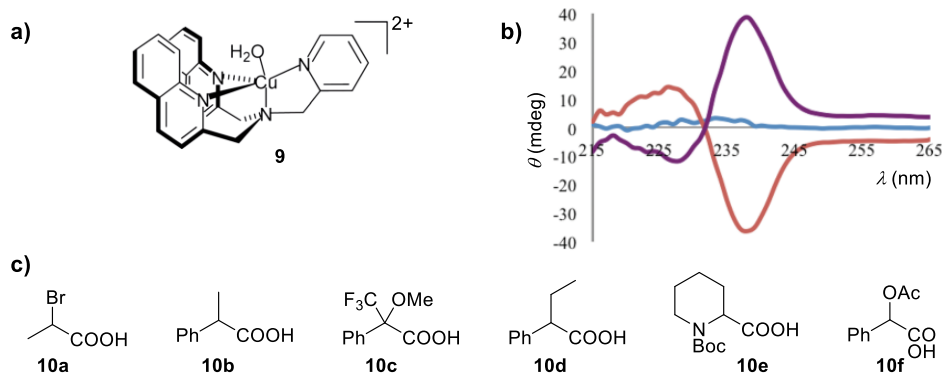
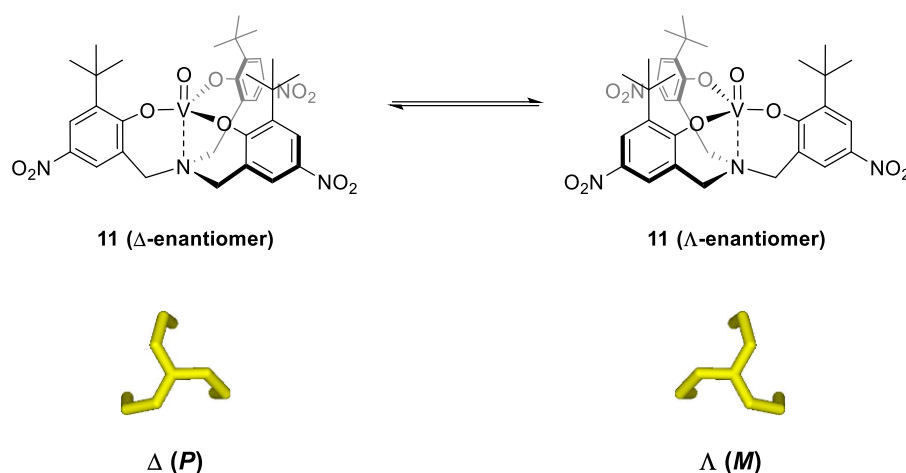


Figure 15. a) Structure of stereodynamic probe **9**. b) CD spectra obtained upon coordination of enantiopure **10d** (0.5 M of **9** in 3:1 MeCN/H₂O + 20 mM HEPES buffer at pH = 7.4 and 2 equivalents of **10d**): CD spectrum of **9** (blue), CD spectrum of **9-(R)-10d** (pink), and CD spectrum of **9-(S)-10d** (purple). c) Structures of chiral carboxylic acids **10a-f** tested. [b] is adapted from ref. [51].

One last example comes from the research group where this thesis has been carried out, where Zonta *et al.* investigated an oxo-vanadium(V) aminotriphenolate (TPA) complex **11** as stereodynamic probe for chirality sensing (Scheme 5).^[53] Like the

previous example, also TPA ligands exhibit the distinctive propeller-like conformation around the metal centre, consequently this complex assumes a C_3 -symmetric bipyramidal trigonal geometry. At room temperature, this arrangement undergoes a dynamic equilibrium between the two helical conformers, generating a racemic mixture of them, hence no CD signal will be detected.



Scheme 5. Top: rapid equilibrium existing between the two enantiomeric forms of stereodynamic sensor **11**. Bottom: schematic representation of the two propeller-like conformations of TPA ligand seen from the nitrogen atom along the nitrogen-vanadium axis.

Furthermore, this probe is decorated with a bulky *tert*-butyl group on the upper part of the phenol rings with the intents of avoiding formation of metal aggregates and enhancing the energy differentiation of the complex diastereomers upon binding of chiral analytes, and with a nitro group in *para*-position to the phenol oxygen in order to generate a strong chromophore and to increment the electrophilicity of the vanadium centre. Indeed, chiroptical sensor **11** was analysed by UV-vis spectroscopy in dry CHCl_3 , showing two strong absorption bands at 308 nm and 450 nm. These electronic transitions are associated to ligand-to-metal charge transfer (LMCT) from the oxygen on the phenolate ring to the empty d orbitals located on the vanadium(V) centre. In addition to that, when **11** is in the presence of Lewis bases (not necessarily chiral) or it is dissolved in typical coordinating solvents (*e.g.* THF, Et_2O *etc.*), both absorption bands red-shift. The band found at 450 nm is the most important one, because it displays a shift up to 600 nm, which is associated to an intense colour variation of the solution from orange to deep blue (Figure 16).

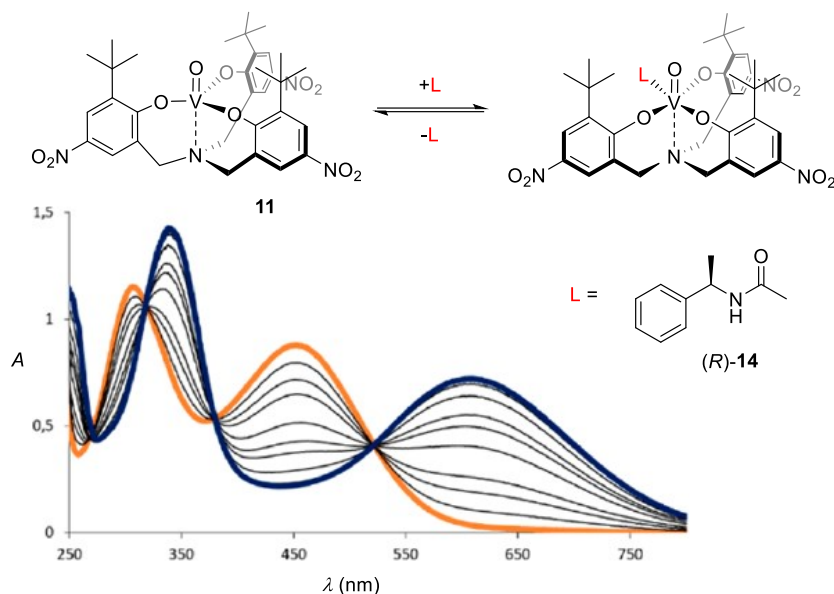
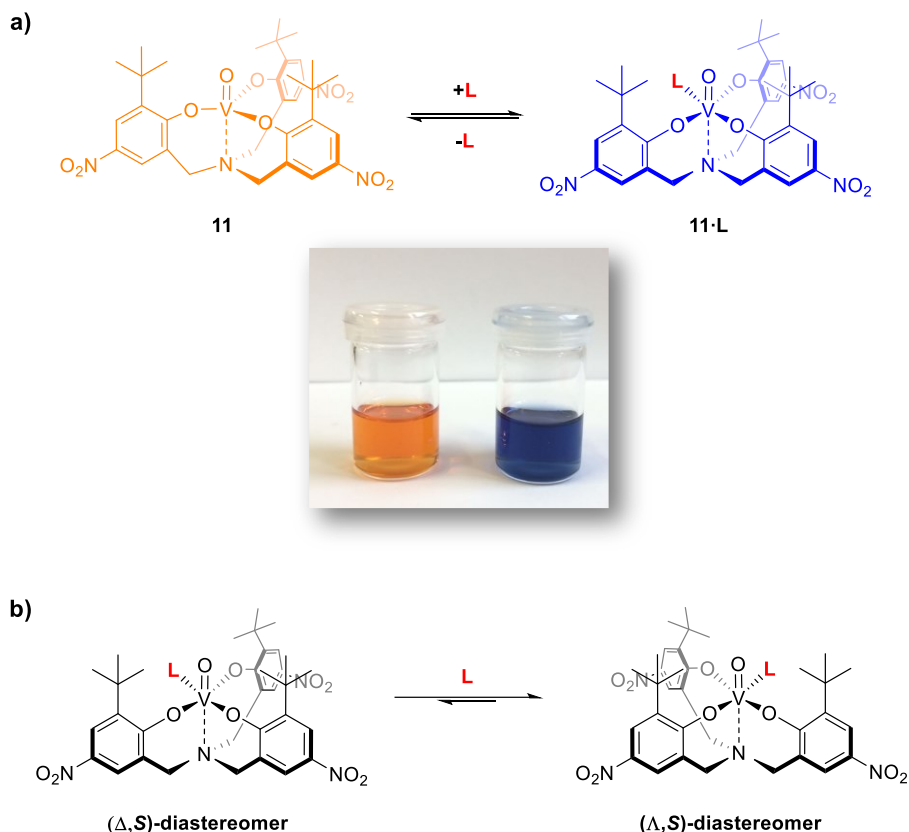


Figure 16. UV-vis titration of a solution of **11** with (*R*)-*N*-(1-phenylethyl)acetamide (*R*)-**14** (5.0×10^{-5} M of **11** in dry CHCl_3). The spectrum of pure **11** (orange line) and the one in the presence of 20 eq of (*R*)-**14** (deep blue line) are highlighted. Adapted from ref. [53].

Using NMR and crystallographic analysis, observations of the tendency of this complex to coordinate an additional monodentate ligand were collected, and the consequent shift toward an octahedral geometry was verified. The crystallographic structure of the adduct between complex **11** and amide (*S*)-**14** confirmed the twisted propeller-like arrangement of the TPA ligand in *M* (Λ) conformation when (*S*)-**14** coordinates to the vanadium atom (Figure 20). In solution, both conformations of stereodynamic metal complex **11** are present simultaneously, specifically Λ -conformer and Δ -conformer, which are enantiomers. These two rapidly interconvert through an equilibrium (Scheme 5). Nonetheless, it is logical to think that the interaction with a chiral analyte leads the complex to adopt a preferential helical conformation. This is due to the perturbation of the chiral environment of **11** by the chirality of the substrate, thus a diastereomeric interaction arises from this molecular recognition process. The preference for a helical conformation rather than the other depends on the difference of thermodynamic stability of the two diastereomers, but it is fundamental that both diastereomers are found in solution, only in different amount (e.g. 45:55 preference for one of the two conformations possible). The various amides do not modify the structure of **11**, or at least they do it slightly. What they really change is the energy difference between the two diastereomers generated, hence the relative population of the two, and eventually the intensity of the CD signal. In the end, the purpose of the chiroptical sensor is to differentiate the amide enantiomers or, in other words, to weight

them. In this particular example, since the preference of (*S*)-**14** in regard to the *M* (Δ) conformation in the solid state, in solution (Δ,S)-diastereomer is found in higher amount than (Δ,S)-diastereomer (Scheme 6b).



Scheme 6. a) Colour change of the species involved in the equilibrium between the free and complexed form of stereodynamic probe **11** with a generic donor ligand **L**. b) Equilibrium in solution of the two diastereomers generated after molecular recognition of (*S*)-**14** (*L* = ligand) by sensor **11**. Here the equilibrium is not 50:50 anymore.

The stereodynamic complex was tested with an extremely wide range of classes of chiral analytes, obtaining intense CD signals, with the relation between absolute configuration of the substrate and type of Cotton effect depending on the chemical class of the chiral molecules (Figure 17). Taking into account the previous example by Canary and Anslyn or the Wolf's one in paragraph 1.3.2, both sensors have exhibited a good linear relationship between enantiomeric excess and CD output, but a critical requirement is to know the exact composition of the sample, hence the concentration of the probe and the chiral analyte. Nonetheless, a huge and innovative advantage brought to attention by this stereodynamic probe is the possibility to conduct concentration-independent CD measurements, meaning that enantiomeric excess determination can be conducted without knowing the exact concentration of the various species in solution. Indeed, prior to this work, applications of the anisotropic

g-factor for the quantification of enantiomeric excess had never been reported. The main reason was the complexity to define a wavelength region where only the chiroptically active diastereomeric adduct between the chiroptical sensor and the chiral analyte would absorb.

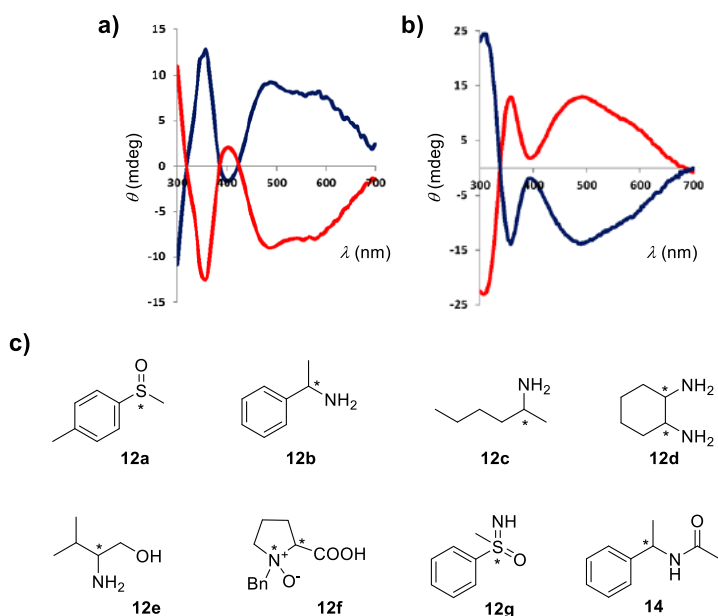


Figure 17. a) CD spectrum of sensor **11** (10^{-4} M) in the presence of **12a** (2×10^{-4} M in CHCl_3) (R)-enantiomer (red) and (S)-enantiomer (blue). b) CD spectrum of sensor **11** (10^{-4} M) in the presence of **12g** (2×10^{-3} M in CHCl_3) (R)-enantiomer (red) and (S)-enantiomer (blue). c) Structures of selected substrates tested. [a] and b) are adapted from ref. [53].

However, in the context of stereodynamic vanadium complex **11**, only the octahedral species absorbs in the spectral region above 600 nm (Figure 16). This was a major discovery, because the CD signal recorded in this region for a sample of **11** in the presence of a chiral substrate is directly related to the enantiomeric excess of the analyte through the *g*-factor. Moreover, this peculiar feature allows to avoid the complete conversion of sensor **11** to the octahedral adduct, hence sparing analyte that may be expensive or available in contained amount. This is true as long as there are no other Lewis bases in solution. To quest this purpose, *g*-factor spectra were collected and analysed (Figure 18a). Following these observations, either the concentration of the sensor or of the chiral substrate were varied, keeping the enantiomeric excess of the latter constant, in order to verify whether the probe was truly concentration-independent or not. The results obtained were highly consistent with the hypothesis, and an exquisite linear correlation between *g*-factor and enantiomeric excess was built (Figure 18b), upholding the use of this stereodynamic vanadium

complex in HTA for the assignment of absolute configuration and to quantify enantiomeric excess of a wide range of chiral substrates.

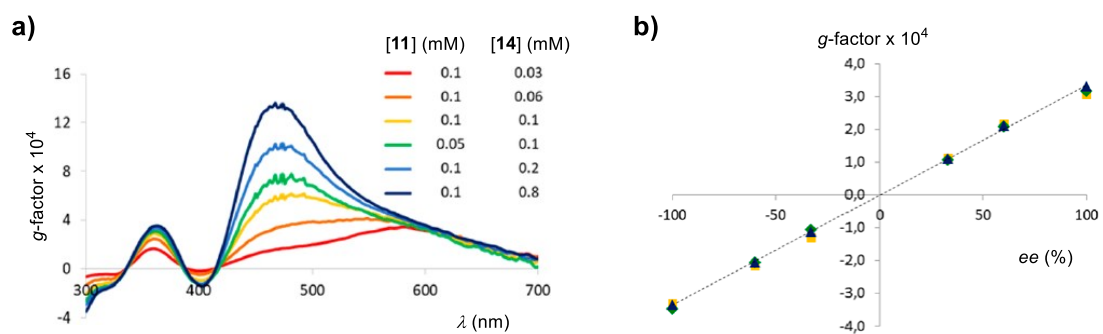


Figure 18. a) *g*-factor spectra of six samples containing **II** and (R)-**14** in different concentrations. b) Calibration curve of *g*-factor values in the range 590-620 nm against the enantiomeric excess of (R)-**14**. Adapted from ref. [53].

2. AIM OF THE THESIS

As reported in the introduction, a large interest in the chemical community has been dedicated to the possibility to implement chiral high-throughput analysis routines in synthetic related fields. Within this context, chiroptical spectroscopies have received a significant attention as a consequence of their intrinsic properties. However, a huge drawback of chiroptical spectroscopies is the impossibility to build a calibration curve in the absence of enantiopure analytes, or at least in the presence of samples of known enantiomeric excess.

In the research group where this thesis has been carried out, it was recently disclosed the application of an oxo-vanadium(V) aminotriphenolate (TPA) complex **11** as stereodynamic probe for chirality sensing which exhibits an activity on a widespread ensemble of different organic compounds.^[53]

The aim of this thesis is to investigate the existence of a multivariate model capable of predicting the electronic circular dichroism readout of different chiral amides using stereodynamic probe **11**. The long-term ambition is to prepare a model able to predict chiroptical output of chiral amides for which enantiopure samples are not available. More in detail, the three main objectives of this work are *i*) the design and synthesis of a class of structurally-related chiral amides, *ii*) the measurement of their chiroptical activity in the presence of stereodynamic probe **11** and *iii*) the multivariate regression of the obtained chiroptical readouts for the elaboration of a model able to describe the experimental results.

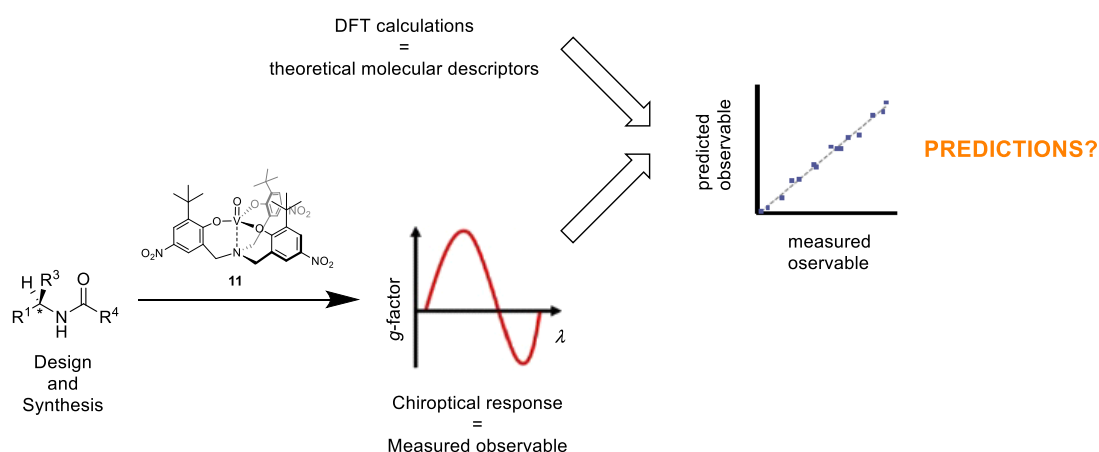


Figure 19. Schematic representation of the methodological approach applied of this thesis.

3. RESULTS AND DISCUSSION

As stated before, this thesis aims to investigate the possibility to develop a multivariate model able to predict the CD output of different chiral analytes using stereodynamic metal complex **11** as chiroptical sensor. The development of the model requires: *i*) the design and preparation of a class of structurally related molecular compounds, *ii*) the measurement of their optical activity in the presence of the stereodynamic probe and *iii*) the multivariate regression of the obtained experimental data. To this end, the preparation of a library of chiral substrates to analyse spectroscopically with the probe will be prepared. In particular, amide substrates have been chosen as target compounds due to their high signal and high binding constant ((*S*)-**14**, $K = 5 \times 10^4 \text{ M}^{-1}$).^[53]

3.1. DESIGN AND SYNTHESIS OF THE LIBRARY OF CHIRAL AMIDES

The first part of the thesis has been focused on the design, followed by the synthesis, of chiral amide substrates. Design is necessary to create a library of substrates in which different electronic and steric features can “cover” the chemical space of possible analytes.

To this end, crystallographic data of the adduct obtained between complex **11** and amide (*S*)-**14**, which was crystallized by the group where this thesis has been carried out, has been used as starting information for the design of the different amides (Figure 20).

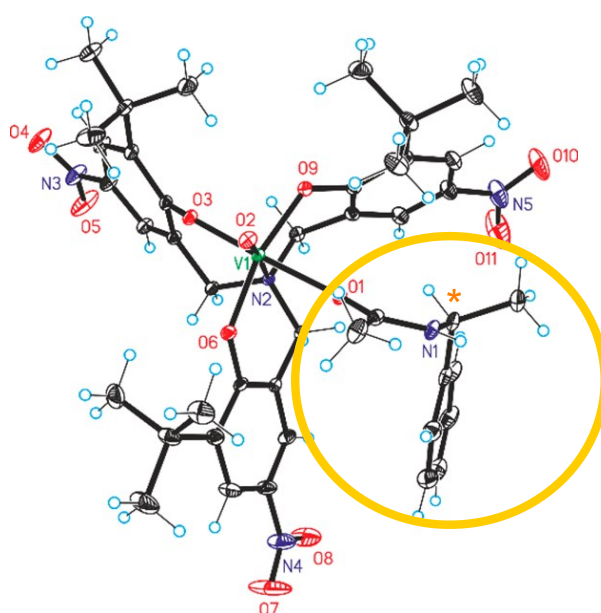


Figure 20. ORTEP representation of the adduct between stereodynamic probe **11** and amide (*S*)-**14** (yellow circle). The yellow asterisk indicates the stereogenic carbon. Adapted from ref. ^[53].

The structure displayed a twisted propeller-like arrangement of the TPA ligand in $M(\Lambda)$ conformation when (*S*)-**14** coordinates to the vanadium centre through the carbonyl oxygen, switching the system geometry from trigonal bipyramidal to octahedral.^[53] As already stated in the introduction to this thesis, both enantiomers of stereodynamic vanadium complex **11** are present simultaneously in solution and are rapidly interconverting. Coordination of a chiral analyte shifts the equilibrium, leading probe **11** to adopt a preferential helical conformation. This diastereomeric imbalance is responsible for the detection of a CD signal of specific intensity and sign. More generally, the interactions arising between chiroptical sensor **11** and the chiral analyte can be seen as a combination of steric and electronic factors. Specifically for the system under examination, the steric hindrance of the phenyl ring in (*S*)-**14** was initially ascribed as the first responsible for the handedness of the TPA ligand around the vanadium centre. Purpose of this thesis is to verify if the substitution structural features of amide substrates can be correlated to the CD experimental readouts. With this considerations, different chiral amides were prepared varying both amine and acid moieties (Figure 21).

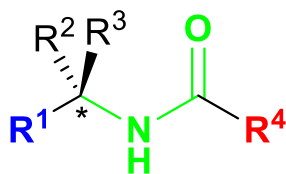


Figure 21. General structure of secondary chiral amides substituted in *N*- α -position. In green is indicated the amide scaffold, which was never modified in the substrates synthesized. R^1 (blue) and R^4 (red) are the two groups varied to study steric and electronic effects. In each compound, $R^2 = H$ or $R^3 = H$, depending on the absolute configuration of the stereogenic centre.

Modifications were primarily conducted on acyl substituent R^4 and on *N*- α -substituent R^1 with the purpose of tuning steric and electronic characteristics of the molecules. To a lesser extent, also R^2 and R^3 substituents were modified, inserting in the compounds steric bulk or ring strain. In Table 1 are collected all of the thirty substrates synthesized (green slots). In particular, the Table is organised to have along the rows compounds with the same enantiopure amine moiety, whereas along the columns are collected the groups R^4 chosen on the acyl moiety.

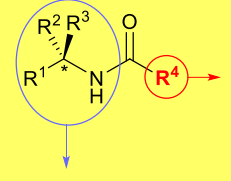
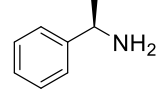
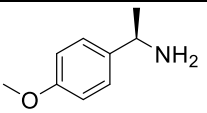
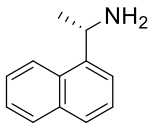
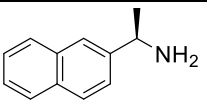
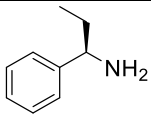
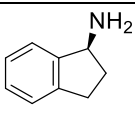
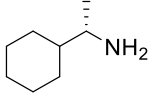
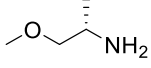
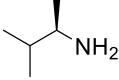
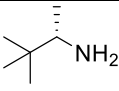
	Me	Et	<i>i</i> -Pr	<i>t</i> -Bu	<i>neo</i> -Pe	Ph	Bn	2-Tp
	(R)-14	(R)-15	(R)-16	(R)-17		(R)-18	(R)-19	
	(R)-21	(R)-22						(R)-23
	(S)-25	(S)-26			(S)-27			(S)-28
	(S)-30		(R)-31			(R)-32		
	(R)-34			(R)-35			(R)-36	
	(S)-38				(S)-39			
	(S)-41		(S)-42		(S)-43		(S)-44	
				(S)-46				
		(R)-48						(R)-49
					(S)-51		(S)-52	

Table 1. Ensemble of enantiopure secondary *N*- α -substituted amides synthesized. Each green slot corresponds to an amide substrate prepared, which is given by coupling reaction between an enantiopure amine (rows) and an acyl chloride (columns). Here are specified just the R^4 substituents (red) and not the entire structures of the acyl chlorides. Legend: Me = methyl, Et = ethyl, *i*-Pr = isopropyl, *t*-Bu = tert-butyl, *neo*-Pe = neopentyl, Ph = phenyl, Bn = benzyl, 2-Tp = 2-thiophenyl.

The distribution of compounds has been planned in order to have a balance between time consumption and the selection able to sample the widest dataset of structures to examine by means of electronic circular dichroism spectroscopy.

In the following, it is given a brief insight into the design of these amides, with a focus on the different structural and electronic aspects considered. Beginning with (*R*)-*N*-(1-phenylethyl)acetamide (*R*)-**14** as first substrate, various amides have been prepared changing the acyl moiety with a propionyl, an isobutyryl, a pivaloyl, a benzoyl, and a 2-phenylacetyl group (Table 1, amides **15-19**). The crystallographic structure (Figure 20) of the adduct between **11** and (*S*)-**14** shows that the methyl substituent in α -position relative to the carbonyl is directed almost in parallel to and in the same sense of the vanadium-oxygen double bond. From this observation, it was hypothesized that an increase of the steric bulk in the acyl moiety would lead to a higher hindrance, therefore to a decrease of the binding affinity and also to the potential subsequent decrease in the differentiation between the two conformations of the propeller-like arrangements of the TPA ligand. This latter statement is due to the fact that a larger acyl moiety would be so bulky that neither the Λ nor the Δ conformation would be preferred to accommodate the analyte molecule. This would lead to a diastereomeric equilibrium with a tendency to equilibrate the concentrations of the two species (the equilibrium would tend to 50:50 preference between the two helical conformations). Ultimately, all of this would be revealed through CD measurements, with an expected drop of the signal incrementing the steric bulk. For these reasons, propionyl, isobutyryl, and pivaloyl have been chosen as R⁴ groups. Benzoyl and 2-phenylacetyl groups have been tested mainly to study electronic aspects, even if they surely contribute in a certain part to steric effects. In particular, it was considered interesting to check the possible interactions arising between the phenyl moiety and the oxo or *t*-butyl groups.

Then, a similar procedure of substituents modification was repeated, this time increasing the electron density of the phenyl group with a methoxy group in *para*-position on the phenyl ring in *N*- α -position (Table 1, amides **21-23**). A thiophenyl substituent was inserted on the acyl moiety, to see if a heteroaromatic system would have led to different properties.

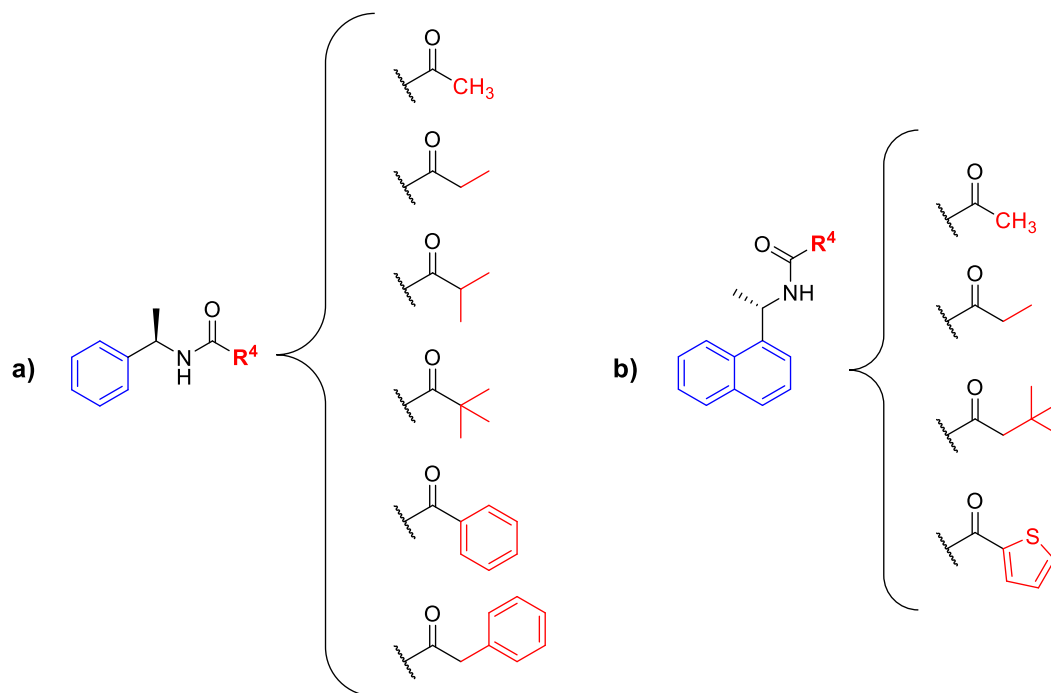


Figure 22. Schematic example showing the modifications in the acyl substituent R^4 in the design process of different enantiopure amides prepared starting from a) (*R*)-1-phenylethylamine (*R*)-**13** and b) (*S*)-1-(1-naphthyl)ethylamine (*S*)-**24**.

Steric effects were investigated also on the side of the amine moiety. For this reason, two constitutional isomers of naphthalene have been employed in *N*- α -position, namely 1-naphthyl and 2-naphthyl substituents (Table 1, amides **25-28**, **30-32**). The modification of the acyl moiety was done using similarly as before, but the 3,3-dimethylbutyryl substituent was also tested. This choice had the purpose to study the aliphatic equivalent of the 2-phenylacetyl group.

Nevertheless, also a modification of electronic effects may be expected. Indeed, the last example described here took into account the substitution of the phenyl ring located in *N*- α -position in (*S*)-**14** with its respective aliphatic substituent, *i.e.* cyclohexyl (Table 1, amides **41-44**). The crystallographic structure of the adduct between **11** and (*S*)-**14** exhibits the phenyl ring of (*S*)-**14** located a bit far but almost in parallel to the phenolate ring of the stereodynamic metal complex (Figure 20). Hence, the purpose of the substitution of the phenyl with a cyclohexyl was to drastically reduce electron density on the substituent by removing pi bonds of the aromatic ring. This was conducted to investigate if electronic effects were important in the overall properties of the host-guest adduct. Then, the acyl moiety was modified again with the same principles already introduced for the previous substrates.

For the different synthesis, as general strategy for the preparation of the compounds, a coupling reaction between an enantiopure α -substituted amine and an activated derivative of a carboxylic acid has been adopted. As a general example, in the synthesis of (*R*)-*N*-(1-phenylethyl)acetamide (*R*)-**14**, the experimental procedure is the reaction between one equivalent of (*R*)- α -phenylethylamine (*R*)-**13** and one equivalent of acetyl chloride in stirred solution at room temperature, obtaining through crystallization the desired product as a white solid with an 80% yield (Scheme 7).



Scheme 7. Base-catalysed coupling reaction for the synthesis of (*R*)-*N*-(1-phenylethyl)acetamide (*R*)-**14**.

The identity and purity of the compound was confirmed by ¹H NMR and ¹³C NMR spectroscopy, and by ESI-MS analysis. The ¹H NMR spectrum (Figure 23) of amide (*R*)-**14** showed the distinctive singlet of the amide proton at 6.77 ppm indicative of the formation of the secondary amide and the signal relative to the proton on the stereogenic carbon centred at 5.03 ppm, which is typically at least one ppm higher than the same proton on the amine reactant. These two are peculiar signals found in the 5.0 - 7.0 ppm region for all thirty chiral secondary *N*- α -substituted amides prepared. The signal around 7.0 ppm related to the five aromatic protons, the singlet at 1.88 ppm is associated to the methyl group in α -position in regard to the carbonyl, and the doublet at 1.40 ppm of the methyl group on the stereogenic carbon.

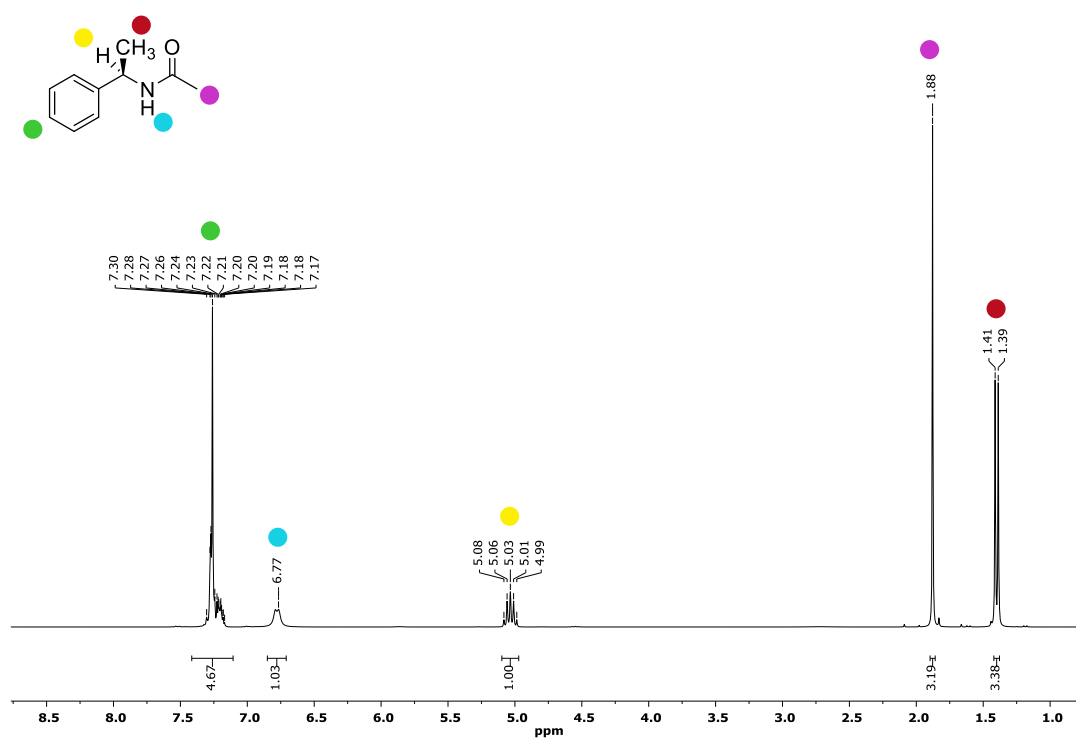


Figure 23. ^1H NMR spectrum (300 MHz, 301 K, CDCl_3) of (R)-N-(1-phenylethyl)acetamide (R)-14.

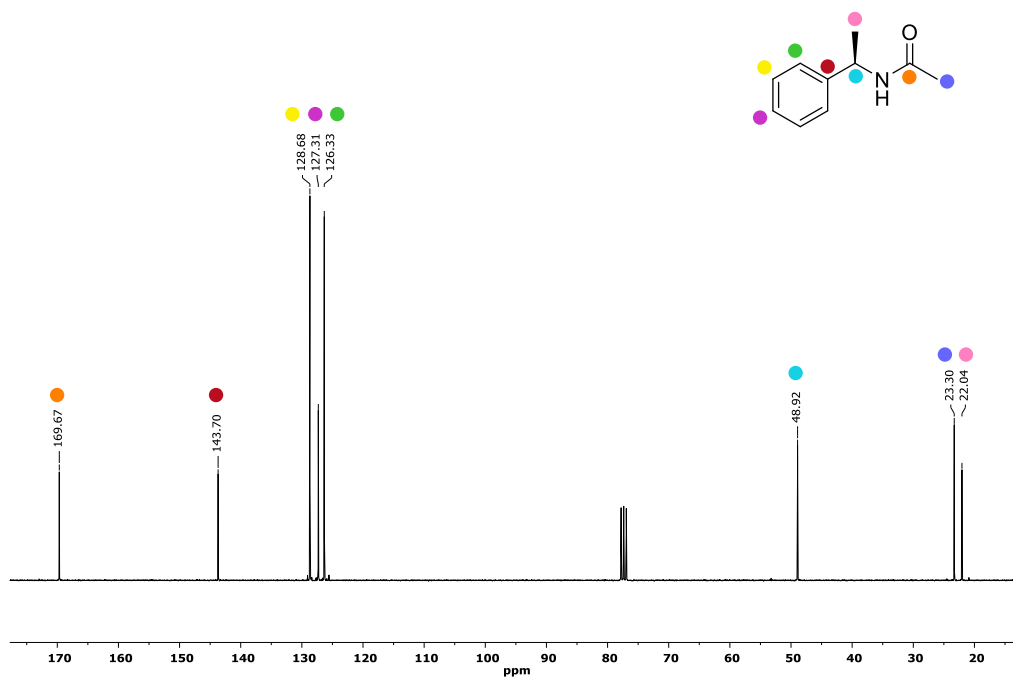
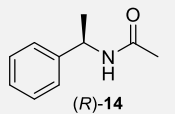
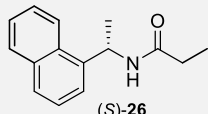
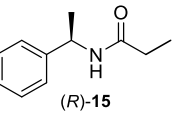
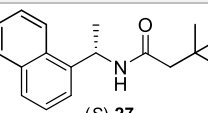
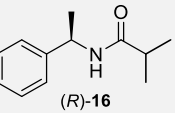
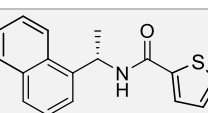
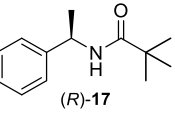
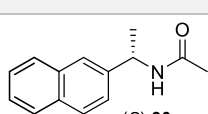
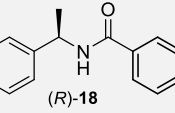
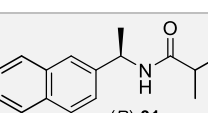
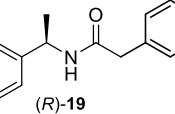
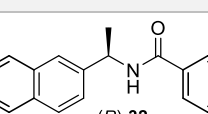
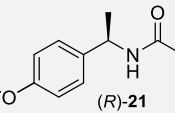
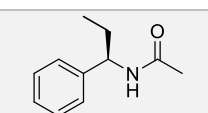
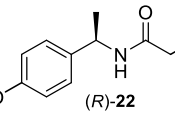
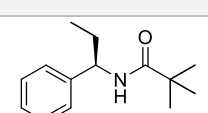
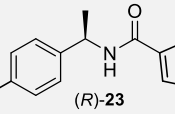
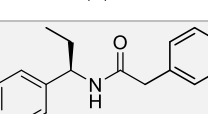
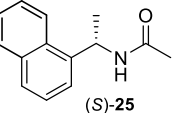
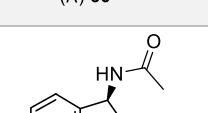


Figure 24. ^{13}C NMR spectrum (75 MHz, 301 K, CDCl_3) spectrum of (R)-N-(1-phenylethyl)acetamide (R)-14.

The ^{13}C NMR spectrum (Figure 24) of amide (*R*)-**14** displayed the exact number of non-equivalent carbon atoms, such as the carbonyl carbon at 169.67 ppm, the aromatic carbons between 120-150 ppm, and the aliphatic carbons under 50 ppm.

Compound (*R*)-**14** had been already synthesized in the previous work. In this thesis it was synthesized again following the same experimental procedure. The characterization data are in agreement with the data reported in literature.

Structure	Conditions Purification	Yield [α] $^{20}_D$	Structure	Conditions Purification	Yield [α] $^{20}_D$
 (<i>R</i>)- 14	A Crystn ^f	80% +135.7	 (<i>S</i>)- 26	B ^c Washing	61% -104.0
 (<i>R</i>)- 15	A Crystn ^f	78% +120.9	 (<i>S</i>)- 27	B ^c Washing	57% -66.2
 (<i>R</i>)- 16	A Crystn ^f	79% +119.8	 (<i>S</i>)- 28	A Crystn ^g	92% +31.6
 (<i>R</i>)- 17	A Crystn ^f	73% +109.5	 (<i>S</i>)- 30	A Crystn ^f	85% -181.2
 (<i>R</i>)- 18	A Crystn ^f	76% +20.4	 (<i>R</i>)- 31	B ^c Washing	65% +172.0
 (<i>R</i>)- 19	A Crystn ^f	70% +3.7	 (<i>R</i>)- 32	B ^c Washing	73% +35.8
 (<i>R</i>)- 21	B Washing	65% +147.2	 (<i>R</i>)- 34	B Washing	72% +130.6
 (<i>R</i>)- 22	B Washing	70% +149.6	 (<i>R</i>)- 35	B ^c Washing	50% +108.8
 (<i>R</i>)- 23	A Crystn ^g	90% +30.8	 (<i>R</i>)- 36	B ^c Washing	52% +11.9
 (<i>S</i>)- 25	B Washing	70% -123.6	 (<i>S</i>)- 38	B ^d Washing	15% -80.0

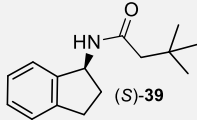
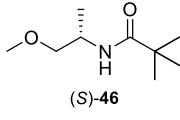
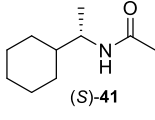
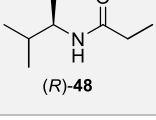
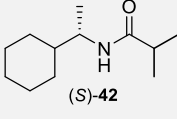
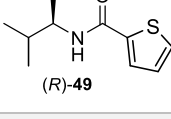
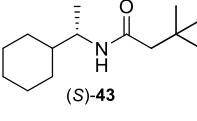
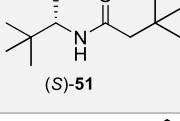
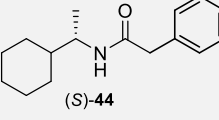
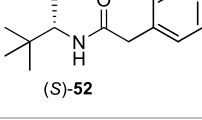
Structure	Conditions Purification	Yield [α] ³⁰ _D	Structure	Conditions Purification	Yield [α] ³⁰ _D
 (S)-39	A ^c Washing	55% -33.5	 (S)-46	A -	91% -20.0
 (S)-41	A Crystn ^g	84% -23.7	 (R)-48	A Crystn ^g	94% -9.7
 (S)-42	A Crystn ^g	88% -18.4	 (R)-49	A Crystn ^g	90% -37.2
 (S)-43	A Crystn ^g	82% -7.6	 (S)-51	A Crystn ^g	96% +16.5
 (S)-44	A Crystn ^g	85% +28.6	 (S)-52	A Crystn ^g	87% +32.1

Table 2. Chiral amides synthesized in this thesis. A) 10 mL of DCM, 6 h. B) 10 mL of THF, 2 h. ^{c)} 2.5 h. ^{d)} 10 mL of toluene. ^{e)} 2 h. Crystn = crystallization ^{f)} from DCM/n-hexane or ^{g)} cooling from solution of boiling n-hexane. Washing = washing three times with Et₂O.

Table 2 gathers all chiral substrates synthesized in this work. ¹H NMR and ¹³C NMR spectra of these amides were in line with the type of features previously seen for the spectra of amide (R)-14. All characterizations to determine identity and enantiopurity of compounds already present in literature were in accordance with reported data.

3.2. ELECTRONIC CIRCULAR DICHROISM ANALYSIS

Following the synthesis of the library of chiral amides, in the second part of the thesis, electronic circular dichroism measurements have been conducted. This analysis was fundamental to collect the experimental observable data used for the development of a multivariate model.

Taking as an example the circular dichroism measurement of (*R*)-*N*-[1-(4-methoxyphenyl)ethyl]acetamide (*R*)-**21** done in this thesis, the preparation of the sample solution started from the preparation of a stock solution of **11** (2.0×10^{-3} M) and a solution of (*R*)-**21** (8.0×10^{-3} M) both in dry CHCl_3 . Solutions were mixed in order to obtain a final ratio 1:20 between **11** and (*R*)-**21**, at a final 10^{-4} M concentration of **11**. After the addition of the chiral amide to the vanadium complex, the distinctive colour change of the solution from orange to deep blue was observed. The CD measurements were performed between 300 and 700 nm and in triplicates. The decision to use 20 equivalents is due to experimental evidences already reported in the previous work for a similar context, where the molecules of **11** were saturated with chiral analyte (*S*)-**14**, whose excess in solution is irrelevant to the measurement since it does not absorb in the wavelength range of interest.^[53] The CD spectrum obtained displays strong Cotton effects in the visible region, particularly between 350 and 600 nm (Figure 25). When the same CD analysis was conducted with either pure sensor **11** or chiral substrate (*R*)-**21**, no dichroic signal was noticed.

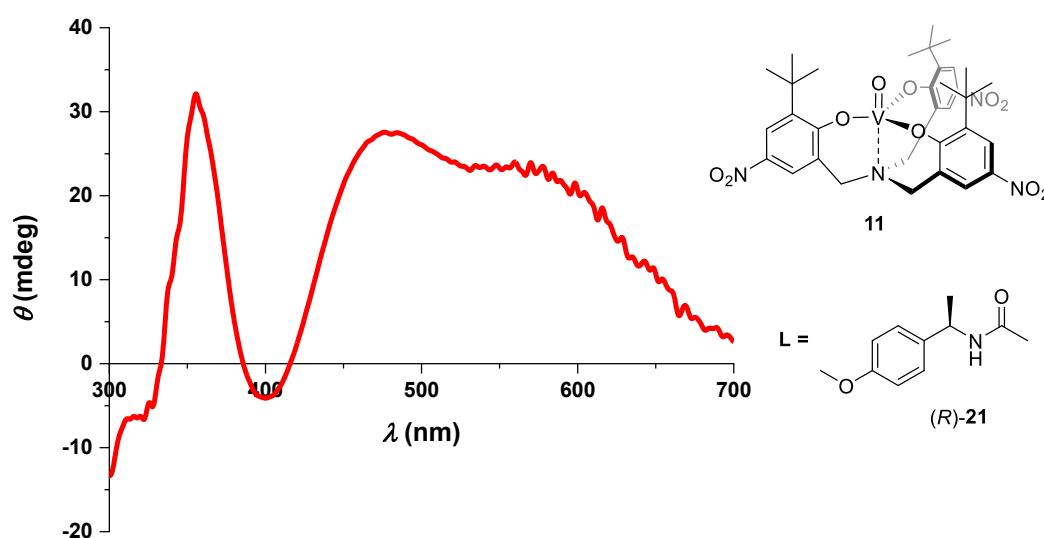


Figure 25. Electronic circular dichroism spectrum ($T = 298.15$ K) recorded within the range 300-700 nm of stereodynamic probe **11** (10^{-4} M) in the presence of the ligand (**L**) (*R*)-*N*-[1-(4-methoxyphenyl)ethyl]acetamide (*R*)-**21** (2×10^{-3} M) in dry CHCl_3 .

Using a CD spectrophotometer with a detector able to measure simultaneously both circular dichroism (*CD*) and the conventional absorbance of non-polarized light (*A*), the anisotropy *g*-factor was readily evaluated (eqn (5)). As elucidated in the introduction to this thesis, the use of this physical quantity allows to carry out experiments without knowing the concentration of the analyte bound to the stereodynamic complex. This is a consequence of the distinctive feature of the oxovanadium TPA complex **11** to red-shift upon coordination of donor species. Specifically, the interest focuses on the octahedral adduct, which is responsible for a strong absorption of the electromagnetic radiation in the wavelength region above 600 nm (Figure 16). As expected, the *g*-factor spectrum obtained for the solution of **11** in the presence of (*R*)-**21** (Figure 26) displays the same sign of the Cotton effects observed in the CD spectrum of the same sample (Figure 25).

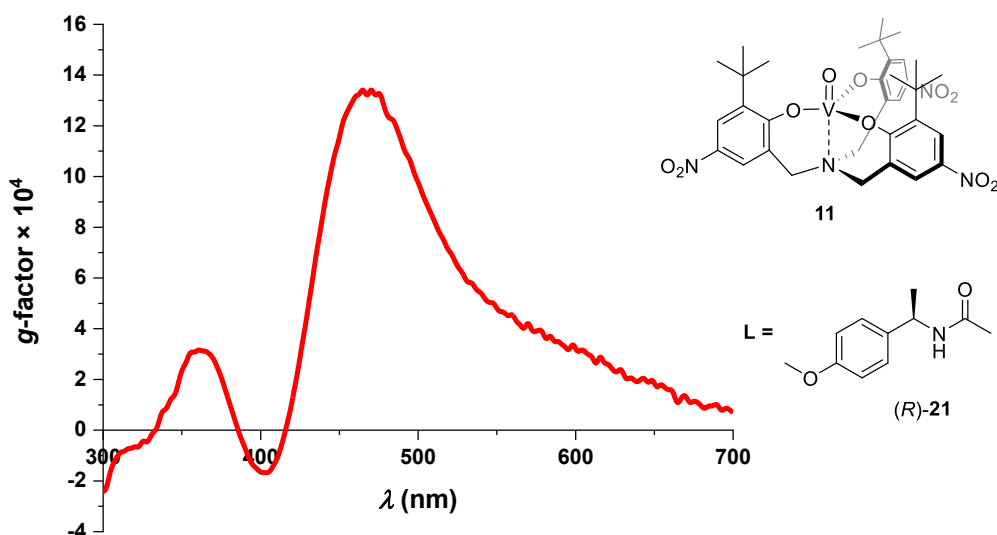


Figure 26. *g*-factor spectrum ($T = 298.15\text{ K}$) recorded within the range 300-700 nm of stereodynamic probe **11** (10^{-4} M) in the presence of the ligand (**L**) (*R*)-*N*-[1-(4-methoxyphenyl)ethyl]acetamide (*R*)-**21** ($2 \times 10^{-3}\text{ M}$) in dry CHCl_3 .

Following this procedure, all thirty enantiopure secondary *N*- α -substituted amides have been tested by means of electronic circular dichroism in the wavelength region between 300 and 700 nm. The different CD spectra obtained were all converted into *g*-factor spectra.

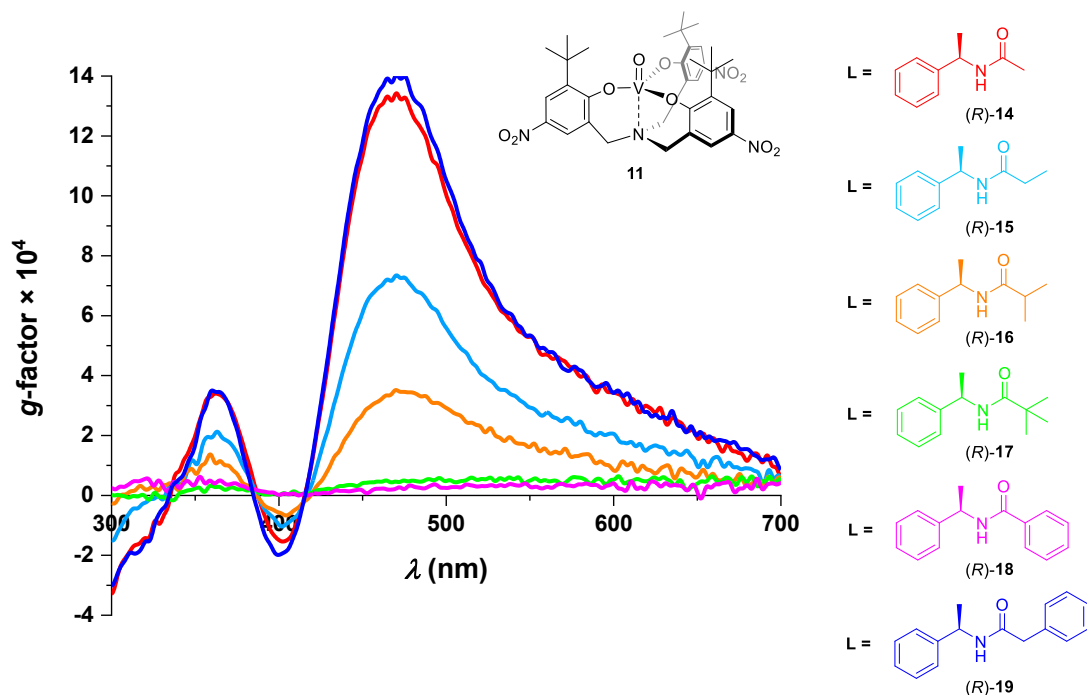


Figure 27. *g*-factor spectra ($T = 298.15$ K) recorded within the range 300–700 nm of stereodynamic probe **11** (1×10^{-4} M) in the presence of different chiral amides **L** (2×10^{-3} M) in dry CHCl_3 : (R)-**14** (red), (R)-**15** (light blue), (R)-**16** (orange), (R)-**17** (green), (R)-**18** (magenta), and (R)-**19** (blue).

Superimposition of structurally related amides **14–19** provided some insight into the differences and similarities between the different adduct formed (Figure 27). Interestingly, the bands at about 360 and 470 nm are located at the same wavelengths even if the substrates structurally change. The second meaningful point is the intensity variation related to the modification of the structure of the analytes. Particularly, in the compound reported in Figure 27, only the acyl part was modified. From acetamide (R)-**14** to pivalamide (R)-**17**, the steric bulk gradually increases and simultaneously the *g*-factor value of the adducts with **11** decreases. Even if it would be expected that the phenyl group on the carbonyl moiety enriches the carbonyl with additional electron density, adduct between **11** and benzamide (R)-**18** exhibits a signal of a comparable magnitude than with pivalamide (R)-**17**. This is quite surprising, but at the same time it might be justified with the steric hindrance that is inserted in the system, in a position so close to the *t*-butyl groups on the upper part of the phenolate rings. Unexpectedly, adduct between **11** and 2-phenylacetamide (R)-**19** showed a signal of intensity essentially equal to the one with acetamide (R)-**14** which own only a methyl group. Since both propionamide (R)-**15** and 2-phenylacetamide (R)-**19** exhibit a methylene group near the carbonyl, the only difference comes from the substituent attached to it, respectively a methyl group and a phenyl group. This might be associated to the

existence of specific interactions between that phenyl substituent and the upper part of complex **11**.

Moving to (*R*)-*N*-[1-(4-methoxyphenyl)ethyl] amides **21-23**, the spectra exhibit trend analogous to the previous case (Figure 28). The *g*-factor spectra of acetamide (*R*)-**14** and acetamide (*R*)-**21**, owning the same structure except for the methoxy group in *para*-position on the phenyl ring, show the same intensity. This suggests that the enhancement of electron density on the aromatic ring does not have a substantial impact on the CD signal.

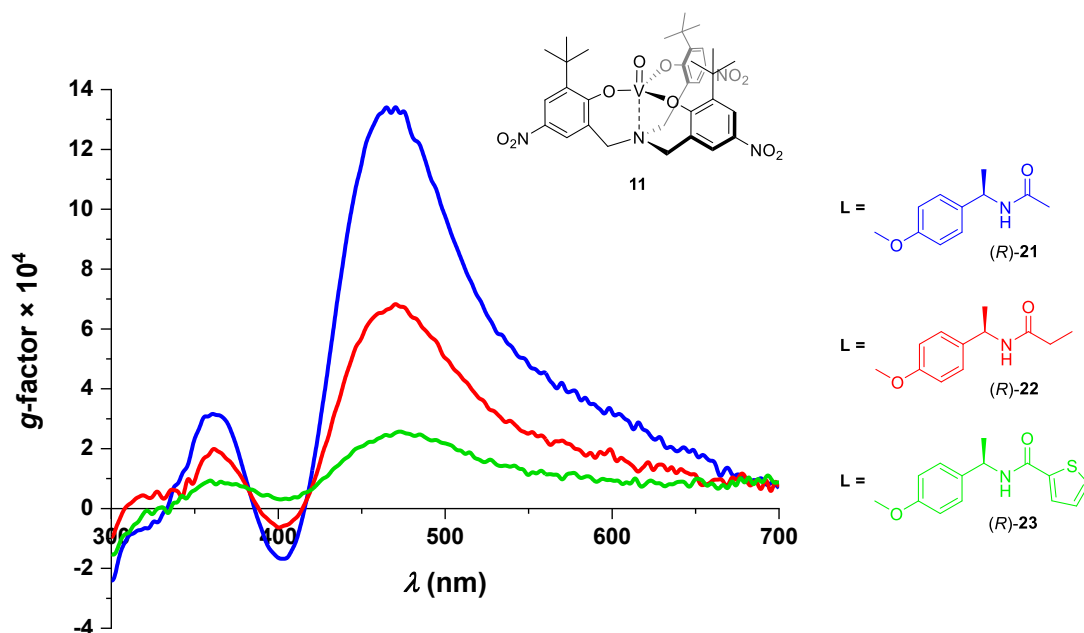


Figure 28. *g*-factor spectra ($T = 298.15$ K) recorded within the range 300-700 nm of stereodynamic probe **11** (1×10^{-4} M) in the presence of different chiral amides **L** (2×10^{-3} M) in dry CHCl₃: (*R*)-**21** (blue), (*R*)-**22** (red), and (*R*)-**23** (green).

The *g*-factor spectra of different adducts between **11** and acetamide (*S*)-**30**, isobutyramide (*R*)-**31**, and benzamide (*R*)-**32**, which are *N*- α -substituted with a 2-naphthyl group, all display similar trends compared to the ones already illustrated (Figure 29). Comparing the chiroptical output of these amides with the structurally related (*R*)-*N*-(1-phenylethyl) **14-19** (Figure 27), an increase of the signal intensity was noticed. This might indicate that the greater steric bulk of the naphthalene substituent may not provoke clash with the same phenolate ring, as it was hypothesised during the design phase. This is somehow supported by the crystallographic structure of the adduct between **11** and acetamide (*S*)-**14** (Figure 20), which shows that the phenyl ring of the amide is pretty much parallel to the phenolate ring.

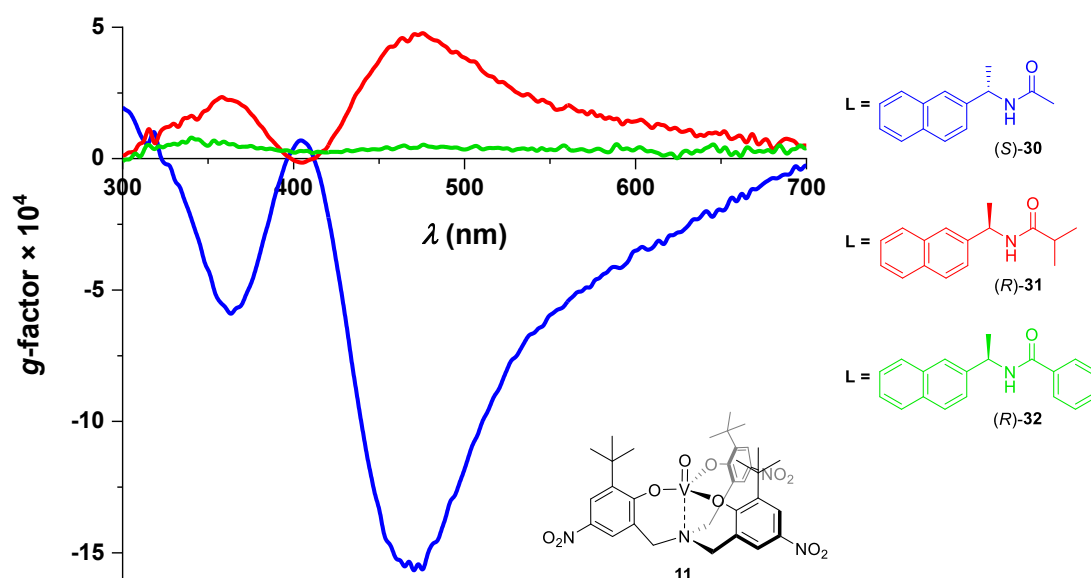


Figure 29. *g*-factor spectra ($T = 298.15$ K) recorded within the range 300–700 nm of stereodynamic probe **11** (1×10^{-4} M) in the presence of different chiral amides **L** (2×10^{-3} M) in dry CHCl_3 : (S)-**30** (blue), (R)-**31** (red), and (R)-**32** (green).

When the aromatic substituent in *N*- α -position was substituted with an aliphatic ring (Figure 30), the dichroic signal experienced a huge drop in intensity. The same was also observed also for a general acyclic aliphatic substituent, modestly or highly branched.

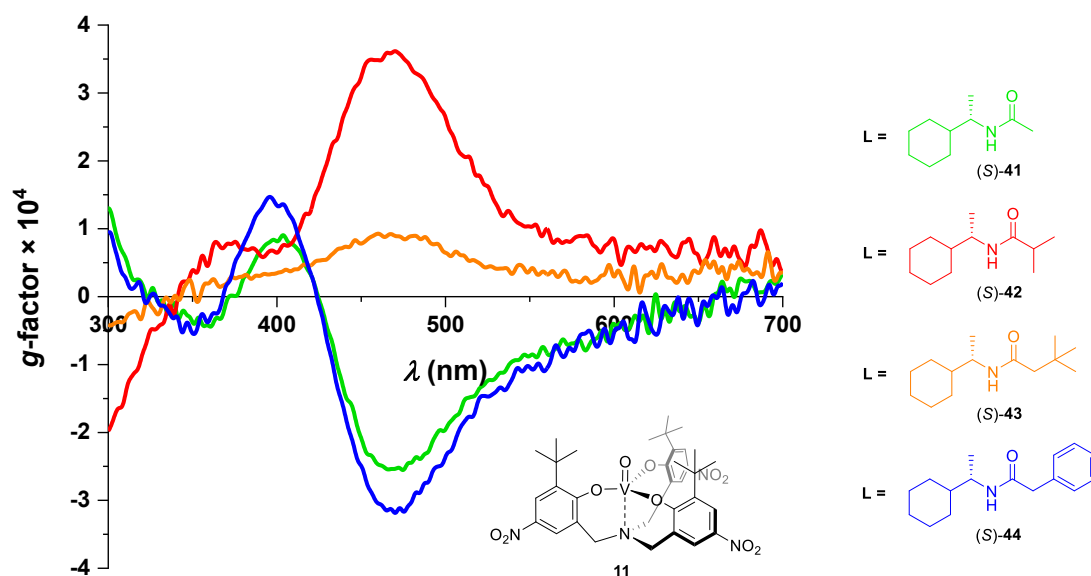


Figure 30. *g*-factor spectra ($T = 298.15$ K) recorded within the range 300–700 nm of stereodynamic probe **11** (1×10^{-4} M) in the presence of different chiral amides **L** (2×10^{-3} M) in dry CHCl_3 : (S)-**41** (green), (S)-**42** (red), (S)-**43** (orange), and (S)-**44** (blue).

Based on the experimental observations extracted from *g*-factor spectra analysed until this point, it was not possible to do hypothesis about the critical features that come into play in this last context. For example, it would have been expected that the adduct

between **11** and isobutyramide (*S*)-**42** exhibited a much lower signal than both acetamide (*S*)-**41** and 2-phenylacetamide (*S*)-**44**. Nevertheless, its signal is even higher than each of the other two amides, and it is also different in sign.

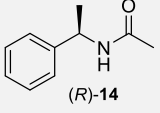
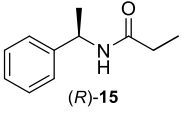
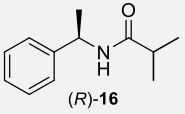
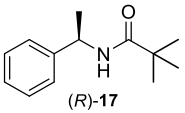
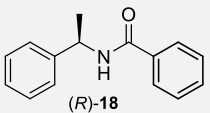
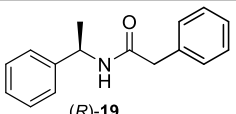
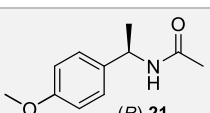
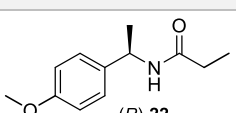
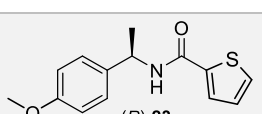
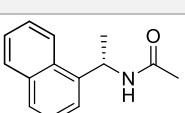
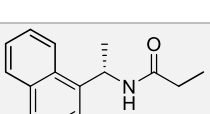
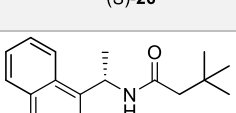
Still, some general aspects were seen pooling similar classes of amides. One example was the sign of the dichroic signal of the adduct between stereodynamic probe **11** and *N*- α -aromatic amides. Indeed, almost the totality of them exhibit a recurring pattern in the sign of the CD signal dependent on the absolute configuration of the stereogenic carbon. In completely general terms, positive CD is associated to *R*-configuration, whereas negative CD is associated to *S*-configuration. Anomalies might be described as dissimilar structures in terms of properties. For example, (*S*)-3,3-dimethyl-*N*-(indan-1-yl)butyramide (*S*)-**39** is an *N*- α -aromatic amide which displays a positive *g*-factor spectra, despite the absolute configuration of the stereogenic centre. However, this molecule is a bit different for example from acetamide (*S*)-**14**, because it presents a condensed five-membered ring between the aromatic ring and the stereogenic carbon: an extra ring strain factor is added, and it may be the discriminating factor in the observed difference.

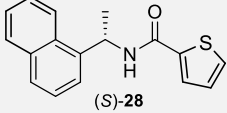
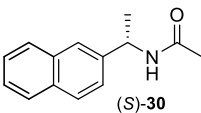
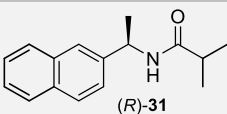
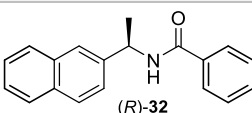
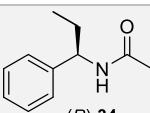
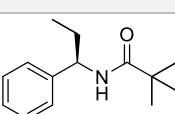
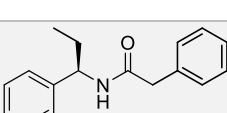
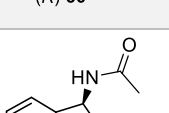
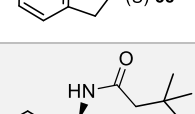
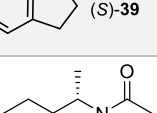
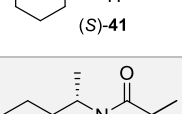
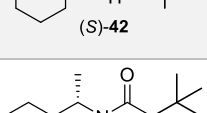
Nonetheless, other general considerations were standing for all the substrates investigated, such as the fact that the electronic effects of substrates in *N*- α -position are crucial to achieve a strong dichroic output, and that highly bulky acyl moieties (*i.e.* pivaloyl, 3,3-dimethylbutyryl, benzoyl, and 2-thiophenecarbonyl) suppress this very signal.

3.3. DEVELOPMENT OF A PREDICTIVE MULTIVARIATE MODEL

The last part of this thesis has been focused on the investigation and development of a multivariate model able to reproduce the observed results reported in the previous paragraph. In particular, the application of a data-driven strategy was performed to obtain a physical-organic description, which should correlate the molecular structure with chiroptical response.^[54] Predictive methods are employed to understand relations between experimental and theoretical parameters, but also to predict relationships existing between structure and activity or properties. They represent somehow an evolution of seminal linear free energy relationships (LFERs, *e.g.* Hammett, Taft *etc.*), which were used to relate a single parameter with the chemical reactivity of the investigated systems. Nonetheless, older LFERs were quite incapable to predict the behaviour of complex systems in which more variables are present. Computational progresses have allowed the rise of novel disciplines, such as chemometrics and chemoinformatics, up to the most modern approaches, like artificial intelligence and machine learning. In particular, a methodological approach developed by Sigman and coworkers was adapted in this thesis, which employs multivariate linear regression (MLR) models for reaction optimization and system interrogation.^[55] This method correlates empirical outputs with calculated molecular descriptors.

The experimental observable chosen in this thesis was the average anisotropic *g*-factor (g^{avg}), defined as the *g*-factor in the spectral region included between 595 and 605 nm. This wavelength region was chosen because it is the first spectral region where the free form of the vanadium complex **11** does not absorb, and at the same time it still allows to obtain a good absorption of circularly polarized light. From *g*-factor spectra of each chiral amide synthesized, g^{avg} values were extracted. g^{avg} values lower than 1×10^{-5} were not considered in the regression due to potential interference by the underlying noise (Table 3). As a result of this restriction, amides (*S*)-**38** and (*R*)-**49** were excluded from the dataset of substrates employed for the subsequent investigation.

Structure	$g^{avg} \times 10^4$
 (R)-14	3.35
 (R)-15	1.90
 (R)-16	1.04
 (R)-17	0.44
 (R)-18	0.30
 (R)-19	3.38
 (R)-21	3.14
 (R)-22	1.64
 (R)-23	0.93
 (S)-25	-4.58
 (S)-26	-2.23
 (S)-27	0.16

Structure	$g^{avg} \times 10^4$
 (S)-28	-0.70
 (S)-30	-3.71
 (R)-31	1.43
 (R)-32	0.34
 (R)-34	3.89
 (R)-35	0.21
 (R)-36	4.06
 (S)-38	< 0.10
 (S)-39	0.26
 (S)-41	-0.50
 (S)-42	0.75
 (S)-43	0.32

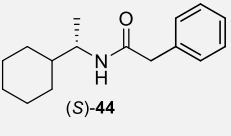
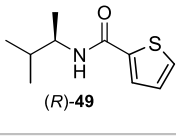
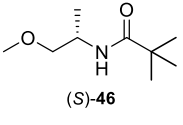
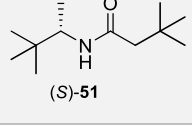
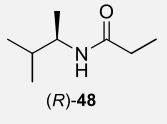
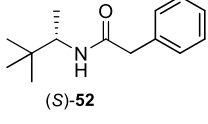
Structure	$g^{avg} \times 10^4$	Structure	$g^{avg} \times 10^4$
 (S)-44	-0.56	 (R)-49	< 0.10
 (S)-46	0.30	 (S)-51	0.23
 (R)-48	-0.63	 (S)-52	0.42

Table 3. g^{avg} values extracted from the g -factor spectra of each chiral secondary N - α -substituted amide investigated in this thesis. In red are highlighted the substrates displaying a value of g^{avg} lower than 1×10^{-5} (cutoff).

The computationally based methodological approach adopted to achieve the last aim of the thesis was divided in five main phases (Figure 31). At the beginning, a library of conformers was created by conducting a conformational analysis on each one of the synthesized amides. This was followed by DFT calculations on each conformer in order to optimize its geometry and to calculate the vibrational frequencies. At this stage, a comparison was made among the outputs and only structures displaying ΔE within $3 \text{ kcal}\cdot\text{mol}^{-1}$ from the most stable one were kept for the model development. This energy value was a cutoff in order to consider only the relevant structures in the subsequent weighting procedure. On the remaining structures, molecular descriptors, which will be described more in detail in the following paragraph, were extrapolated and weighted according to a Boltzmann distribution (eqn (6) and (7)):

$$descriptor_{weighted}^a = \sum_{i=1}^n c_i \cdot descriptor_i^a \quad (6)$$

$$c_i = \frac{e^{-\frac{\Delta E_i}{RT}}}{\sum_{j=1}^n e^{-\frac{\Delta E_j}{RT}}} \quad (7)$$

where c_i is the coefficient multiplying the molecular descriptor a (e.g. descriptor $a = E_{HOMO}$) of the i -th conformer ($i = 1, 2, 3, \dots, n$), n is the number of retained conformers of the considered substrate, R is the universal gas constant, and T is the

temperature set at 298.15 K. At the end, the use of multivariate regression analysis to elaborate a model able to describe the experimental results was performed.

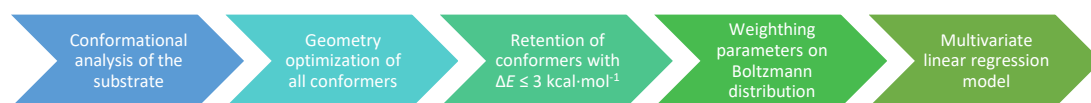


Figure 31. Schematic representation of the adopted protocol to obtain the final correlation for the description of the behaviour of stereodynamic sensor **II** towards chiral secondary *N*- α -substituted amides.

The conformational research was conducted through calculations with PM6 semiempirical method using Spartan '14 1.1.0 software, setting up 10^3 cycles (command: *GEOMETRYCYCLES=1000*) between all the possible candidates. For each substrate, a different number of conformers was obtained, ranging from 5 to 86 depending on the molecular complexity (Table 4). DFT calculations M06-2X/Def2TZVP were subsequently carried out using Gaussian 16 software^[56] over all conformers found. These calculations were conducted alongside analysis of natural bond orbital (NBO)^[57], in order to produce a large variety of molecular descriptors. Among the overall number of conformers, the ones within 3 kcal·mol⁻¹ from the most stable conformer were kept (Table 4). In the case of conformers converging to the same structure, only one structure was considered in the Boltzmann distribution.

Amide	n° conformers (total)	n° conformers (kept)
(<i>R</i>)-14	5	3
(<i>R</i>)-15	14	7
(<i>R</i>)-16	14	6
(<i>R</i>)-17	6	3
(<i>R</i>)-18	6	3
(<i>R</i>)-19	11	5
(<i>R</i>)-21	10	6
(<i>R</i>)-22	29	13
(<i>R</i>)-23	24	10
(<i>S</i>)-25	9	3
(<i>S</i>)-26	25	5
(<i>S</i>)-27	24	3
(<i>S</i>)-28	19	4
(<i>S</i>)-30	10	7
(<i>R</i>)-31	29	10
(<i>R</i>)-32	12	5
(<i>R</i>)-34	14	8
(<i>R</i>)-35	12	5
(<i>R</i>)-36	32	14
(<i>S</i>)-38	4	3
(<i>S</i>)-39	14	4
(<i>S</i>)-41	27	9
(<i>S</i>)-42	86	13
(<i>S</i>)-43	80	11
(<i>S</i>)-44	55	13
(<i>S</i>)-46	36	10
(<i>R</i>)-48	34	13
(<i>R</i>)-49	31	12
(<i>S</i>)-51	14	4
(<i>S</i>)-52	10	5

Table 4. Number of conformers obtained from the conformational analysis, along with the number of conformers kept after geometry optimization.

In order to elaborate a model able to describe the obtained experimental results, physically meaningful molecular descriptors relative to the investigated molecules were chosen from the properties determined by those DFT calculations (Table 5). The descriptors used in this thesis were chosen after an investigation of the most often applied in multivariate linear regression analysis reported in the literature.^[58] These computationally derived molecular descriptors are parameters able to cluster molecules based on their steric and electronic features. Steric effects play a relevant role in molecular recognition processes, since the spatial orientation of the interacting partners might be important in the little energy discrimination of the two generated diastereomeric adducts. Indeed, if the substrate is highly bulky in a critical position, the two diastereomers formed with the probe could have practically the same energy, because there could not be a preferred helical conformation of the stereodynamic complex capable to reduce steric hindrance over the other conformation. Specifically, buried volumes^[59] and Sterimol parameters^[60] have been considered useful for the description of the tested substrates. The percent buried volume ($\%V_{\text{bur}}$) is a physical quantity defined as the percent of the volume occupied of a hypothetical sphere of appropriate diameter (d), where that specific atom is positioned at the centre of the sphere (Figure 32a).^[61] Sterimol values are a set of three different parameters associated to each substituent considered, instead of an individual and cumulative value used to represent the entire spatial information of the substituent. In this way, the steric knowledge of a molecular moiety is interpreted in a more comprehensive way. In detail, Sterimol values included in this dissertation are the maximum distance along the bond axis (L), the minimum and the maximum radius perpendicular to the same axis (respectively B_1 and B_5) (Figure 32b). These Sterimol parameters were collected from reported data in literature.^[60]

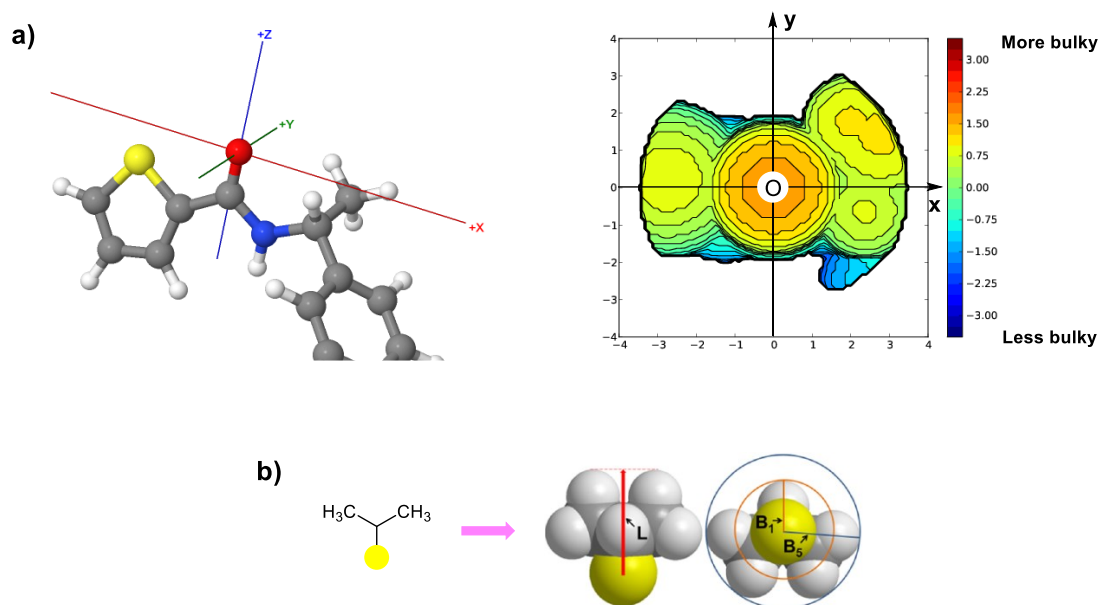


Figure 32. a) Steric map of a conformer of amide (*R*)-**23**. Only a portion of the amide is considered, and it is oriented according to the scheme on the left and the sphere of $d = 3.5 \text{ \AA}$ is centred on the oxygen atom of the carbonyl group; the steric map is reported on the right. b) Representation of the Sterimol parameters for the isopropyl substituent.

Along with steric effects, also electronic effects show a key role in the molecular recognition process, since even remote variations of the electronic property of the substrate may culminate in critical changes in the capability to interact strongly with the stereodynamic sensor. The most significant electronic parameters chosen are IR frequencies, atomic charges, and orbital energies. For the host-guest system investigated in this thesis, it was decided to consider predominantly bonding molecular orbital (from HOMO to HOMO-4) and the LUMO as antibonding molecular orbital. The reason is that the vanadium centre is in electronic configuration d^0 and in high oxidation state (+5), thus it prefers to attract and hold electron density around itself in order to saturate its electron deficiency, therefore it should not be prone to undergo backdonation toward orbitals of the carbonyl moiety. Furthermore, after an initial analysis, also the energy of the two lone pairs of the carbonyl oxygen atom (LP1(O) and LP2(O)) were included in the parameters pool, to verify if it could be relevant for an enhanced donation toward the vanadium centre in the coordination process. These energies of these two lone pairs were available in the DFT calculation output in combination with the NBO analysis. These energies were considered since preliminary calculations showed that HOMO- m ($m = 0, 1, 2, 3, 4$) did not exhibit the same electron density distribution on the carbonyl unit (Figure 33). As an example, the HOMO and the HOMO-1 for amide (*S*)-**26** are distributed mainly on the aromatic ring, whereas

for amide (*S*)-**41** they are also quite present on the carbonyl oxygen atom. This would have caused a bias in the potential participation of one of these orbitals in the correlation, because the same type of orbital would have described a different part of the molecule for different substrates.

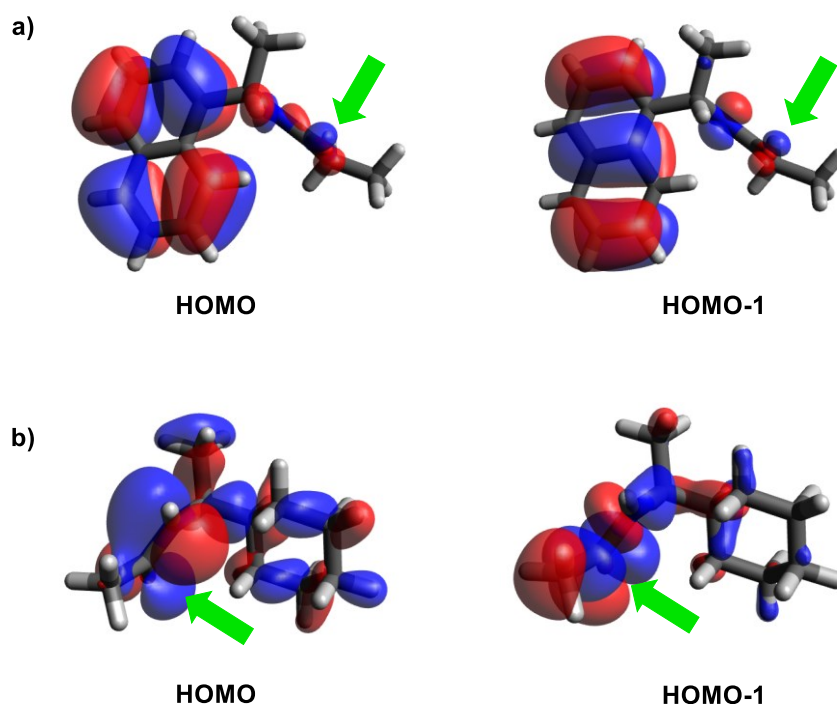


Figure 33. Calculated distribution of HOMO and HOMO-1 in the most stable conformer of amide a) (*S*)-26 and b) (*S*)-41. The green arrows indicate the location of the oxygen atom of the carbonyl group.

An important point to stress is the fact that these several molecular descriptors available in the calculation outputs were carefully chosen, considering mainly the chemical characteristics of the investigated system, thus of the adduct between stereodynamic probe **11** and the secondary *N*- α -substituted amides (Table 5). Only dipole moment and polarizability descriptors were chosen as “filler-parameters”, to test just if they could have been potentially important, but without any chemical reasoning.

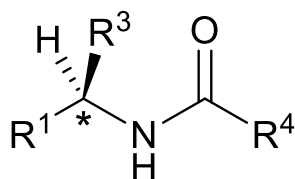


Figure 34. Representative structure of *N*- α -substituted amides indicating the considered substituents. To simplify the modelling, $R^2 = H$ always. To take into account this aspect, the sign of g^{avg} values was inverted accordingly to the inversion of R^2 and R^3 , if it occurred.

CLASS OF PARAMETER	PARAMETER	UNIT OF MEASURE
IR frequencies	ν_{CO}	cm ⁻¹
	ν_{NH}	
Atomic charges	charge O	-
	charge H ^N	
	charge H [*]	
	charge C ^{α-CO}	
	average charge H _{prox} ^{NH}	
	average charge H _{prox} ^{CO}	
Dipole moment	μ	Debye
Polarizability	α	a.u.
Orbital energies	E_{LUMO}	eV
	E_{HOMO}	
	E_{HOMO-1}	
	E_{HOMO-2}	
	E_{HOMO-3}	
	E_{HOMO-4}	
	$E_{LP1(O)}$	
	$E_{LP2(O)}$	
Buried volumes	$\%V_{bur}^O (d = 3.5 \text{ \AA})$	-
	$\%V_{bur}^* (d = 3.5 \text{ \AA})$	
	$\%V_{bur}^{\alpha-CO} (d = 3.5 \text{ \AA})$	
Sterimol parameters	L^{R1}	-
	B_1^{R1}	
	B_5^{R1}	
	L^{R3}	
	B_1^{R3}	
	B_5^{R3}	
	L^{R4}	
	B_1^{R4}	
	B_5^{R4}	

Table 5. Ensemble of computationally-derived molecular descriptors chosen to describe the investigated host-guest system. H^N = amide H; H^{*} = H on the stereogenic carbon; C ^{α -CO} = C in α -position to the carbonyl C; H_{prox}^{NH} = H atoms proximal to N; H_{prox}^{CO} = H atoms proximal to the carbonyl C; $\%V_{bur}^*$ = buried volume centred on the stereogenic C.

Finally, gathering together the experimental observable (g^{avg}) with the computationally derived molecular descriptors, a 28×31 matrix was achieved (28 amides on the rows, 1 empirical + 30 calculated parameters on the columns). Through the application of a MATLAB routine, the realized matrix was employed as dataset in the multivariate regression analysis. In this specific context, this routine sought correlations between the g^{avg} and one or more theoretical molecular descriptors, repeating cycles where these descriptors were continuously and alternatively added or subtracted, with the final goal of reaching the correlation with the best R^2 value. The multivariate model describing the predicted chiroptical readout (Figure 35) was defined by five variables and dependent on four different molecular descriptors (two steric and two electronic), namely the charge on the amide hydrogen atom, the energy of the HOMO-1, the percent buried volume in a sphere of $d = 3.5 \text{ \AA}$ centred on the carbon atom in α -position to the carbonyl group, and the Sterimol parameter L of the large substituent in N - α -position (R^1). The rationalization of the steric descriptor $\%V_{\text{bur}}^{\alpha\text{-CO}}$ is more straightforward and it is coherent with the experimental observation done in paragraph 3.2, which is the importance of the steric bulk of the acyl moiety; whereas, for the steric descriptor L^1 , the situation is not so obvious, and it was not much noticed previously. The comprehension of the two electronic descriptors is instead not straightforward to assign. However, an attempt was made, particularly regarding the energy of the HOMO-1. The introduction of the energy of the lone pairs on the oxygen atom in the molecular descriptors list was done to investigate if the entity of the charge-dipole interaction between the vanadium centre and the carbonyl was significant. Nevertheless, these are not appearing in the formula. Instead, the two electronic parameters appearing are the charge on the amide hydrogen atom, which is not easily ascribable to the recognition phenomena, and the energy of the HOMO-1, which might instead reflect the different distribution in aliphatic and aromatic amides of that orbital (Figure 33). In first approximation, the energy of this orbital can be regarded as the presence of pi stacking between aromatic rings. The determined mathematical relationship is not linear in all terms, since it includes a second-order variable, which mixes electronic and steric effects. Unfortunately, in contrast to first-order parameters, it is usually not possible to interpret second-order ones.

$$g^{\text{avg}} = 0.01 + 0.56\text{chargeH}_N + 0.29E_{\text{HOMO}-1} - 0.85\%V_{\text{bur}}^{\alpha\text{-CO}} + 0.23L^{\text{R1}} + 0.28\text{chargeH}_N \cdot L^{\text{R1}}$$

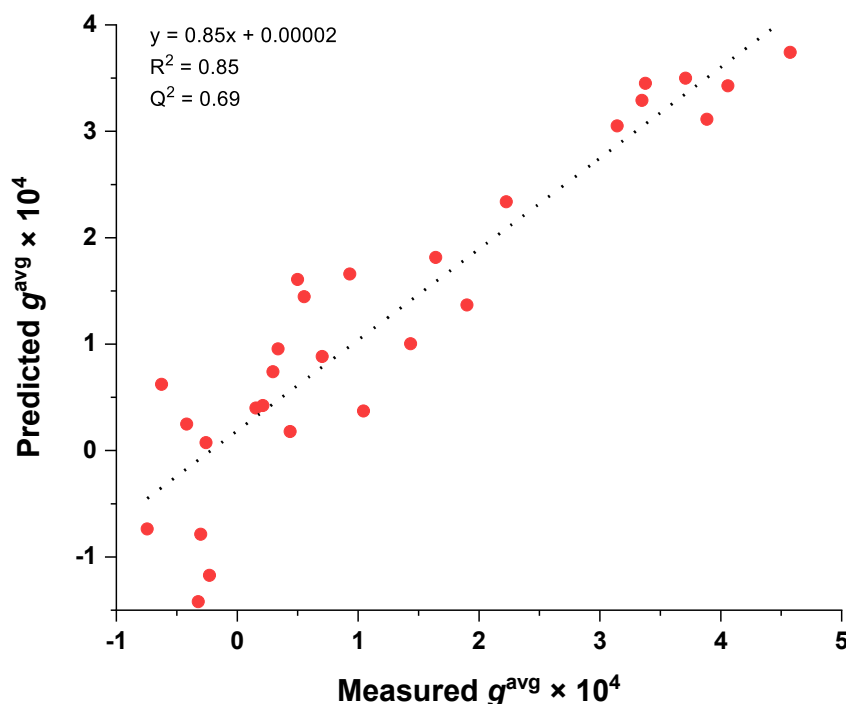


Figure 35. Multivariate model correlating the chiroptical output with the physically meaningful molecular descriptors crucial in the molecular recognition event by stereodynamic sensor **II** of both aliphatic and aromatic *N*- α -substituted amides with $g^{\text{avg}} > 1 \times 10^{-5}$.

This multivariate model exhibits a good correlation with these descriptors ($R^2 = 0.85$). Each red dot in Figure 35 corresponds to a tested amide, and the g^{avg} in the formula is the predicted one. Knowing the structure of a structurally-similar amide, determining computationally the molecular descriptors values displayed in the equation with the same procedure previously illustrated, and substituting them in the equation in Figure 35 leads to obtain the predicted g^{avg} for that specific enantiopure amide. However, this correlation is still far to be implemented for a predictive capability of the chiroptical output. Moreover, a significant drop in the Q^2 ($= 0.69$, as determined by 5-fold cross-validation procedure) when compared to the R^2 was found, which suggests possible overfitting of the data by the model. Therefore, to improve the model, a dataset resizing to a representative sub-class of compounds was attempted, aiming at isolating a fewer number of key interactions with consequent simplification of the recognition pattern. As already showed in paragraph 3.2, experimental evidences from g -factor spectra suggest a quite interesting trend in the dichroic outputs of different amides substituted with an aromatic group in *N*- α -position. Moreover, a very simple linear relationship was noticed already correlating g^{avg} with the percent buried volume in a sphere of $d = 3.5 \text{ \AA}$ centred on the carbon atom in α -position to the carbonyl group (Figure 36).

Interestingly, it was noticed that the two *N*- α -aromatic and phenylacetyl substituted amides (*R*)-**19** and (*R*)-**36** behaves as outliers, because they have a steric bulk on the acyl moiety that should correlate with more or less a half of the chiroptical signal that they actually display. Indeed, taking out those two points, the new linear correlation remarkably improves (from $R^2 = 0.70$ to $R^2 = 0.90$, see black vs. red lines in Figure 36). This suggests that possibly not all of the significant molecular descriptors were taken into account, otherwise these two substrates should be found in proximity to the red line. In particular, it might be necessary to include parameters capable of describing the possible interactions of the benzyl substituent with complex **11**.

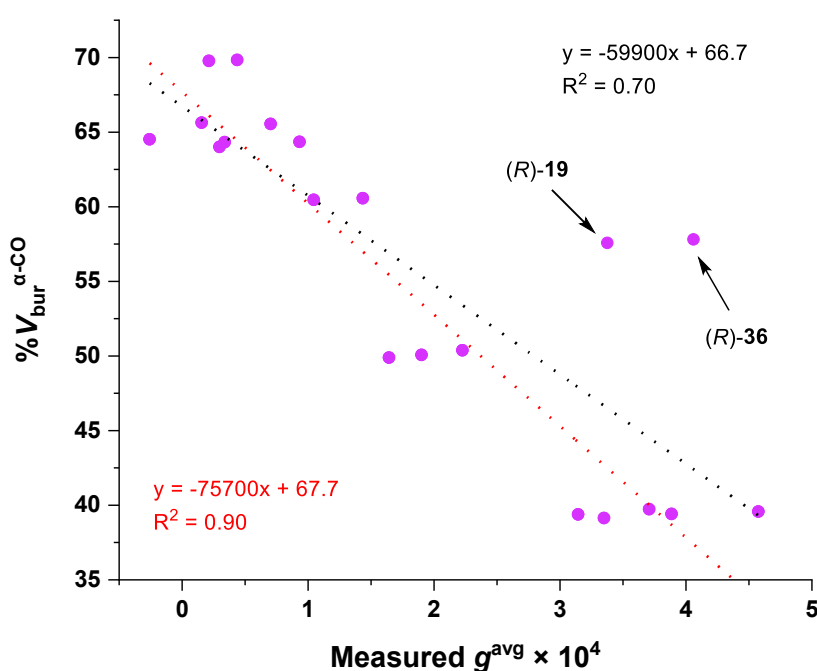


Figure 36. Correlation of % $V_{bur}^{\alpha-CO}$ ($d = 3.5 \text{ \AA}$) of *N*- α -aromatic substituted amides with measured g^{avg} a) considering all points (black dotted line) or b) excluding amides (*R*)-**19** and (*R*)-**36** (red dotted line).

Nevertheless, it was investigated the possibility to generate a multivariate model to relate the twenty *N*- α -aromatics amides with the computationally derived parameters defined previously (Figure 37).

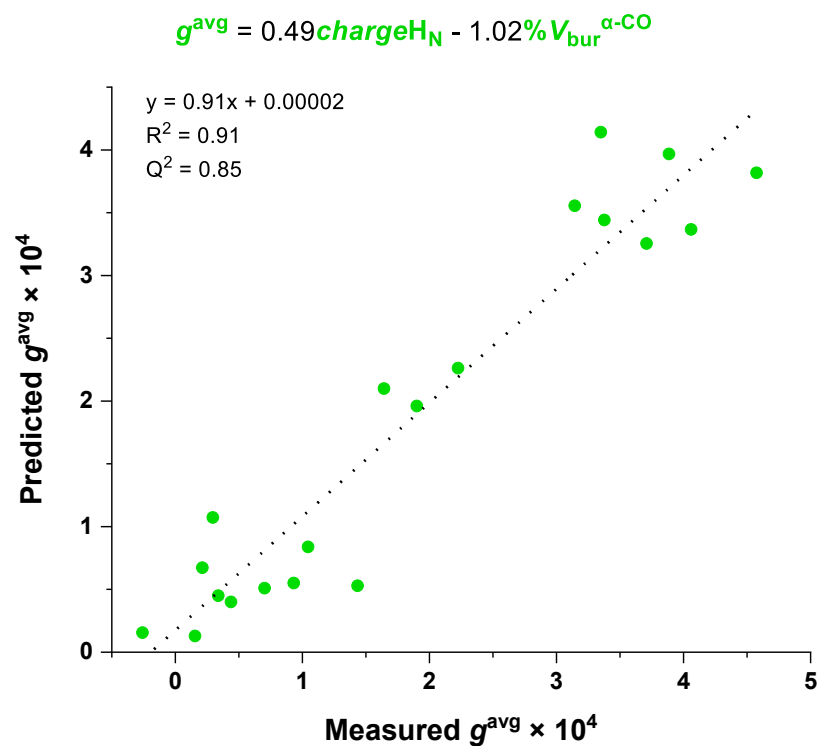


Figure 37. Multivariate model correlating the chiroptical output with the physically meaningful molecular descriptors crucial in the molecular recognition event by stereodynamic sensor **II** of *N*- α -aromatic substituted amides with $g^{\text{avg}} > 1 \times 10^{-5}$.

The multivariate model describing the predicted chiroptical readout was indeed much better than the previous one. Here, the predicted g^{avg} is dependent only on two parameters, one electronic and one steric, which were found and contextualized also in the previous model. Each green dot indicates one *N*- α -aromatic substituted amine.

4. CONCLUSIONS

Aim of this thesis has been to build a multivariate model capable to reproduce and predict the experimental electronic circular dichroism readout of the different chiral amides using supramolecular stereodynamic probe **11**.

To this end a library of thirty chiral amides have been designed and prepared. The design was conducted investigating modifications primarily conducted on the acyl substituent and on the larger *N*- α -substituent, with the goal of tuning steric and electronic characteristics of the molecules. To a lesser extent, also the other two *N*- α -substituents were modified.

In the second part of this thesis, electronic circular dichroism measurements have been carried out on the adduct between stereodynamic vanadium complex **11** and each amide synthesized in the previous part. The chiroptical outputs exhibited interesting features about all these supramolecular adducts, such as the importance of electronic effects of substituents in *N*- α -position and steric effects on the acyl moieties in the achievement of a strong dichroic signal.

The third and last part of this thesis has been focused on the investigation and development of a multivariate model able to reproduce the experimental data obtained in the precedent part of this work. In particular, the method applied was able to correlate the empirical outputs with computationally-derived molecular descriptors. The obtained results are promising, because a good mathematical relationship was found between the g^{avg} experimental data and both steric and electronic properties of the tested substrates. Furthermore, even better results were obtained considering a sub-class of compounds, namely the *N*- α -aromatic substituted amides. Specifically, this multivariate model exhibits a simpler and enhanced correlation between electronic and steric molecular descriptors. However, it was observed that not all substrates are adequately described, such as amides displaying the 2-phenylacetyl moiety, and that other aspects must be examined more deeply, for example including appropriate descriptors for non-covalent interactions. In conclusion, it is not possible to do predictions at this stage, and further investigations will be necessary to conduct, enlarging the library of amides and considering further molecular aspects that may be important in the description of this system, and this methodological approach could be even applied to investigate other classes of organic compounds.

5. EXPERIMENTAL SECTION

5.1. GENERAL METHODS

^1H NMR and ^{13}C NMR spectra were recorded at 301 K on Bruker Avance 300 MHz or Bruker Avance Neo 400 MHz instruments. All the ^1H NMR spectra were referenced to residual isotopic impurity of CDCl_3 (7.26 ppm); the same was done for ^{13}C NMR spectra (77.36 ppm). The following abbreviations are used to report the multiplicity for NMR resonances: s = singlet, d = doublet, t = triplet, q = quartet, p = quintet, hept = septet, and m = multiplet. The NMR data were processed using Bruker Topspin 3.5 pl2 and MestReNova 12.0.2.

ESI-MS spectra have been acquired with an Acquity UPLC H-Class System with Xevo G2-XS QToF (Waters) or an Agilent Technology LC/MSD Trap SL, interfaced to an Agilent 1100 binary pump. The samples were preventively diluted in acetonitrile and then injected via direct infusion with a Hamilton syringe at a rate of 0.05 ml/min. MS peak intensity for each analysis is reported as monoisotopic mass and the data were processed with Data Explorer 4.2 or with MestReNova 12.0.2. The isotopic distribution simulations have been performed through www.envipat.eawag.ch.

ECD spectra were recorded with a Jasco J-1500 spectrometer and processed with Spectra Manager Version 2.15.3.1 or OriginPro 2018 (64-bit) SR1 b9.5.1.195.

Optical rotation values were measured on a Jasco P-1010 polarimeter.

The conformational analysis was carried out with Spartan '14 1.1.0.

The computational searches of the most stable structures and the calculations of vibrational frequencies were carried out with Gaussian 16 package Revision C.01^[56,57] and processed with GaussView 6.0.16^[62] or Avogadro 1.2.0.

Calculations of buried volumes have been performed with SambVca 2.1 through www.molnac.unisa.it/OMtools/sambvca2.1.^[61]

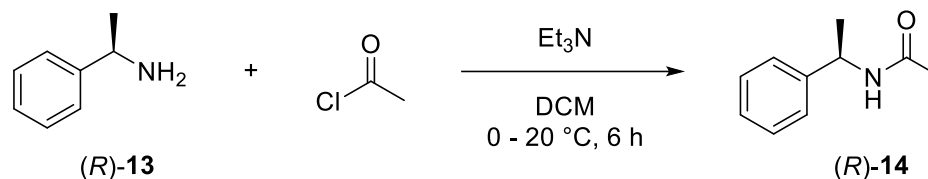
MLR modelling was conducted using Excel 2016 and MATLAB R2023a Update 2.

Chemicals were purchased from Aldrich, FluoroChem, or Alfa Aesar and used without further purification.

5.2.ABBREVIATIONS

ACN	Acetonitrile
DCM	Dichloromethane
Et₂O	Diethyl ether
EtOAc	Ethyl Acetate
THF	Tetrahydrofuran
Tol	Toluene
Et₃N	Triethylamine

5.3. SYNTHESIS OF (*R*)-*N*-(1-PHENYLETHYL)ACETAMIDE (*R*)-14



The synthesis was performed adapting reported procedures.^[63,64] In a 50 mL flask, (*R*)-1-phenylethylamine (*R*)-13 (255 μ L, 2.0 mmol) and Et₃N (420 μ L, 3.0 mmol) were mixed with DCM (10 mL). Under stirring at 0 °C, acetyl chloride (142 μ L, 2.0 mmol) was added dropwise. The colourless solution was left under stirring for 6 hours at room temperature. The mixture was then poured into a saturated solution of aqueous NH₄Cl (25 mL) and extracted with DCM (3 x 50 mL). The combined organic phases were washed with brine solution (50 mL), dried over anhydrous Na₂SO₄, and the solvent was evaporated under reduced pressure. The remaining solid was then precipitated by crystallization: after being dissolved in DCM, *n*-hexane was slowly added. After 24 hours, the white solid was filtered and dried out, yielding the desired product (261 mg, 80%). All characterizations were in agreement with data reported in literature.

¹H NMR (300 MHz, CDCl₃) δ (ppm): 7.30 - 7.17 (m, 5H, ArH), 6.77 (s, 1H, NH), 5.03 (p, *J* = 7.1 Hz, 1H, CH), 1.88 (s, 3H, C(=O)CH₃), 1.40 (d, *J* = 6.9 Hz, 3H, CHCH₃).

¹³C NMR (75 MHz, CDCl₃) δ (ppm): 169.67, 143.70, 128.68, 127.31, 126.33, 48.92, 23.30, 22.04.

ESI-MS (*m/z*): calculated 164.1 [M+H]⁺, found 164.1 [M+H]⁺; calculated 186.1 [M+Na]⁺, found 186.0 [M+Na]⁺.

$[\alpha]^{30}_{\text{D}} = +135.7$ (*c* = 0.121, CHCl₃).

5.4. SYNTHESIS OF (*R*)-*N*-(1-PHENYLETHYL)PROPIONAMIDE (*R*)-15



The synthesis was performed adapting reported procedures.^[63,64] In a 50 mL flask, (*R*)-1-phenylethylamine (*R*)-13 (255 μ L, 2.0 mmol) and Et₃N (420 μ L, 3.0 mmol) were mixed with DCM (10 mL). Under stirring at 0 °C, propionyl chloride (175 μ L, 2.0 mmol) was added dropwise. The colourless solution was left under stirring for 6 hours at room temperature. The mixture was then poured into a saturated solution of aqueous NH₄Cl (25 mL) and extracted with DCM (3 x 50 mL). The combined organic phases were washed with brine solution (50 mL), dried over anhydrous Na₂SO₄, and the solvent was evaporated under reduced pressure. The remaining solid was then precipitated by crystallization: after being dissolved in DCM, *n*-hexane was slowly added. After 24 hours, the white solid was filtered and dried out, yielding the desired product (277 mg, 78%). All characterizations were in agreement with data reported in literature.

¹H NMR (300 MHz, CDCl₃) δ (ppm): 7.27 - 7.16 (m, 5H, ArH), 6.97 (s, 1H, NH), 5.05 (p, $J = 7.2$ Hz, 1H, CH), 2.14 (q, $J = 7.6$ Hz, 2H, CH₂), 1.39 (d, $J = 7.0$ Hz, 3H, CHCH₃), 1.07 (t, $J = 7.6$ Hz, 3H, CH₂CH₃).

¹³C NMR (75 MHz, CDCl₃) δ (ppm): 173.33, 143.89, 128.46, 127.01, 126.14, 48.56, 29.49, 22.01, 9.98.

ESI-MS (m/z): calculated 178.1 [M+H]⁺, found 178.1 [M+H]⁺; calculated 200.1 [M+Na]⁺, found 200.0 [M+Na]⁺.

$[\alpha]^{30}_{\text{D}}$ = +120.9 ($c = 0.238$, CHCl₃).

5.5. SYNTHESIS OF (*R*)-*N*-(1-PHENYLETHYL)ISOBUTYRAMIDE (*R*)-16



The synthesis was performed adapting reported procedures.^[63,64] In a 50 mL flask, (*R*)-1-phenylethylamine (*R*)-13 (255 μ L, 2.0 mmol) and Et₃N (420 μ L, 3.0 mmol) were mixed with DCM (10 mL). Under stirring at 0 °C, isobutyryl chloride (210 μ L, 2.0 mmol) was added dropwise. The colourless solution was left under stirring for 6 hours at room temperature. The mixture was then poured into a saturated solution of aqueous NH₄Cl (25 mL) and extracted with DCM (3 x 50 mL). The combined organic phases were washed with brine solution (50 mL), dried over anhydrous Na₂SO₄, and the solvent was evaporated under reduced pressure. The remaining solid was then precipitated by crystallization: after being dissolved in DCM, *n*-hexane was slowly added. After 24 hours, the white solid was filtered and dried out, yielding the desired product (302 mg, 79%). All characterizations were in agreement with data reported in literature.

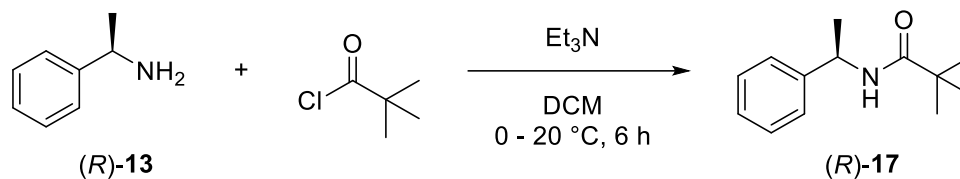
¹H NMR (300 MHz, CDCl₃) δ (ppm): 7.30 - 7.17 (m, 5H, ArH), 6.22 (s, 1H, NH), 5.06 (p, J = 7.1 Hz, 1H, CHNH), 2.33 (hept, J = 6.8 Hz, 1H, C(=O)CH), 1.41 (d, J = 6.9 Hz, 3H, CHCH₃), 1.07 (d, J = 6.9 Hz, 6H, CH(CH₃)₂).

¹³C NMR (75 MHz, CDCl₃) δ (ppm): 176.34, 143.83, 128.73, 127.29, 126.27, 48.52, 35.63, 22.03, 19.75.

ESI-MS (m/z): calculated 192.1 [M+H]⁺, found 192.1 [M+H]⁺; calculated 214.1 [M+Na]⁺, found 214.0 [M+Na]⁺.

$[\alpha]^{30}_{\text{D}}$ = +119.8 (c = 0.345, CHCl₃).

5.6. SYNTHESIS OF (*R*)-*N*-(1-PHENYLETHYL)PIVALAMIDE (*R*)-17



The synthesis was performed adapting reported procedures.^[63,64] In a 50 mL flask, (*R*)-1-phenylethylamine (*R*)-13 (255 μL , 2.0 mmol) and Et_3N (420 μL , 3.0 mmol) were mixed with DCM (10 mL). Under stirring at 0 °C, pivaloyl chloride (246 μL , 2.0 mmol) was added dropwise. The colourless solution was left under stirring for 6 hours at room temperature. The mixture was then poured into a saturated solution of aqueous NH_4Cl (25 mL) and extracted with DCM (3 x 50 mL). The combined organic phases were washed with brine solution (50 mL), dried over anhydrous Na_2SO_4 , and the solvent was evaporated under reduced pressure. The remaining solid was then precipitated by crystallization: after being dissolved in DCM, *n*-hexane was slowly added. After 24 hours, the white solid was filtered and dried out, yielding the desired product (300 mg, 73%). All characterizations were in agreement with data reported in literature.

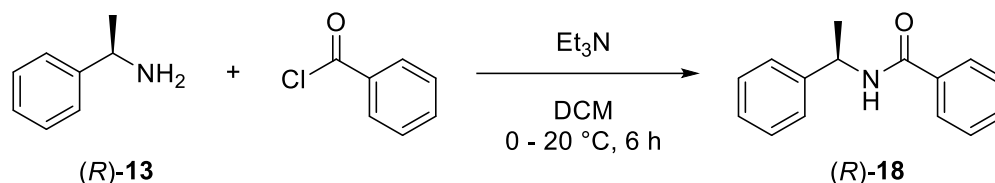
^1H NMR (300 MHz, CDCl_3) δ (ppm): 7.31 - 7.17 (m, 5H, ArH), 5.85 (s, 1H, NH), 5.06 (p, $J = 7.1$ Hz, 1H, CH), 1.42 (d, $J = 6.9$ Hz, 3H, CHCH₃), 1.15 (s, 9H, C(CH₃)₃).

^{13}C NMR (75 MHz, CDCl_3) δ (ppm): 177.67, 143.81, 128.87, 127.42, 126.25, 48.68, 38.80, 27.79, 21.98.

ESI-MS (m/z): calculated 206.2 $[\text{M}+\text{H}]^+$, found 206.1 $[\text{M}+\text{H}]^+$; calculated 228.1 $[\text{M}+\text{Na}]^+$, found 228.1 $[\text{M}+\text{Na}]^+$.

$[\alpha]^{30}_{\text{D}}$ = +109.5 ($c = 0.484$, CHCl_3).

5.7. SYNTHESIS OF (*R*)-*N*-(1-PHENYLETHYL)BENZAMIDE (*R*)-18



The synthesis was performed adapting reported procedures.^[63,64] In a 50 mL flask, (*R*)-1-phenylethylamine (*R*)-13 (255 μ L, 2.0 mmol) and Et₃N (420 μ L, 3.0 mmol) were mixed with DCM (10 mL). Under stirring at 0 °C, benzoyl chloride (232 μ L, 2.0 mmol) was added dropwise. The colourless solution was left under stirring for 6 hours at room temperature. The mixture was then poured into a saturated solution of aqueous NH₄Cl (25 mL) and extracted with DCM (3 x 50 mL). The combined organic phases were washed with brine solution (50 mL), dried over anhydrous Na₂SO₄, and the solvent was evaporated under reduced pressure. The remaining solid was then precipitated by crystallization: after being dissolved in DCM, *n*-hexane was slowly added. After 24 hours, the white solid was filtered and dried out, yielding the desired product (342 mg, 76%). All characterizations were in agreement with data reported in literature.

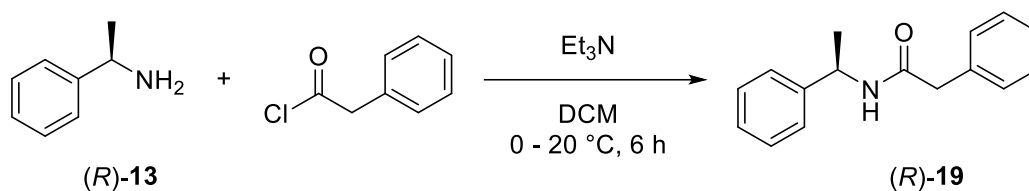
¹H NMR (300 MHz, CDCl₃) δ (ppm): 7.69 - 7.65 (m, 2H, ArH), 7.38 - 7.12 (m, 8H, ArH), 6.61 (s, 1H, NH), 5.21 (p, $J = 7.1$ Hz, 1H, CH), 1.46 (d, $J = 6.9$ Hz, 3H, CH₃).

¹³C NMR (75 MHz, CDCl₃) δ (ppm): 166.92, 143.53, 134.83, 131.63, 128.92, 128.72, 127.59, 127.27, 126.51, 49.45, 21.98.

ESI-MS (m/z): calculated 226.1 [M+H]⁺, found 226.1 [M+H]⁺; calculated 248.1 [M+Na]⁺, found 248.1 [M+Na]⁺.

$[\alpha]^{30}_{\text{D}} = +20.4$ ($c = 0.270$, CHCl₃).

5.8. SYNTHESIS OF (*R*)-2-PHENYL-*N*-(1-PHENYLETHYL)ACETAMIDE (*R*)-19



The synthesis was performed adapting reported procedures.^[63,64] In a 50 mL flask, (*R*)-1-phenylethylamine (*R*)-13 (255 μ L, 2.0 mmol) and Et₃N (420 μ L, 3.0 mmol) were mixed with DCM (10 mL). Under stirring at 0 °C, 2-phenylacetyl chloride (264 μ L, 2.0 mmol) was added dropwise. The colourless solution was left under stirring for 6 hours at room temperature. The mixture was then poured into a saturated solution of aqueous NH₄Cl (25 mL) and extracted with DCM (3 x 50 mL). The combined organic phases were washed with brine solution (50 mL), dried over anhydrous Na₂SO₄, and the solvent was evaporated under reduced pressure. The remaining solid was then precipitated by crystallization: after being dissolved in DCM, *n*-hexane was slowly added. After 24 hours, the white solid was filtered and dried out, yielding the desired product (335 mg, 70%). All characterizations were in agreement with data reported in literature.

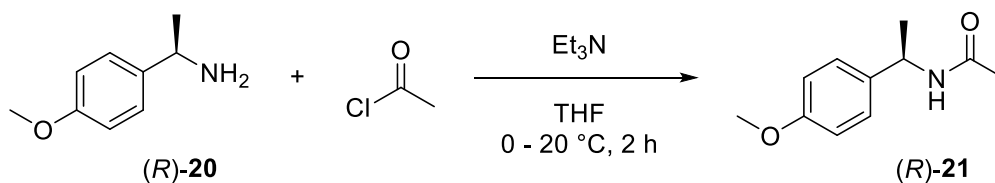
¹H NMR (300 MHz, CDCl₃) δ (ppm): 7.41 - 7.25 (m, 10H, ArH), 6.50 (s, 1H, NH), 5.16 (p, $J = 7.1$ Hz, 1H, CH), 3.55 (s, 2H, CH₂), 1.44 (d, $J = 7.0$ Hz, 3H, CH₃).

¹³C NMR (75 MHz, CDCl₃) δ (ppm): 170.38, 143.49, 135.36, 129.42, 128.95, 128.68, 127.30, 127.24, 126.16, 48.90, 43.68, 22.01.

ESI-MS (m/z): calculated 240.1 [M+H]⁺, found 240.1 [M+H]⁺; calculated 262.1 [M+Na]⁺, found 262.1 [M+Na]⁺.

$[\alpha]^{30}_{\text{D}}$ = +3.7 ($c = 0.367$, CHCl₃).

5.9. SYNTHESIS OF (R)-N-[1-(4-METHOXYPHENYL)ETHYL] ACETAMIDE (R)-21



The synthesis was performed adapting reported procedures.^[63,64] In a 50 mL flask, (R)-1-(4-methoxyphenyl)ethylamine (R)-20 (295 μ L, 2.0 mmol) and Et₃N (420 μ L, 3.0 mmol) were mixed with THF (10 mL). Under stirring at 0 °C, acetyl chloride (142 μ L, 2.0 mmol) was added dropwise. The colourless solution was left under stirring for 2 hours at room temperature. The mixture was then poured into a saturated solution of aqueous NH₄Cl (25 mL) and extracted with EtOAc (3 x 50 mL). The combined organic phases were washed with brine solution (50 mL), dried over anhydrous Na₂SO₄, and the solvent was evaporated under reduced pressure. The remaining solid was washed with Et₂O to remove amine and acid impurities, and then dried out to yield the white solid product (251 mg, 65%). All characterizations were in agreement with data reported in literature.

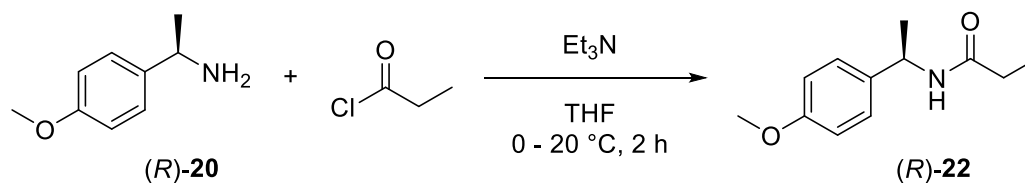
¹H NMR (300 MHz, CDCl₃) δ (ppm): 7.21 (d, J = 8.2 Hz, 2H, ArH), 6.82 (d, J = 8.2 Hz, 2H, ArH), 6.30 (s, 1H, NH), 5.02 (p, J = 7.1 Hz, 1H, CH), 3.75 (s, 3H, OCH₃), 1.91 (s, 3H, C(=O)CH₃), 1.42 (d, J = 6.9 Hz, 3H, CHCH₃).

¹³C NMR (75 MHz, CDCl₃) δ (ppm): 169.45, 158.94, 135.74, 127.61, 114.14, 55.48, 48.37, 23.52, 21.92.

ESI-MS (m/z): calculated 194.1 [M+H]⁺, found 194.0 [M+H]⁺; calculated 216.1 [M+Na]⁺, found 216.0 [M+Na]⁺.

$[\alpha]^{30}_{\text{D}} = +147.2$ ($c = 0.148$, CHCl₃).

5.10. SYNTHESIS OF (R)-N-[1-(4-METHOXYPHENYL)ETHYL] PROPIONAMIDE (R)-22



The synthesis was performed adapting reported procedures.^[63,64] In a 50 mL flask, (R)-1-(4-methoxyphenyl)ethylamine (R)-20 (295 μ L, 2.0 mmol) and Et₃N (420 μ L, 3.0 mmol) were mixed with THF (10 mL). Under stirring at 0 °C, propionyl chloride (175 μ L, 2.0 mmol) was added dropwise. The colourless solution was left under stirring for 2 hours at room temperature. The mixture was then poured into a saturated solution of aqueous NH₄Cl (25 mL) and extracted with EtOAc (3 x 50 mL). The combined organic phases were washed with brine solution (50 mL), dried over anhydrous Na₂SO₄, and the solvent was evaporated under reduced pressure. The remaining solid was washed with Et₂O to remove amine and acid impurities, and then dried out to yield the white solid product (290 mg, 70%).

¹H NMR (300 MHz, CDCl₃) δ (ppm): 7.25 (d, J = 8.3 Hz, 2H, ArH), 6.87 (d, J = 8.3 Hz, 2H, ArH), 5.82 (s, 1H, NH), 5.09 (p, J = 7.1 Hz, 1H, CH), 3.80 (s, 3H, OCH₃), 2.19 (q, J = 7.6 Hz, 2H, CH₂), 1.47 (d, J = 6.9 Hz, 3H, CHCH₃), 1.15 (t, J = 7.6 Hz, 3H, CH₂CH₃).

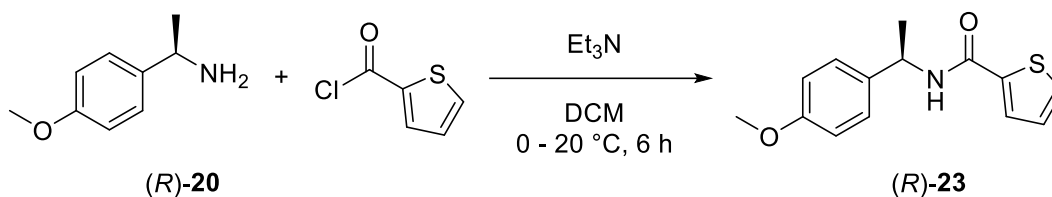
¹³C NMR (75 MHz, CDCl₃) δ (ppm): 173.03, 159.06, 135.80, 127.66, 114.25, 55.57, 48.27, 30.06, 21.94, 10.12.

ESI-MS (m/z): calculated 230.1 [M+Na]⁺, found 230.1215 [M+Na]⁺.

$[\alpha]^{30}_{\text{D}}$ = +149.6 (c = 0.400, CHCl₃).

Elemental analysis: C 69.37%, H 8.41%, N 6.81%, O 15.41%.

5.11. SYNTHESIS OF *N*-[(1*R*)-1-(4-METHOXYPHENYL)ETHYL]THIOPHENE-2-CARBOXAMIDE (*R*)-23



The synthesis was performed adapting reported procedures.^[63,64] In a 50 mL flask, (*R*)-1-(4-methoxyphenyl)ethylamine (*R*)-20 (295 μ L, 2.0 mmol) and Et₃N (420 μ L, 3.0 mmol) were mixed with DCM (10 mL). Under stirring at 0 °C, 2-thiophenecarbonyl chloride (235 μ L, 2.2 mmol) was added dropwise. The colourless solution was left under stirring for 6 hours at room temperature. The mixture was then poured into a saturated solution of aqueous NH₄Cl (25 mL) and extracted with DCM (3 x 50 mL). The combined organic phases were extracted once with a saturated solution of NaHCO₃ (50 mL), then washed with brine solution (50 mL), dried over anhydrous MgSO₄, and the solvent was evaporated under reduced pressure. The remaining solid was solubilized in the minimum amount of boiling *n*-hexane, then slowly cooled down until room temperature. The crystals obtained were filtered, washed with cold *n*-hexane, then dried out, yielding the desired product as a white solid (470 mg, 90%).

¹H NMR (400 MHz, CDCl₃) δ (ppm): 7.46 (ddd, J = 8.0, 4.4, 1.2 Hz, 2H, TpH), 7.33 – 7.30 (m, 2H, ArH), 7.05 (dd, J = 5.0, 3.7 Hz, 1H, TpH), 6.91 – 6.87 (m, 2H, ArH), 6.12 (s, 1H, NH), 5.26 (p, J = 7.1 Hz, 1H, CH), 3.80 (s, 3H, OCH₃), 1.58 (d, J = 6.9 Hz, 3H, CHCH₃).

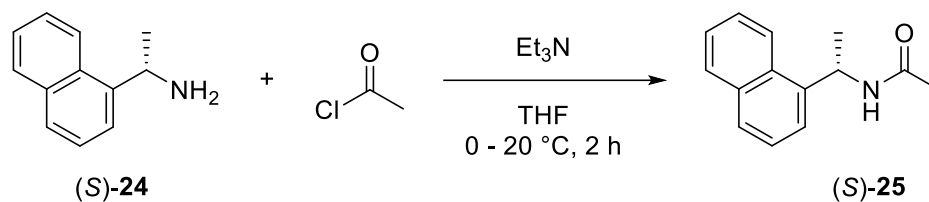
¹³C NMR (100 MHz, CDCl₃) δ (ppm): 161.26, 159.30, 139.43, 135.34, 130.18, 128.27, 127.89, 127.87, 114.42, 55.66, 49.00, 21.85.

ESI-MS (m/z): calculated 284.1 [M+Na]⁺, found 284.0739 [M+Na]⁺.

$[\alpha]^{30D} = +30.8$ ($c = 0.502$, CHCl₃).

Elemental analysis: C 64.40%, H 5.77%, N 5.36%, O 12.15%, S 12.32%.

5.12. SYNTHESIS OF (S)-N-[1-(1-NAPHTHYL)ETHYL]ACETAMIDE (S)-25



The synthesis was performed adapting reported procedures.^[63,64] In a 50 mL flask, (S)-1-(1-naphthyl)ethylamine (S)-24 (323 μ L, 2.0 mmol) and Et₃N (420 μ L, 3.0 mmol) were mixed with THF (10 mL). Under stirring at 0 °C, acetyl chloride (142 μ L, 2.0 mmol) was added dropwise. The pale-yellow solution was left under stirring for 2 hours at room temperature. The mixture was then poured into a saturated solution of aqueous NH₄Cl (25 mL) and extracted with EtOAc (3 x 50 mL). The combined organic phases were washed with brine solution (50 mL), dried over anhydrous Na₂SO₄, and the solvent was evaporated under reduced pressure. The remaining solid was washed with Et₂O to remove amine and acid impurities, and then dried out to yield the white solid product (299 mg, 70%). All characterizations were in agreement with data reported in literature.

¹H NMR (300 MHz, CDCl₃) δ (ppm): 8.09 (d, J = 8.1 Hz, 1H, ArH), 7.88 – 7.78 (m, 2H, ArH), 7.57 – 7.42 (m, 4H, ArH), 5.91 (p, J = 6.8 Hz, 1H, CH), 5.83 (s, 1H, NH), 1.94 (s, 3H, C(=O)CH₃), 1.65 (d, J = 6.7 Hz, 3H, CHCH₃).

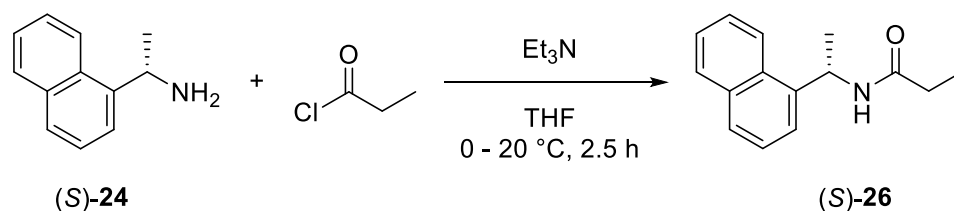
¹³C NMR (75 MHz, CDCl₃) δ (ppm): 169.27, 138.54, 134.24, 131.44, 129.09, 128.71, 126.92, 126.21, 125.50, 123.76, 122.87, 44.95, 23.66, 20.96.

ESI-MS (m/z): calculated 214.1 [M+H]⁺, found 214.0 [M+H]⁺; calculated 236.1 [M+Na]⁺, found 236.0 [M+Na]⁺.

$[\alpha]^{30}_{\text{D}} = -123.6$ ($c = 0.325$, CHCl₃).

5.13. SYNTHESIS OF (S)-N-[1-(1-NAPHTHYL)ETHYL]PROPIONAMIDE

(S)-26



The synthesis was performed adapting reported procedures.^[63,64] In a 50 mL flask, (S)-1-(1-naphthyl)ethan-1-amine (S)-24 (323 μ L, 2.0 mmol) and Et₃N (420 μ L, 3.0 mmol) were mixed with THF (10 mL). Under stirring at 0 °C, propionyl chloride (175 μ L, 2.0 mmol) was added dropwise. The pale-yellow solution was left under stirring for 2.5 hours at room temperature. The mixture was then poured into a saturated solution of aqueous NH₄Cl (25 mL) and extracted with EtOAc (3 x 50 mL). The combined organic phases were washed with brine solution (50 mL), dried over anhydrous Na₂SO₄, and the solvent was evaporated under reduced pressure. The remaining solid was washed with Et₂O to remove amine and acid impurities, and then dried out to yield the white solid product (277 mg, 61%). All characterizations were in agreement with data reported in literature.

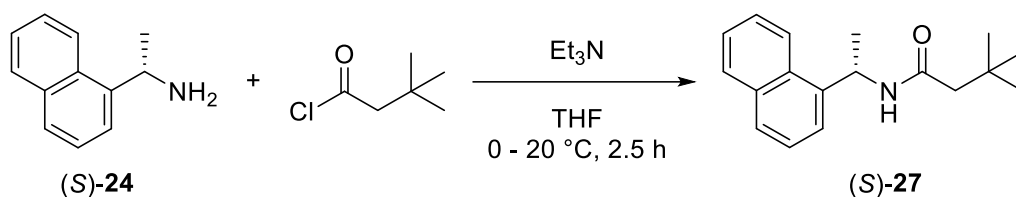
¹H NMR (300 MHz, CDCl₃) δ (ppm): 8.11 – 8.08 (m, 1H, ArH), 7.88 – 7.78 (m, 2H, ArH), 7.57 – 7.42 (m, 4H, ArH), 5.93 (p, J = 7.0 Hz, 1H, CH), 5.72 (s, 1H, NH), 2.17 (q, J = 7.5 Hz, 2H, CH₂), 1.66 (d, J = 6.7 Hz, 3H, CHCH₃), 1.14 (t, J = 7.6 Hz, 3H, CH₂CH₃).

¹³C NMR (75 MHz, CDCl₃) δ (ppm): 172.95, 138.66, 134.26, 131.49, 129.08, 128.70, 126.88, 126.21, 125.50, 123.82, 122.87, 44.79, 30.11, 20.99, 10.21.

ESI-MS (m/z): calculated 228.1 [M+H]⁺, found 228.1 [M+H]⁺.

$[\alpha]^{30}_{\text{D}}$ = -104.0 (c = 0.176, CHCl₃).

5.14. SYNTHESIS OF (S)-3,3-DIMETHYL-N-[1-(1-NAPHTHYL)ETHYL] BUTYRAMIDE (S)-27



The synthesis was performed adapting reported procedures.^[63,64] In a 50 mL flask, (S)-1-(1-naphthyl)ethanamine (S)-24 (323 μL , 2.0 mmol) and Et_3N (420 μL , 3.0 mmol) were mixed with THF (10 mL). Under stirring at 0 $^\circ\text{C}$, 3,3-dimethylbutyryl chloride (278 μL , 2.0 mmol) was added dropwise. The pale-yellow solution was left under stirring for 2.5 hours at room temperature. The mixture was then poured into a saturated solution of aqueous NH_4Cl (25 mL) and extracted with EtOAc (3 x 50 mL). The combined organic phases were washed with brine solution (50 mL), dried over anhydrous Na_2SO_4 , and the solvent was evaporated under reduced pressure. The remaining solid was washed with Et_2O to remove amine and acid impurities, and then dried out to yield the white solid product (307 mg, 57%).

$^1\text{H NMR}$ (300 MHz, CDCl_3) δ (ppm): 8.13 – 8.10 (m, 1H, ArH), 7.87 – 7.78 (m, 2H, ArH), 7.55 – 7.41 (m, 4H, ArH), 5.94 (p, $J = 6.9$ Hz, 1H, CH), 5.75 (s, 1H, NH), 2.00 (s, 2H, CH_2), 1.66 (d, $J = 6.7$ Hz, 3H, CHCH_3), 1.01 (s, 9H, $\text{C}(\text{CH}_3)_3$).

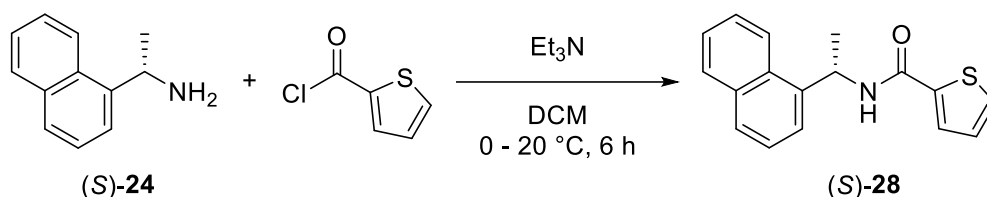
$^{13}\text{C NMR}$ (75 MHz, CDCl_3) δ (ppm): 170.83, 138.63, 134.20, 131.46, 128.99, 128.63, 126.79, 126.18, 125.42, 123.99, 122.89, 50.81, 44.63, 31.26, 30.13, 20.87.

ESI-MS (m/z): calculated 292.2 $[\text{M}+\text{Na}]^+$, found 292.1709 $[\text{M}+\text{Na}]^+$.

$[\alpha]^{30}_{\text{D}} = -66.2$ ($c = 0.365$, CHCl_3).

Elemental analysis: C 80.11%, H 8.59%, N 5.23%, O 6.07%.

5.15. SYNTHESIS OF *N*-[(1*S*)-1-(1-NAPHTHYL)ETHYL]THIOPHENE-2-CARBOXAMIDE (*S*)-28



The synthesis was performed adapting reported procedures.^[63,64] In a 50 mL flask, (*S*)-1-(1-naphthyl)ethylamine (*S*)-24 (323 μ L, 2.0 mmol) and Et₃N (420 μ L, 3.0 mmol) were mixed with DCM (10 mL). Under stirring at 0 °C, 2-thiophenecarbonyl chloride (235 μ L, 2.2 mmol) was added dropwise. The pale-yellow solution was left under stirring for 6 hours at room temperature. The mixture was then poured into a saturated solution of aqueous NH₄Cl (25 mL) and extracted with DCM (3 x 50 mL). The combined organic phases were extracted once with a saturated solution of NaHCO₃ (50 mL), then washed with brine solution (50 mL), dried over anhydrous MgSO₄, and the solvent was evaporated under reduced pressure. The remaining solid was solubilized in the minimum amount of boiling *n*-hexane, then slowly cooled down until room temperature. The crystals obtained were filtered, washed with cold *n*-hexane, and then dried out, yielding the desired product as a white solid (518 mg, 92%).

¹H NMR (300 MHz, CDCl₃) δ (ppm): 8.16 – 8.13 (m, 1H, ArH), 7.89 – 7.80 (m, 2H, ArH), 7.60 – 7.40 (m, 4H + 2H, ArH + TpH), 6.99 (dd, $J = 5.0, 3.8$ Hz, 1H, TpH), 6.31 (s, 1H, NH), 6.06 (p, $J = 7.0$ Hz, 1H, CH), 1.75 (d, $J = 6.7$ Hz, 3H, CH₃).

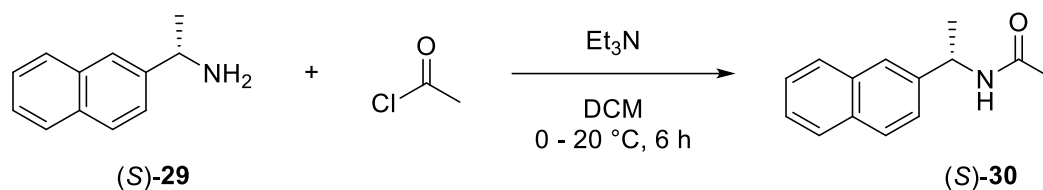
¹³C NMR (75 MHz, CDCl₃) δ (ppm): 161.19, 139.21, 138.30, 134.27, 131.49, 130.28, 129.09, 128.85, 128.33, 127.86, 127.02, 126.24, 125.51, 123.72, 123.06, 45.51, 21.03.

ESI-MS (m/z): calculated 282.1 [M+H]⁺, found 282.1000 [M+H]⁺; calculated 304.1 [M+Na]⁺, found 304.0769 [M+Na]⁺.

$[\alpha]^{30}_{\text{D}} = +31.6$ ($c = 0.183$, CHCl₃).

Elemental analysis: C 72.50%, H 5.32%, N 5.06%, O 5.71%, S 11.41%.

5.16. SYNTHESIS OF (*S*)-*N*-[1-(2-NAPHTHYL)ETHYL]ACETAMIDE (*S*)-30



The synthesis was performed adapting reported procedures.^[63,64] In a 50 mL flask, (*S*)-1-(2-naphthyl)ethylamine (*S*)-29 (342 mg, 2.0 mmol) and Et₃N (420 μ L, 3.0 mmol) were mixed with DCM (10 mL). Under stirring at 0 °C, acetyl chloride (142 μ L, 2.0 mmol) was added dropwise. The colourless solution was left under stirring for 6 hours at room temperature. The mixture was then poured into a saturated solution of aqueous NH₄Cl (25 mL) and extracted with DCM (3 x 50 mL). The combined organic phases were washed with brine solution (50 mL), dried over anhydrous Na₂SO₄, and the solvent was evaporated under reduced pressure. The remaining solid was then precipitated by crystallization: after being dissolved in DCM, *n*-hexane was slowly added. After 24 hours, the white solid was filtered and dried out, yielding the desired product (363 mg, 85%). All characterizations were in agreement with data reported in literature.

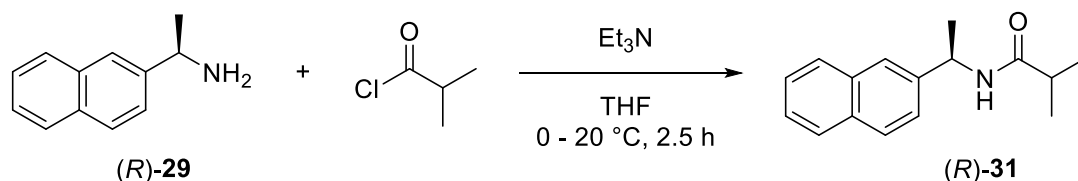
¹H NMR (300 MHz, CDCl₃) δ (ppm): 7.81 - 7.73 (m, 4H, ArH), 7.51 - 7.39 (m, 3H, ArH), 6.40 (s, 1H, NH), 5.25 (p, $J = 7.1$ Hz, 1H, CH), 1.95 (s, 3H, C(=O)CH₃), 1.52 (d, $J = 6.9$ Hz, 3H, CHCH₃).

¹³C NMR (75 MHz, CDCl₃) δ (ppm): 169.62, 140.96, 133.56, 132.91, 128.64, 128.09, 127.84, 126.43, 126.07, 125.02, 124.75, 49.06, 23.56, 21.92.

ESI-MS (m/z): calculated 214.1 [M+H]⁺, found 214.1 [M+H]⁺; calculated 236.1 [M+Na]⁺, found 236.0 [M+Na]⁺.

$[\alpha]^{30}_{\text{D}} = -181.2$ ($c = 0.421$, CHCl₃).

5.17. SYNTHESIS OF (*R*)-*N*-[1-(2-NAPHTHYL)ETHYL]ISOBUTYRAMIDE (*R*)-31



The synthesis was performed adapting reported procedures.^[63,64] In a 50 mL flask, (*R*)-1-(2-naphthyl)ethanamine (*R*)-29 (110 mg, 0.64 mmol) and Et₃N (227 μL, 1.64 mmol) were mixed with THF (10 mL). Under stirring at 0 °C, isobutyryl chloride (67 μL, 0.64 mmol) was added dropwise. The colourless solution was left under stirring for 2.5 hours at room temperature. The mixture was then poured into a saturated solution of aqueous NH₄Cl (25 mL) and extracted with EtOAc (3 x 50 mL). The combined organic phases were washed with brine solution (50 mL), dried over anhydrous Na₂SO₄, and the solvent was evaporated under reduced pressure. The remaining solid was washed with Et₂O to remove amine and acid impurities, and then dried out to yield the white solid product (100 mg, 65%).

¹H NMR (300 MHz, CDCl₃) δ (ppm): 7.83 - 7.74 (m, 4H, ArH), 7.51 - 7.41 (m, 3H, ArH), 5.84 (s, 1H, NH), 5.29 (p, *J* = 7.1 Hz, 1H, CHNH), 2.36 (hept, *J* = 6.9 Hz, 1H, CH(CH₃)₂), 1.57 (d, *J* = 6.9 Hz, 3H, CHCH₃), 1.16 (dd, *J* = 9.1, 6.9 Hz, 6H, CH(CH₃)₂).

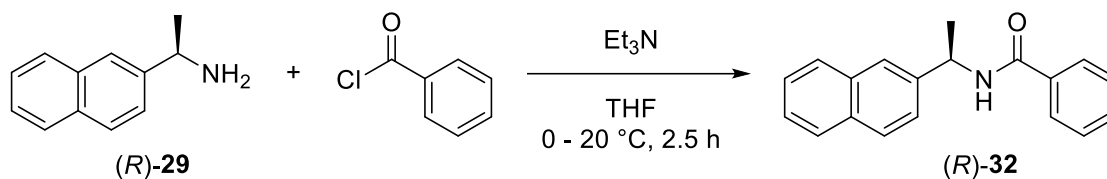
¹³C NMR (75 MHz, CDCl₃) δ (ppm): 176.38, 141.07, 133.65, 133.00, 128.78, 128.19, 127.91, 126.52, 126.17, 125.07, 124.76, 48.75, 35.99, 21.90, 19.93, 19.89.

ESI-MS (*m/z*): calculated 242.2 [M+H]⁺, found 242.2894 [M+H]⁺; calculated 264.1 [M+Na]⁺, found 264.1398 [M+Na]⁺.

[α]³⁰_D = +172.0 (*c* = 0.154, CHCl₃).

Elemental analysis: C 79.62%, H 7.90%, N 5.90%, O 6.58%.

5.18. SYNTHESIS OF (*R*)-*N*-[1-(2-NAPHTHYL)ETHYL]BENZAMIDE (*R*)-32



The synthesis was performed adapting reported procedures.^[63,64] In a 50 mL flask, (*R*)-1-(2-naphthyl)ethylamine (*R*)-29 (100 mg, 0.58 mmol) and Et₃N (222 μ L, 1.58 mmol) were mixed with THF (10 mL). Under stirring at 0 °C, benzoyl chloride (68 μ L, 0.58 mmol) was added dropwise. The colourless solution was left under stirring for 2.5 hours at room temperature. The mixture was then poured into a saturated solution of aqueous NH₄Cl (25 mL) and extracted with EtOAc (3 x 50 mL). The combined organic phases were washed with brine solution (50 mL), dried over anhydrous Na₂SO₄, and the solvent was evaporated under reduced pressure. The remaining solid was washed with Et₂O to remove amine and acid impurities, and then dried out to yield the white solid product (117 mg, 73%). All characterizations were in agreement with data reported in literature.

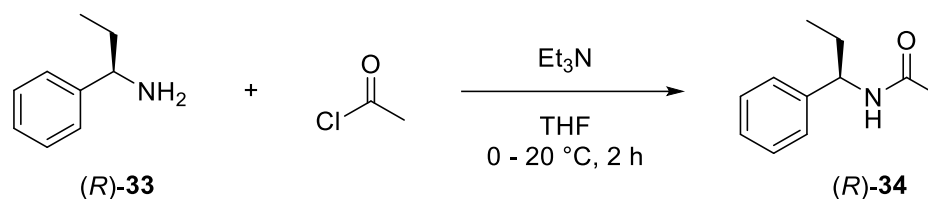
¹H NMR (300 MHz, CDCl₃) δ (ppm): 7.86 - 7.78 (m, 6H, ArH), 7.53 - 7.39 (m, 6H, ArH), 6.44 (s, 1H, NH), 5.52 (p, $J = 7.1$ Hz, 1H, CH), 1.70 (d, $J = 6.9$ Hz, 3H, CH₃).

¹³C NMR (75 MHz, CDCl₃) δ (ppm): 166.94, 140.80, 134.90, 133.70, 133.12, 131.84, 128.94, 128.92, 128.26, 127.97, 127.28, 126.61, 126.29, 125.14, 124.99, 49.62, 21.96.

ESI-MS (m/z): calculated 276.1 [M+H]⁺, found 276.2 [M+H]⁺; calculated 298.1 [M+Na]⁺, found 298.2 [M+Na]⁺.

$[\alpha]^{30}_{\text{D}} = +35.8$ ($c = 0.156$, CHCl₃).

5.19. SYNTHESIS OF (*R*)-*N*-(1-PHENYLPROPYL)ACETAMIDE (*R*)-34



The synthesis was performed adapting reported procedures.^[63,64] In a 50 mL flask, (*R*)-1-phenylpropylamine (*R*)-33 (288 μ L, 2.0 mmol) and Et₃N (420 μ L, 3.0 mmol) were mixed with THF (10 mL). Under stirring at 0 °C, acetyl chloride (142 μ L, 2.0 mmol) was added dropwise. The colourless solution was left under stirring for 2 hours at room temperature. The mixture was then poured into a saturated solution of aqueous NH₄Cl (25 mL) and extracted with EtOAc (3 x 50 mL). The combined organic phases were washed with brine solution (50 mL), dried over anhydrous Na₂SO₄, and the solvent was evaporated under reduced pressure. The remaining solid was washed with Et₂O to remove amine and acid impurities, and then dried out to yield the white solid product (255 mg, 72%). All characterizations were in agreement with data reported in literature.

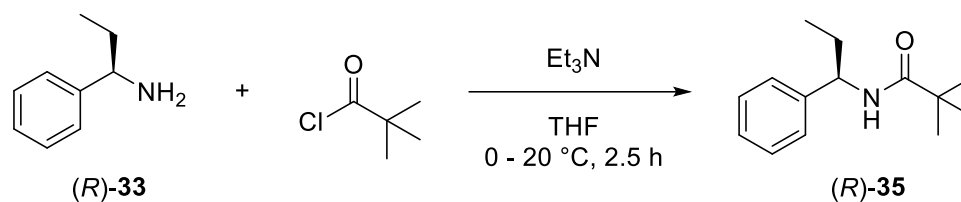
¹H NMR (300 MHz, CDCl₃) δ (ppm): 7.33 – 7.19 (m, 5H, ArH), 6.32 (s, 1H, NH), 4.84 (q, J = 7.6 Hz, 1H, CH), 1.93 (s, 3H, C(=O)CH₃), 1.84 - 1.73 (m, 2H, CH₂), 0.86 (t, J = 7.4 Hz, 3H, CH₂CH₃).

¹³C NMR (75 MHz, CDCl₃) δ (ppm): 169.77, 142.56, 128.79, 127.47, 126.92, 55.24, 29.38, 23.55, 11.04.

ESI-MS (m/z): calculated 178.1 [M+H]⁺, found 178.1 [M+H]⁺; calculated 200.1 [M+Na]⁺, found 200.0 [M+Na]⁺.

$[\alpha]^{30}_{\text{D}} = +130.6$ ($c = 0.212$, CHCl₃).

5.20. SYNTHESIS OF (*R*)-*N*-(1-PHENYLPROPYL)PIVALAMIDE (*R*)-35



The synthesis was performed adapting reported procedures.^[63,64] In a 50 mL flask, (*R*)-1-phenylpropylamine (*R*)-33 (288 μ L, 2.0 mmol) and Et₃N (420 μ L, 3.0 mmol) were mixed with THF (10 mL). Under stirring at 0 °C, pivaloyl chloride (246 μ L, 2.0 mmol) was added dropwise. The colourless solution was left under stirring for 2.5 hours at room temperature. The mixture was then poured into a saturated solution of aqueous NH₄Cl (25 mL) and extracted with EtOAc (3 x 50 mL). The combined organic phases were washed with brine solution (50 mL), dried over anhydrous Na₂SO₄, and the solvent was evaporated under reduced pressure. The remaining solid was washed with Et₂O to remove amine and acid impurities, and then dried out to yield the white solid product (219 mg, 50%).

¹H NMR (300 MHz, CDCl₃) δ (ppm): 7.35 – 7.21 (m, 5H, ArH), 5.81 (s, 1H, NH), 4.86 (q, *J* = 7.5 Hz, 1H, CH), 1.81 (p, *J* = 7.3 Hz, 2H, CH₂), 1.19 (s, 9H, C(CH₃)₃), 0.89 (t, *J* = 7.4 Hz, 3H, CH₂CH₃).

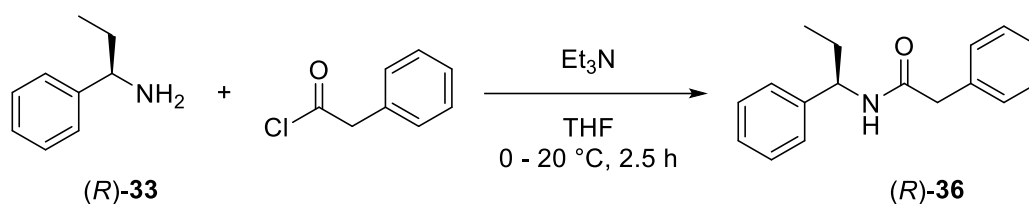
¹³C NMR (75 MHz, CDCl₃) δ (ppm): 177.95, 142.81, 128.93, 127.50, 126.76, 54.87, 39.01, 29.54, 27.92, 11.03.

ESI-MS (*m/z*): calculated 220.2 [M+H]⁺, found 220.1736 [M+H]⁺; calculated 242.2 [M+Na]⁺, found 242.1558 [M+Na]⁺.

$[\alpha]^{30}_{\text{D}} = +108.8$ (*c* = 0.311, CHCl₃).

Elemental analysis: C 76.70%, H 9.64%, N 6.42%, O 7.24%.

5.21. SYNTHESIS OF (R)-2-PHENYL-N-(1-PHENYLPROPYL) ACETAMIDE (R)-36



The synthesis was performed adapting reported procedures.^[63,64] In a 50 mL flask, (*R*)-1-phenylpropylamine (*R*)-**33** (288 μ L, 2.0 mmol) and Et₃N (420 μ L, 3.0 mmol) were mixed with THF (10 mL). Under stirring at 0 °C, 2-phenylacetyl chloride (309 μ L, 2.0 mmol) was added dropwise. The colourless solution was left under stirring for 2.5 hours at room temperature. The mixture was then poured into a saturated solution of aqueous NH₄Cl (25 mL) and extracted with EtOAc (3 x 50 mL). The combined organic phases were washed with brine solution (50 mL), dried over anhydrous Na₂SO₄, and the solvent was evaporated under reduced pressure. The remaining solid was washed with Et₂O to remove amine and acid impurities, and then dried out to yield the white solid product (263 mg, 52%).

¹H NMR (300 MHz, CDCl₃) δ (ppm): 7.38 – 7.13 (m, 10H, ArH), 5.85 (s, 1H, NH), 4.87 (q, J = 7.6 Hz, 1H, CH), 3.55 (d, J = 3.1 Hz, 2H, C(=O)CH₂), 1.70 (pd, J = 7.3, 1.5 Hz, 2H, CH₂CH₃), 0.80 (t, J = 7.4 Hz, 3H, CH₃).

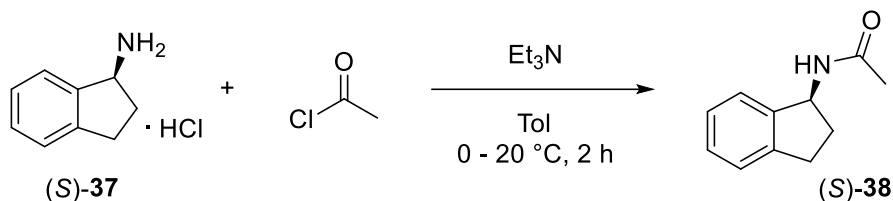
¹³C NMR (75 MHz, CDCl₃) δ (ppm): 170.53, 142.40, 135.36, 129.63, 129.24, 128.80, 127.56, 127.46, 126.67, 55.06, 44.10, 29.46, 10.83.

ESI-MS (m/z): calculated 254.2 [M+H]⁺, found 254.1578 [M+H]⁺; calculated 276.1 [M+Na]⁺, found 276.1382 [M+Na]⁺.

$[\alpha]^{30}_{\text{D}} = +11.9$ ($c = 0.497$, CHCl₃).

Elemental analysis: C 80.49%, H 7.59%, N 5.39%, O 6.53%.

5.22. SYNTHESIS OF (*S*)-*N*-(INDAN-1-YL)ACETAMIDE (*S*)-38



The synthesis was performed adapting reported procedures.^[63,65] In a 50 mL flask, (*S*)-1-aminoindane hydrochloride (*S*)-37 (339 mg, 2.0 mmol) and Et₃N (697 μ L, 5.0 mmol) were mixed with toluene (10 mL), but the amine did not completely solubilize. Under stirring at 0 °C, acetyl chloride (142 μ L, 2.0 mmol) was added dropwise. The pale-yellow solution was left under stirring for 2 hours at room temperature. The homogeneous mixture was then poured into a saturated solution of aqueous NH₄Cl (25 mL) and extracted with EtOAc (3 x 50 mL). The combined organic phases were washed with brine solution (50 mL), dried over anhydrous Na₂SO₄, and the solvent was evaporated under reduced pressure. The remaining solid was washed with Et₂O to remove amine and acid impurities, and then dried out to yield the white solid product (53 mg, 15%). All characterizations were in agreement with data reported in literature.

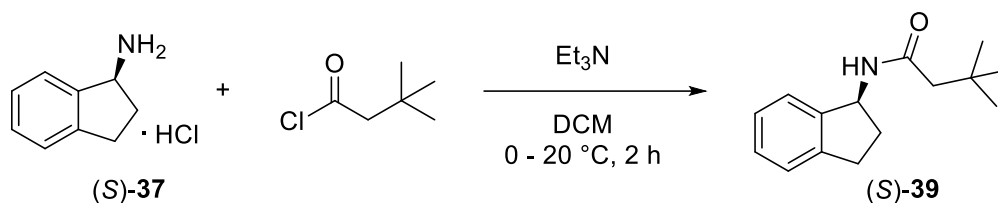
¹H NMR (300 MHz, CDCl₃) δ (ppm): 7.33 – 7.20 (m, 4H, ArH), 5.67 (s, 1H, NH), 5.50 (q, J = 7.6 Hz, 1H, CH), 3.05 – 2.83 (m, 2H, ArCH₂), 2.68 – 2.57 and 1.88 – 1.76 (m, 2H, CHCH₂), 2.05 (s, 3H, CH₃).

¹³C NMR (75 MHz, CDCl₃) δ (ppm): 170.14, 143.81, 143.44, 128.38, 127.13, 125.19, 124.36, 55.14, 34.43, 30.56, 23.80.

ESI-MS (m/z): calculated 176.1 [M+H]⁺, found 176.0 [M+H]⁺.

$[\alpha]^{30}_{\text{D}} = -80.0$ ($c = 0.104$, CHCl₃).

5.23. SYNTHESIS OF (*S*)-3,3-DIMETHYL-*N*-(INDAN-1-YL)BUTYRAMIDE (*S*)-39



The synthesis was performed adapting reported procedures.^[63,64] In a 50 mL flask, (*S*)-1-aminoindane hydrochloride (*S*)-37 (509 mg, 3.0 mmol) and Et₃N (980 μL, 7.0 mmol) were mixed with DCM (10 mL), but the amine did not completely solubilize. Under stirring at 0 °C, 3,3-dimethylbutyryl chloride (417 μL, 3.0 mmol) was added dropwise. The pale-yellow solution was left under stirring for 2 hours at room temperature. The homogeneous mixture was then poured into a saturated solution of aqueous NH₄Cl (25 mL) and extracted with DCM (3 x 50 mL). The combined organic phases were washed with brine solution (50 mL), dried over anhydrous Na₂SO₄, and the solvent was evaporated under reduced pressure. The remaining solid was washed with Et₂O to remove amine and acid impurities, and then dried out to yield the white solid product (381 mg, 55%).

¹H NMR (300 MHz, CDCl₃) δ (ppm): 7.30 – 7.19 (m, 4H, ArH), 5.53 – 5.46 (m, 1H + 1H, NH + CH), 3.03 – 2.81 (m, 2H, ArCH₂), 2.67 – 2.56 and 1.85 – 1.73 (m, 2H, CHCH₂), 2.09 (s, 2H, C(=O)CH₂), 1.07 (s, 9H, C(CH₃)₃).

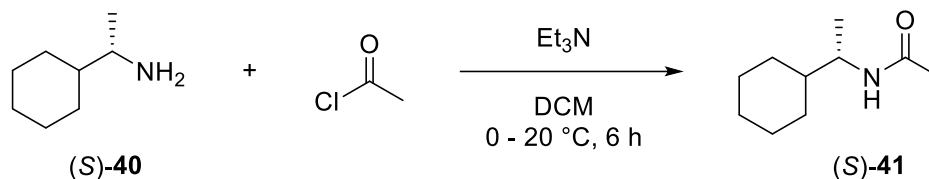
¹³C NMR (75 MHz, CDCl₃) δ (ppm): 171.68, 143.85, 143.64, 128.27, 127.10, 125.17, 124.35, 54.91, 51.15, 46.13, 34.58, 31.25, 30.23, 8.96.

ESI-MS (m/z): calculated 232.2 [M+H]⁺, found 232.1724 [M+H]⁺; calculated 254.2 [M+Na]⁺, found 254.1513 [M+Na]⁺.

[α]³⁰_D = -33.5 (*c* = 0.108, CHCl₃).

Elemental analysis: C 77.77%, H 9.00%, N 6.14%, O 7.09%.

5.24. SYNTHESIS OF (*S*)-*N*-(1-CYCLOHEXYLETHYL)ACETAMIDE (*S*)-41



The synthesis was performed adapting reported procedures.^[63,64] In a 50 mL flask, (*S*)-1-cyclohexylethylamine (*S*)-40 (297 μ L, 2.0 mmol) and Et₃N (420 μ L, 3.0 mmol) were mixed with DCM (10 mL). Under stirring at 0 °C, acetyl chloride (142 μ L, 2.0 mmol) was added dropwise. The colourless solution was left under stirring for 6 hours at room temperature. The mixture was then poured into a saturated solution of aqueous NH₄Cl (25 mL) and extracted with DCM (3 x 50 mL). The combined organic phases were washed with brine solution (50 mL), dried over anhydrous Na₂SO₄, and the solvent was evaporated under reduced pressure. The remaining solid was then precipitated by crystallization: after being dissolved in DCM, *n*-hexane was slowly added. After 24 hours, the white solid was filtered and dried out, yielding the desired product (284 mg, 84%). All characterizations were in agreement with data reported in literature.

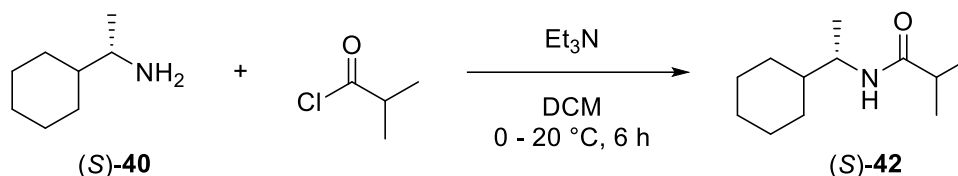
¹H NMR (300 MHz, CDCl₃) δ (ppm): 6.18 (s, 1H, NH), 3.76 – 3.64 (m, 1H, CHNH), 1.86 (s, 3H, C(=O)CH₃), 1.67 – 1.50 and 1.25 – 0.79 (m, 14H, *c*-HexH + CHCH₃).

¹³C NMR (75 MHz, CDCl₃) δ (ppm): 169.67, 49.52, 43.10, 29.33, 29.10, 26.49, 26.26, 23.43, 17.88.

ESI-MS (m/z): calculated 170.2 [M+H]⁺, found 170.1 [M+H]⁺.

$[\alpha]^{30}_{\text{D}} = -23.7$ ($c = 0.565$, CHCl₃).

5.25. SYNTHESIS OF (*S*)-*N*-(1-CYCLOHEXYLETHYL)ISOBUTYRAMIDE (*S*)-42



The synthesis was performed adapting reported procedures.^[63,64] In a 50 mL flask, (*S*)-1-cyclohexylethylamine (*S*)-40 (297 μ L, 2.0 mmol) and Et₃N (420 μ L, 3.0 mmol) were mixed with DCM (10 mL). Under stirring at 0 °C, isobutyryl chloride (230 μ L, 2.2 mmol) was added dropwise. The colourless solution was left under stirring for 6 hours at room temperature. The mixture was then poured into a saturated solution of aqueous NH₄Cl (25 mL) and extracted with DCM (3 x 50 mL). The combined organic phases were extracted once with a saturated solution of NaHCO₃ (50 mL), then washed with brine solution (50 mL), dried over anhydrous MgSO₄, and the solvent was evaporated under reduced pressure. The remaining solid was solubilized in the minimum amount of boiling *n*-hexane, then slowly cooled down until room temperature. The crystals obtained were filtered, washed with cold *n*-hexane, and then dried out, yielding the desired product as a white solid (347 mg, 88%).

¹H NMR (300 MHz, CDCl₃) δ (ppm): 5.62 (s, 1H, NH), 3.81 – 3.69 (m, 1H, CHNH), 2.28 (hept, *J* = 6.6 Hz, 1H, CH(CH₃)₂), 1.68 – 1.58 and 1.28 – 0.84 (m, 20H, c-HexH + CHCH₃ + CH(CH₃)₂).

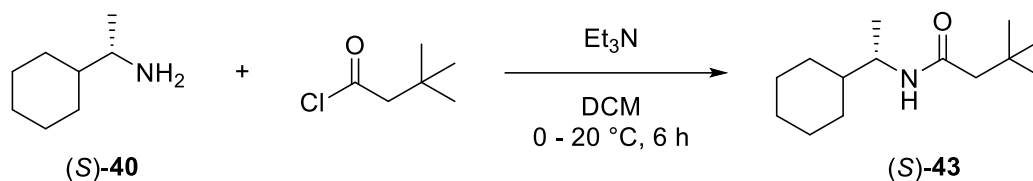
¹³C NMR (75 MHz, CDCl₃) δ (ppm): 176.38, 49.08, 43.30, 35.87, 29.33, 26.59, 26.36, 20.08, 19.75, 18.14.

ESI-MS (*m/z*): calculated 198.2 [M+H]⁺, found 198.1884 [M+H]⁺.

$[\alpha]^{30}_{\text{D}} = -18.4$ (*c* = 0.961, CHCl₃).

Elemental analysis: C 73.40%, H 12.05%, N 6.95%, O 7.60%.

5.26. SYNTHESIS OF (S)-3,3-DIMETHYL-N-(1-CYCLOHEXYLETHYL) BUTYRAMIDE (S)-43



The synthesis was performed adapting reported procedures.^[63,64] In a 50 mL flask, (S)-1-cyclohexylethylamine (S)-40 (297 μL , 2.0 mmol) and Et_3N (420 μL , 3.0 mmol) were mixed with DCM (10 mL). Under stirring at 0 $^\circ\text{C}$, 3,3-dimethylbutyryl chloride (306 μL , 2.2 mmol) was added dropwise. The colourless solution was left under stirring for 6 hours at room temperature. The mixture was then poured into a saturated solution of aqueous NH_4Cl (25 mL) and extracted with DCM (3 x 50 mL). The combined organic phases were extracted once with a saturated solution of NaHCO_3 (50 mL), then washed with brine solution (50 mL), dried over anhydrous MgSO_4 , and the solvent was evaporated under reduced pressure. The remaining solid was solubilized in the minimum amount of boiling *n*-hexane, then slowly cooled down until room temperature. The crystals obtained were filtered, washed with cold *n*-hexane, and then dried out, yielding the desired product as a white solid (370 mg, 82%).

$^1\text{H NMR}$ (300 MHz, CDCl_3) δ (ppm): 5.39 (s, 1H, NH), 3.80 (dp, $J = 9.0, 6.7$ Hz, 1H, CHCH₃), 1.98 (s, 2H, C(=O)CH₂), 1.73 – 1.58 and 1.31 – 0.84 (m, 23H, c-HexH + CHCH₃ + C(CH₃)₃).

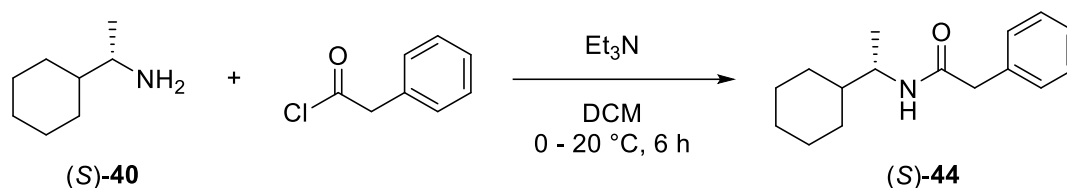
$^{13}\text{C NMR}$ (75 MHz, CDCl_3) δ (ppm): 171.13, 51.09, 49.44, 43.20, 31.07, 30.12, 29.39, 29.30, 26.68, 26.42, 18.26.

ESI-MS (m/z): calculated 226.2 [M+H]⁺, found 226.2193 [M+H]⁺.

$[\alpha]^{30}_{\text{D}} = -7.6$ ($c = 0.920$, CHCl_3).

Elemental analysis: C 74.85%, H 12.60%, N 6.08%, O 6.47%.

5.27. SYNTHESIS OF (S)-2-PHENYL-N-(1-CYCLOHEXYLETHYL) ACETAMIDE (S)-44



The synthesis was performed adapting reported procedures.^[63,64] In a 50 mL flask, (*S*)-1-cyclohexylethylamine (*S*)-**40** (297 μ L, 2.0 mmol) and Et₃N (420 μ L, 3.0 mmol) were mixed with DCM (10 mL). Under stirring at 0 °C, 2-phenylacetyl chloride (290 μ L, 2.2 mmol) was added dropwise. The colourless solution was left under stirring for 6 hours at room temperature. The mixture was then poured into a saturated solution of aqueous NH₄Cl (25 mL) and extracted with DCM (3 x 50 mL). The combined organic phases were extracted once with a saturated solution of NaHCO₃ (50 mL), then washed with brine solution (50 mL), dried over anhydrous MgSO₄, and the solvent was evaporated under reduced pressure. The remaining solid was solubilized in the minimum amount of boiling *n*-hexane, then slowly cooled down until room temperature. The crystals obtained were filtered, washed with cold *n*-hexane, and then dried out, yielding the desired product as a white solid (417 mg, 85%).

¹H NMR (300 MHz, CDCl₃) δ (ppm): 7.38 – 7.23 (m, 5H, ArH), 5.23 (s, 1H, NH), 3.82 (dp, *J* = 9.1, 6.7 Hz, 1H, CHCH₃), 3.55 (s, 2H, C(=O)CH₂), 1.71 – 1.52 and 1.27 – 0.71 (m, 14H, c-HexH + CHCH₃).

¹³C NMR (75 MHz, CDCl₃) δ (ppm): 170.47, 135.51, 129.69, 129.26, 127.57, 49.69, 44.35, 43.20, 29.30, 29.03, 26.67, 26.39, 18.09.

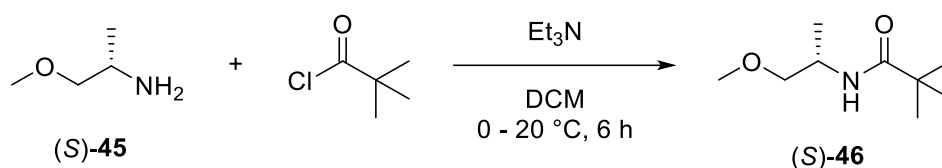
ESI-MS (*m/z*): calculated 246.2 [M+H]⁺, found 246.1926 [M+H]⁺.

$[\alpha]^{30}_{\text{D}} = +28.6$ (*c* = 0.235, CHCl₃).

Elemental analysis: C 78.92%, H 9.77%, N 5.42%, O 5.89%.

5.28. SYNTHESIS OF *N*-[(2*S*)-1-METHOXYPROPAN-2-YL]PIVALAMIDE

(*S*)-46



The synthesis was performed adapting reported procedures.^[63,64] In a 50 mL flask, (*S*)-1-methoxy-2-propylamine (*S*)-45 (211 μ L, 2.0 mmol) and Et₃N (420 μ L, 3.0 mmol) were mixed with DCM (10 mL). Under stirring at 0 °C, pivaloyl chloride (271 μ L, 2.2 mmol) was added dropwise. The colourless solution was left under stirring for 6 hours at room temperature. The mixture was then poured into a saturated solution of aqueous NH₄Cl (25 mL) and extracted with DCM (3 x 50 mL). The combined organic phases were extracted once with a saturated solution of NaHCO₃ (50 mL), then washed with brine solution (50 mL), and dried over anhydrous MgSO₄. The solvent was evaporated under reduced pressure, yielding the desired product as a transparent and colourless oil (315 mg, 91%).

¹H NMR (300 MHz, CDCl₃) δ (ppm): 5.83 (s, 1H, NH), 4.17 – 4.05 (m, 1H, CH), 3.34 (s + d, 3H + 2H, OCH₃ + CH₂), 1.17 (s, 9H, C(CH₃)₃), 1.15 (d, *J* = 6.8 Hz, 3H, CHCH₃).

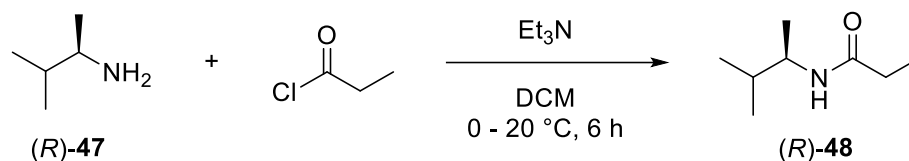
¹³C NMR (75 MHz, CDCl₃) δ (ppm): 178.23, 75.83, 59.39, 44.86, 38.93, 27.86, 17.94.

ESI-MS (*m/z*): calculated 174.1 [M+H]⁺, found 174.1513 [M+H]⁺; calculated 196.1 [M+Na]⁺, found 196.1336 [M+Na]⁺.

$[\alpha]^{30}_{\text{D}} = -20.0$ (*c* = 0.530, CHCl₃).

Elemental analysis: C 62.15%, H 10.96%, N 8.06%, O 18.83%.

5.29. SYNTHESIS OF (*R*)-*N*-(1,2-DIMETHYLPROPYL)PROPIONAMIDE (*R*)-48



The synthesis was performed adapting reported procedures.^[63,64] In a 50 mL flask, (*R*)-1,2-dimethylpropylamine (*R*)-47 (232 μ L, 2.0 mmol) and Et₃N (420 μ L, 3.0 mmol) were mixed with DCM (10 mL). Under stirring at 0 °C, propionyl chloride (192 μ L, 2.2 mmol) was added dropwise. The colourless solution was left under stirring for 6 hours at room temperature. The mixture was then poured into a saturated solution of aqueous NH₄Cl (25 mL) and extracted with DCM (3 x 50 mL). The combined organic phases were extracted once with a saturated solution of NaHCO₃ (50 mL), then washed with brine solution (50 mL), dried over anhydrous MgSO₄, and the solvent was evaporated under reduced pressure. The remaining solid was solubilized in the minimum amount of boiling *n*-hexane, then slowly cooled down until room temperature. The crystals obtained were filtered, washed with cold *n*-hexane, and then dried out, yielding the desired product as a white solid (269 mg, 94%).

¹H NMR (300 MHz, CDCl₃) δ (ppm): 5.66 (s, 1H, NH), 3.84 – 3.72 (m, 1H, CHNH), 2.13 (q, $J = 7.7$ Hz, 2H, CH₂), 1.69 – 1.53 (m, 1H, CH(CH₃)₂), 1.08 (t, $J = 7.6$ Hz, 3H, CH₂CH₃), 0.99 (d, $J = 6.8$ Hz, 3H, CHCH₃), 0.82 (d, $J = 6.9$ Hz, 6H, CH(CH₃)₂).

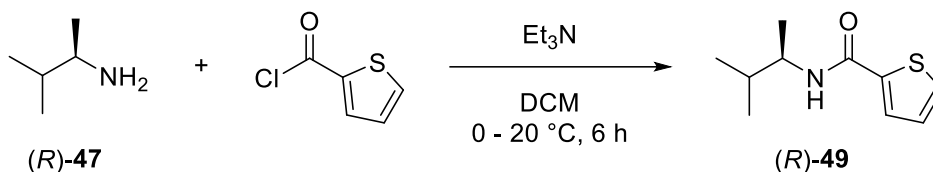
¹³C NMR (75 MHz, CDCl₃) δ (ppm): 173.37, 49.95, 33.16, 30.11, 18.82, 18.63, 17.75, 10.31.

ESI-MS (m/z): calculated 144.1 [M+H]⁺, found 144.1416 [M+H]⁺.

$[\alpha]^{30}_{\text{D}} = -9.7$ ($c = 0.530$, CHCl₃).

Elemental analysis: C 67.53%, H 12.36%, N 9.64%, O 10.47%.

5.30. SYNTHESIS OF *N*-[(1*R*)-1,2-DIMETHYLPROPYL]THIOPHENE-2 CARBOXAMIDE (*R*)-49



The synthesis was performed adapting reported procedures.^[63,64] In a 50 mL flask, (*R*)-1,2-dimethylpropylamine (*R*)-47 (232 μ L, 2.0 mmol) and Et₃N (420 μ L, 3.0 mmol) were mixed with DCM (10 mL). Under stirring at 0 °C, 2-thiophenecarbonyl chloride (235 μ L, 2.2 mmol) was added dropwise. The colourless solution was left under stirring for 6 hours at room temperature. The mixture was then poured into a saturated solution of aqueous NH₄Cl (25 mL) and extracted with DCM (3 x 50 mL). The combined organic phases were extracted once with a saturated solution of NaHCO₃ (50 mL), then washed with brine solution (50 mL), dried over anhydrous MgSO₄, and the solvent was evaporated under reduced pressure. The remaining solid was solubilized in the minimum amount of boiling *n*-hexane, then slowly cooled down until room temperature. The crystals obtained were filtered, washed with cold *n*-hexane, and then dried out, yielding the desired product as a white solid (355 mg, 90%).

¹H NMR (300 MHz, CDCl₃) δ (ppm): 7.50 (dd, $J = 3.7, 1.2$ Hz, 1H, TpH), 7.42 (dd, $J = 5.0, 1.2$ Hz, 1H, TpH), 7.03 (dd, $J = 5.0, 3.7$ Hz, 1H, TpH), 6.02 (s, 1H, NH), 4.00 (dp, 1H, CHNH), 1.85 – 1.70 (m, 1H, CH(CH₃)₂), 1.15 (d, $J = 6.7$ Hz, 3H, CHCH₃), 0.93 (dd, $J = 6.8, 3.9$ Hz, 6H, CH(CH₃)₂).

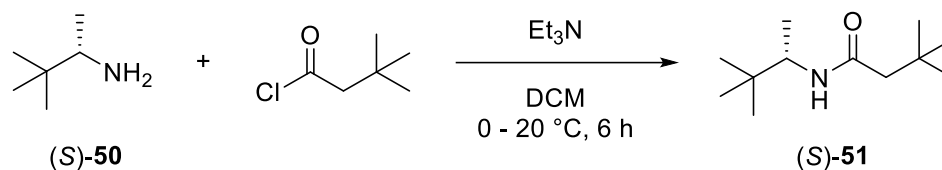
¹³C NMR (75 MHz, CDCl₃) δ (ppm): 161.57, 139.87, 129.84, 127.91, 127.79, 50.89, 33.43, 18.98, 18.85, 17.95.

ESI-MS (m/z): calculated 198.1 [M+H]⁺, found 198.0963 [M+H]⁺.

$[\alpha]^{30}_{\text{D}} = -37.2$ ($c = 0.404$, CHCl₃).

Elemental analysis: C 60.21%, H 7.42%, N 7.16%, O 8.29%, S 16.92%.

5.31. SYNTHESIS OF (S)-3,3-DIMETHYL-N-(3,3-DIMETHYL-2-BUTYL) BUTYRAMIDE (S)-51



The synthesis was performed adapting reported procedures.^[63,64] In a 50 mL flask, (S)-3,3-dimethyl-2-butylamine (S)-50 (272 μ L, 2.0 mmol) and Et₃N (420 μ L, 3.0 mmol) were mixed with DCM (10 mL). Under stirring at 0 °C, 3,3-dimethylbutyryl chloride (306 μ L, 2.2 mmol) was added dropwise. The colourless solution was left under stirring for 6 hours at room temperature. The mixture was then poured into a saturated solution of aqueous NH₄Cl (25 mL) and extracted with DCM (3 x 50 mL). The combined organic phases were extracted once with a saturated solution of NaHCO₃ (50 mL), then washed with brine solution (50 mL), dried over anhydrous MgSO₄, and the solvent was evaporated under reduced pressure. The remaining solid was solubilized in the minimum amount of boiling *n*-hexane, then slowly cooled down until room temperature. The crystals obtained were filtered, washed with cold *n*-hexane, and then dried out, yielding the desired product as a white solid (383 mg, 96%).

¹H NMR (300 MHz, CDCl₃) δ (ppm): 5.27 (s, 1H, NH), 3.83 (dq, *J* = 9.7, 6.8 Hz, 1H, CH), 2.00 (s, 2H, CH₂), 1.00 (d, *J* = 6.7 Hz, 3H, CHCH₃), 1.00 (s, 9H, CH₂C(CH₃)₃), 0.85 (s, 9H, CHC(CH₃)₃).

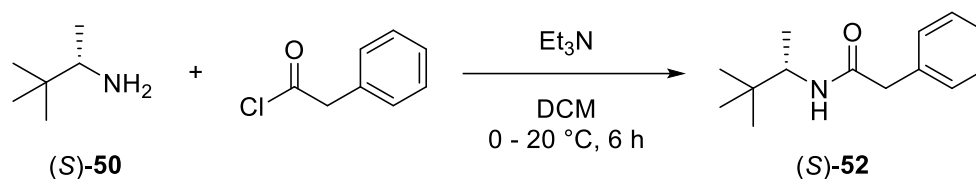
¹³C NMR (75 MHz, CDCl₃) δ (ppm): 171.16, 52.81, 51.30, 34.20, 31.15, 30.16, 26.53, 16.59.

ESI-MS (*m/z*): calculated 200.2 [M+H]⁺, found 200.2076 [M+H]⁺.

$[\alpha]^{30}_{\text{D}} = +16.5$ (*c* = 0.690, CHCl₃).

Elemental analysis: C 72.31%, H 13.04%, N 6.76%, O 7.49%.

5.32. SYNTHESIS OF (S)-2-PHENYL-N-(3,3-DIMETHYL-2-BUTYL) ACETAMIDE (S)-52



The synthesis was performed adapting reported procedures.^[63,64] In a 50 mL flask, (S)-3,3-dimethyl-2-butylamine (S)-50 (272 μ L, 2.0 mmol) and Et₃N (420 μ L, 3.0 mmol) were mixed with DCM (10 mL). Under stirring at 0 °C, 2-phenylacetyl chloride (290 μ L, 2.2 mmol) was added dropwise. The colourless solution was left under stirring for 6 hours at room temperature. The mixture was then poured into a saturated solution of aqueous NH₄Cl (25 mL) and extracted with DCM (3 x 50 mL). The combined organic phases were extracted once with a saturated solution of NaHCO₃ (50 mL), then washed with brine solution (50 mL), dried over anhydrous MgSO₄, and the solvent was evaporated under reduced pressure. The remaining solid was solubilized in the minimum amount of boiling *n*-hexane, then slowly cooled down until room temperature. The crystals obtained were filtered, washed with cold *n*-hexane, and then dried out, yielding the desired product as a white solid (381 mg, 87%).

¹H NMR (300 MHz, CDCl₃) δ (ppm): 7.36 – 7.21 (m, 5H, ArH), 5.34 (s, 1H, NH), 3.81 (dq, $J = 9.7, 6.8$ Hz, 1H, CH), 3.54 (d, $J = 3.2$ Hz, 2H, CH₂), 0.93 (d, $J = 6.8$ Hz, 3H, CHCH₃), 0.73 (s, 9H, C(CH₃)₃).

¹³C NMR (75 MHz, CDCl₃) δ (ppm): 170.30, 135.46, 129.60, 129.20, 127.52, 52.90, 44.29, 34.30, 26.22, 16.15.

ESI-MS (m/z): calculated 220.1 [M+H]⁺, found 220.1736 [M+H]⁺; calculated 242.2 [M+Na]⁺, found 242.1558 [M+Na]⁺.

$[\alpha]^{30}_{\text{D}}$ = +32.1 ($c = 0.864$, CHCl₃).

Elemental analysis: C 76.77%, H 9.72%, N 6.33%, O 7.18%.

5.33. CD MEASUREMENTS AND *g*-FACTOR SPECTRA

The solutions necessary for the CD measurements were prepared with a final concentration appropriate for obtaining values of absorbance within the linearity range of the Lambert-Beer law. Firstly, it was prepared a stock solution (**V**) of vanadium complex **11** (2.0×10^{-3} M) in dry chloroform (orange colour). Secondly, a stock solution (**L**) of chiral amide (8.0×10^{-3} M) was prepared, again in dry chloroform (colourless). Finally, the sample solution was prepared mixing together a determined amount of solution **V** and a determined amount of solution **L**, obtaining the peculiar colour transition from orange to deep blue. This last step was achieved in order to obtain a determined concentration of vanadium complex (1.0×10^{-4} M) and of chiral amide (2.0×10^{-3} M), hence a solution with a final ratio 1:20 between **11** and the amide. This was repeated for each chiral amide synthesized in this work. The vanadium complex **11** used was already available from previous uses and its purity was assessed through ^1H NMR, ^{13}C NMR and ^{51}V NMR spectroscopy, and by ESI-MS analysis.

All the electronic circular dichroism spectra were recorded with a cuvette of 1 cm pathlength in the spectral region between 300 and 700 nm, at a temperature of 298.15 K. The CD measurements were performed using a bandwidth of 2.0 nm, 1.0 s of integration time, a data pitch of 0.2 nm, a scanning speed of 100 nm/min, and 4 accumulations. The *g*-factor spectra were obtained straightaway from the CD spectrophotometer, which was capable to measure simultaneously also the UV-vis absorption spectra of the various samples analysed. Both CD and UV-vis spectra were previously corrected with the blank subtraction. Additional CD measurements were also conducted in order to obtain better data of g^{avg} . Specifically, these measurements were performed in the wavelength region between 590 and 610 nm, using a bandwidth of 2.0 nm, 2.0 s of integration time, a data pitch of 0.5 nm, a scanning speed of 20 nm/min, and 8 accumulations.

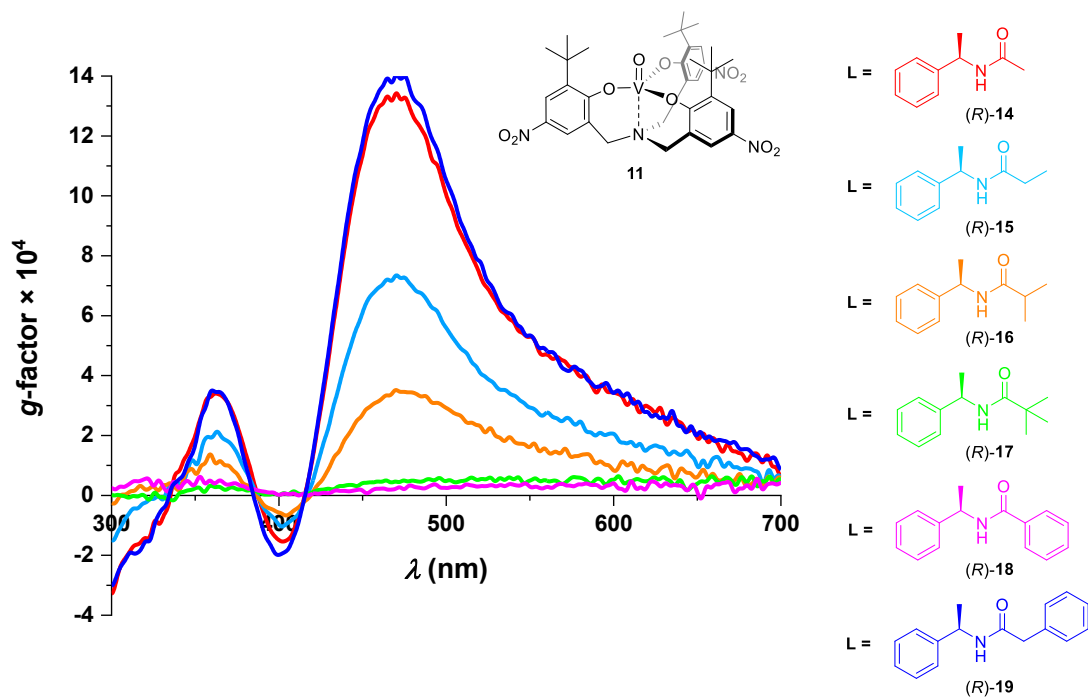


Figure S1. g -factor spectra ($T = 298.15$ K) recorded within the range 300-700 nm of stereodynamic probe **11** (1×10^{-4} M) in the presence of different chiral amides **L** (2×10^{-3} M) in dry CHCl_3 : (R)-14 (red), (R)-15 (light blue), (R)-16 (orange), (R)-17 (green), (R)-18 (magenta), and (R)-19 (blue).

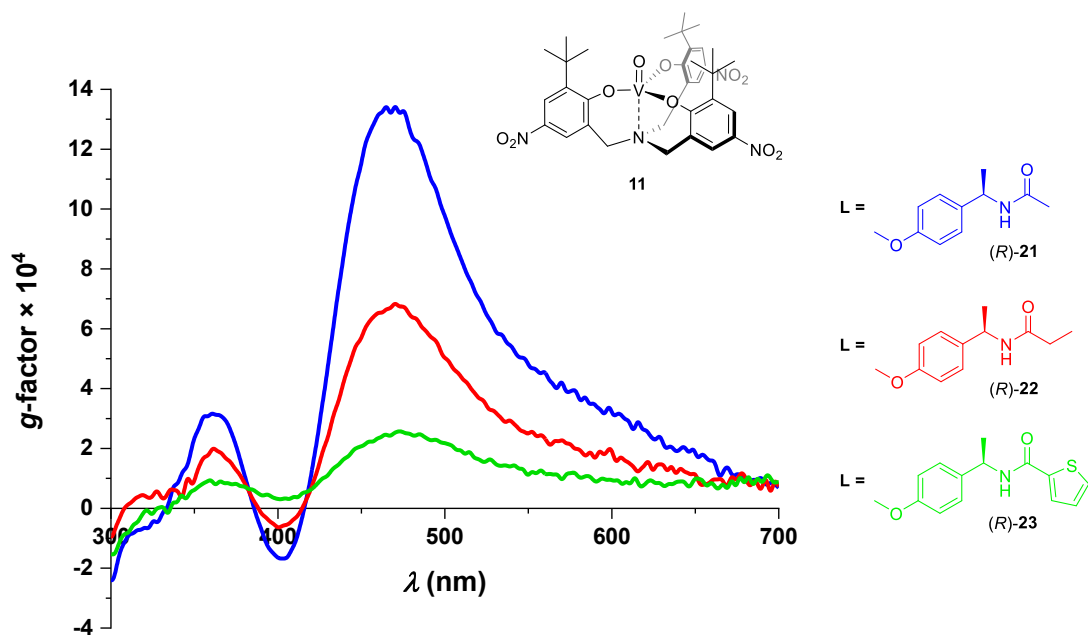


Figure S2. g -factor spectra ($T = 298.15$ K) recorded within the range 300-700 nm of stereodynamic probe **11** (1×10^{-4} M) in the presence of different chiral amides **L** (2×10^{-3} M) in dry CHCl_3 : (R)-21 (blue), (R)-22 (red), and (R)-23 (green).

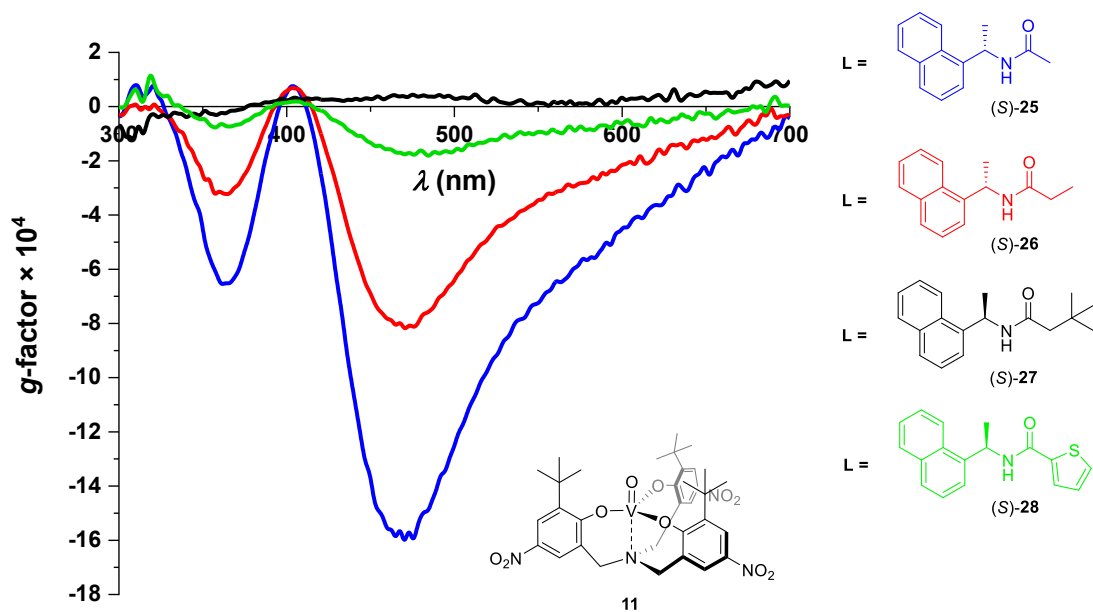


Figure S3. *g*-factor spectra ($T = 298.15$ K) recorded within the range 300-700 nm of stereodynamic probe **11** (1×10^{-4} M) in the presence of different chiral amides **L** (2×10^{-3} M) in dry CHCl_3 : (S)-**25** (blue), (S)-**26** (red), (S)-**27** (black), and (S)-**28** (green).

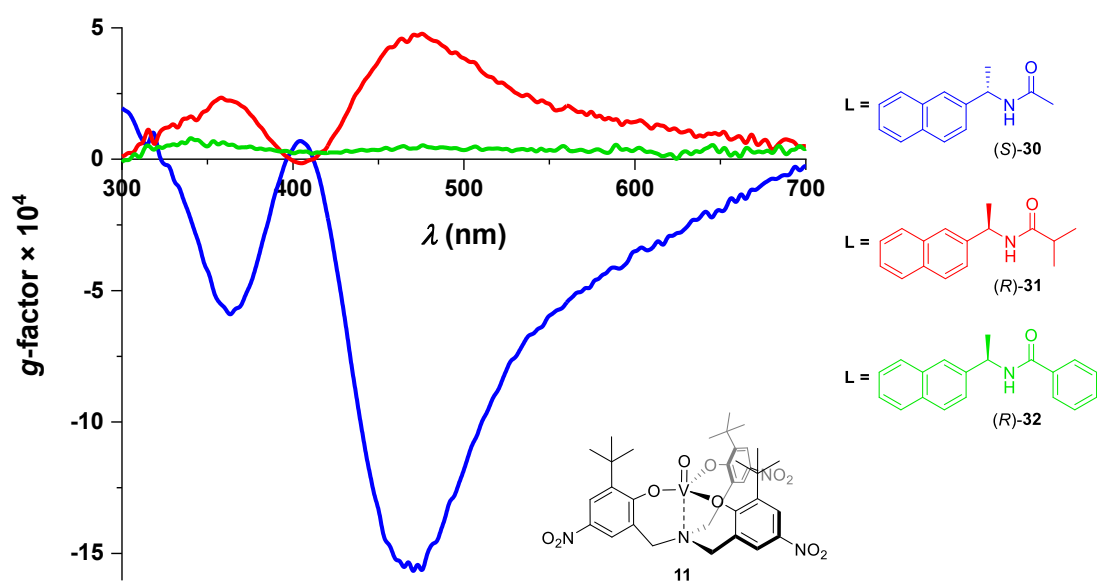


Figure S4. *g*-factor spectra ($T = 298.15$ K) recorded within the range 300-700 nm of stereodynamic probe **11** (1×10^{-4} M) in the presence of different chiral amides **L** (2×10^{-3} M) in dry CHCl_3 : (S)-**30** (blue), (R)-**31** (red), and (R)-**32** (green).

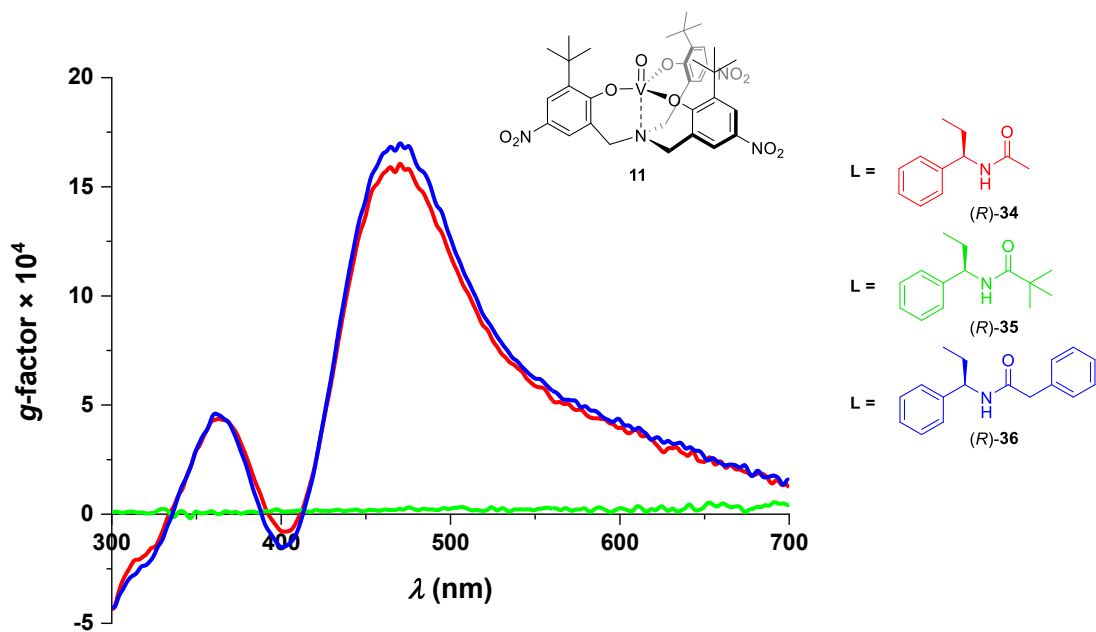


Figure S5. *g*-factor spectra ($T = 298.15$ K) recorded within the range 300-700 nm of stereodynamic probe **11** (1×10^{-4} M) in the presence of different chiral amides **L** (2×10^{-3} M) in dry CHCl_3 : (R)-**34** (red), (R)-**35** (green), and (R)-**36** (blue).

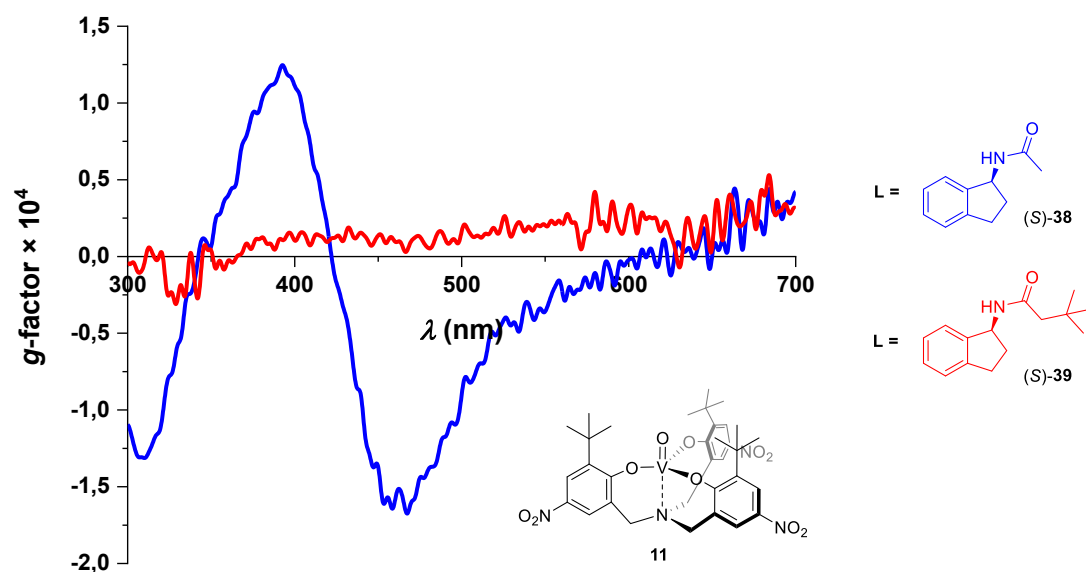


Figure S6. *g*-factor spectra ($T = 298.15$ K) recorded within the range 300-700 nm of stereodynamic probe **11** (1×10^{-4} M) in the presence of different chiral amides **L** (2×10^{-3} M) in dry CHCl_3 : (S)-**38** (blue) and (S)-**39** (red).

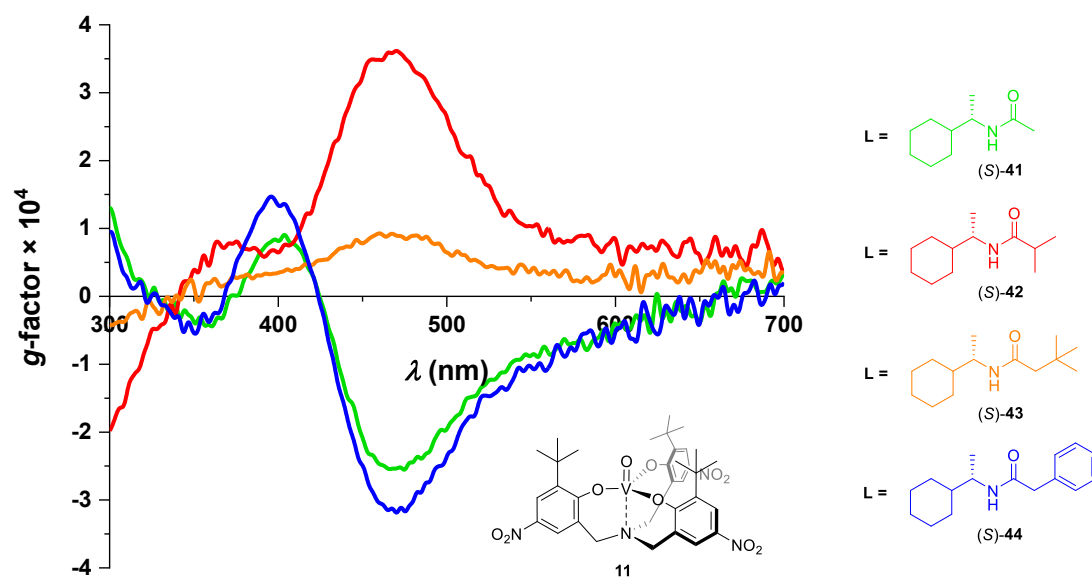


Figure S7. *g*-factor spectra ($T = 298.15\text{ K}$) recorded within the range 300-700 nm of stereodynamic probe **11** ($1 \times 10^{-4}\text{ M}$) in the presence of different chiral amides **L** ($2 \times 10^{-3}\text{ M}$) in dry CHCl_3 : (*S*)-**41** (green), (*S*)-**42** (red), (*S*)-**43** (orange), and (*S*)-**44** (blue).

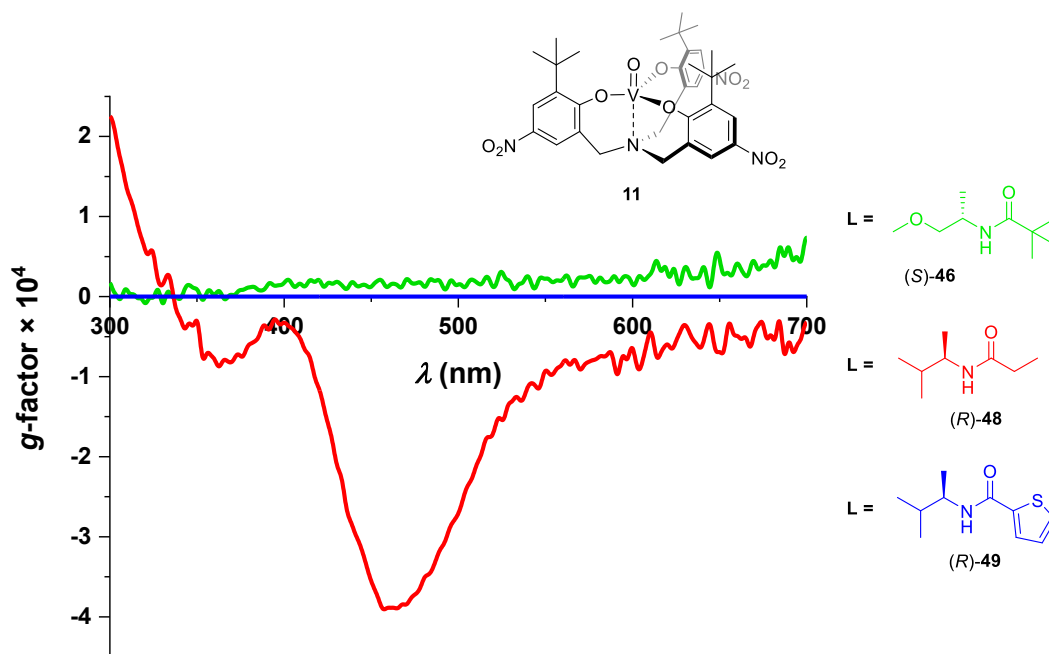


Figure S8. *g*-factor spectra ($T = 298.15\text{ K}$) recorded within the range 300-700 nm of stereodynamic probe **11** ($1 \times 10^{-4}\text{ M}$) in the presence of different chiral amides **L** ($2 \times 10^{-3}\text{ M}$) in dry CHCl_3 : (*S*)-**46** (green), (*R*)-**48** (red), and (*R*)-**49** (blue).

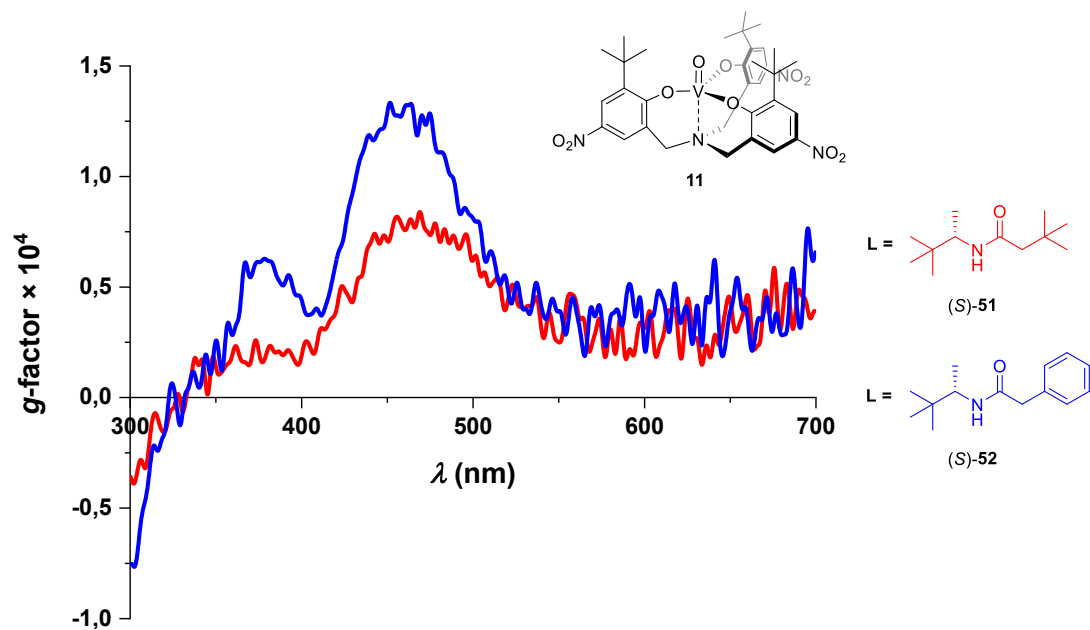


Figure S9. *g*-factor spectra ($T = 298.15\text{ K}$) recorded within the range 300–700 nm of stereodynamic probe **11** ($1 \times 10^{-4}\text{ M}$) in the presence of different chiral amides **L** ($2 \times 10^{-3}\text{ M}$) in dry CHCl_3 : **(S)-51** (red) and **(S)-52** (blue).

5.34. DFT CALCULATIONS

Density functional theory (DFT) calculations were carried out on the ground state of each calculated conformer of the chiral amides tested, in order to optimize their geometry and to calculate their vibrational frequencies. All calculations have been conducted with M06-2X functional and Def2TZVP basis set. These calculations were conducted alongside analysis of natural bond orbital (NBO).

Amide	n° conformers	Energies of the most stable conformer			
		Electronic energy [Hartree]	Thermal correction to Gibbs free energy [Hartree]	Electronic energy (solvation = smd, chloroform) [Hartree]	Gibbs free energy [Hartree]
(R)-14	5	-518.859736	0.172998	-518.877883	-518.704885
(R)-15	14	-558.167060	0.200266	-558.185674	-557.985408
(R)-16	14	-597.475824	0.227130	-597.494850	-597.267720
(R)-17	6	-636.784091	0.255127	-636.803645	-636.548518
(R)-18	6	-710.589908	0.223509	-710.613022	-710.389513
(R)-19	11	-749.898429	0.248585	-749.923252	-749.674667
(R)-21	10	-633.385574	0.204648	-633.404058	-633.199410
(R)-22	29	-672.693295	0.230495	-672.712474	-672.481979
(R)-23	24	-1145.884802	0.219552	-1145.907439	-1145.687887
(S)-25	9	-672.495472	0.219354	-672.517452	-672.298098
(S)-26	25	-711.802894	0.246043	-711.825381	-711.579338
(S)-27	24	-829.730096	0.328652	-829.753582	-829.424930
(S)-28	19	-1184.993945	0.233971	-1185.020022	-1184.786051
(S)-30	10	-672.495409	0.218014	-672.518207	-672.300193
(R)-31	29	-751.111878	0.271680	-751.135505	-750.863825
(R)-32	12	-864.226140	0.267536	-864.253948	-863.986412
(R)-34	14	-558.167543	0.200565	-558.186378	-557.985813
(R)-35	12	-676.092365	0.281501	-676.112161	-675.830660
(R)-36	32	-789.206443	0.275308	-789.231944	-788.956636
(S)-38	4	-556.970328	0.181462	-556.990167	-556.808705
(S)-39	14	-714.203837	0.289450	-714.225570	-713.936120
(S)-41	27	-522.474229	0.243444	-522.490909	-522.247465
(S)-42	86	-601.090798	0.298104	-601.108241	-600.810137
(S)-43	80	-679.708421	0.352510	-679.726784	-679.374274
(S)-44	55	-753.513951	0.319978	-753.536245	-753.216267
(S)-46	36	-559.576558	0.236771	-559.590080	-559.353309
(R)-48	34	-445.054373	0.206195	-445.068473	-444.862278
(R)-49	31	-918.245845	0.195119	-918.263440	-918.068321
(S)-51	14	-602.289505	0.314841	-602.305220	-601.990379
(S)-52	10	-676.095255	0.280179	-676.115587	-675.835408

Table S1. Calculated energies of the most stable conformer found for each examined amide.

5.35. ^1H NMR, ^{13}C NMR, AND ESI-MS CHARACTERIZATIONS

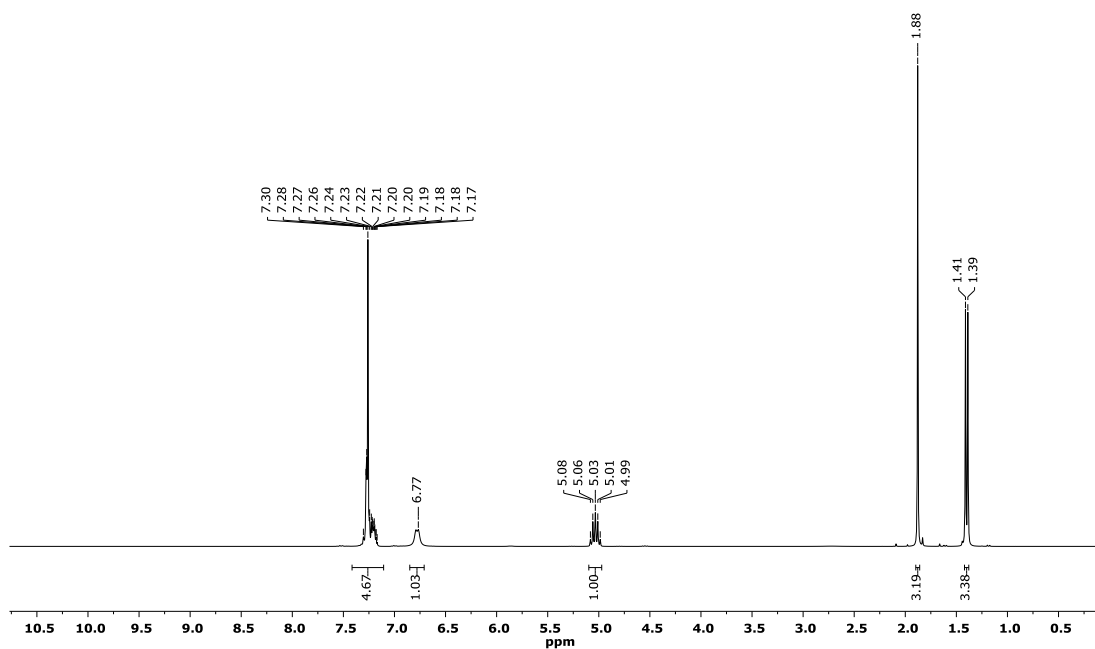


Figure S10. ^1H NMR spectrum (300 MHz, 301 K, CDCl_3) of amide (R)-14.

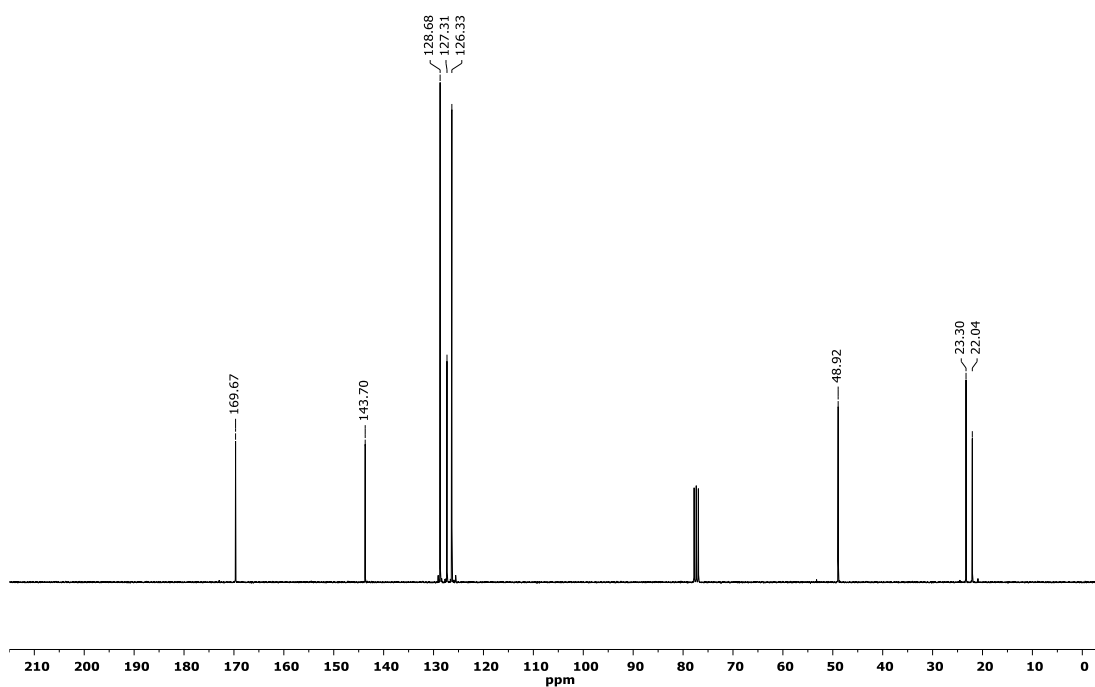


Figure S11. ^{13}C NMR spectrum (75 MHz, 301 K, CDCl_3) of amide (R)-14.

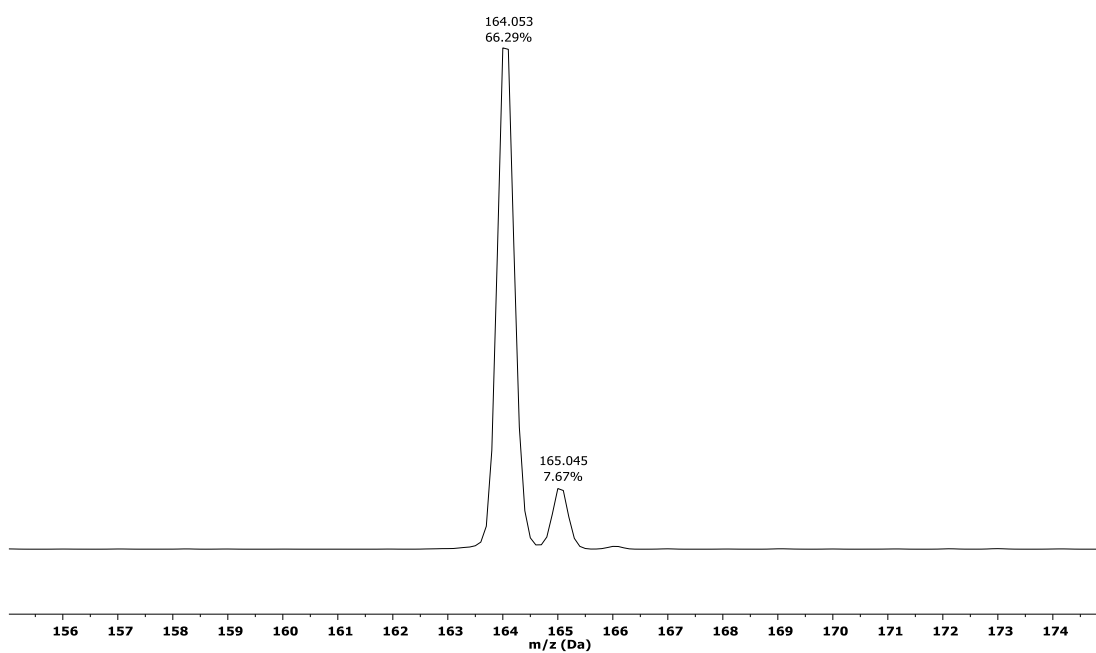


Figure S12. Experimental ESI-MS (ACN/H⁺) of amide (R)-14.

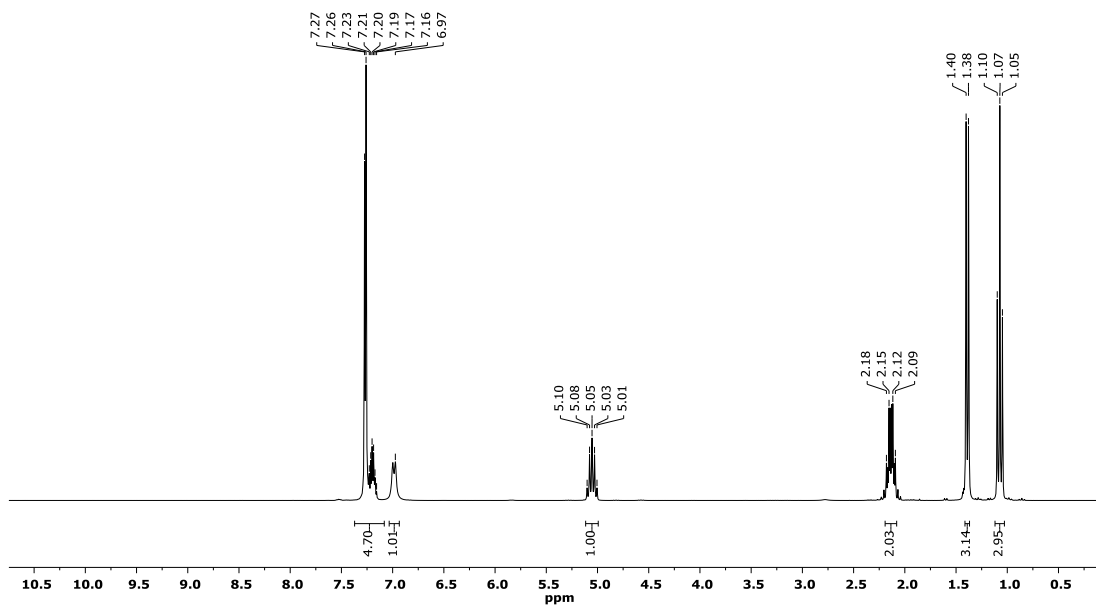


Figure S13. ¹H NMR spectrum (300 MHz, 301 K, CDCl₃) of amide (R)-15.

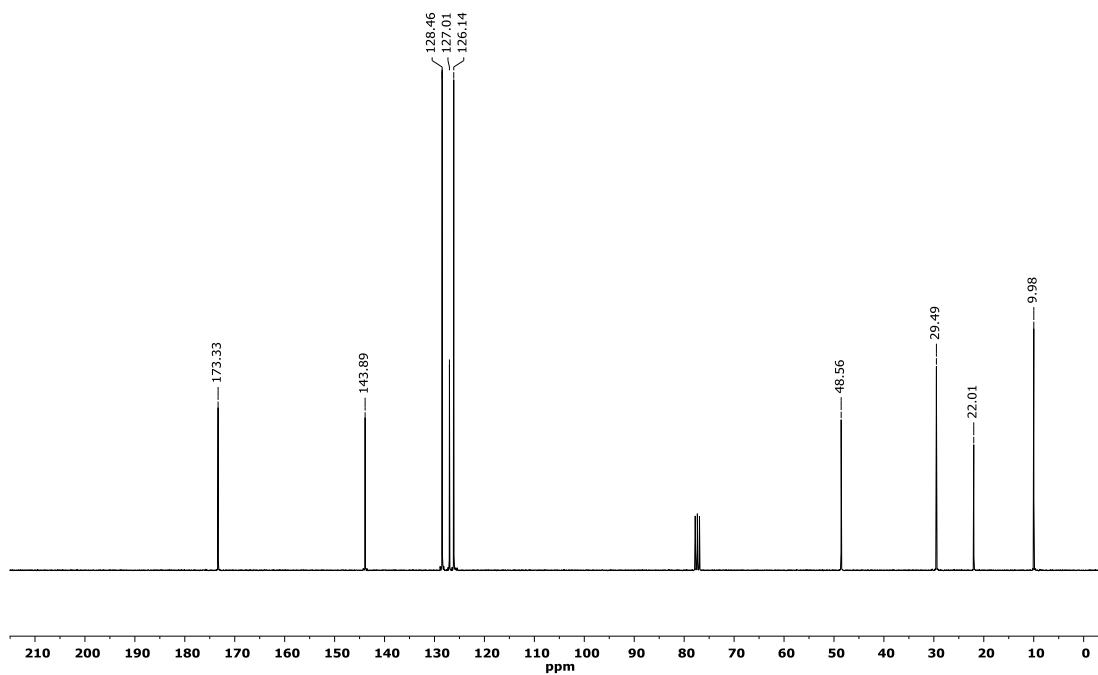


Figure S14. ^{13}C NMR spectrum (75 MHz, 301 K, CDCl_3) of amide (R)-15.

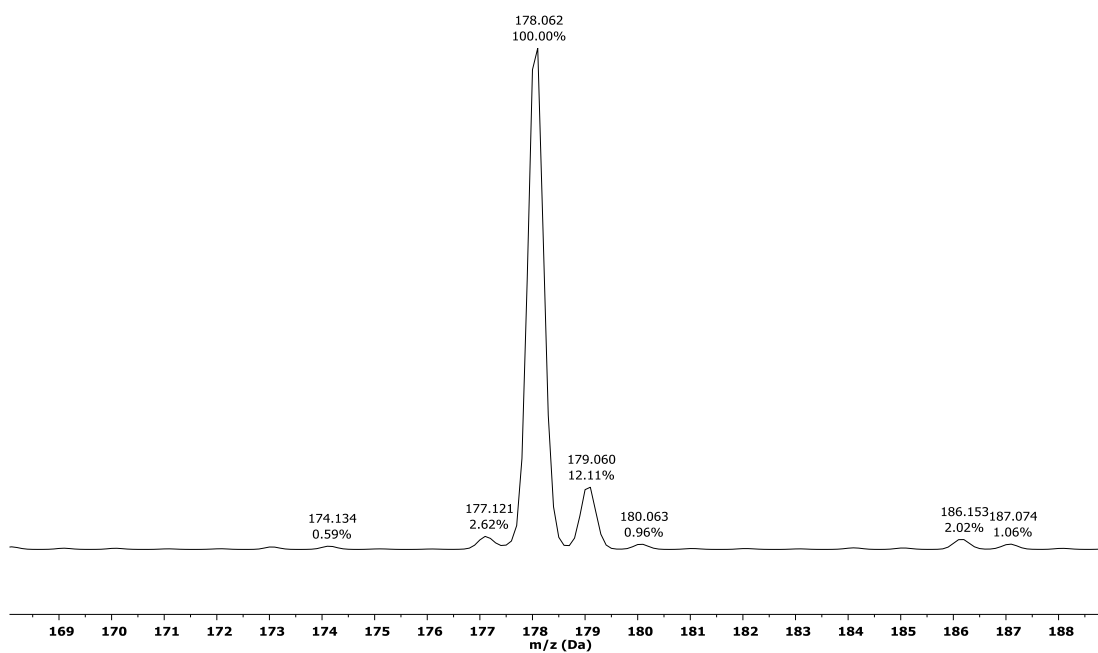


Figure S15. Experimental ESI-MS (ACN/H^+) of amide (R)-15.

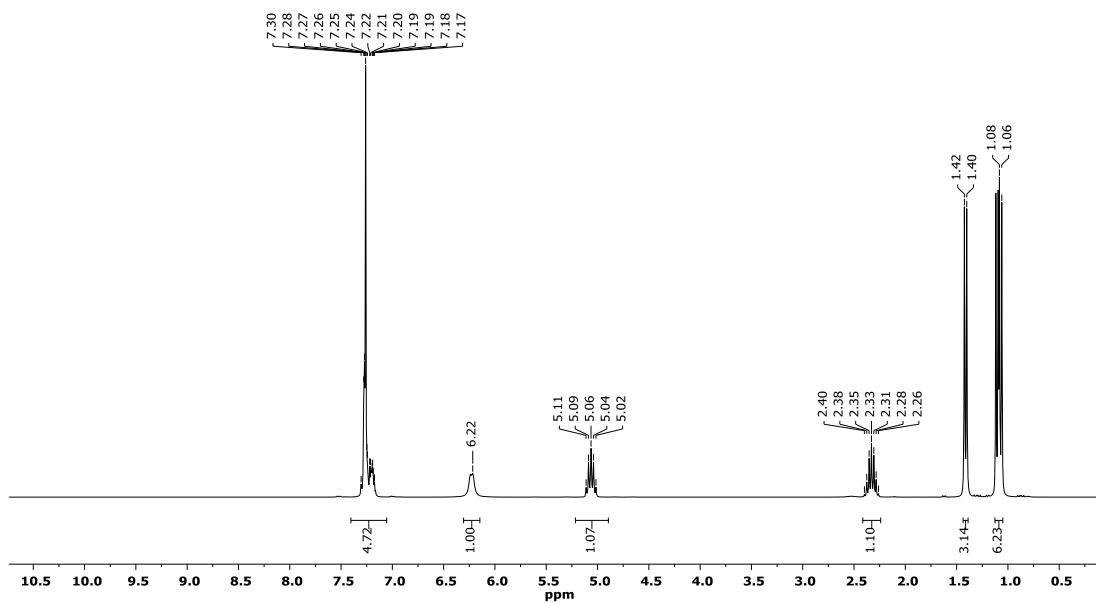


Figure S16. ^1H NMR spectrum (300 MHz, 301 K, CDCl_3) of amide (R)-16.

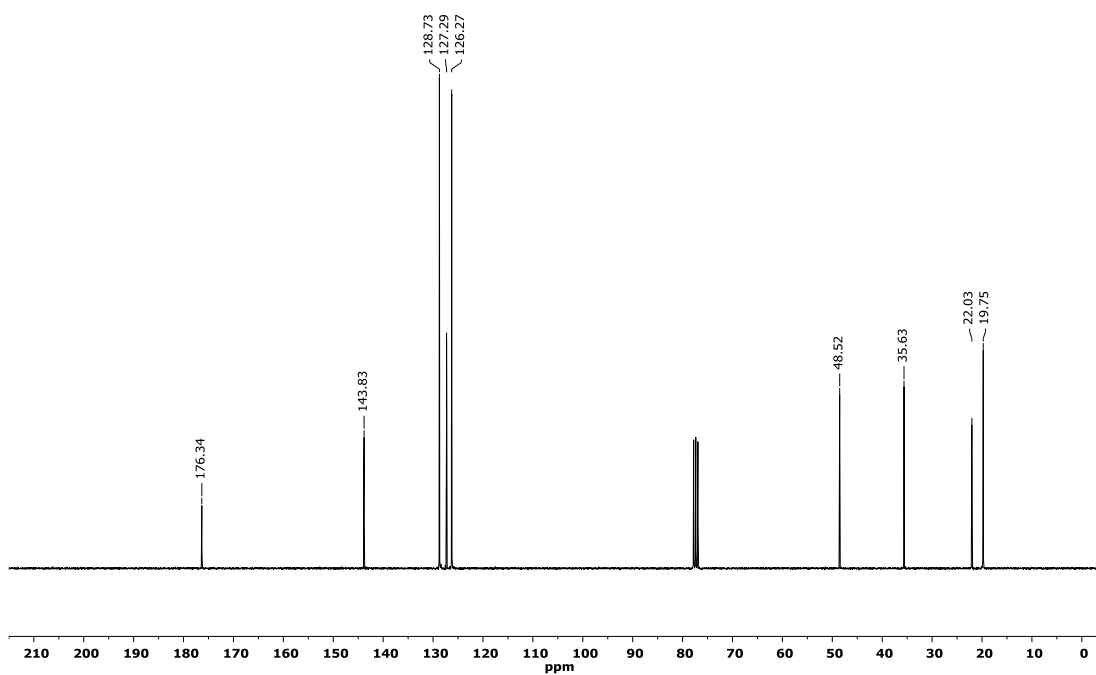


Figure S17. ^{13}C NMR spectrum (75 MHz, 301 K, CDCl_3) of amide (R)-16.

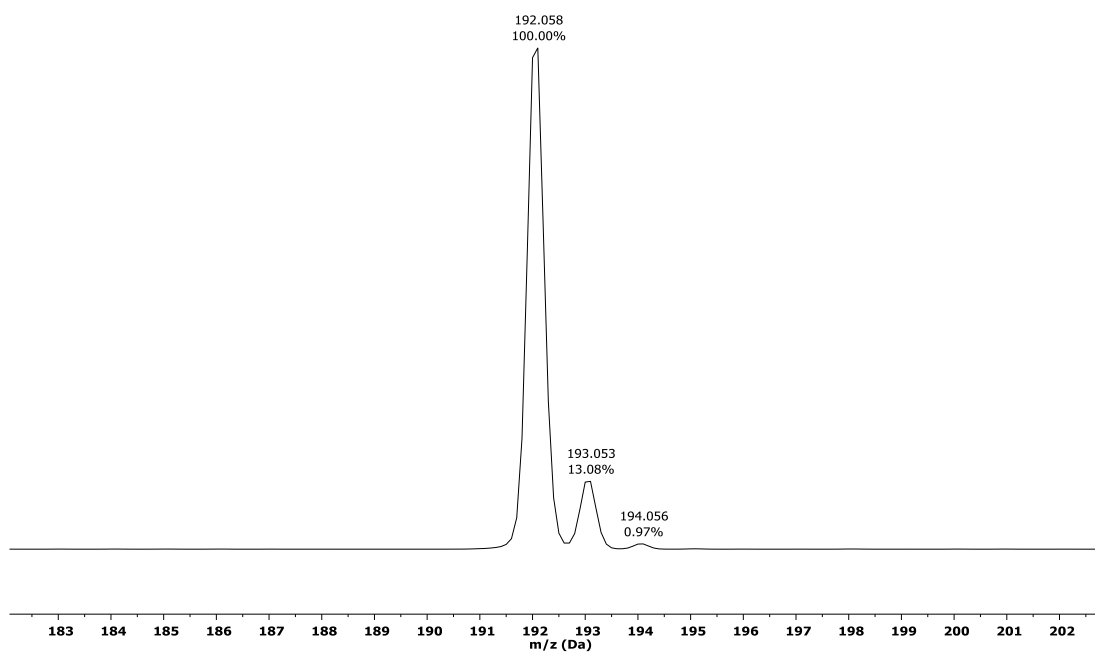


Figure S18. Experimental ESI-MS (ACN/H^+) of amide (R)-16.

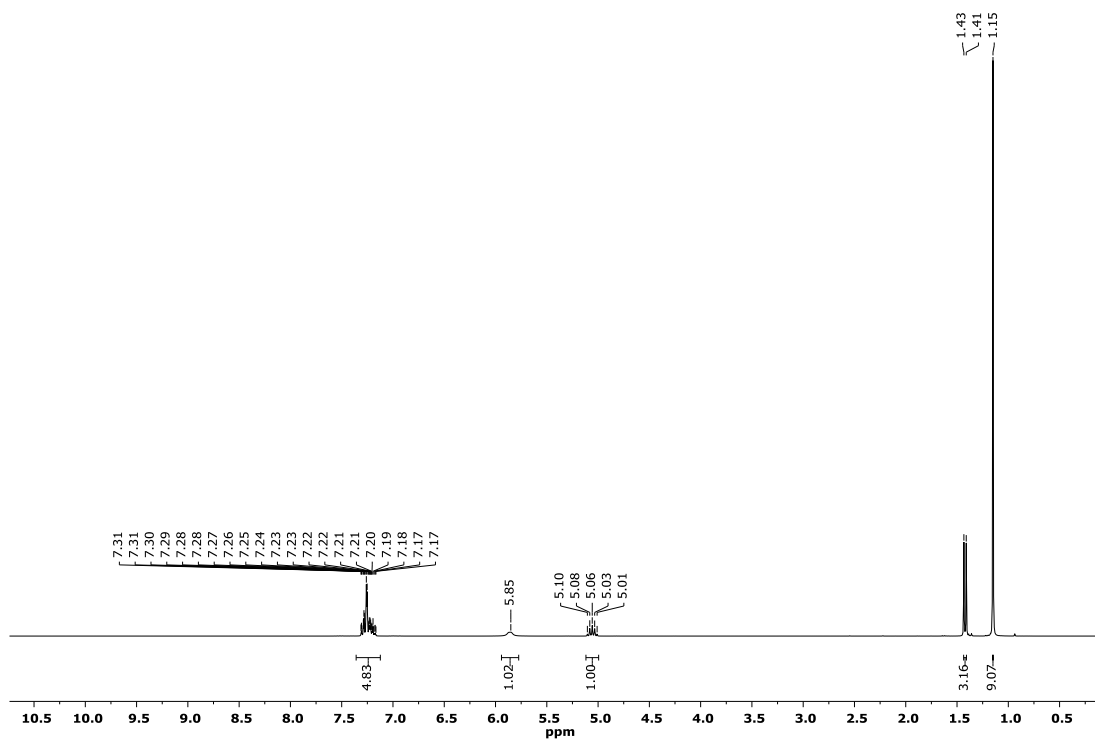


Figure S19. 1H NMR spectrum (300 MHz, 301 K, $CDCl_3$) of amide (R)-17.

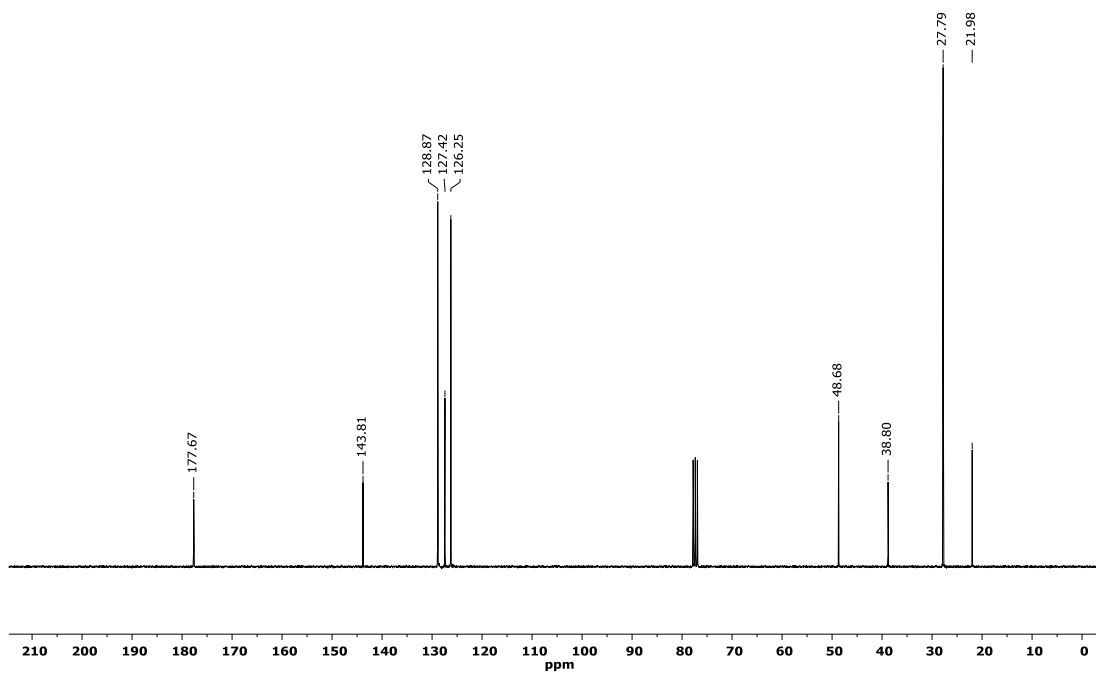


Figure S20. ^{13}C NMR spectrum (75 MHz, 301 K, CDCl_3) of amide (R)-17.

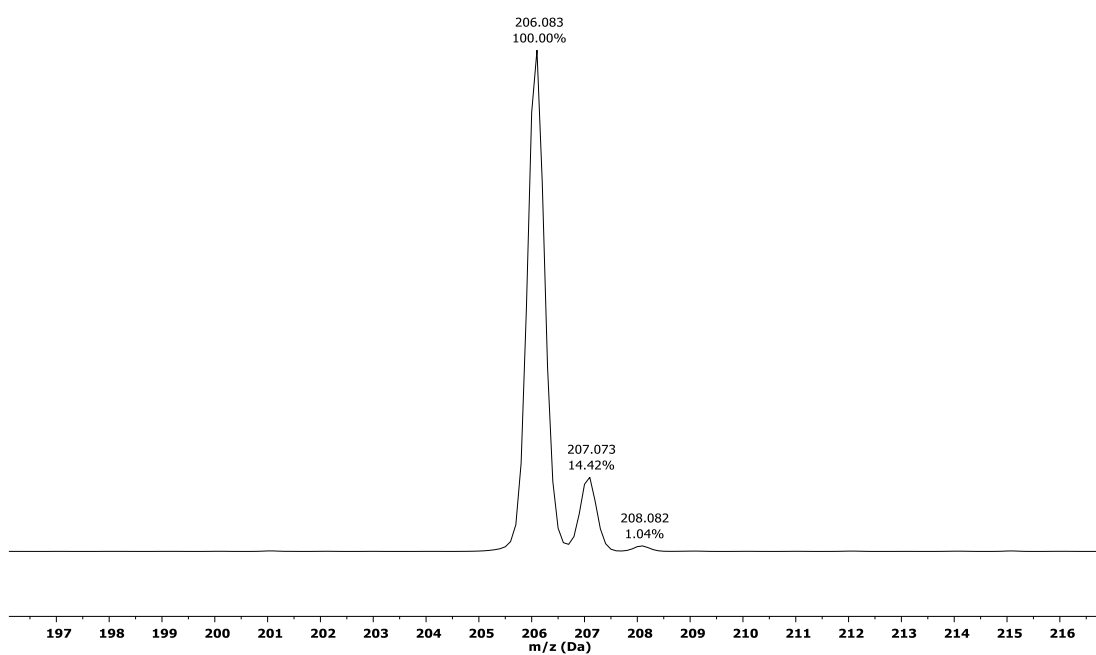


Figure S21. Experimental ESI-MS (ACN/H^+) of amide (R)-17.

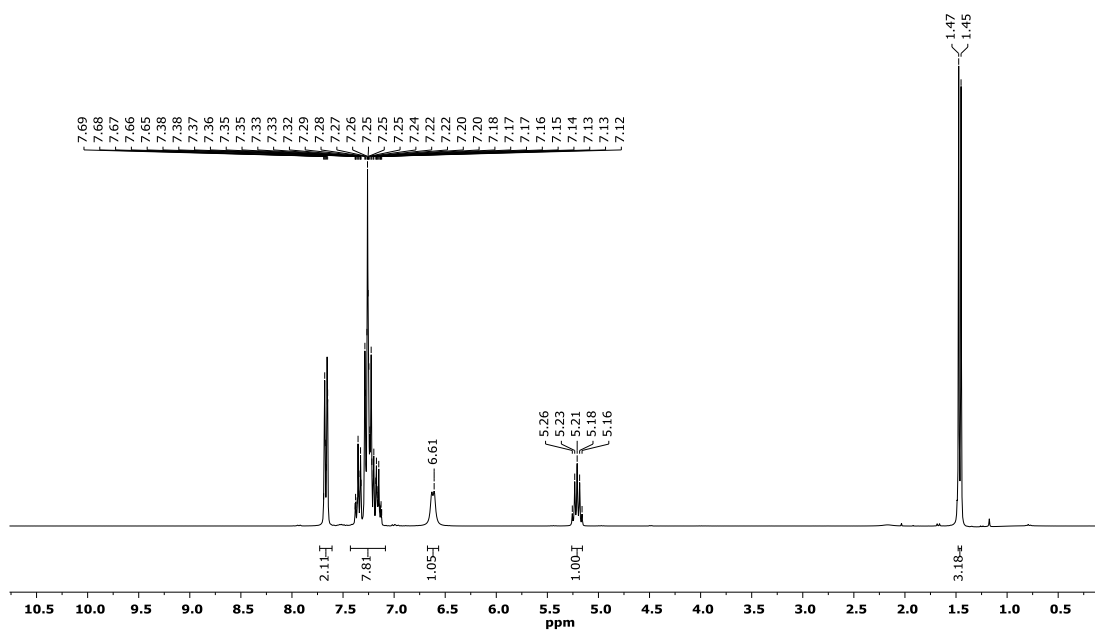


Figure S22. ^1H NMR spectrum (300 MHz, 301 K, CDCl_3) of amide (R)-18.

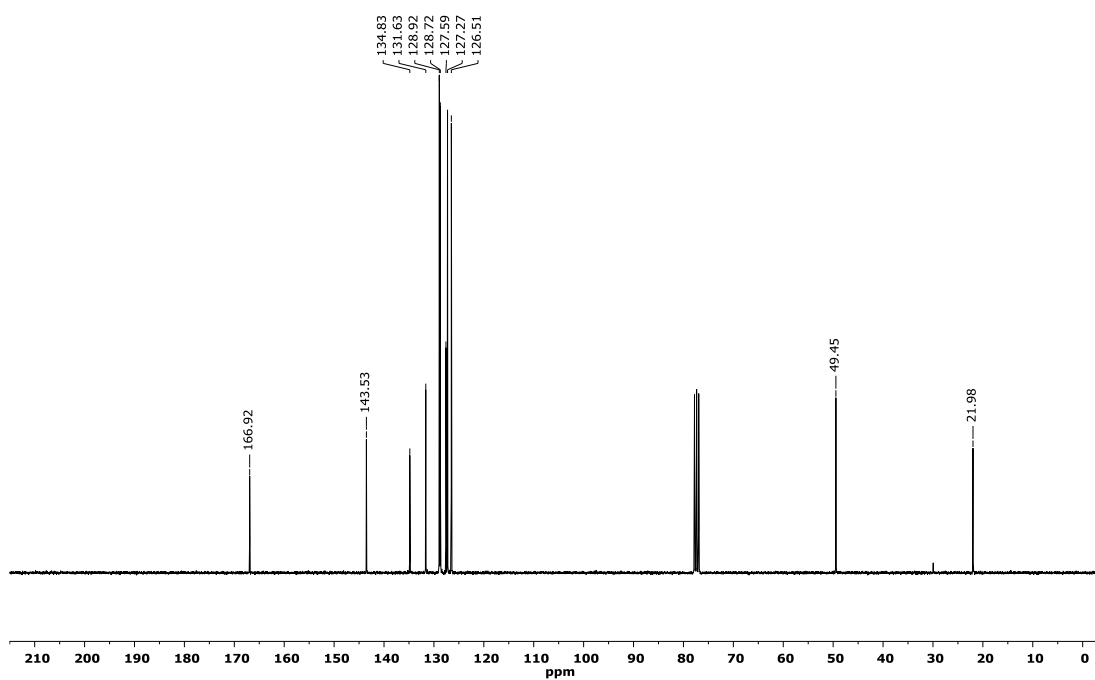


Figure S23. ^{13}C NMR spectrum (75 MHz, 301 K, CDCl_3) of amide (R)-18.

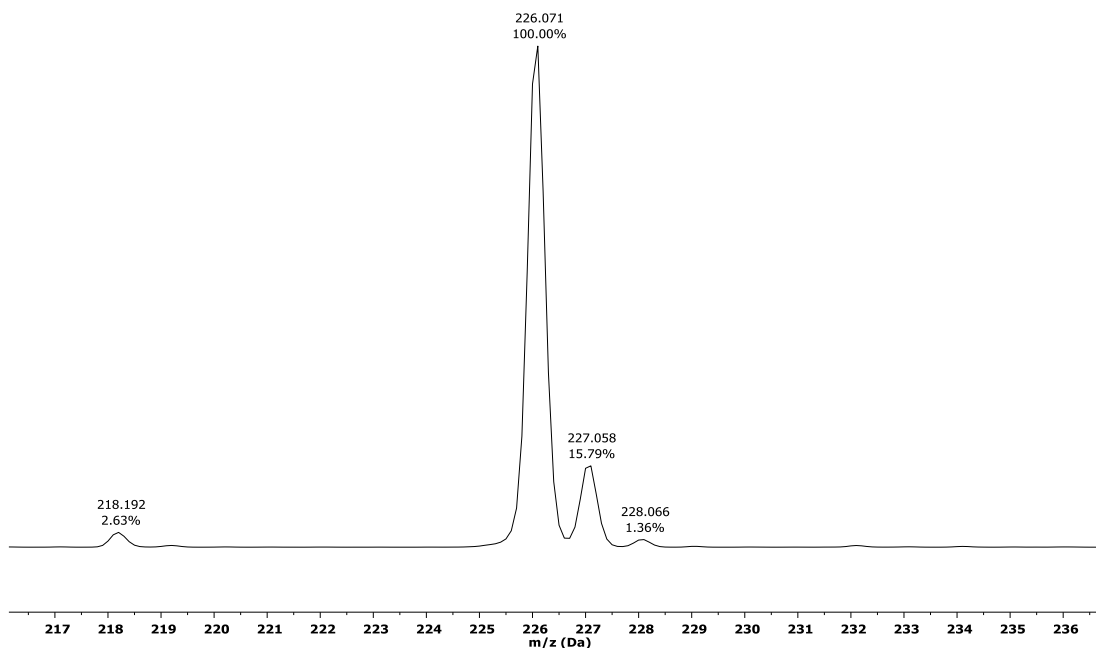


Figure S24. Experimental ESI-MS (ACN/H^+) of amide (R)-18.

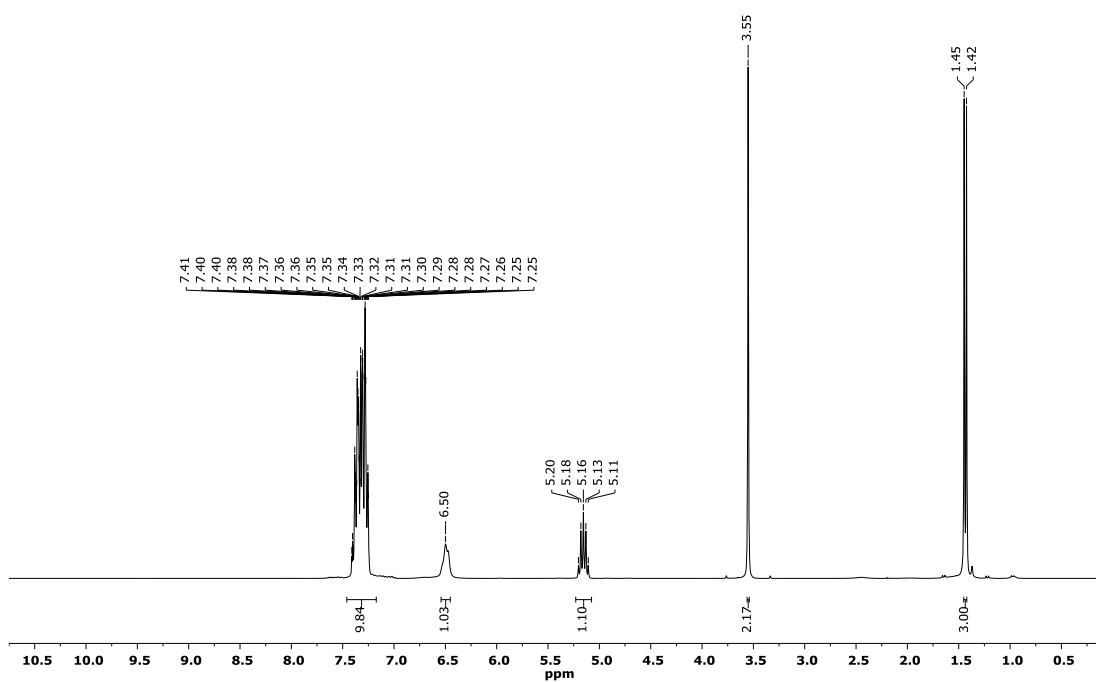


Figure S25. 1H NMR spectrum (300 MHz, 301 K, $CDCl_3$) of amide (R)-19.

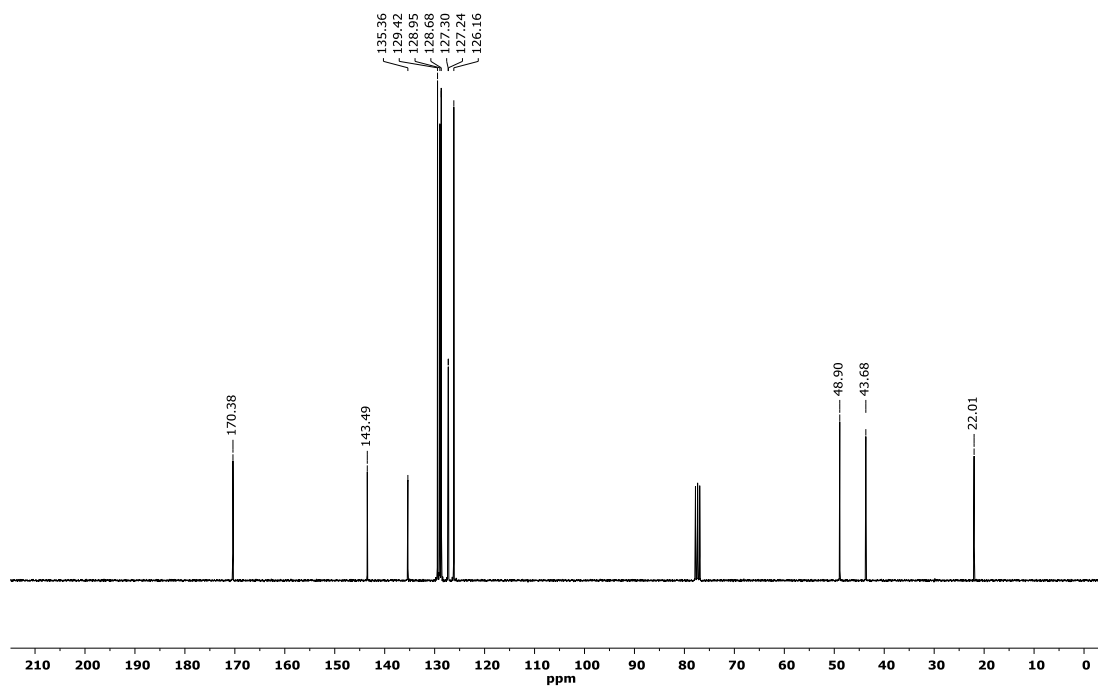


Figure S26. ^{13}C NMR spectrum (75 MHz, 301 K, CDCl_3) of amide (R)-19.

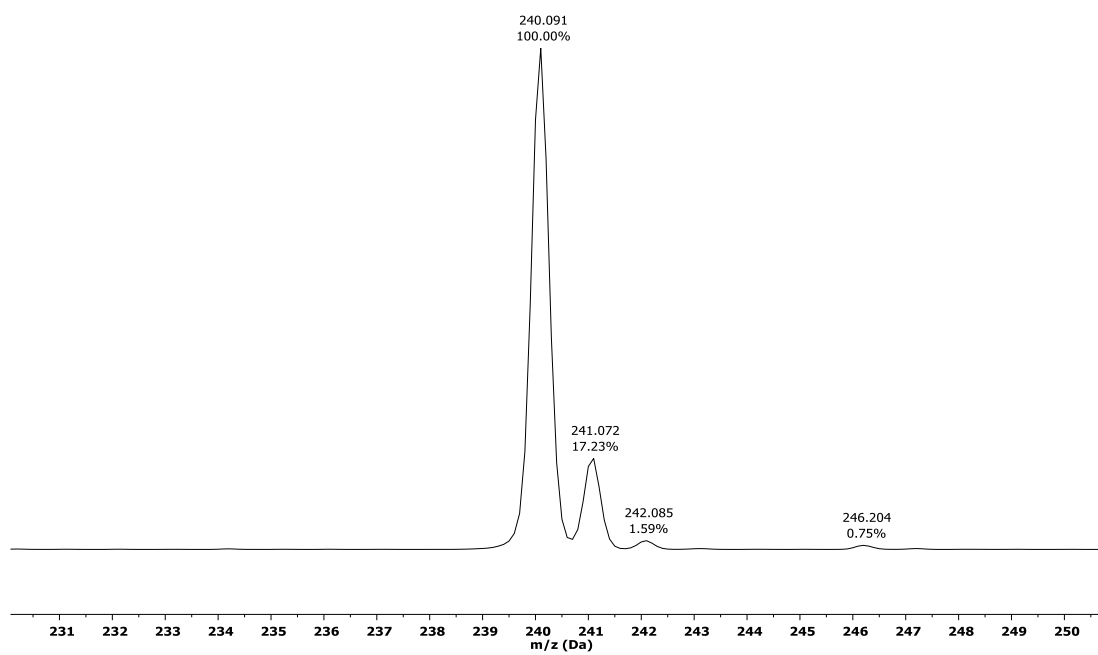


Figure S27. Experimental ESI-MS (ACN/H^+) of amide (R)-19.

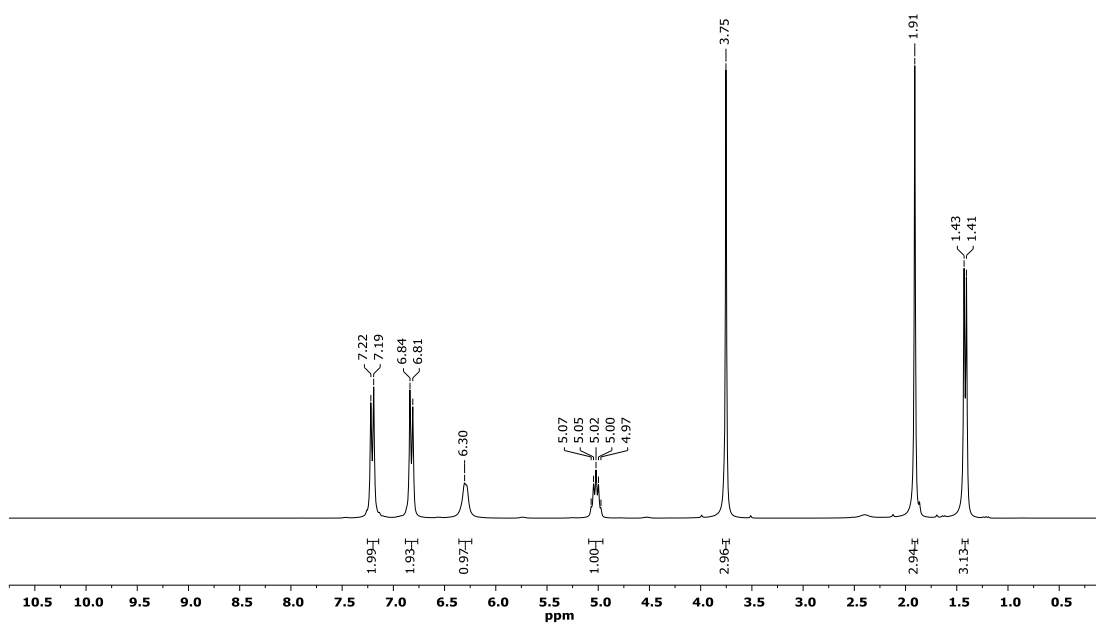


Figure S28. ^1H NMR spectrum (300 MHz, 301 K, CDCl_3) of amide (R)-21.

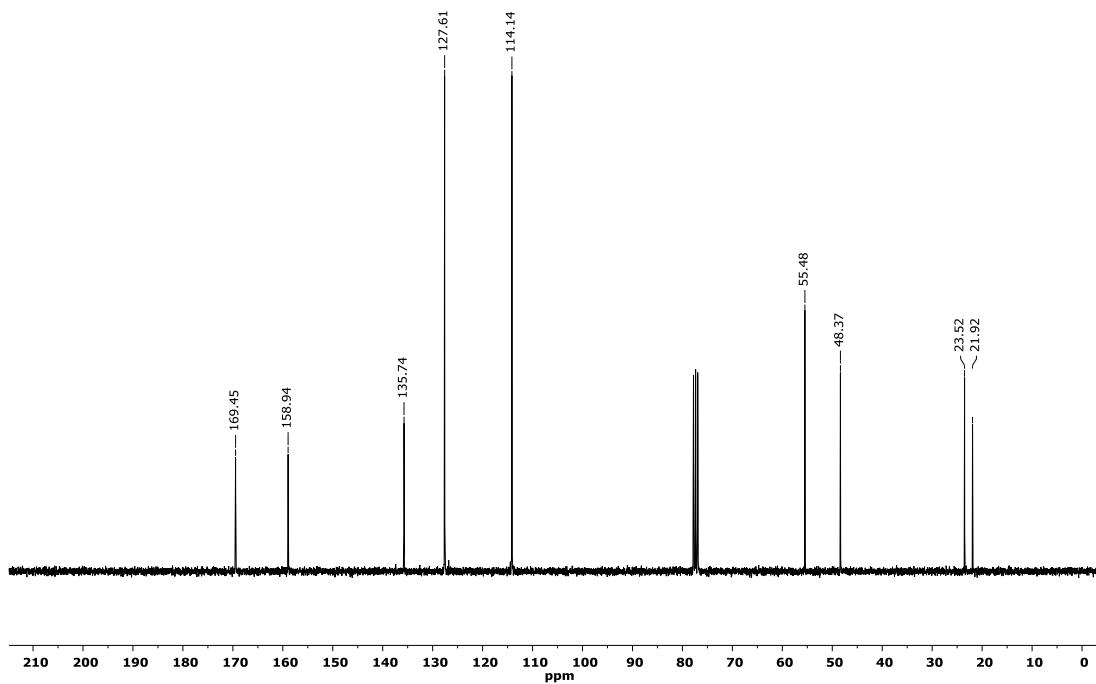


Figure S29. ^{13}C NMR spectrum (75 MHz, 301 K, CDCl_3) of amide (R)-21.

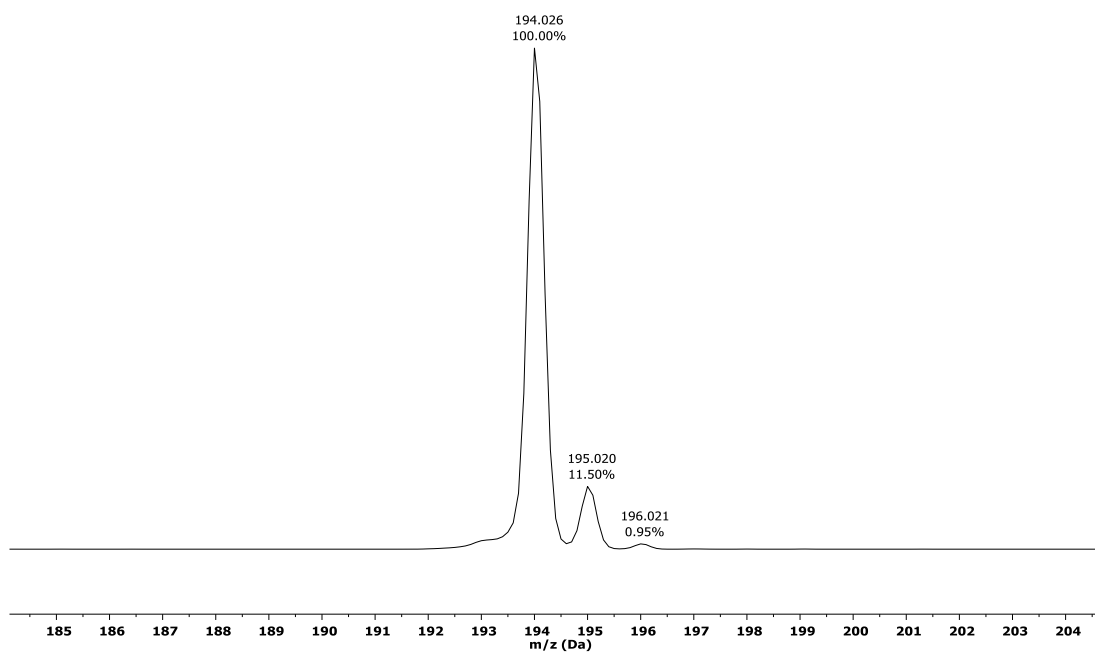


Figure S30. Experimental ESI-MS (ACN/H^+) of amide (R)-21.

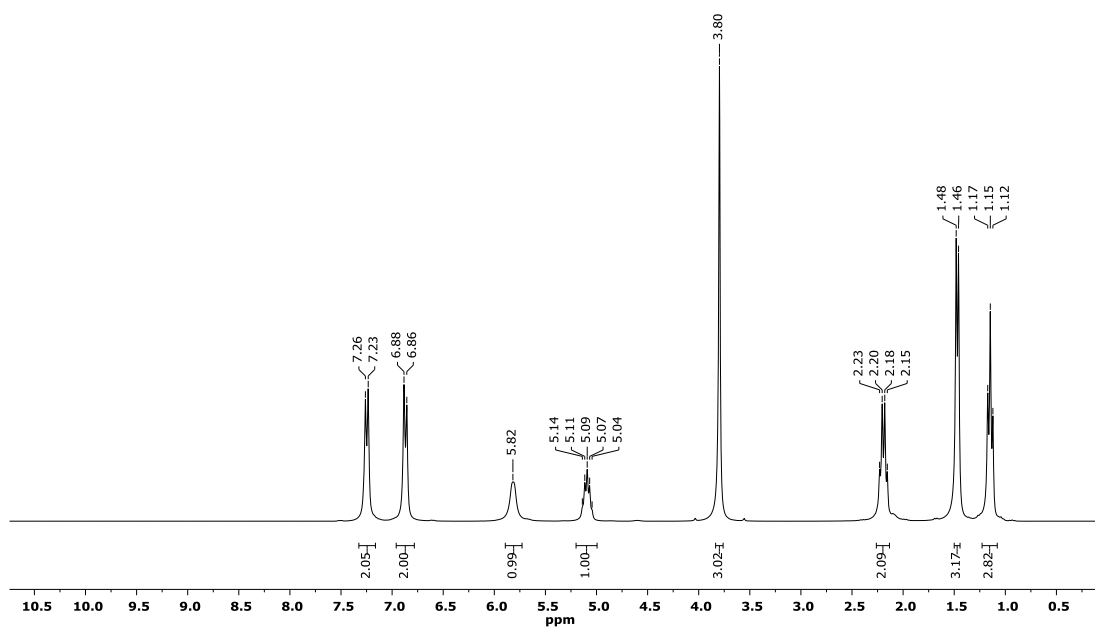


Figure S31. 1H NMR spectrum (300 MHz, 301 K, $CDCl_3$) of amide (R)-22.

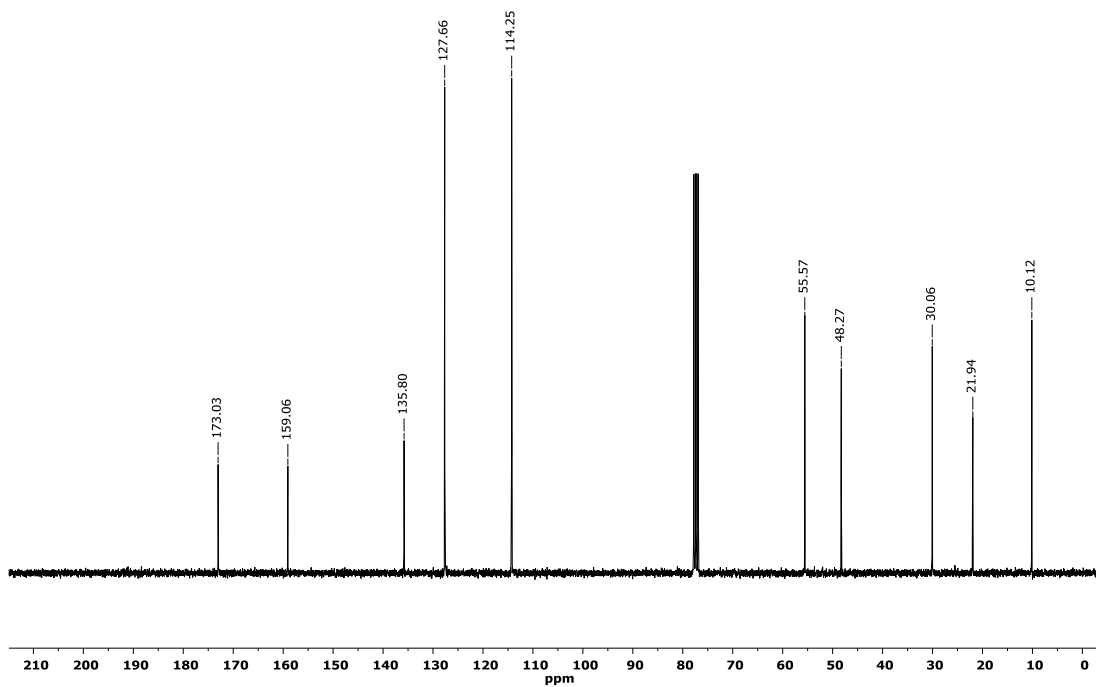


Figure S32. ^{13}C NMR spectrum (75 MHz, 301 K, CDCl_3) of amide (R)-22.

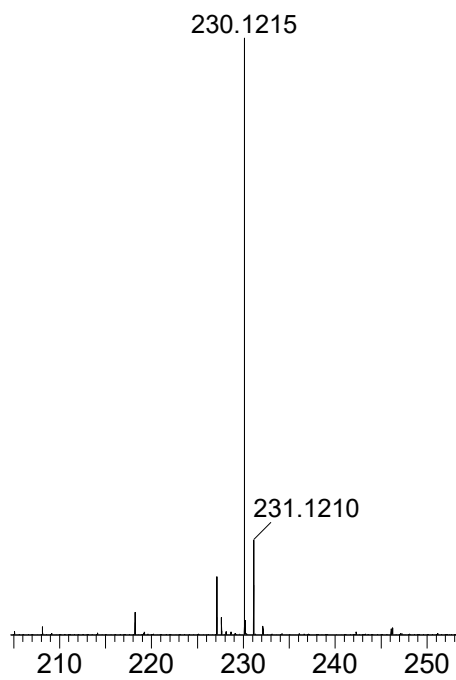


Figure S33. Experimental ESI-MS ($\text{H}_2\text{O}/\text{ACN}$ 50:50 + 0.1% formic acid) of amide (R)-22 $[\text{M}+\text{Na}]^+$.

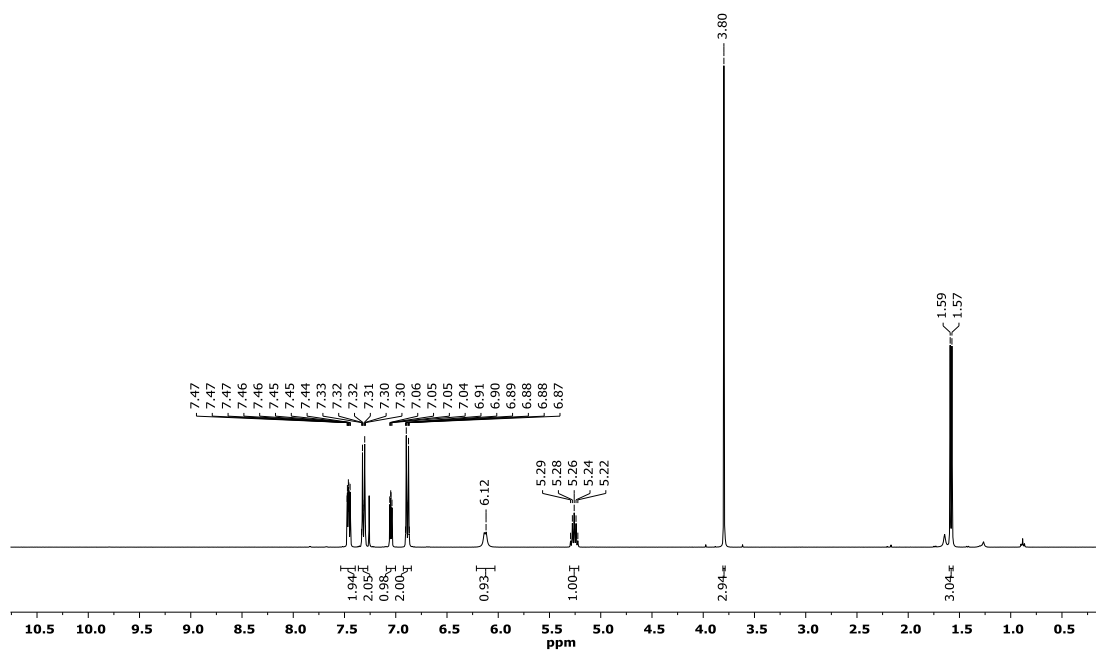


Figure S34. ^1H NMR spectrum (400 MHz, 301 K, CDCl_3) of amide (R)-23.

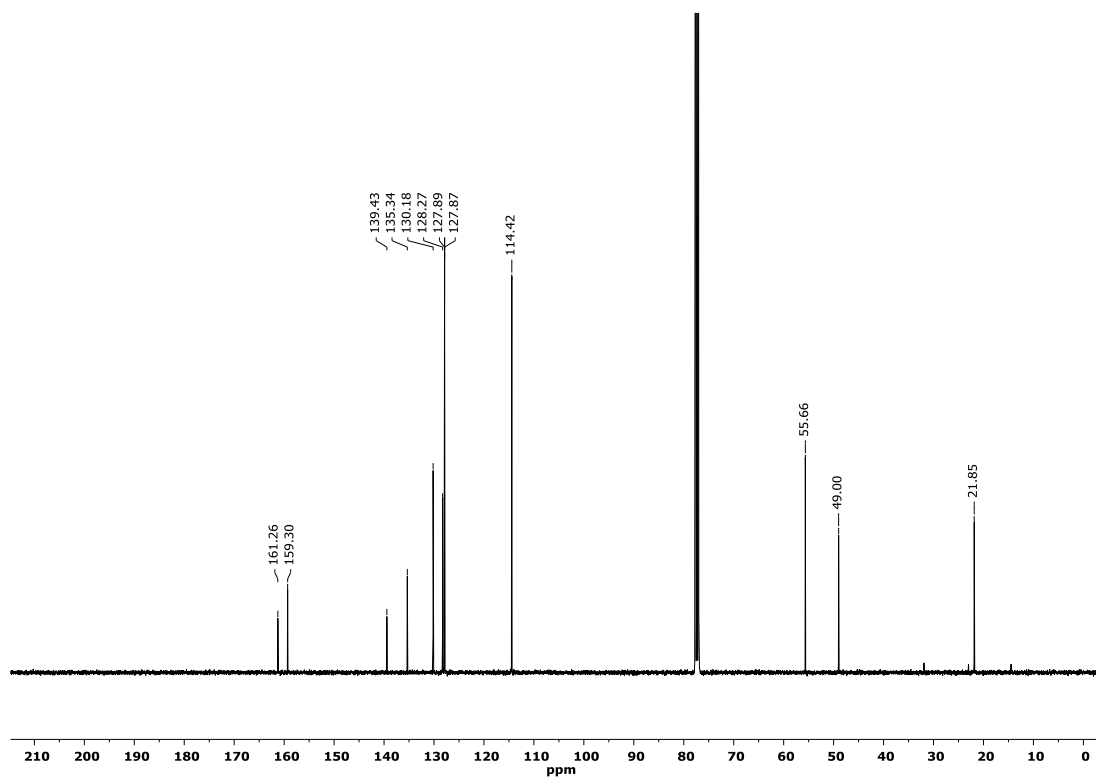


Figure S35. ^{13}C NMR spectrum (100 MHz, 301 K, CDCl_3) of amide (R)-23.

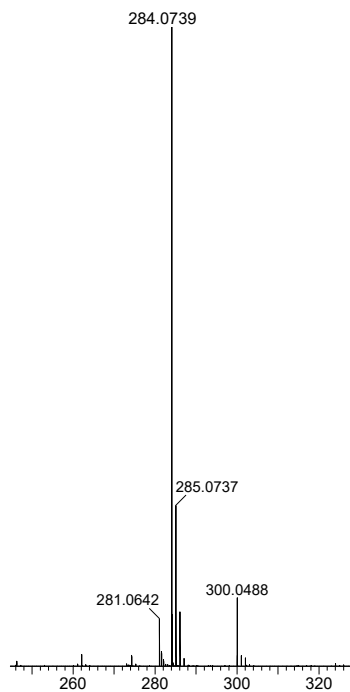


Figure S36. Experimental ESI-MS (H_2O/ACN 50:50 + 0.1% formic acid) of amide (R)-23 $[M+Na]^+$.

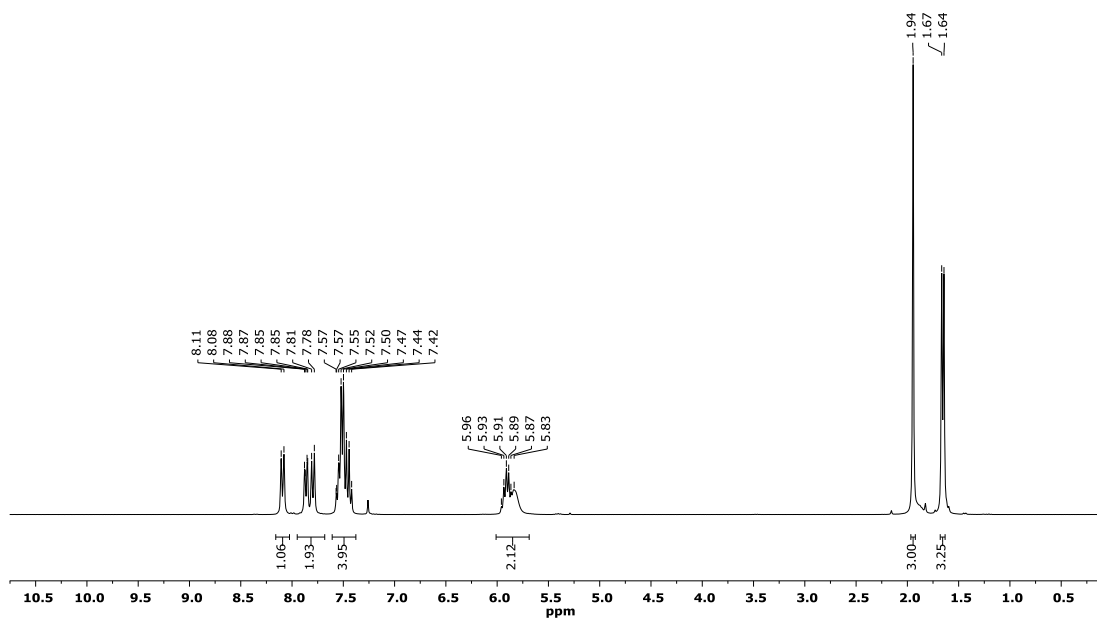


Figure S37. 1H NMR spectrum (300 MHz, 301 K, $CDCl_3$) of amide (S)-25.

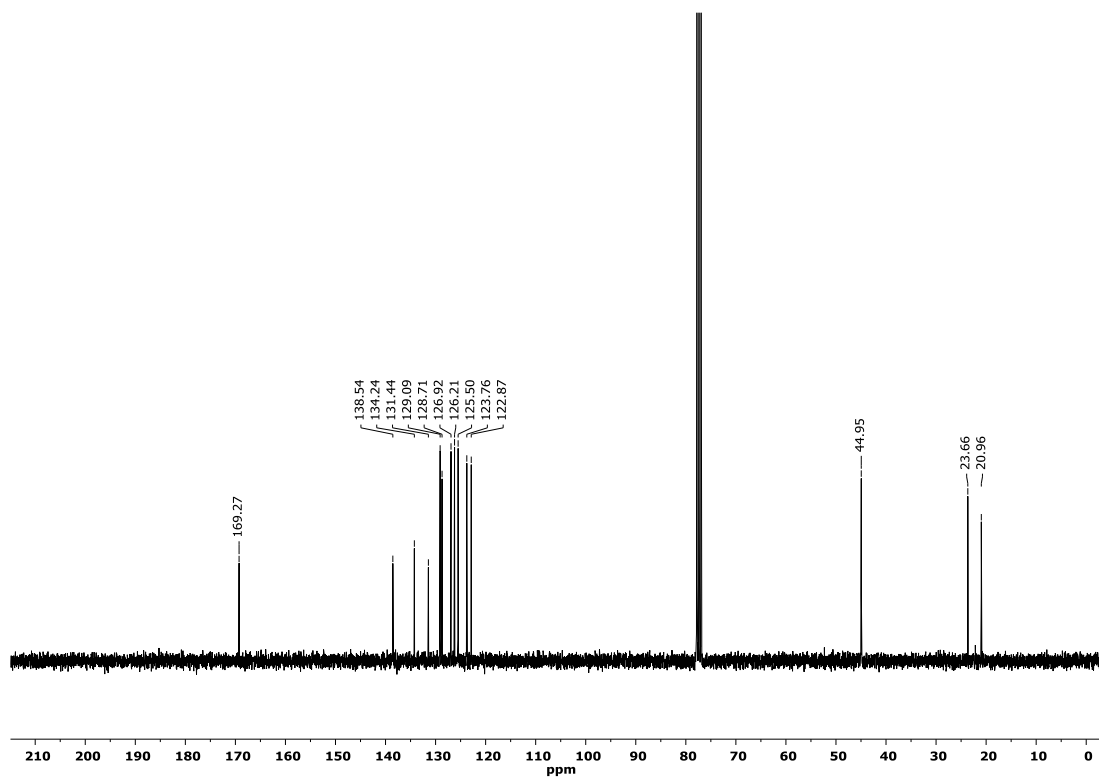


Figure S38. ^{13}C NMR spectrum (75 MHz, 301 K, CDCl_3) of amide (S)-25.

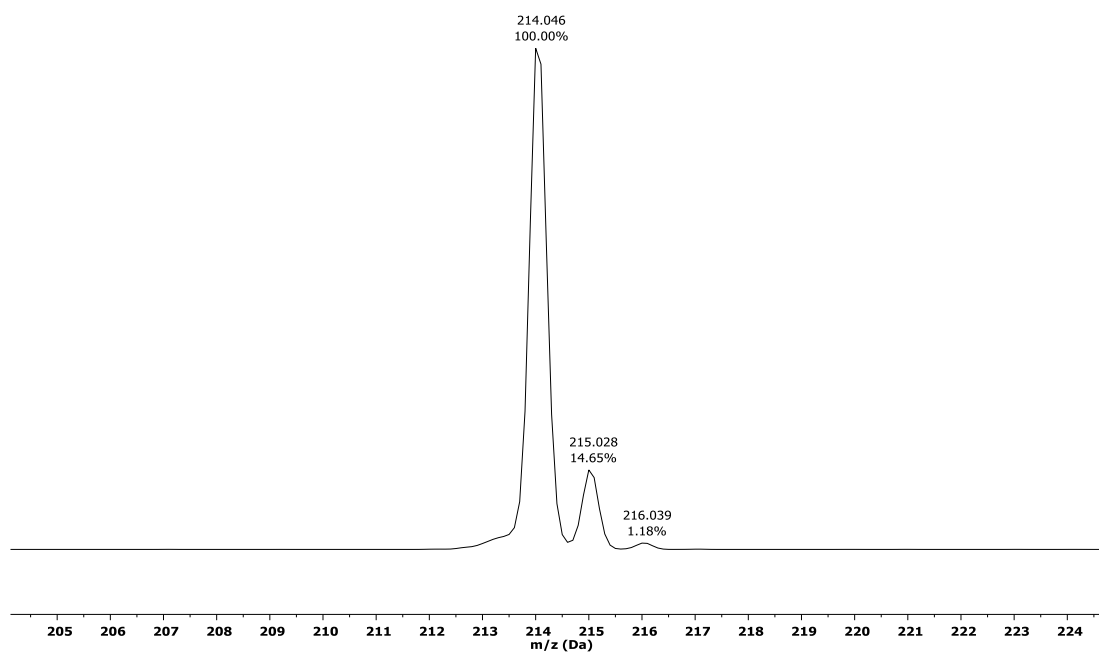


Figure S39. Experimental ESI-MS (ACN/H^+) of amide (S)-25.

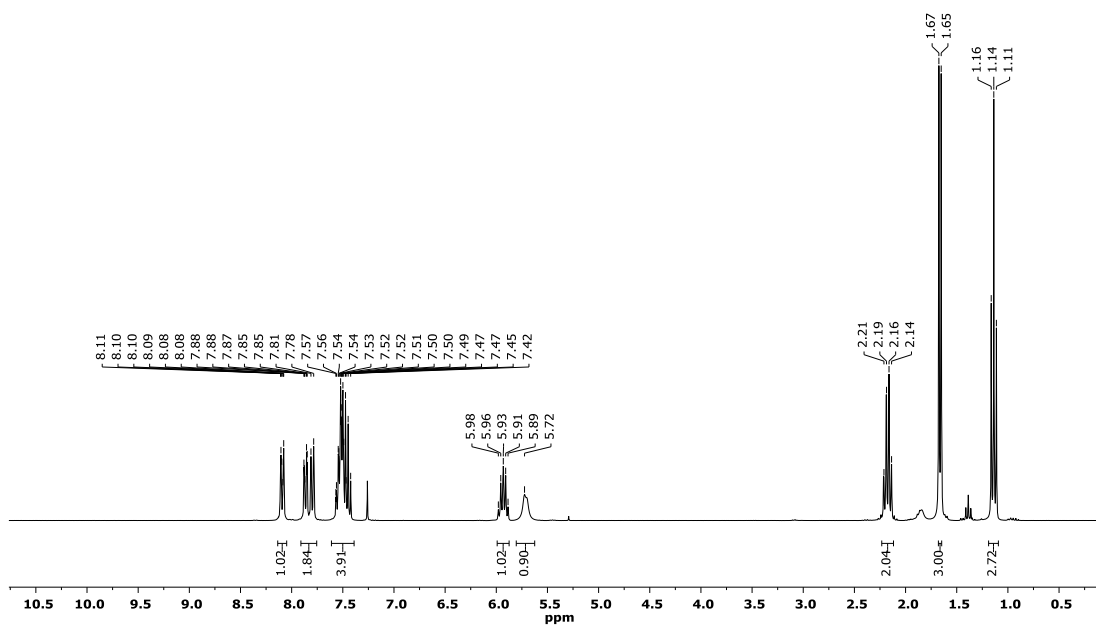


Figure S40. ^1H NMR spectrum (300 MHz, 301 K, CDCl_3) of amide (S)-26.

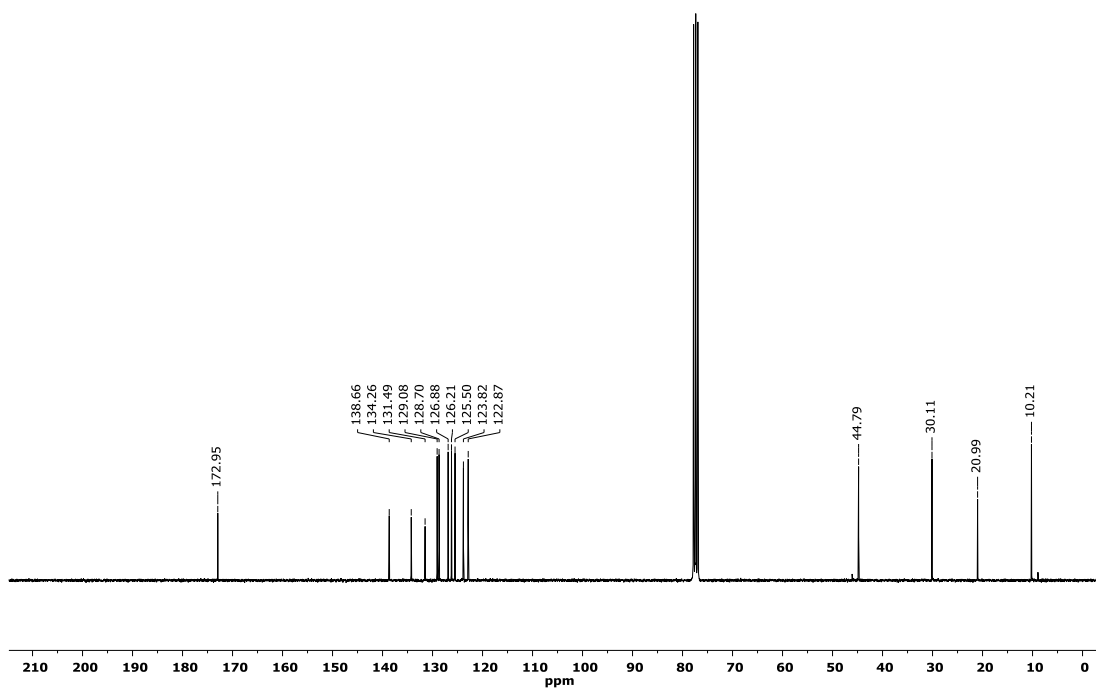


Figure S41. ^{13}C NMR spectrum (75 MHz, 301 K, CDCl_3) of amide (S)-26.

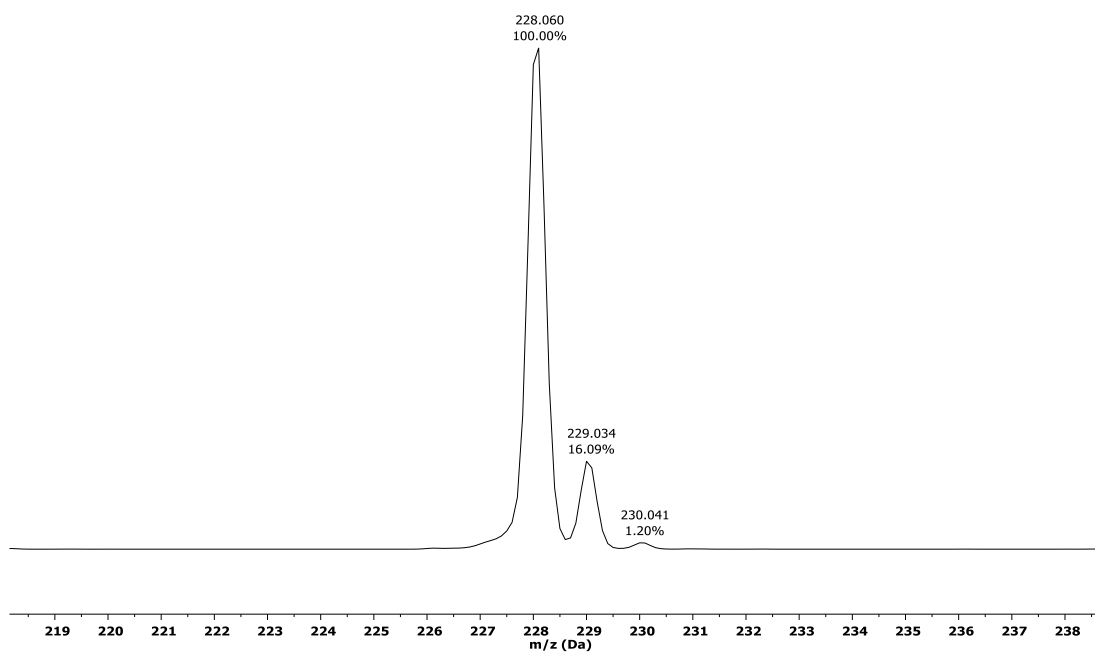


Figure S42. Experimental ESI-MS (ACN/H^+) of amide (S)-26.

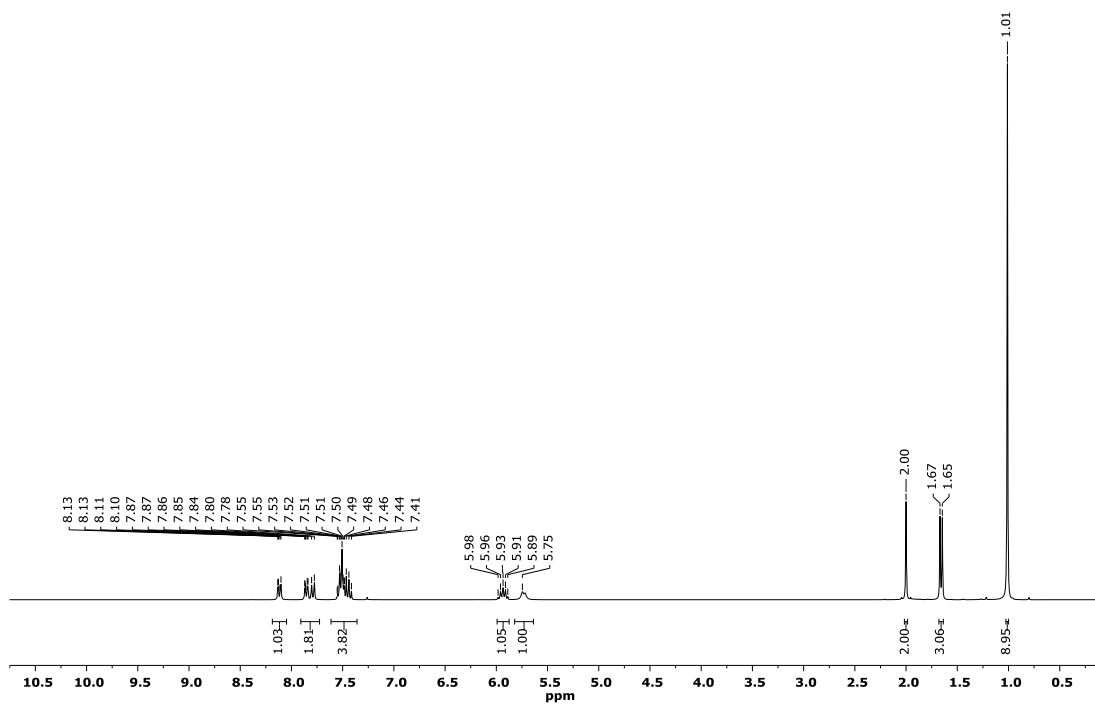


Figure S43. 1H NMR spectrum (300 MHz, 301 K, $CDCl_3$) of amide (S)-27.

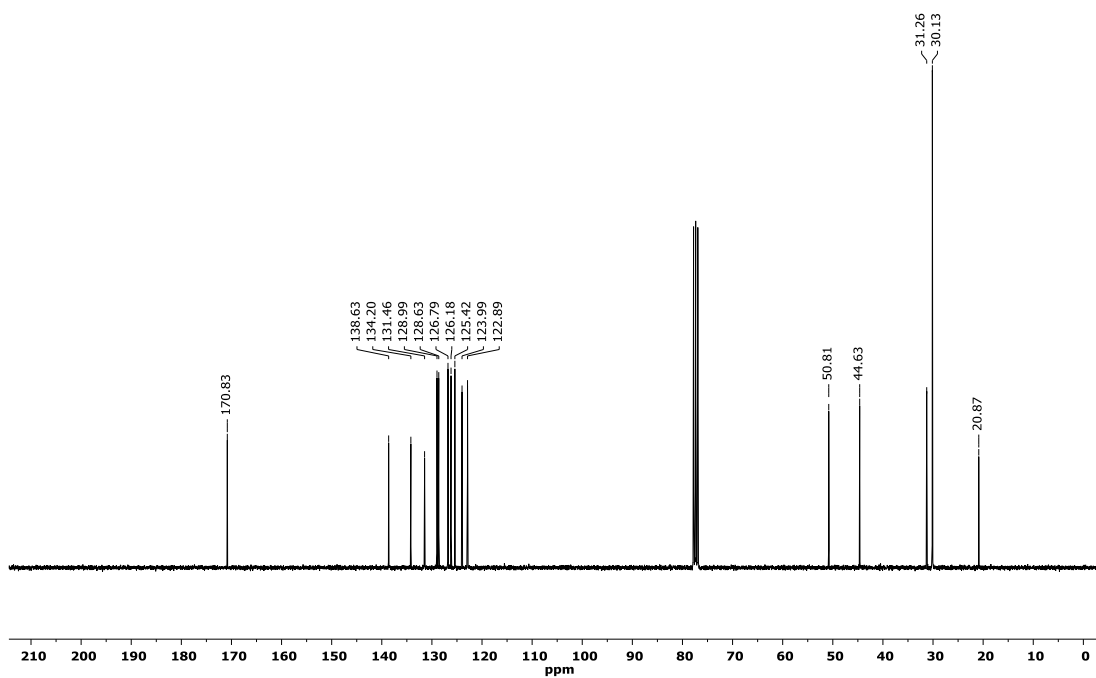


Figure S44. ^{13}C NMR spectrum (75 MHz, 301 K, CDCl_3) of amide (S)-27.

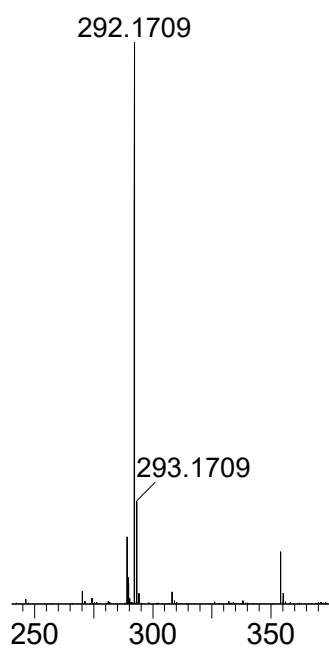


Figure S45. Experimental ESI-MS ($\text{H}_2\text{O}/\text{ACN}$ 50:50 + 0.1% formic acid) of amide (S)-27 $[\text{M}+\text{Na}]^+$.

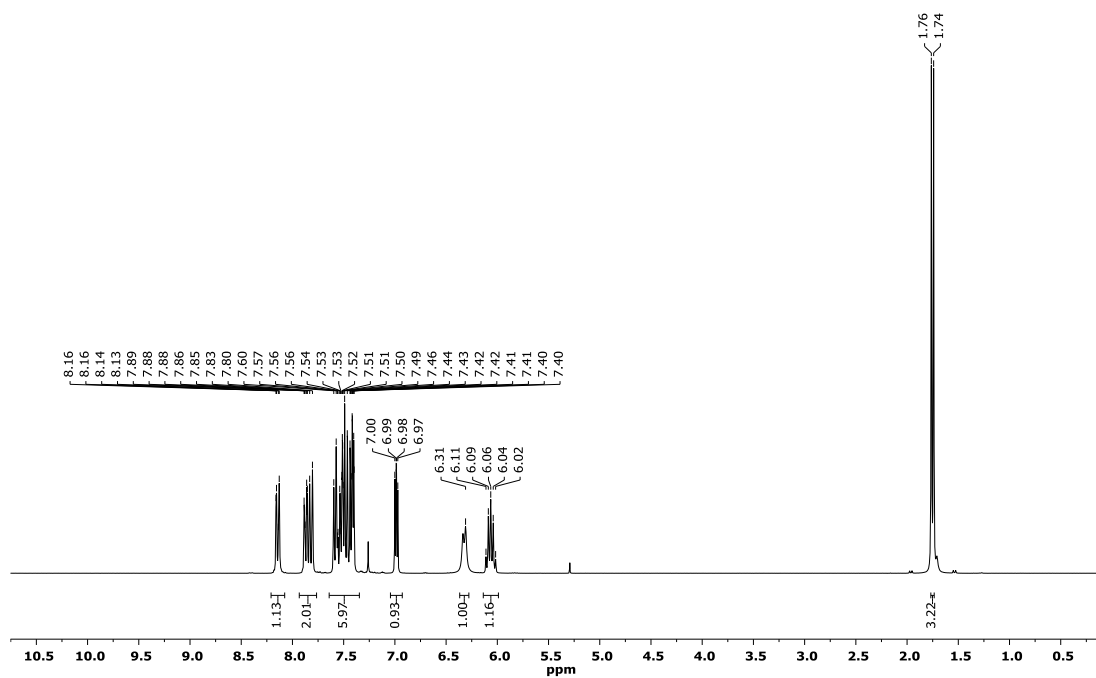


Figure S46. ^1H NMR spectrum (300 MHz, 301 K, CDCl_3) of amide (S)-28.

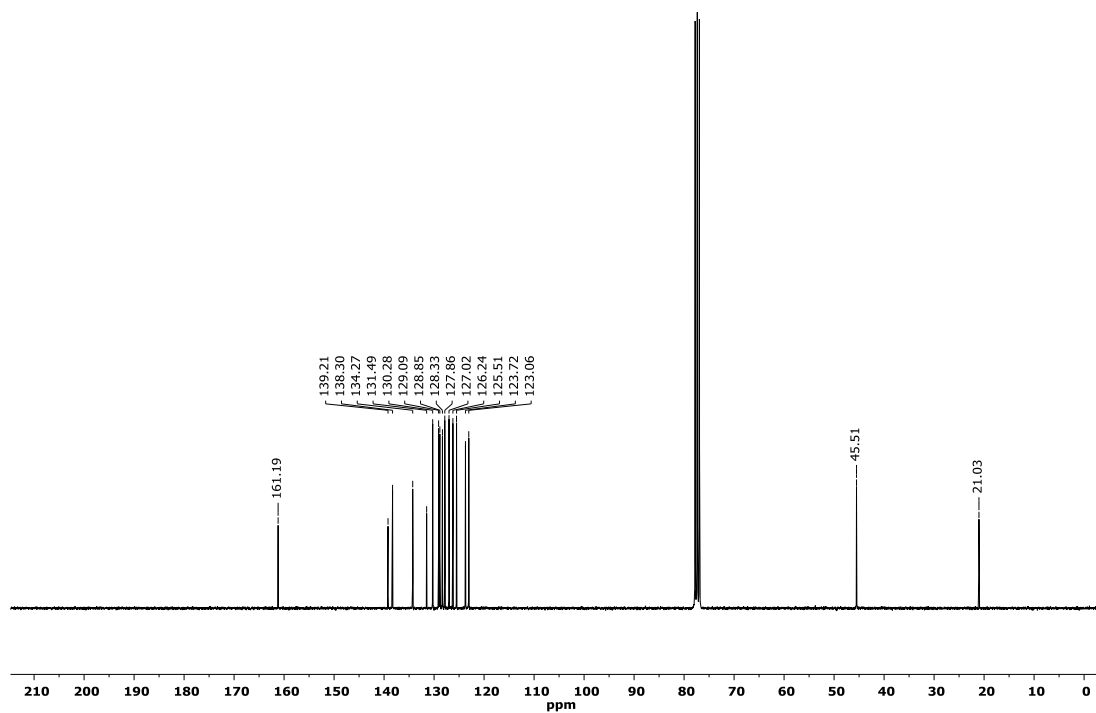


Figure S47. ^{13}C NMR spectrum (75 MHz, 301 K, CDCl_3) of amide (S)-28.

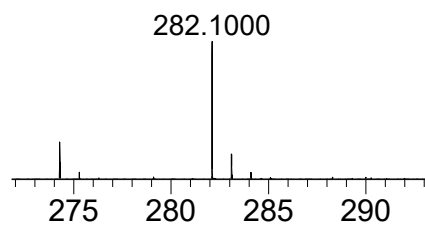


Figure S48. Experimental ESI-MS (H_2O/ACN 50:50 + 0.1% formic acid) of amide (S)-28.

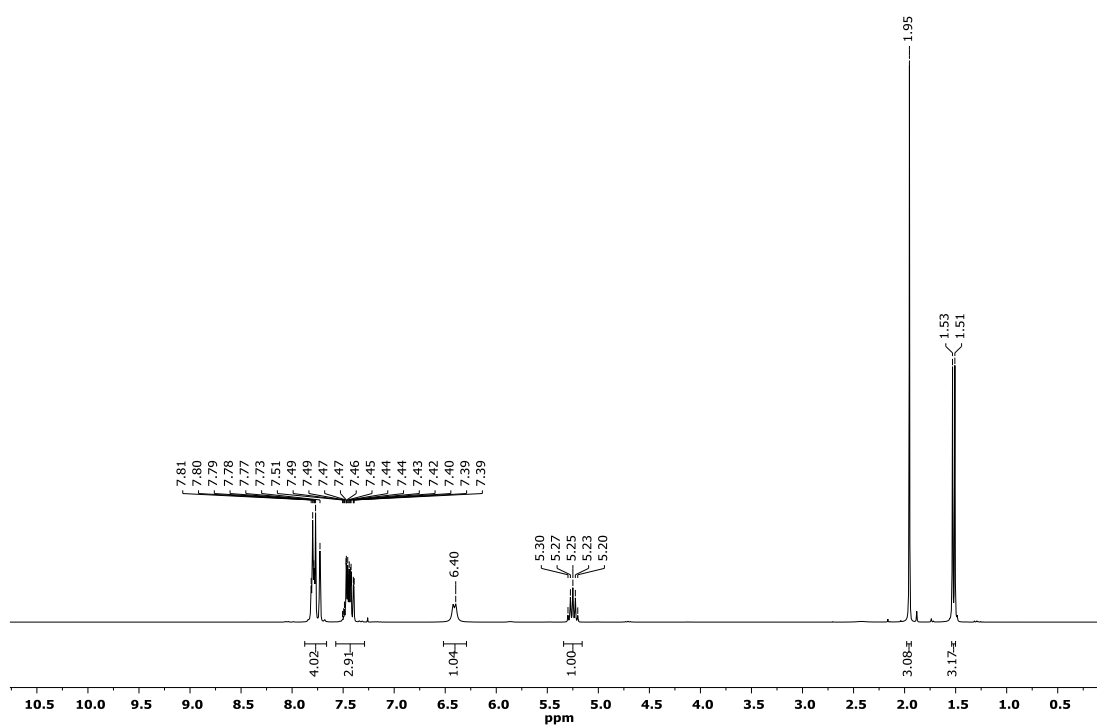


Figure S49. 1H NMR spectrum (300 MHz, 301 K, $CDCl_3$) of amide (S)-30.

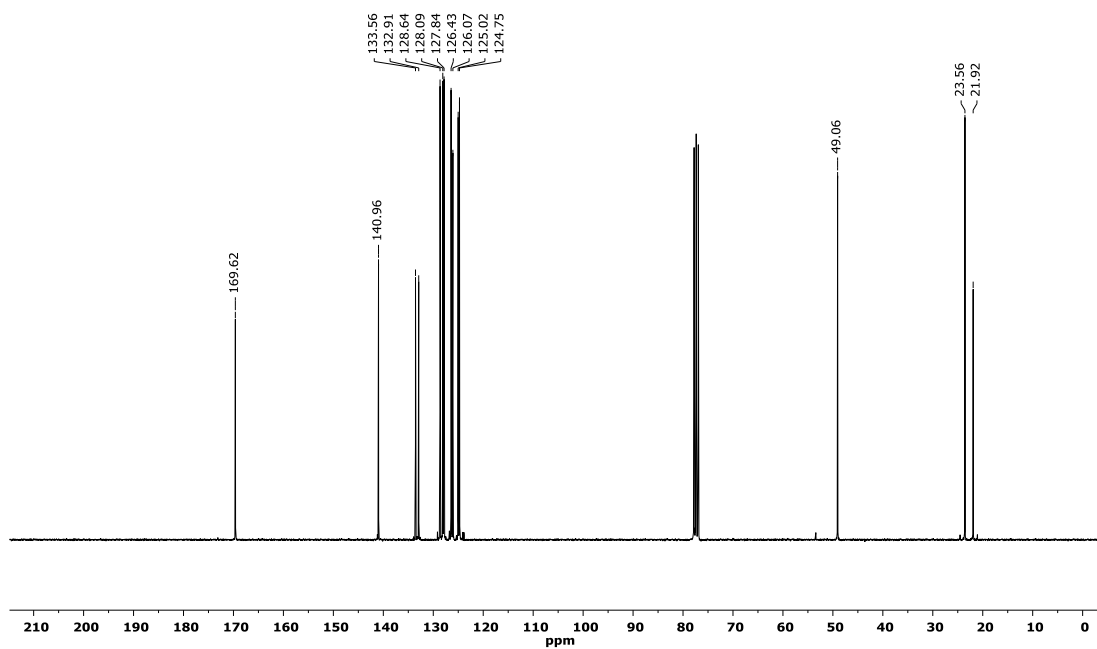


Figure S50. ¹³C NMR spectrum (75 MHz, 301 K, CDCl₃) of amide (S)-30.

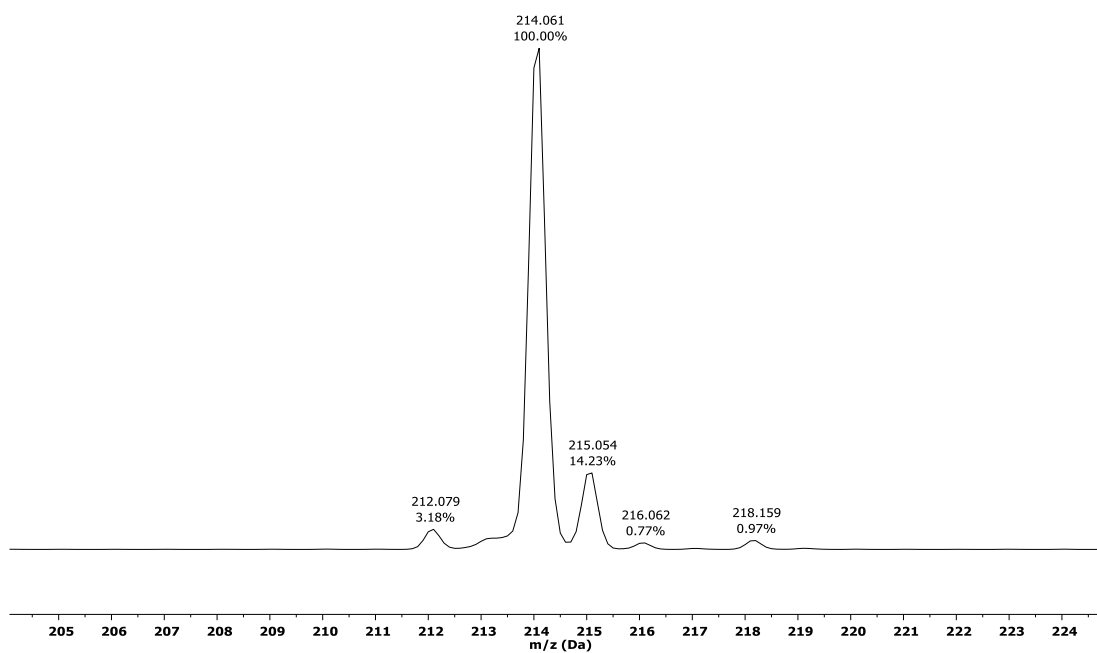


Figure S51. Experimental ESI-MS (ACN/H⁺) of amide (S)-30.

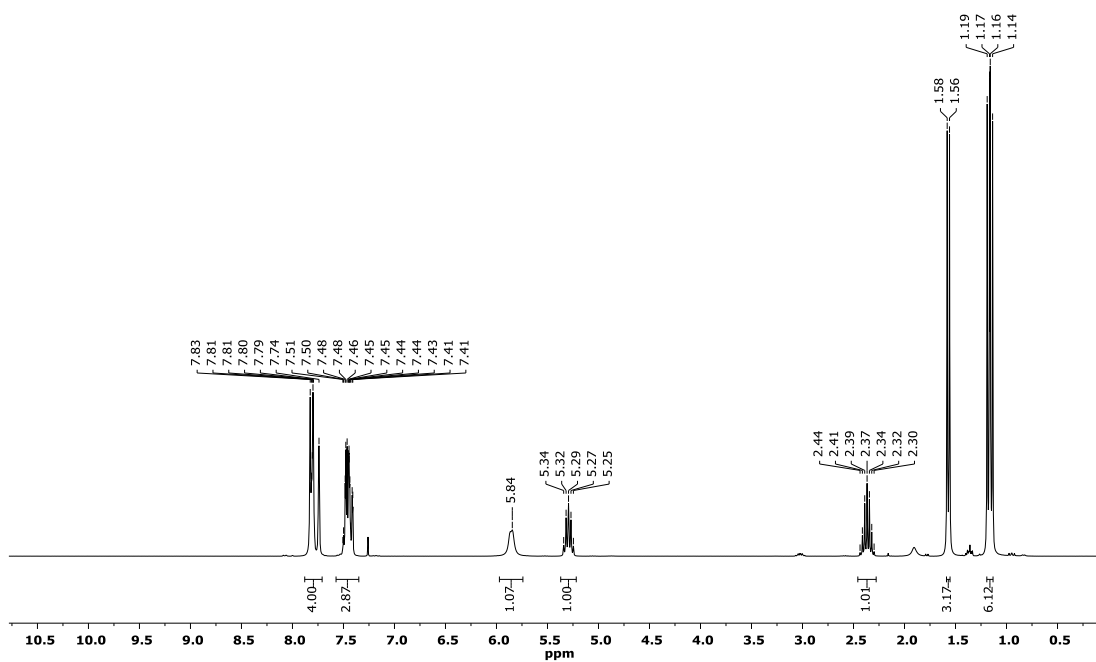


Figure S52. ¹H NMR spectrum (300 MHz, 301 K, CDCl₃) of amide (R)-31.

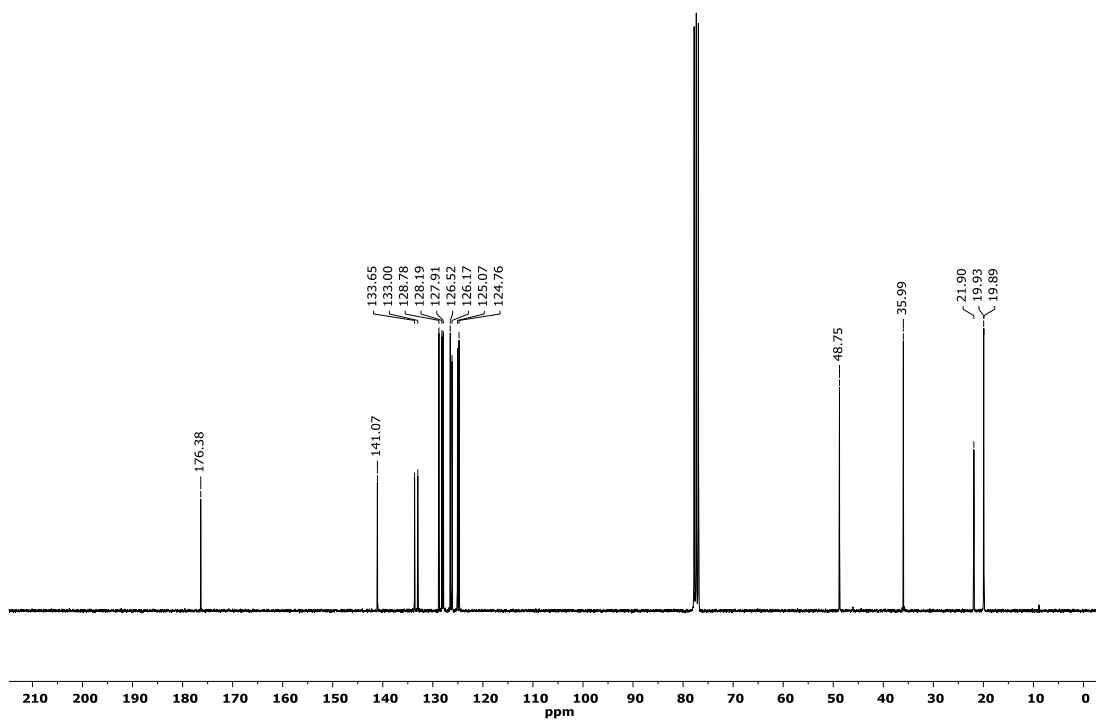


Figure S53. ¹³C NMR spectrum (75 MHz, 301 K, CDCl₃) of amide (R)-31.

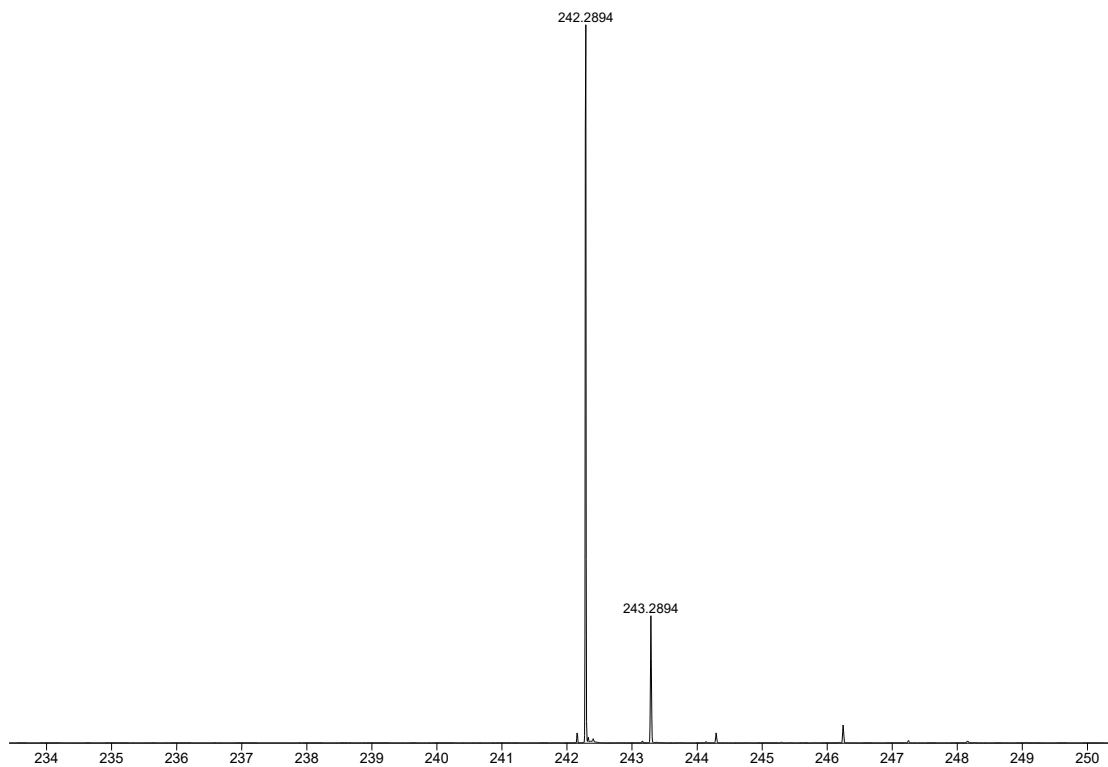


Figure S54. Experimental ESI-MS (H_2O/ACN 50:50 + 0.1% formic acid) of amide (R)-31.

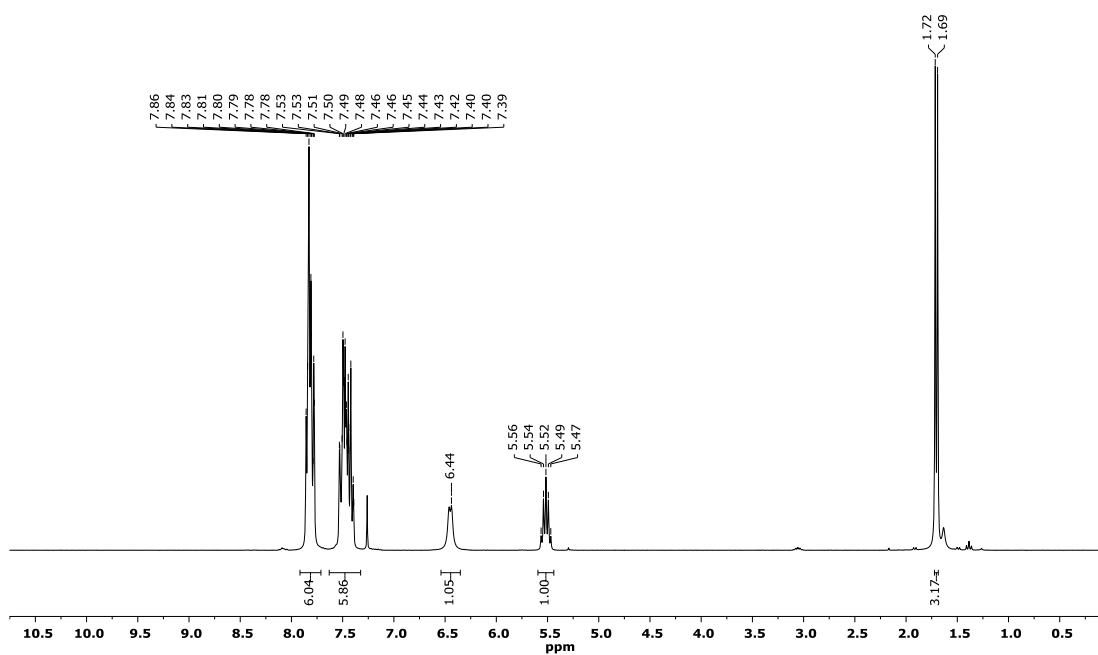


Figure S55. 1H NMR spectrum (300 MHz, 301 K, $CDCl_3$) of amide (R)-32.

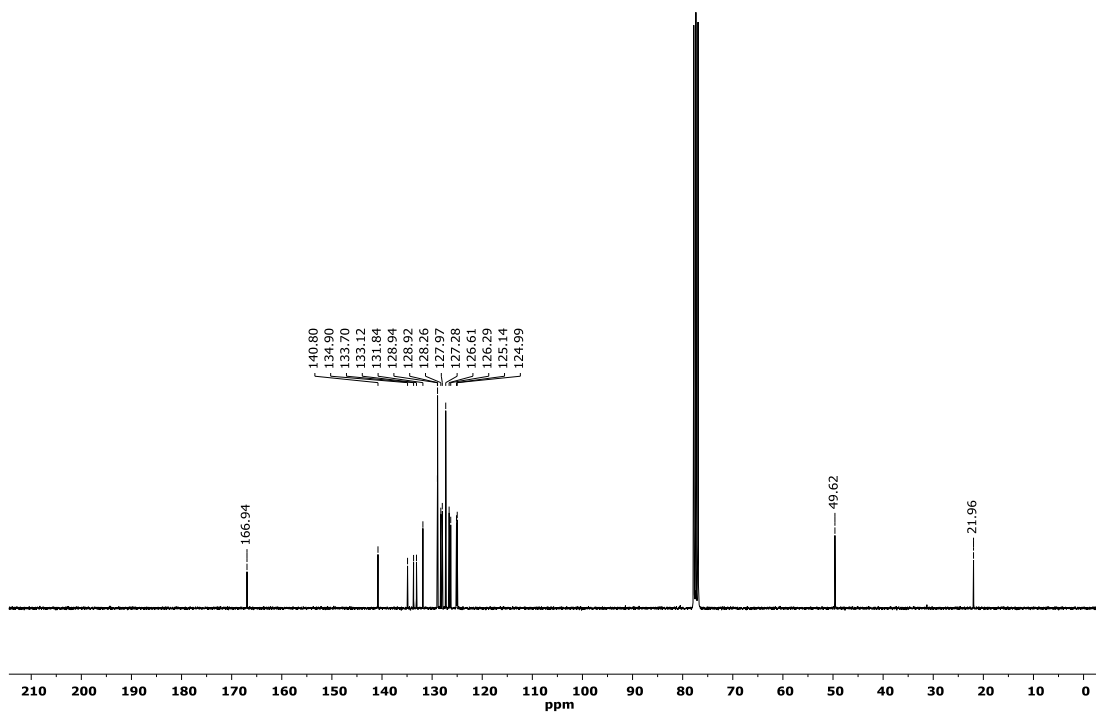


Figure S56. ^{13}C NMR spectrum (75 MHz, 301 K, CDCl_3) of amide (R)-32.

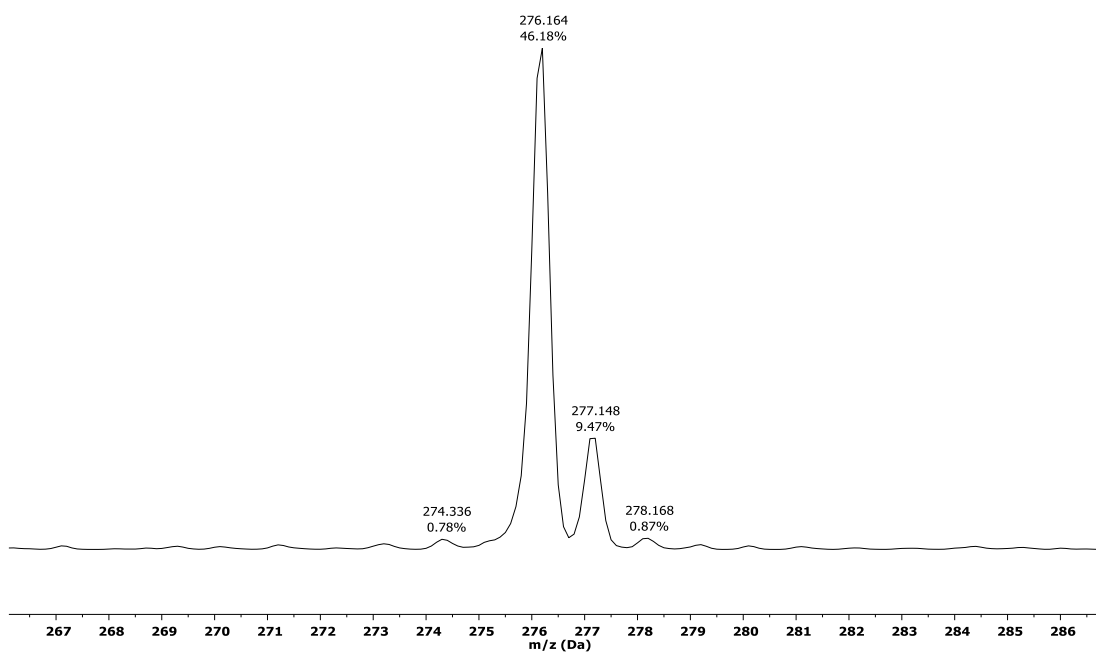


Figure S57. Experimental ESI-MS (ACN/H^+) of amide (R)-32.

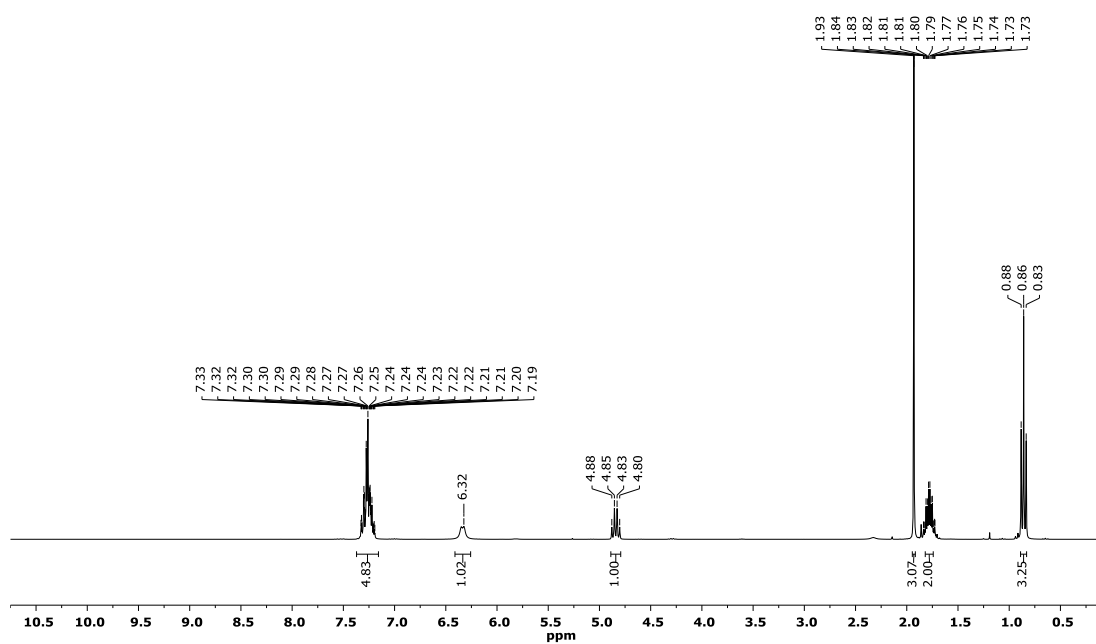


Figure S58. ^1H NMR spectrum (300 MHz, 301 K, CDCl_3) of amide (R)-34.

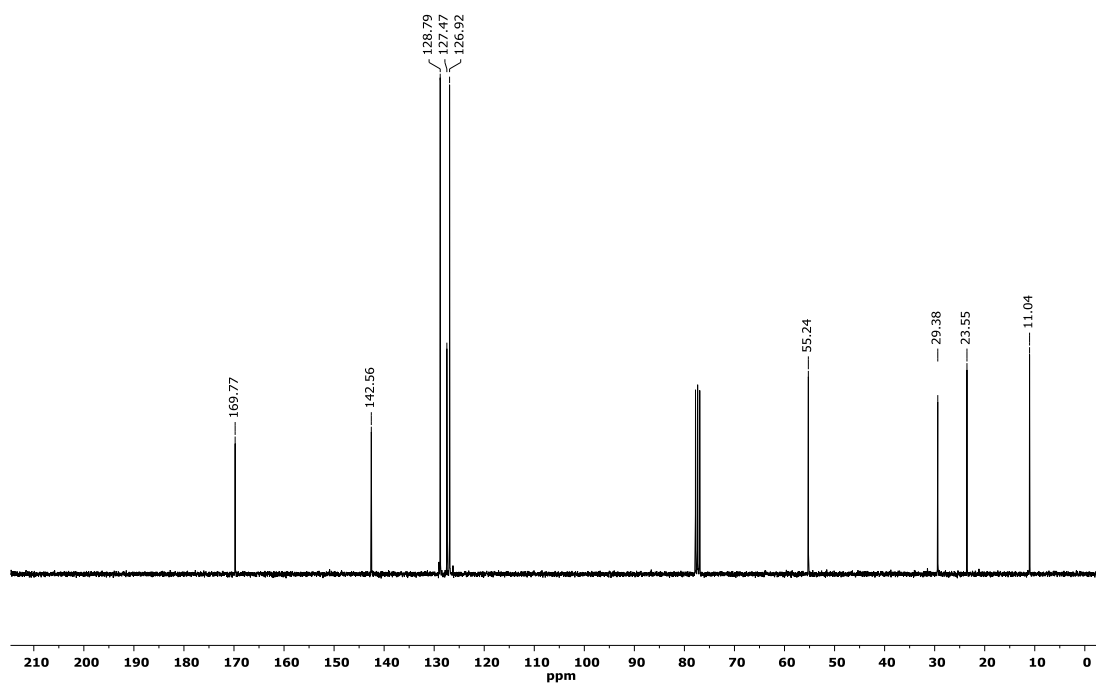


Figure S59. ^{13}C NMR spectrum (75 MHz, 301 K, CDCl_3) of amide (R)-34.

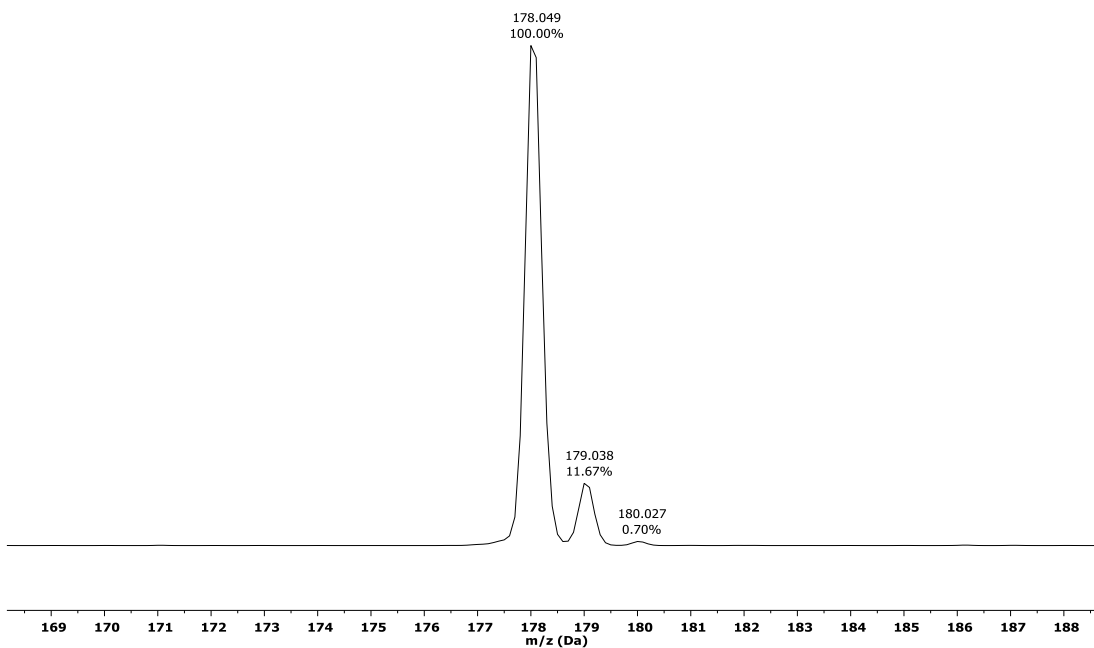


Figure S60. Experimental ESI-MS (ACN/H^+) of amide (R)-34.

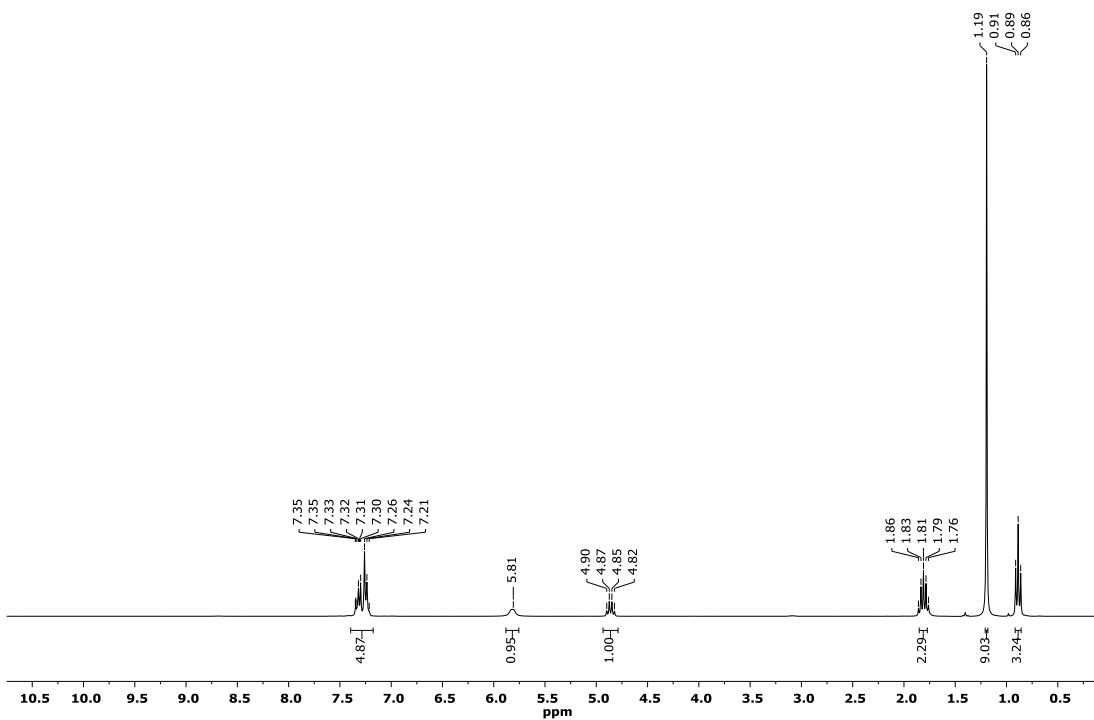


Figure S61. ^1H NMR spectrum (300 MHz, 301 K, CDCl_3) of amide (R)-35.

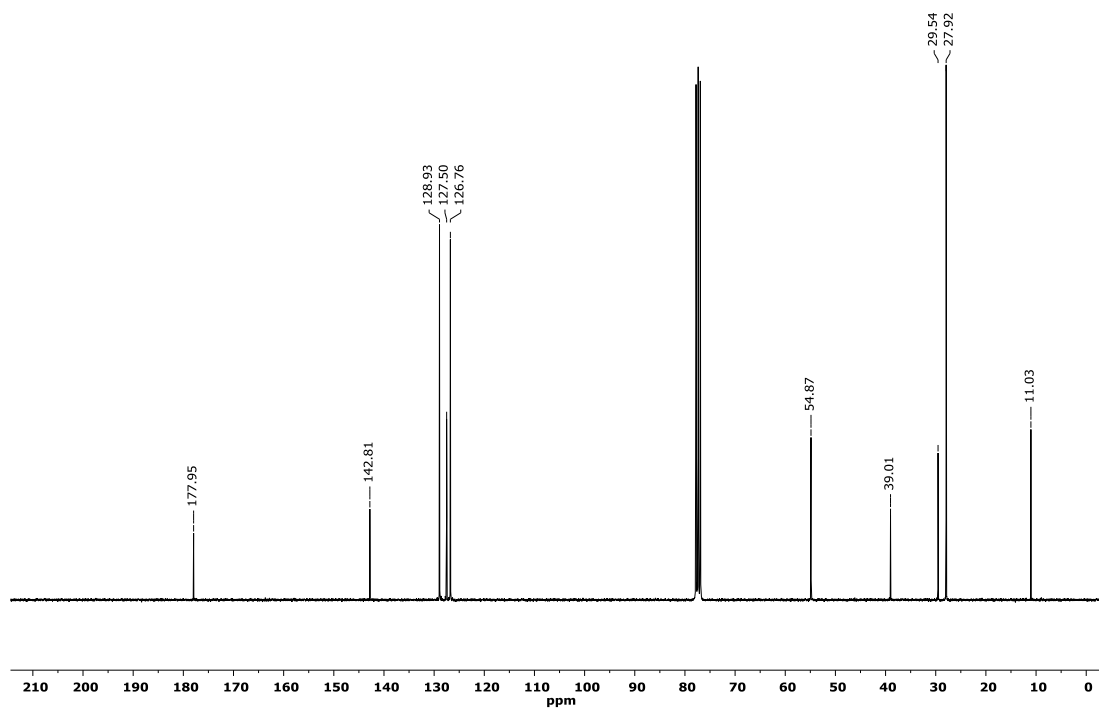


Figure S62. ^{13}C NMR spectrum (75 MHz, 301 K, CDCl_3) of amide (R)-35.

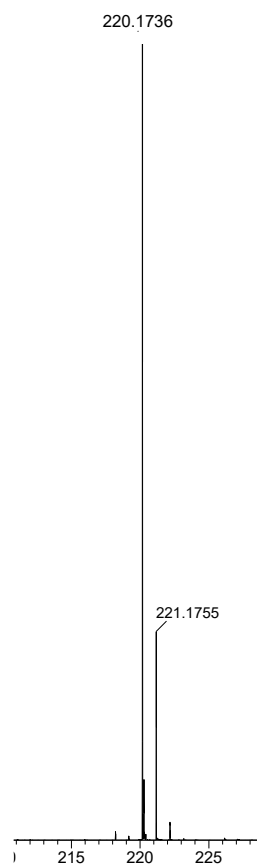


Figure S63. Experimental ESI-MS ($\text{H}_2\text{O}/\text{ACN}$ 50:50 + 0.1% formic acid) of amide (R)-35.

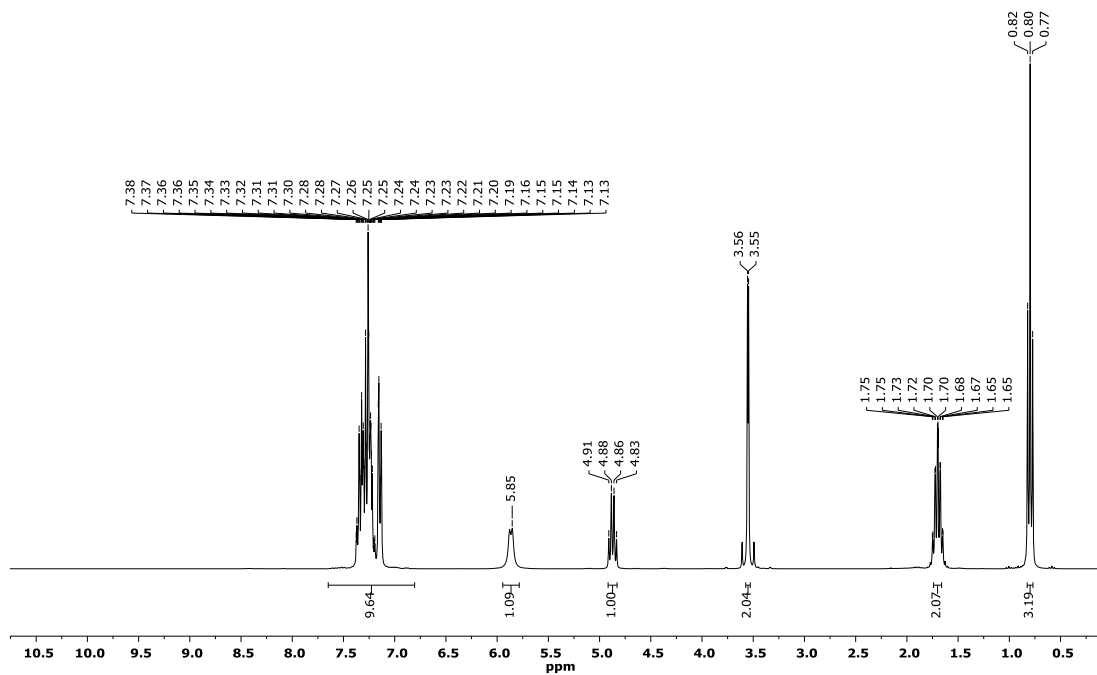


Figure S64. ^1H NMR spectrum (300 MHz, 301 K, CDCl_3) of amide (R)-36.

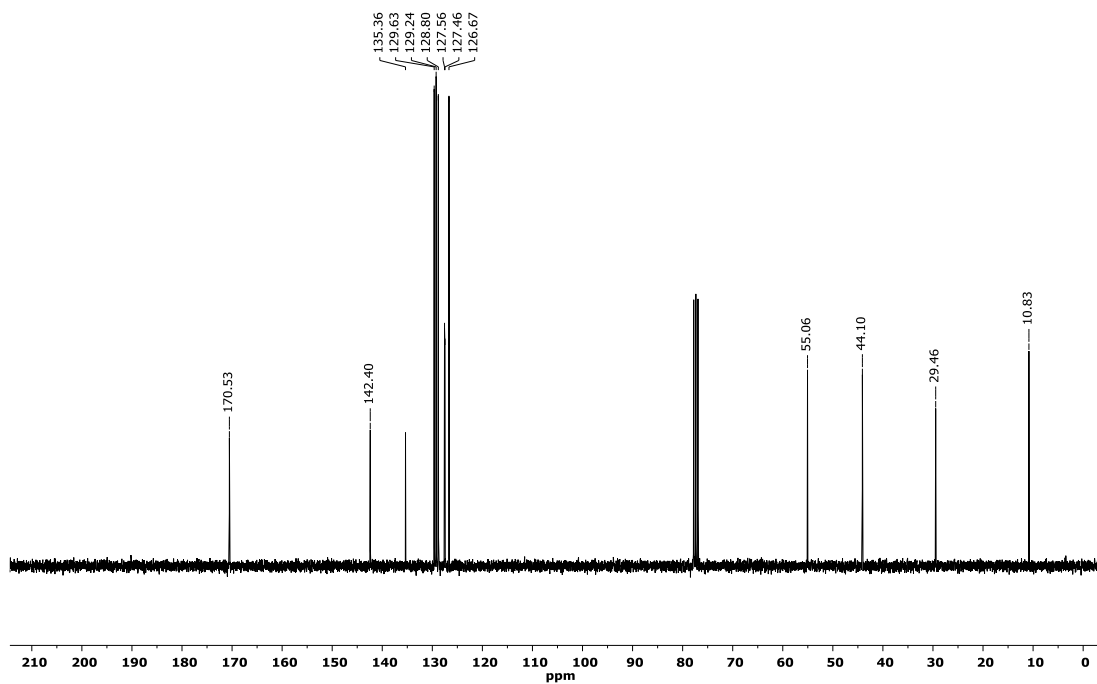


Figure S65. ^{13}C NMR spectrum (75 MHz, 301 K, CDCl_3) of amide (R)-36.

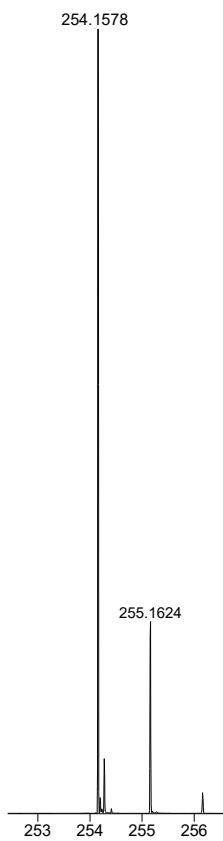


Figure S66. Experimental ESI-MS (H_2O/ACN 50:50 + 0.1% formic acid) of amide (R)-36.

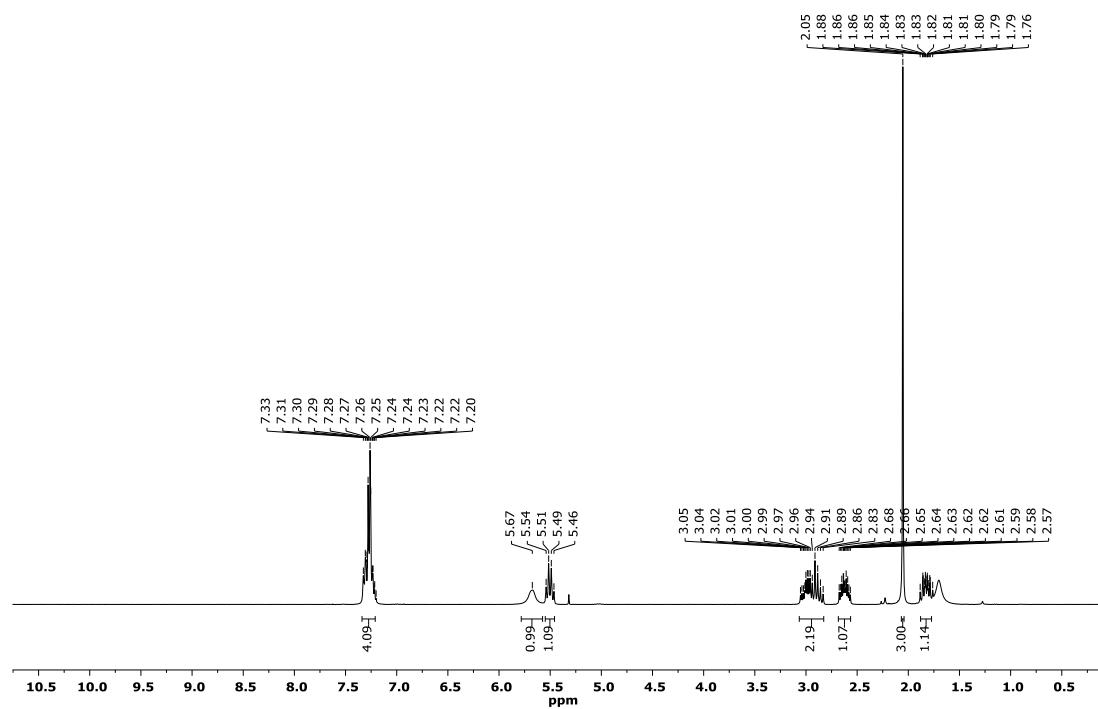


Figure S67. 1H NMR spectrum (300 MHz, 301 K, $CDCl_3$) of amide (S)-38.

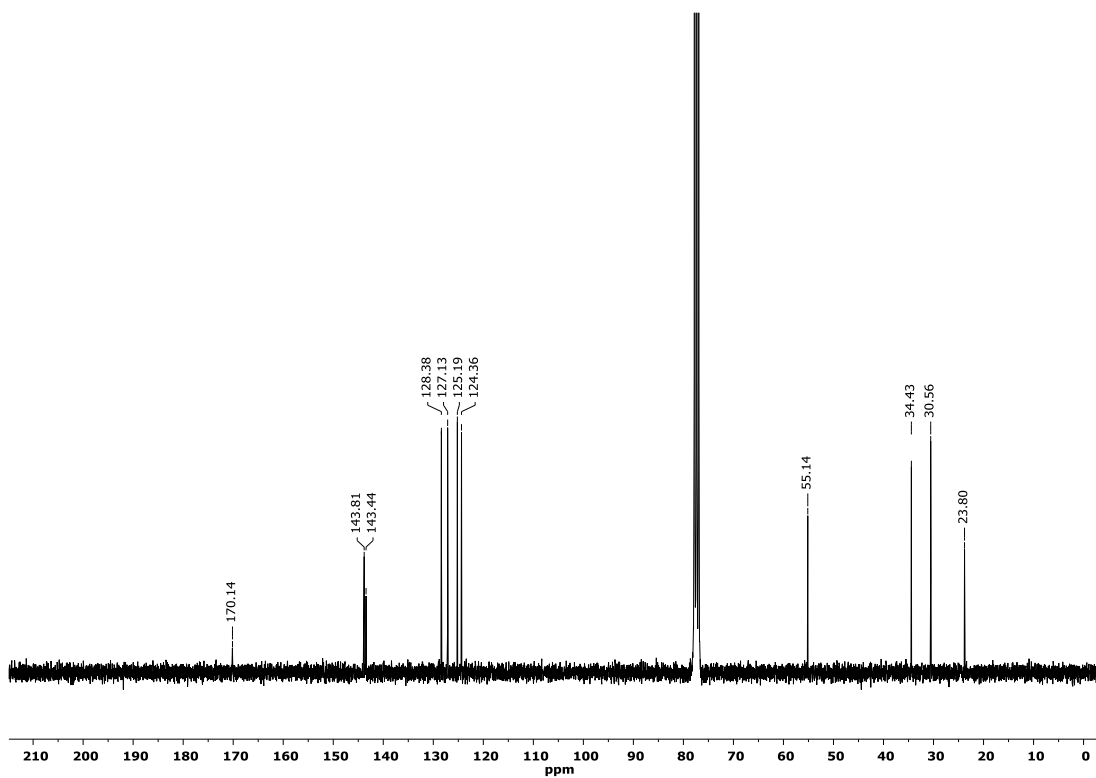


Figure S68. ^{13}C NMR spectrum (75 MHz, 301 K, CDCl_3) of amide (S)-38.

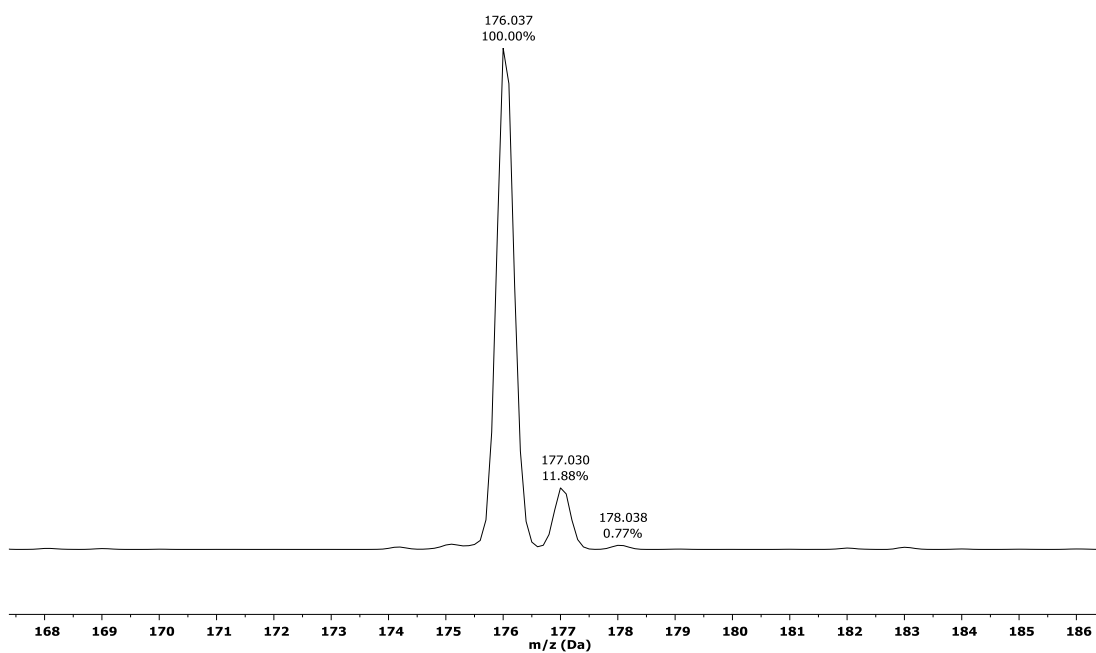


Figure S69. Experimental ESI-MS (ACN/H^+) of amide (S)-38.

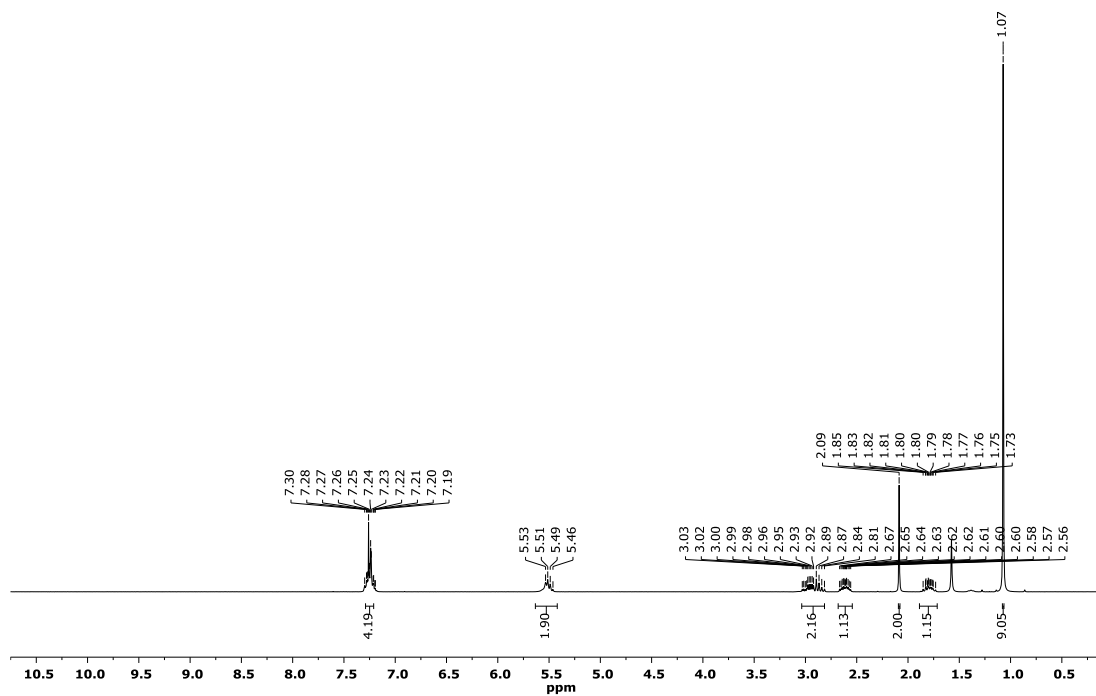


Figure S70. ^1H NMR spectrum (300 MHz, 301 K, CDCl_3) of amide (S)-39.

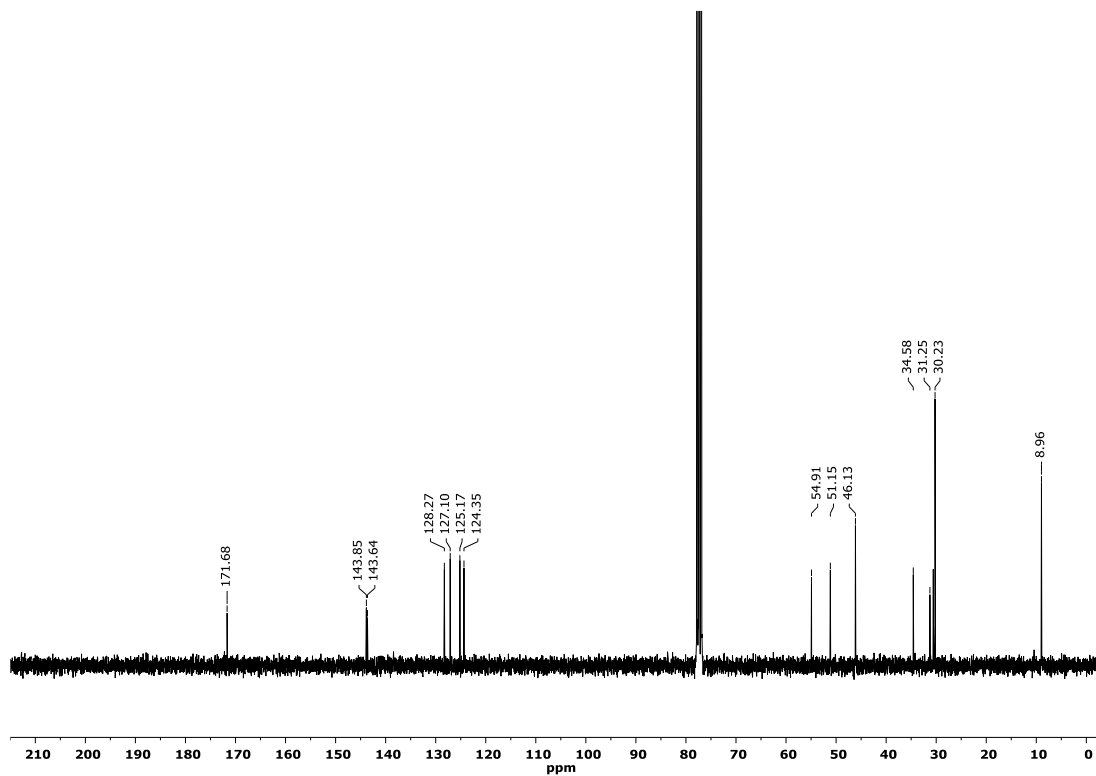


Figure S71. ^{13}C NMR spectrum (75 MHz, 301 K, CDCl_3) of amide (S)-39.

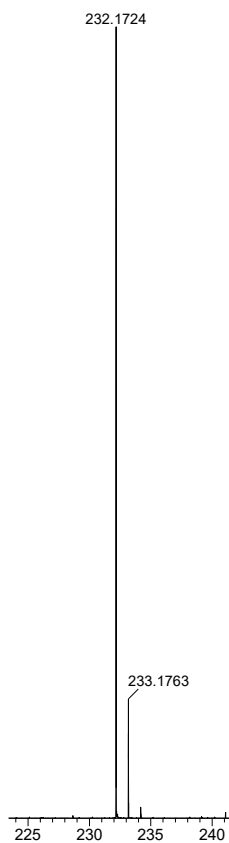


Figure S72. Experimental ESI-MS (H_2O/ACN 50:50 + 0.1% formic acid) of amide (S)-39.

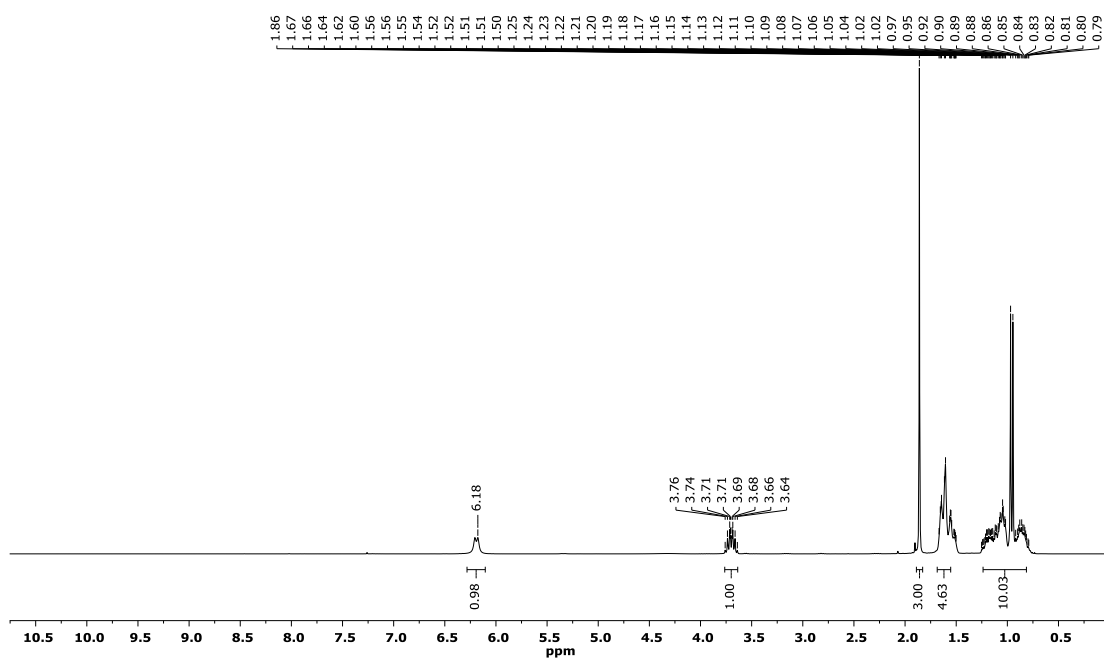


Figure S73. 1H NMR spectrum (300 MHz, 301 K, $CDCl_3$) of amide (S)-41.

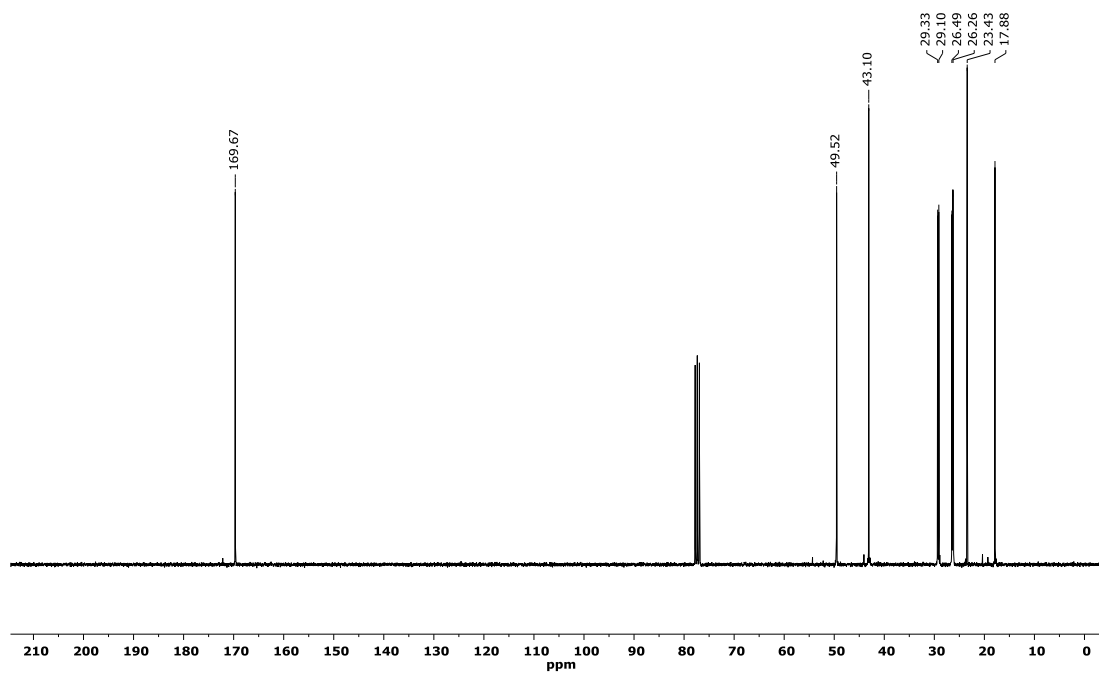


Figure S74. ^{13}C NMR spectrum (75 MHz, 301 K, CDCl_3) of amide (S)-41.

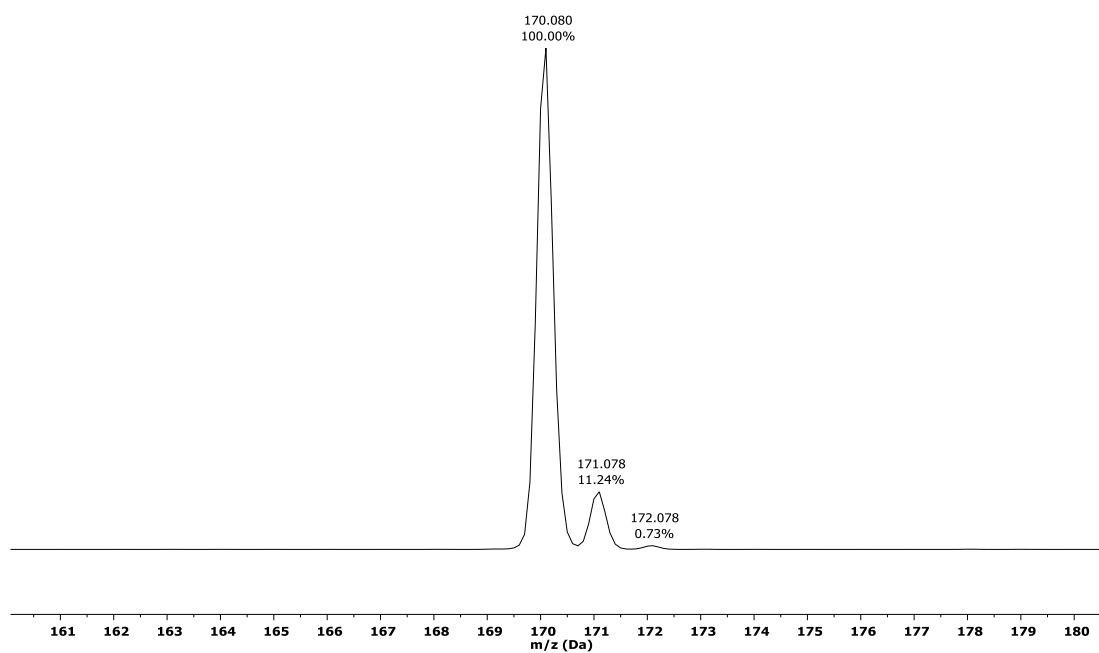


Figure S75. Experimental ESI-MS (ACN/H^+) of amide (S)-41.

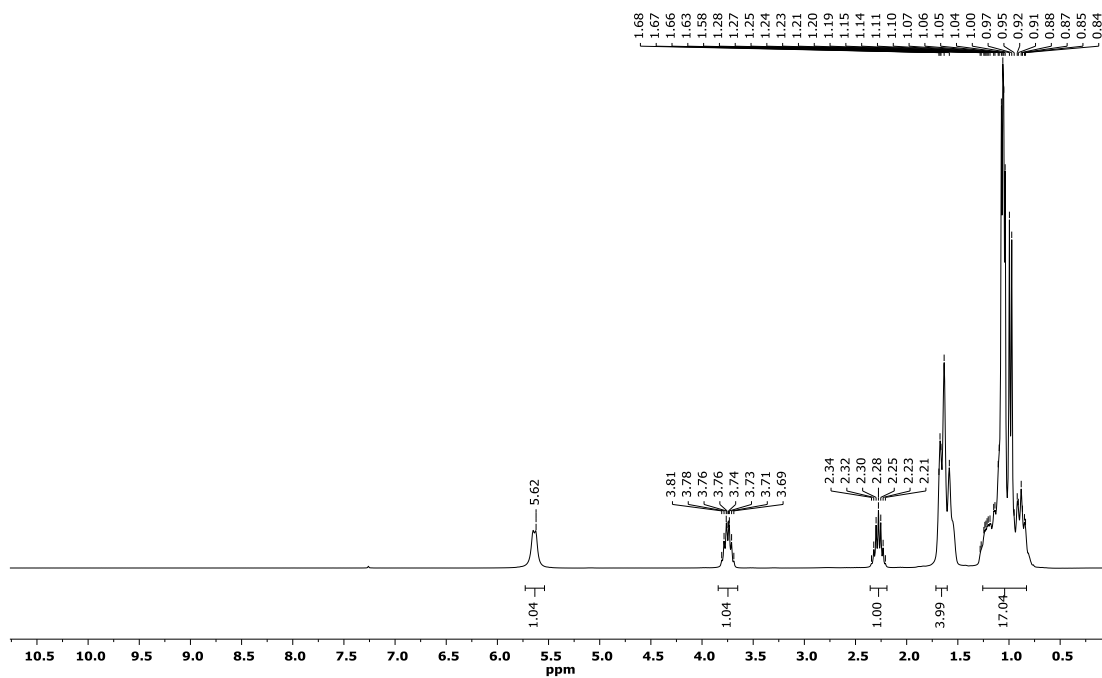


Figure S76. ^1H NMR spectrum (300 MHz, 301 K, CDCl_3) of amide (S)-42.

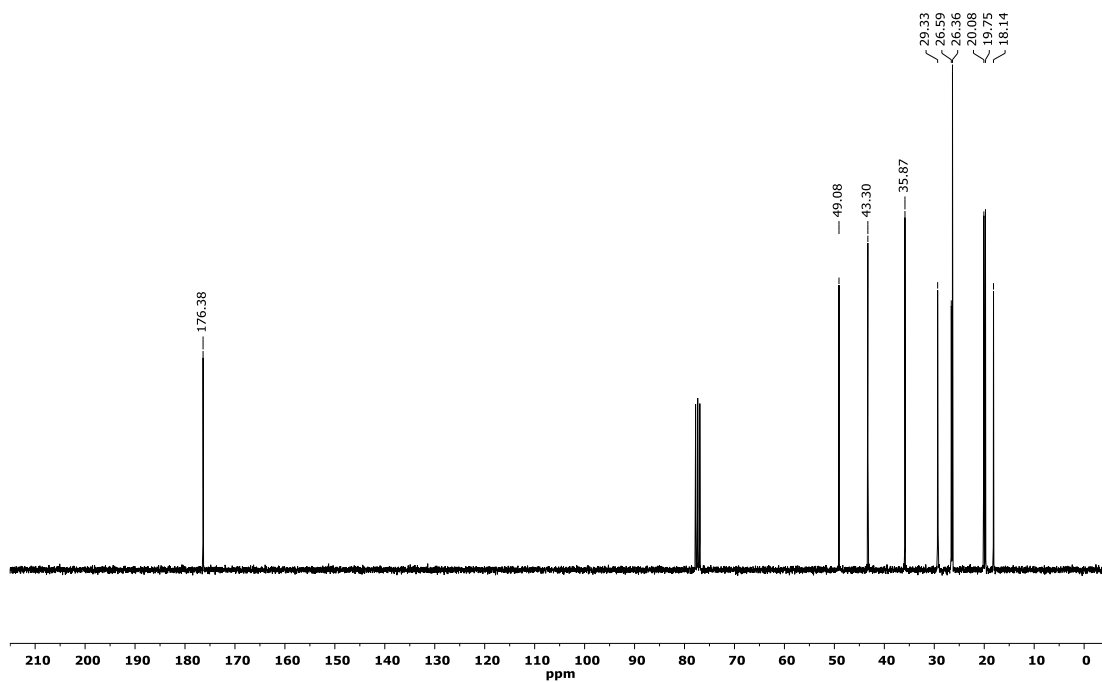


Figure S77. ^{13}C NMR spectrum (75 MHz, 301 K, CDCl_3) of amide (S)-42.

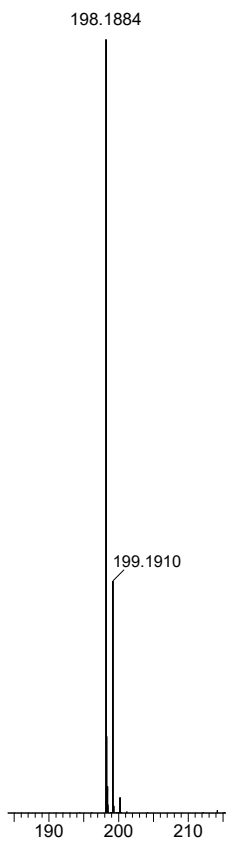


Figure S78. Experimental ESI-MS (H_2O/ACN 50:50 + 0.1% formic acid) of amide (S)-42.

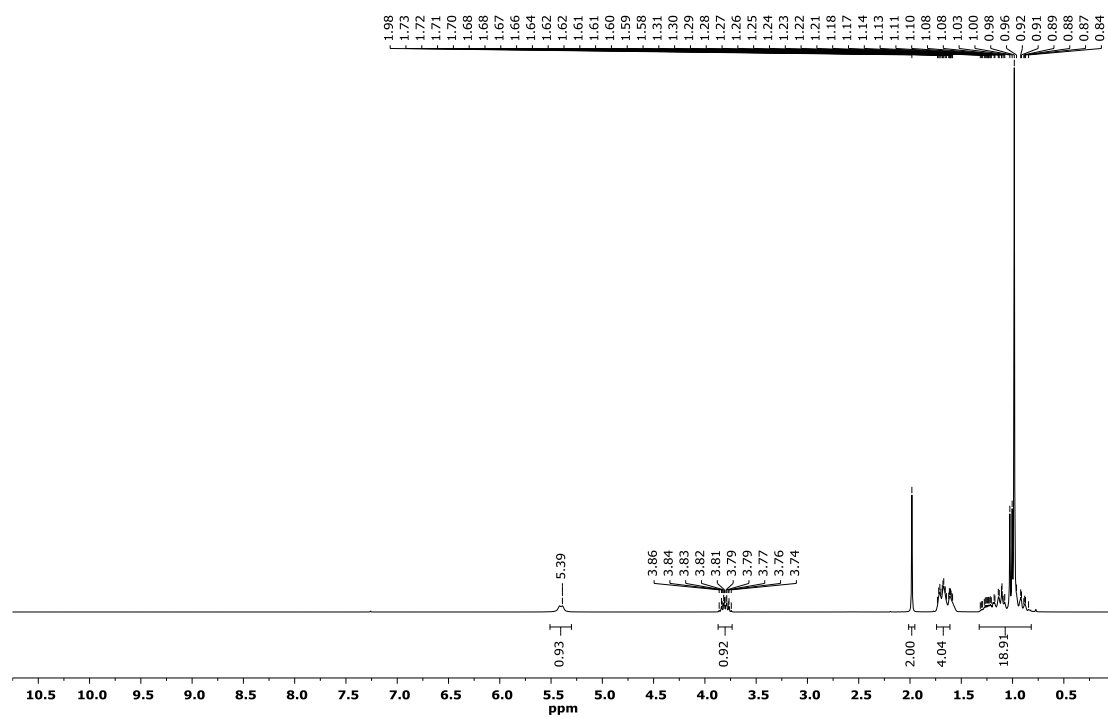


Figure S79. 1H NMR spectrum (300 MHz, 301 K, $CDCl_3$) of amide (S)-43.

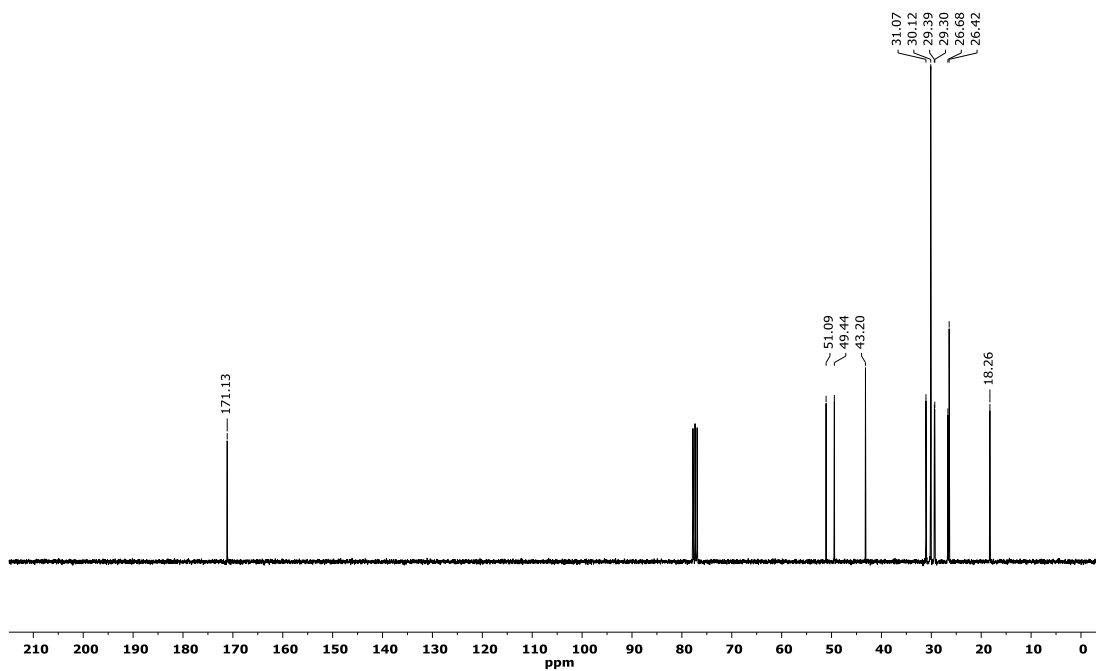


Figure S80. ^{13}C NMR spectrum (75 MHz, 301 K, CDCl_3) of amide (S)-43.

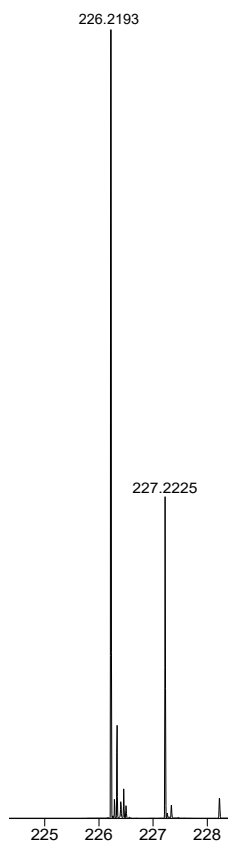


Figure S81. Experimental ESI-MS ($\text{H}_2\text{O}/\text{ACN}$ 50:50 + 0.1% formic acid) of amide (S)-43.

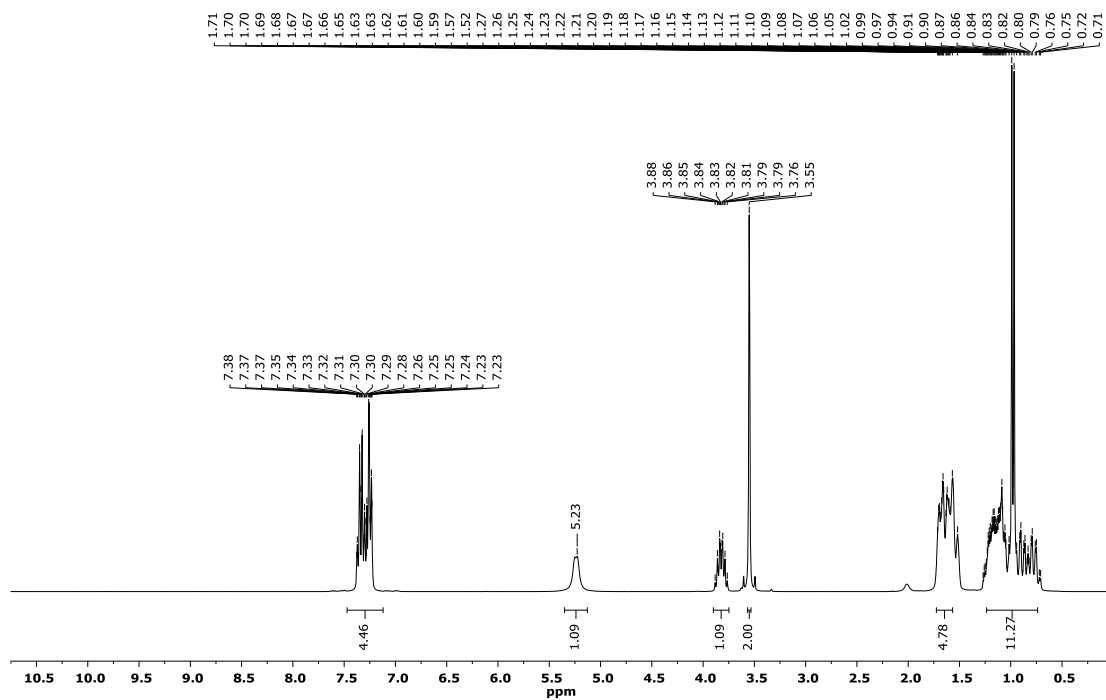


Figure S82. ^1H NMR spectrum (300 MHz, 301 K, CDCl_3) of amide (S)-44.

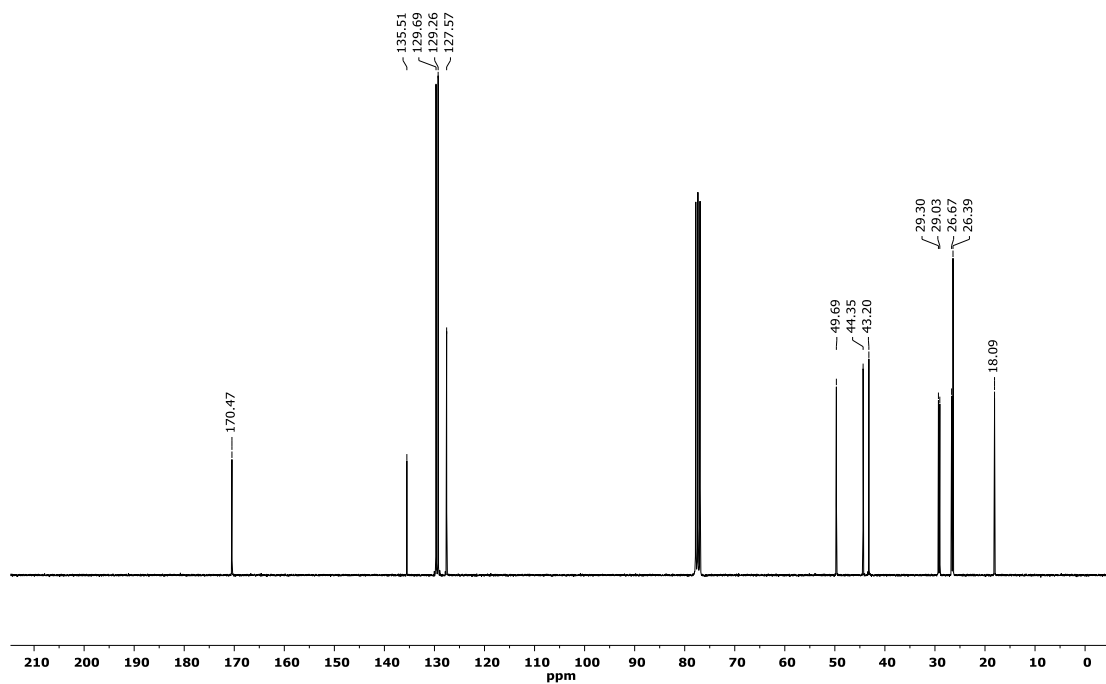


Figure S83. ^{13}C NMR spectrum (75 MHz, 301 K, CDCl_3) of amide (S)-44.

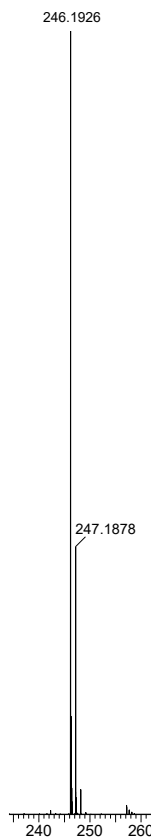


Figure S84. Experimental ESI-MS (H_2O/ACN 50:50 + 0.1% formic acid) of amide (S)-44.

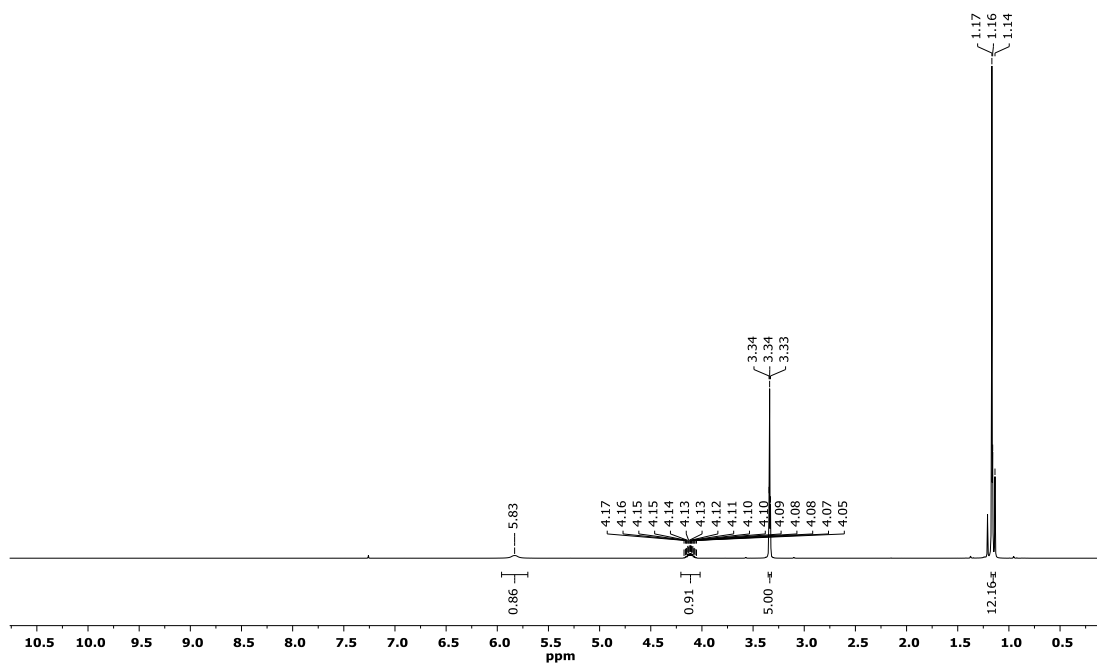


Figure S85. 1H NMR spectrum (300 MHz, 301 K, $CDCl_3$) of amide (S)-46.

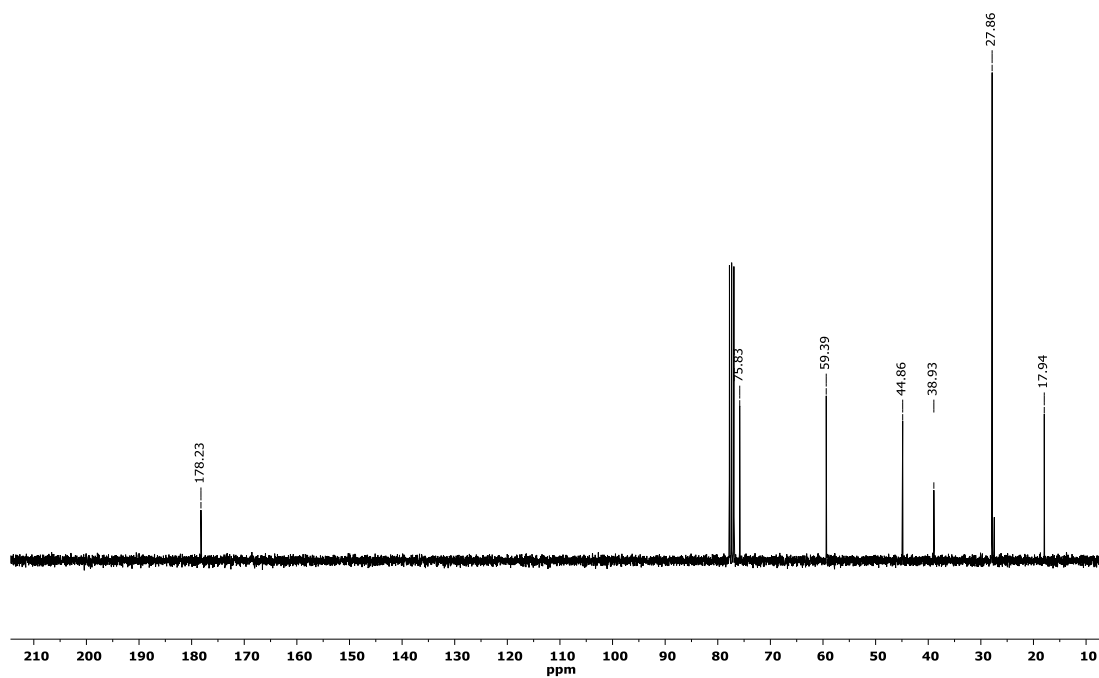


Figure S86. ^{13}C NMR spectrum (75 MHz, 301 K, CDCl_3) of amide (S)-46.

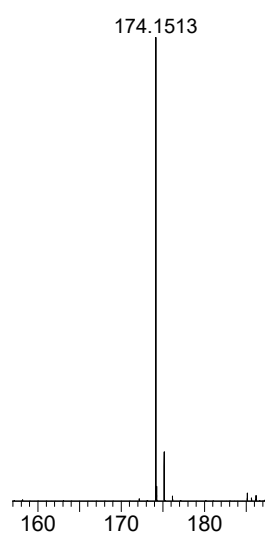


Figure S87. Experimental ESI-MS ($\text{H}_2\text{O}/\text{ACN}$ 50:50 + 0.1% formic acid) of amide (S)-46.

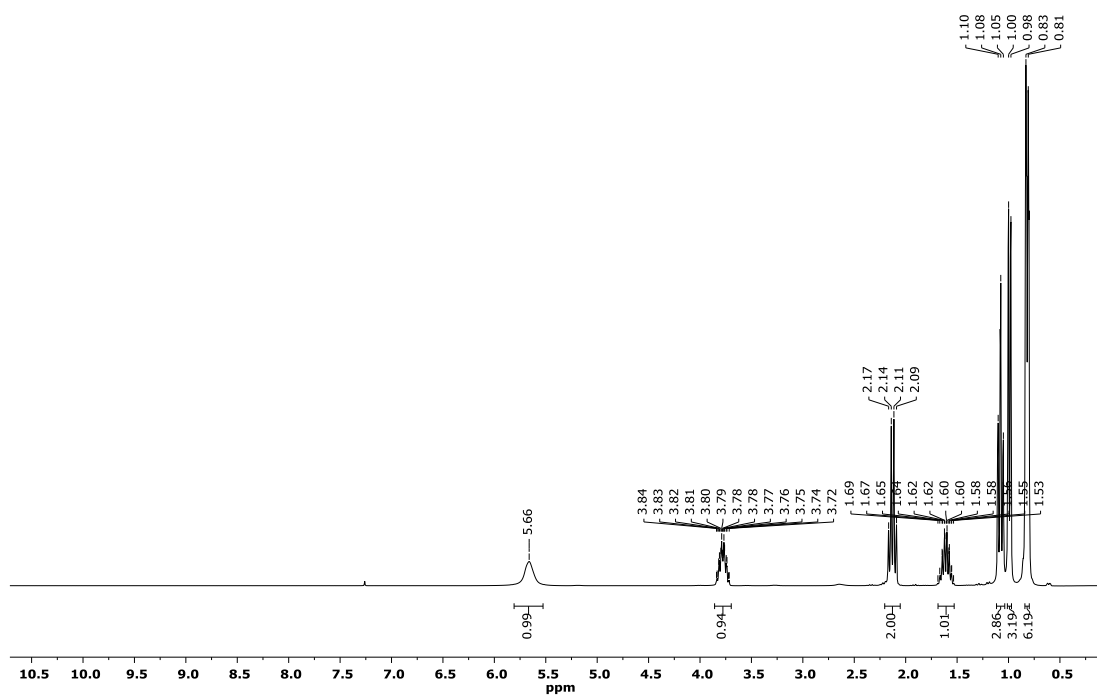


Figure S88. ^1H NMR spectrum (300 MHz, 301 K, CDCl_3) of amide (R)-48.

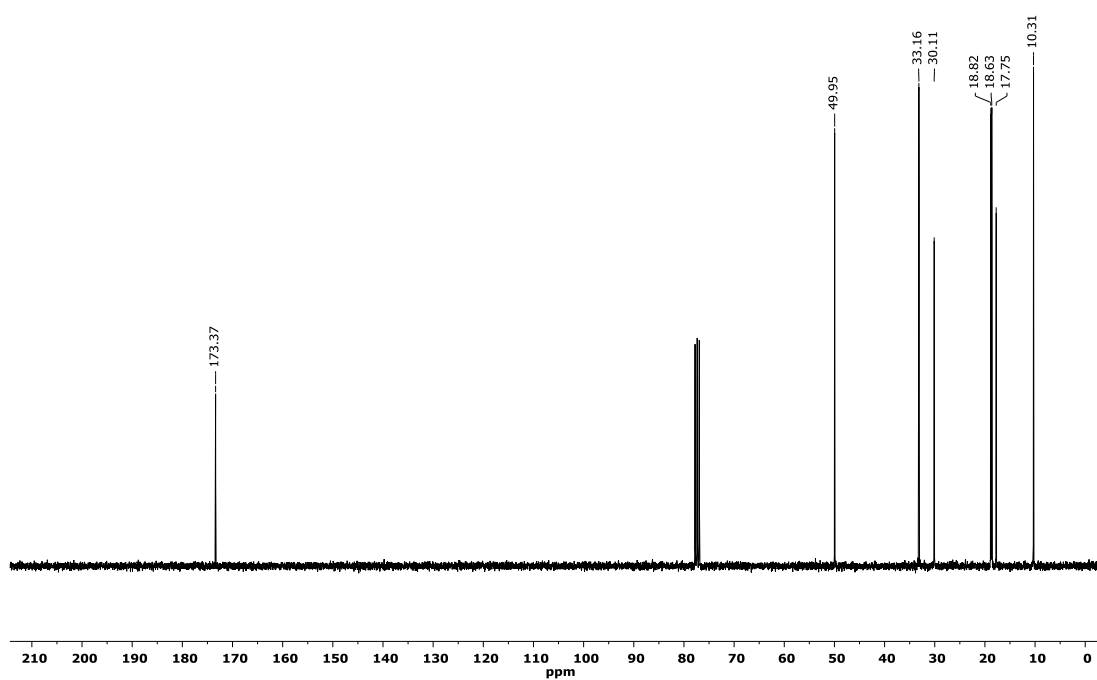


Figure S89. ^{13}C NMR spectrum (75 MHz, 301 K, CDCl_3) of amide (R)-48.

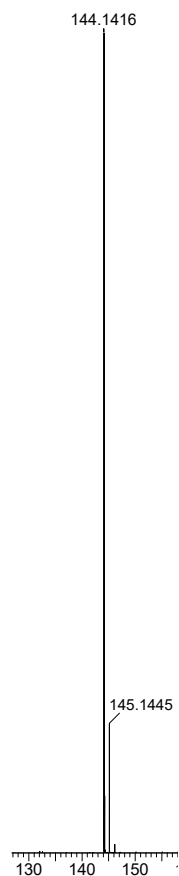


Figure S90. Experimental ESI-MS (H_2O/ACN 50:50 + 0.1% formic acid) of amide (R)-48.

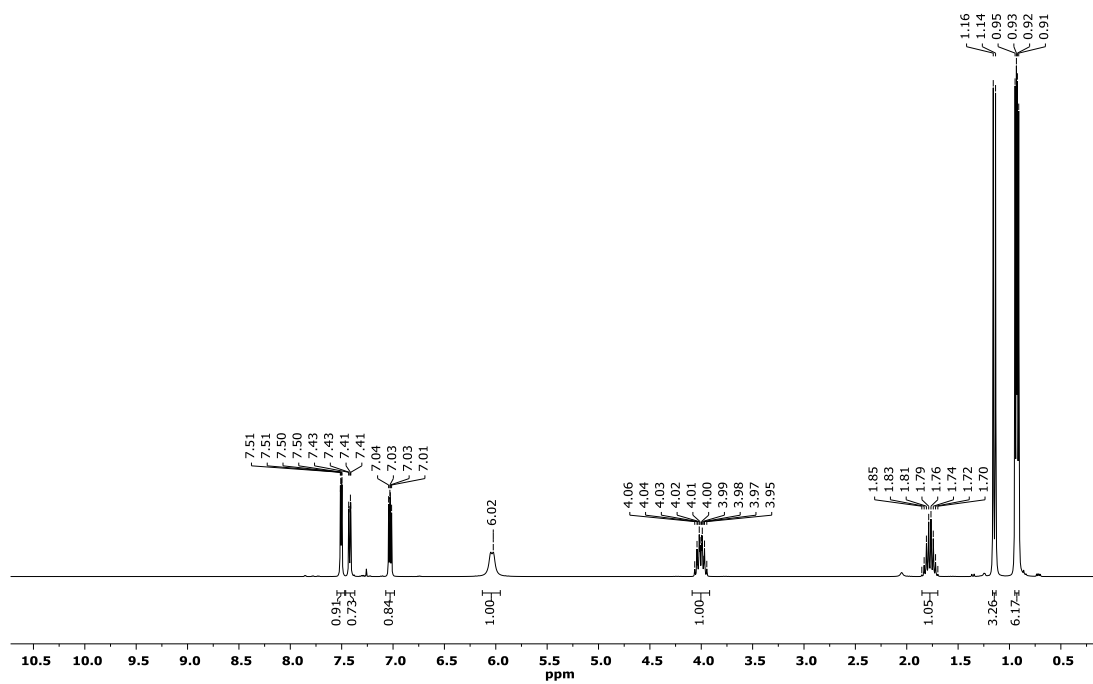


Figure S91. 1H NMR spectrum (300 MHz, 301 K, $CDCl_3$) of amide (R)-49.

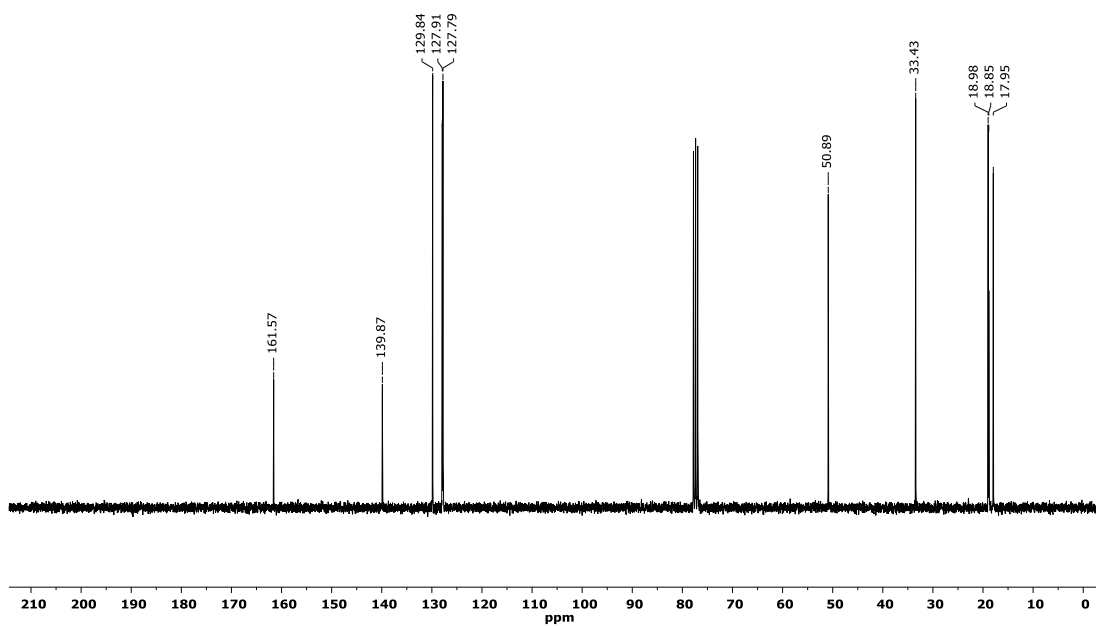


Figure S92. ^{13}C NMR spectrum (75 MHz, 301 K, CDCl_3) of amide (R)-49.

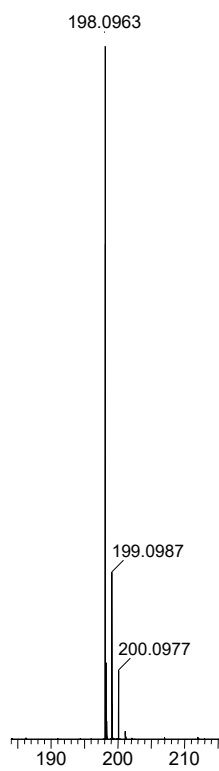


Figure S93. Experimental ESI-MS ($\text{H}_2\text{O}/\text{ACN}$ 50:50 + 0.1% formic acid) of amide (R)-49.

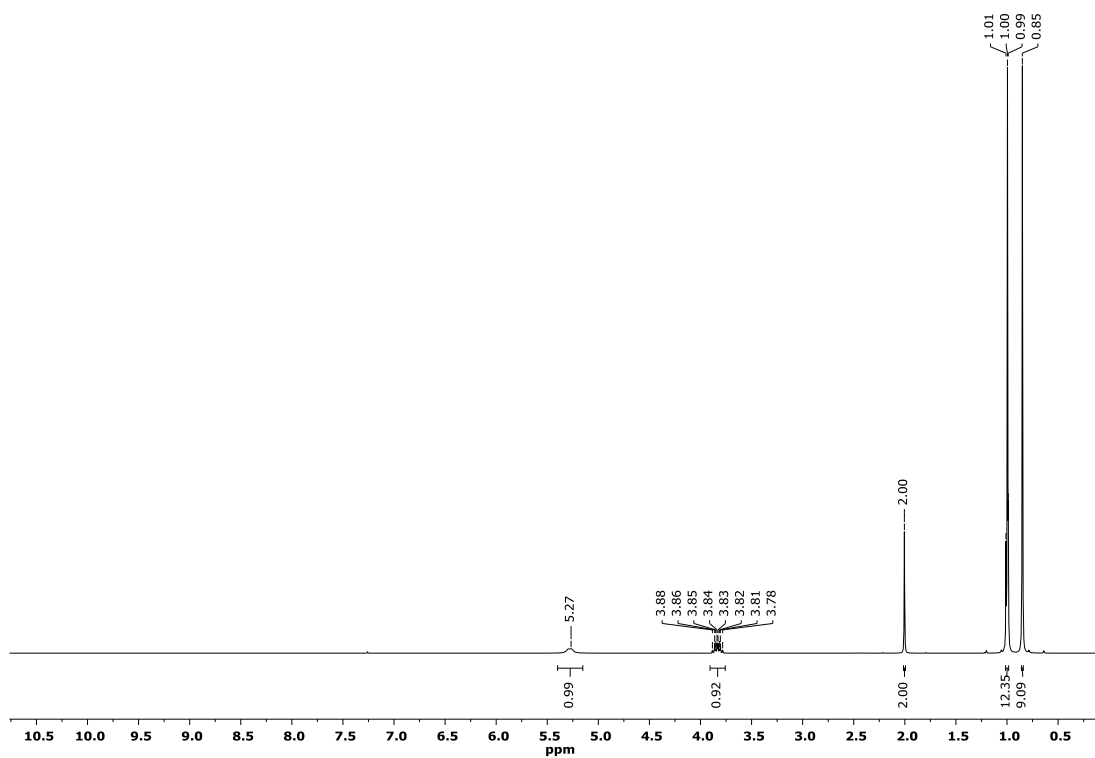


Figure S94. ^1H NMR spectrum (300 MHz, 301 K, CDCl_3) of amide (S)-51.

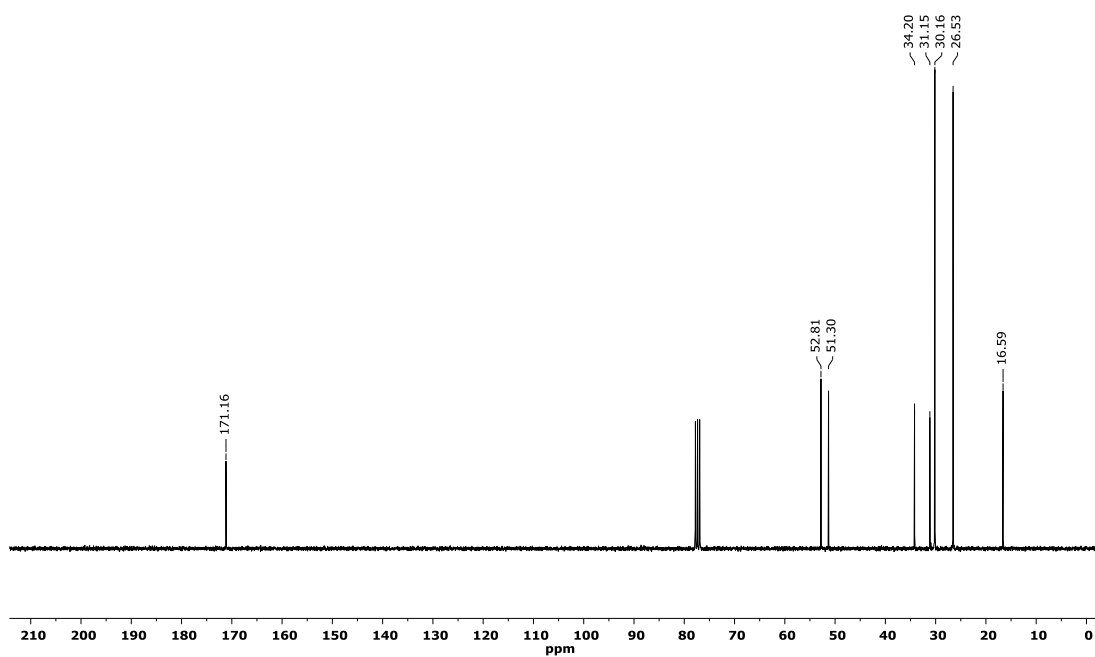


Figure S95. ^{13}C NMR spectrum (75 MHz, 301 K, CDCl_3) of amide (S)-51.

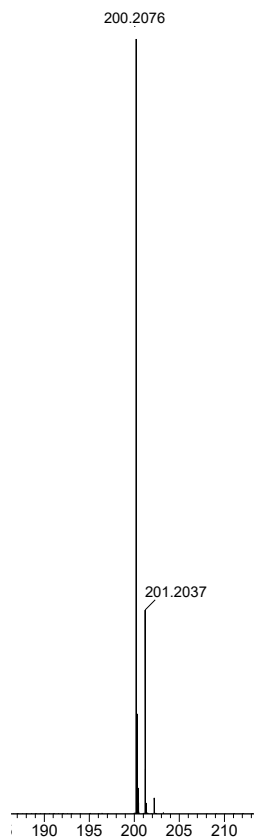


Figure S96. Experimental ESI-MS (H_2O/ACN 50:50 + 0.1% formic acid) of amide (S)-51.

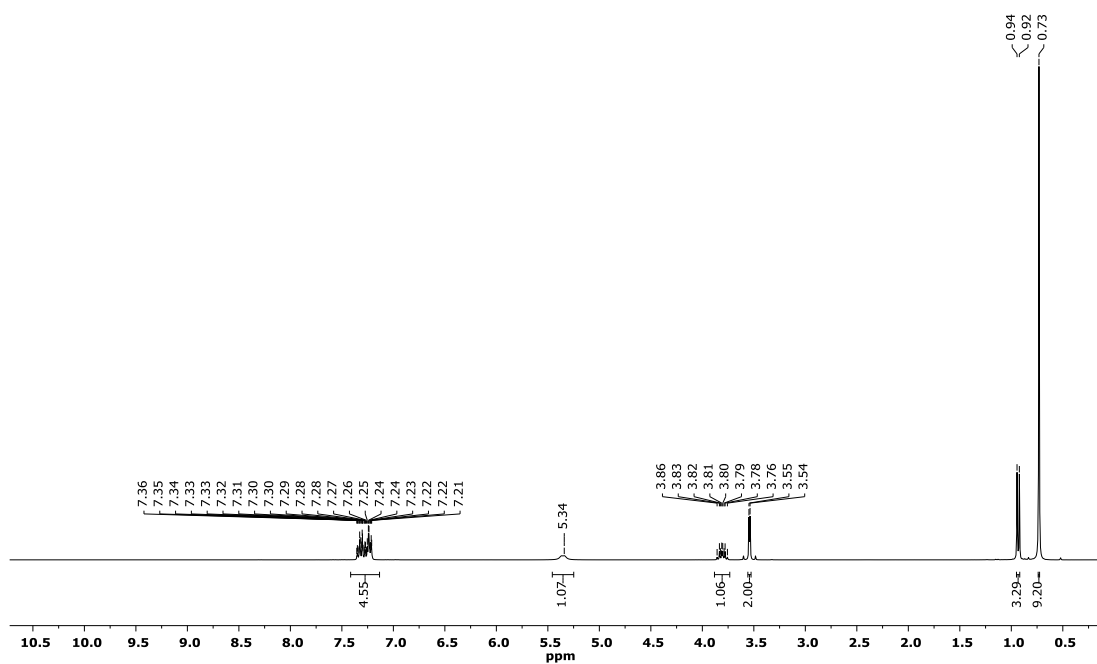


Figure S97. 1H NMR spectrum (300 MHz, 301 K, $CDCl_3$) of amide (S)-52.

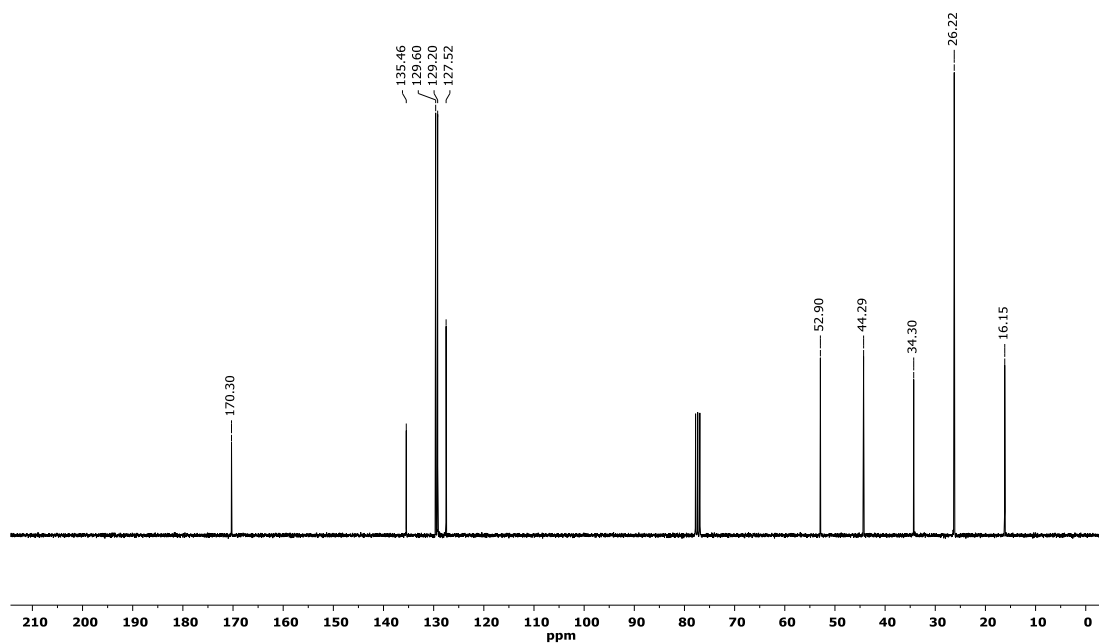


Figure S98. ^{13}C NMR spectrum (75 MHz, 301 K, CDCl_3) of amide (S)-52.

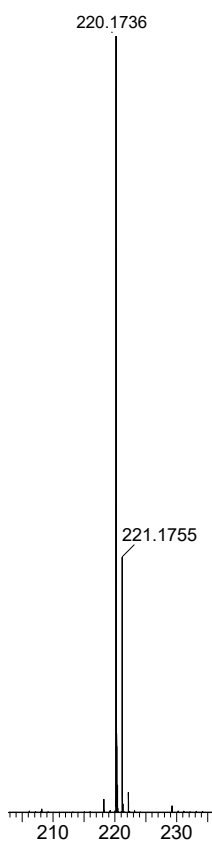


Figure S99. Experimental ESI-MS ($\text{H}_2\text{O}/\text{ACN}$ 50:50 + 0.1% formic acid) of amide (S)-52.

5.36. COORDINATES OF OPTIMIZED STRUCTURES OF THE MOST STABLE CONFORMER FOUND FOR EACH AMIDE

(R)-14				H	4.87689000	-1.39181900	-0.32359200
0 1				H	3.06799900	-2.64388200	0.81627200
C	2.67190500	-0.35313500	0.00815100	H	0.85688400	-1.59751000	1.13580000
O	3.15412900	0.18515400	-0.96875000	H	0.55709300	2.92907500	0.54093100
N	1.37366500	-0.17724800	0.36334500	H	0.03636100	2.41555200	-1.07612400
C	3.48562700	-1.26182600	0.90096500	H	-1.15412100	2.61227800	0.22093400
C	0.48691100	0.70530700	-0.38896700	H	-0.67185900	-0.51954000	-1.08912700
C	-0.94271200	0.23820400	-0.19187300	H	-2.88142800	-2.03617800	-0.34970400
C	-3.55001100	-0.72089900	0.13480000	H	-2.87926900	-0.94886100	-1.72306400
C	-1.28250700	-1.05659200	-0.58641500	H	-4.88396100	0.24884500	-0.77832800
C	-1.92767400	1.04319400	0.36634900	H	-5.22524600	-1.47540300	-0.97916500
C	-3.22448000	0.56629300	0.52848800	H	-0.21998700	0.76136100	1.47176100
C	-2.57186800	-1.53441300	-0.42620600	H	-4.85355000	-0.81068200	0.62149500
C	0.74723300	2.16316500	-0.03607700				
H	1.01898000	-0.61497000	1.19704500	(R)-16			
H	3.96077400	-2.01764700	0.27820300	0 1			
H	2.89592800	-1.74618100	1.67737300	C	-1.97360800	0.07980900	0.27674000
H	0.54619200	2.35209800	1.01983200	O	-2.31458800	0.61365000	1.31558500
H	1.79248200	2.39017600	-0.23940200	N	-0.69234300	0.11772200	-0.16688600
H	4.27465400	-0.67034600	1.36421000	C	-2.96728100	-0.65601400	-0.60967300
H	0.75291300	0.56227200	-1.43966400	C	-3.92843600	0.36932800	-1.21147200
H	0.12494700	2.82701400	-0.63723600	C	-3.71788900	-1.69258200	0.22045800
H	-0.51966500	-1.68884700	-1.02675300	C	0.34724300	0.85170700	0.54863500
H	-1.69328200	2.05260900	0.67655400	C	1.69239900	0.23412300	0.21772400
H	-3.97975200	1.20762800	0.96419800	C	4.13528200	-1.00033100	-0.35915300
H	-4.55936600	-1.09044100	0.26018900	C	1.90556700	-1.10920400	0.53026700
H	-2.81803900	-2.53964900	-0.74324200	C	2.72034000	0.94758300	-0.38558100
				C	3.93540600	0.33375500	-0.67223800
(R)-15				C	3.11332700	-1.72317500	0.24622000
0 1				C	0.23538400	2.34578100	0.27832200
C	-2.25762800	-0.07208700	0.13303000	H	-0.45799800	-0.31062800	-1.04710000
O	-2.66750900	0.56051600	1.08614000	H	0.14524900	0.68674300	1.61027600
N	-0.96396700	-0.00529700	-0.27432800	H	-0.75800200	2.68025900	0.57314700
C	-3.13806000	-1.02027800	-0.66401800	H	0.37803600	2.56297900	-0.78168900
C	-4.61633800	-0.75132200	-0.43884800	H	0.97447300	2.90357700	0.85446400
C	0.01654900	0.83463000	0.40683300	H	2.58430800	1.99149500	-0.63427200
C	1.39665800	0.24519300	0.18558300	H	4.72582200	0.90509400	-1.14169100
C	3.90557700	-0.93613600	-0.18220200	H	5.08122700	-1.47667500	-0.58131500
C	1.64898700	-1.05157200	0.63562500	H	3.26220700	-2.76460900	0.50089200
C	2.41925200	0.93933200	-0.44855600	H	1.10892700	-1.67091700	1.00505800
C	3.66708700	0.35200300	-0.63124000	H	-2.42591800	-1.15823800	-1.41632500
C	2.88934500	-1.63916400	0.45535200	H	-4.66238700	-0.12624800	-1.84787000
C	-0.13870200	2.29177200	-0.00604100	H	-4.45492400	0.88921800	-0.41056600
H	4.45259000	0.90783500	-1.12684900	H	-3.39838300	1.11111000	-1.81100000
H	2.25308000	1.94765300	-0.80317700	H	-4.46482100	-2.19931400	-0.39165700

H	-4.22040400	-1.19856800	1.05186300
H	-3.04071400	-2.44320900	0.62981300
(R)-17			
0 1			
C	1.77370500	0.35632600	-0.37240400
O	2.04570100	1.11109500	-1.28875400
N	0.51113100	0.25269400	0.10855200
C	2.85823800	-0.52130400	0.26746700
C	3.43770700	-1.39340600	-0.85098500
C	2.35268400	-1.40964900	1.40220000
C	3.94124000	0.42494500	0.79514100
C	-0.57924400	1.05783600	-0.43477300
C	-1.88427100	0.31916900	-0.20624500
C	-4.24826100	-1.13060300	0.16238500
C	-2.93580200	0.85509800	0.52641700
C	-2.03397400	-0.95563200	-0.75438700
C	-3.20229900	-1.67588200	-0.57384100
C	-4.11165800	0.13428800	0.70921200
C	-0.53069800	2.47522800	0.11830200
H	-1.21907200	-1.37806800	-1.33170300
H	-3.30200000	-2.66101800	-1.01107300
H	-5.16367400	-1.69002100	0.30430400
H	-4.92122700	0.56774400	1.28220500
H	-2.84890500	1.84273800	0.95897700
H	-1.30732600	3.09607900	-0.32971100
H	-0.66009600	2.47658400	1.20201500
H	0.43931600	2.90882900	-0.11932700
H	0.31042100	-0.35551300	0.88338700
H	-0.39828500	1.11184400	-1.51144800
H	2.68459600	-2.08157100	-1.24088400
H	4.27257200	-1.98247000	-0.46651300
H	4.77671700	-0.15354500	1.19408000
H	3.55178000	1.05924300	1.59438300
H	3.18205500	-2.00015800	1.79430100
H	1.95307100	-0.82253700	2.23249600
H	1.58781600	-2.11125700	1.06092500
H	3.79074800	-0.76865800	-1.66994100
H	4.30375800	1.06565900	-0.00723500

(R)-18

0 1			
C	-1.20465200	1.03420500	-0.00533300
O	-1.29771400	2.23795000	0.14177400
N	-0.01006800	0.42094900	-0.21574800
C	1.23387300	1.18939800	-0.18030100
C	-2.41004000	0.14065700	0.04013000
C	-4.71183100	-1.41260100	0.18792100
C	-3.53814700	0.62234400	0.69598800
C	-2.44553700	-1.11636900	-0.55601800

C	-3.59517300	-1.88988200	-0.48363000
C	-4.68239400	-0.15444900	0.77635800
C	2.39406700	0.24919100	0.04571600
C	4.55554400	-1.47488700	0.44630000
C	2.63797000	-0.80058100	-0.83861700
C	3.24614900	0.42303700	1.12967700
C	4.32356400	-0.43046100	1.32858800
C	3.70792300	-1.65964400	-0.63852800
C	1.40012900	2.00636800	-1.46006000
H	1.98784900	-0.94189700	-1.69525900
H	3.88481000	-2.47097600	-1.33284300
H	5.39268800	-2.14281200	0.60141100
H	4.97898300	-0.28085800	2.17679900
H	3.06301100	1.23401400	1.82447200
H	2.31061200	2.60355000	-1.40385400
H	1.16719700	1.88232000	0.66205400
H	1.47131200	1.34622900	-2.32537700
H	0.54634400	2.66986400	-1.58538800
H	0.04991400	-0.57482600	-0.08128700
H	-1.59098300	-1.48589300	-1.10949400
H	-3.62113900	-2.86202200	-0.95823700
H	-5.60735000	-2.01769500	0.24599800
H	-3.49510800	1.61116900	1.13301500
H	-5.55461400	0.22163100	1.29489500

(R)-19

0 1			
C	0.92297600	2.10121800	-0.34089800
O	0.62719900	3.27526400	-0.45010400
N	0.02087200	1.14462800	-0.03089100
C	2.36468400	1.64163100	-0.56603400
C	2.64933500	0.19067400	-0.30031600
C	3.06933300	-2.52451500	0.22547900
C	2.99111000	-0.24191100	0.97943000
C	2.52148100	-0.75827200	-1.31208400
C	2.72914400	-2.10632200	-1.05327700
C	3.20117500	-1.58787300	1.24220100
C	-1.39073000	1.46396800	0.15860700
C	-2.21220400	0.20262800	0.03282700
C	-3.75136800	-2.12009700	-0.17045800
C	-1.94648400	-0.89845700	0.84530700
C	-3.25834600	0.12486900	-0.87849500
C	-4.02721300	-1.02733600	-0.97858500
C	-2.70618800	-2.05369800	0.74179900
C	-1.61655000	2.16036600	1.50016000
H	2.59913700	1.90314000	-1.59939800
H	2.97896100	2.28464200	0.06540800
H	3.09237700	0.48697200	1.77543300
H	3.47107400	-1.90585600	2.24101000
H	3.23456200	-3.57447800	0.42840700

H	1.88532200	-1.98651100	0.75228300	(S)-26			
H	4.15208400	-3.25219600	1.09412600	O 1			
H	6.18881000	-1.76571400	0.37117400	C	2.58475300	-0.04934800	-0.01094400
H	0.57092200	-0.23307100	0.70504700	O	2.85826500	-0.29667200	1.14817700
H	-0.10264000	1.88408200	-1.17601500	N	1.55845700	0.76850800	-0.35702000
H	-0.33533100	2.35159100	1.82780800	C	3.33423700	-0.66806600	-1.17772100
H	0.77870100	3.14254600	0.69963100	C	4.70386800	-1.18420600	-0.76989100
H	-0.96188700	3.43067200	0.56616700	C	0.65896200	1.37351500	0.62033700
H	-1.02119800	-0.51368100	-1.77752000	C	-1.57239100	2.15615600	-0.25381500
H	-3.15960500	-1.76373500	-1.84184100	C	-0.77542300	1.13486500	0.18777300
H	-2.53822100	1.87496100	1.42390300	C	-3.40616800	0.66276800	-0.69281900
H	-4.64064200	0.64824100	1.36710300	C	-1.29726800	-0.19813300	0.21256600
H	-5.94544700	-1.23587100	1.55392600	C	-2.89468500	1.92482400	-0.69609200
H	-7.03050900	-1.78805400	0.25630600	C	-2.62370700	-0.42780500	-0.23743900
H	-6.58542400	-0.06880700	0.36717300	C	-0.54442000	-1.30721000	0.67894200
				C	-1.08128800	-2.56533200	0.68624200
(S)-25				C	-2.39570700	-2.79045600	0.22834200
O 1				C	-3.14790400	-1.74254500	-0.21937800
C	-2.84390600	-0.66949500	0.24869700	C	1.03345100	2.83170900	0.85215300
O	-3.10745400	-1.04208600	-0.87882400	H	5.33812400	-0.36855100	-0.42375500
N	-1.96771000	0.33599300	0.49749700	H	4.61061400	-1.89616100	0.04769600
C	-3.44614500	-1.33003200	1.46665700	H	5.19571100	-1.67265400	-1.61038600
C	-1.24964200	1.04088600	-0.55989200	H	2.71122200	-1.48720800	-1.55026000
C	0.83550600	2.27246300	0.13978200	H	3.40933100	0.05980400	-1.98870000
C	0.22439800	1.09765900	-0.20598300	H	1.34603800	0.89675500	-1.33353400
C	2.93983000	1.17389100	0.52771100	H	2.05508200	2.87383300	1.22789000
C	0.98708700	-0.11400600	-0.20490900	H	0.98913000	3.40705300	-0.07392100
C	2.19941700	2.31662200	0.50788500	H	0.37182200	3.29490300	1.58463600
C	2.35512200	-0.06688100	0.17059400	H	-1.19421700	3.16953000	-0.26673500
C	0.43411000	-1.36783300	-0.57419900	H	-3.49382800	2.75859100	-1.03817400
C	1.19889300	-2.50192500	-0.56058100	H	-4.41712800	0.47229100	-1.03262000
C	2.55486400	-2.45218100	-0.17722500	H	-4.16218800	-1.89937100	-0.56681600
C	3.11753500	-1.25946800	0.17665400	H	-2.80559700	-3.79201000	0.23938600
C	-1.90474000	2.38855000	-0.83390100	H	-0.49220600	-3.39641900	1.05198100
H	-2.96187400	-2.29768000	1.60235000	H	0.46360700	-1.16478100	1.04697100
H	-4.50248800	-1.50687000	1.27805000	H	0.84130600	0.83380100	1.55053300
H	-3.32561600	-0.74338100	2.37582500				
H	-1.74875200	0.57227000	1.45146300	(S)-27			
H	-1.37561300	0.42454300	-1.45084800	O 1			
H	-1.38056900	2.92517800	-1.62509200	C	-1.83851000	1.23761700	-0.58335600
H	-1.92274000	3.01305700	0.06071100	O	-1.90247000	1.17369900	-1.79840500
H	-2.93367500	2.21902400	-1.14895500	N	-0.70732200	1.61653400	0.06541600
H	0.27360600	3.19674500	0.13164300	C	-3.01192800	0.87683600	0.30447100
H	2.64717300	3.26510100	0.77442700	C	-3.09838700	-0.62349400	0.66389800
H	3.98537100	1.19438200	0.81095700	C	-3.14344900	-1.47795500	-0.60287500
H	4.16035600	-1.20483400	0.46582800	C	-4.38904600	-0.82788300	1.45906800
H	3.14621500	-3.35854200	-0.17092400	C	-1.90710900	-1.04501600	1.52621700
H	0.75938300	-3.44716400	-0.85180700	C	0.53664000	1.96663700	-0.61234200
H	-0.60114600	-1.43660200	-0.88325500	C	0.76193600	3.47219700	-0.54926600
				C	2.62756300	1.66354400	0.76340600

C	1.66544700	1.12347300	-0.04670900
C	3.68292400	-0.47240500	1.09584700
C	1.69899400	-0.27922600	-0.33078400
C	3.64438700	0.86722700	1.33744400
C	2.71461800	-1.07825100	0.25677700
C	0.75609000	-0.91061400	-1.18277500
C	0.81605800	-2.25681900	-1.41925100
C	1.81844400	-3.04895000	-0.82315600
C	2.74755400	-2.46845000	-0.00783500
H	-3.90972400	1.16124700	-0.24596800
H	-2.98096700	1.45987800	1.22933700
H	-2.22212700	-1.38468600	-1.17839200
H	-3.27763200	-2.52886400	-0.33731100
H	-3.96946500	-1.17604300	-1.24944900
H	-4.49716900	-1.87556100	1.74672400
H	-4.38880800	-0.22562000	2.37062400
H	-5.26192300	-0.54777000	0.86577300
H	-1.84183400	-0.43410500	2.43141200
H	-2.01902800	-2.08571600	1.83709400
H	-0.96432400	-0.96326100	0.98223500
H	-0.69949600	1.59688100	1.07307800
H	0.79301700	3.82906800	0.48149000
H	-0.06389000	3.97239700	-1.05358800
H	1.69381400	3.74951600	-1.04258900
H	0.37881000	1.69721700	-1.65673100
H	2.62260000	2.72417600	0.97603500
H	4.38746200	1.33153700	1.97260600
H	4.45362400	-1.09423400	1.53527000
H	3.52883000	-3.06331200	0.45021700
H	1.85200200	-4.11272200	-1.01922200
H	-0.02306000	-0.32815900	-1.65870300
H	0.08695200	-2.71799800	-2.07329900

(S)-28

0 1			
C	1.66429900	-0.62457300	-0.63386700
O	1.77266800	-0.65923500	-1.84770300
N	0.57580900	-1.09431700	0.01886700
C	2.73222900	-0.04308400	0.21537300
C	2.75647300	0.24903600	1.55158000
C	3.98723400	0.81578000	1.96126700
C	4.86321900	0.93891200	0.92189200
S	4.20687700	0.38031700	-0.54526500
C	-0.56962800	-1.66494600	-0.68382000
C	-2.69375700	-1.90177900	0.65169100
C	-1.84389200	-1.11252700	-0.07481600
C	-4.16779200	-0.05664700	1.10737200
C	-2.15007000	0.27576500	-0.24400700
C	-3.86314000	-1.37660200	1.24688400
C	-3.32303900	0.80063900	0.35874500

C	-1.33218900	1.15500100	-1.00022800
C	-1.66253900	2.47499000	-1.13815900
C	-2.82403400	2.99393800	-0.53026200
C	-3.63502600	2.17192700	0.19840200
C	-0.46629900	-3.18433400	-0.71740900
H	4.20899800	1.11993100	2.97335600
H	5.86541600	1.33537800	0.95064900
H	0.53943900	-1.05149600	1.02361700
H	1.92592000	0.08729500	2.22476100
H	-0.48541600	-1.30631500	-1.71040700
H	-0.42783700	-3.60402400	0.28894900
H	0.45151100	-3.45978100	-1.23552500
H	-1.31243800	-3.62149000	-1.24808900
H	-2.47933100	-2.95460000	0.77686800
H	-4.51113900	-2.03231900	1.81364200
H	-5.06011800	0.35816000	1.56069200
H	-4.53440200	2.55555400	0.66530100
H	-3.07089400	4.04105200	-0.64768900
H	-1.02667000	3.12756700	-1.72215200
H	-0.43738800	0.78514100	-1.48400600

(R)-30

0 1			
C	3.54953000	-0.55840700	0.19140600
O	3.70653100	-0.98960200	-0.93385300
N	2.66292200	0.42872200	0.48591300
C	4.33421600	-1.10109900	1.36374100
C	1.77276300	1.02380700	-0.50458200
C	0.38588200	0.41705200	-0.38947200
C	-0.72703800	1.13616600	-0.05695800
C	-0.94410900	-1.60190800	-0.52979100
C	-1.99866300	0.51574000	0.05820400
C	0.26271900	-0.97857100	-0.62989100
C	-2.11161400	-0.87545700	-0.18004500
C	-3.15888700	1.24755900	0.40471700
C	-4.37216500	0.62598500	0.50913100
C	-4.48407200	-0.76053400	0.27089400
C	-3.37927700	-1.49217300	-0.06599600
H	3.99383700	-2.11772500	1.56063800
H	4.22562400	-0.50602500	2.26883500
H	5.38356300	-1.15080400	1.08067700
H	2.51115900	0.66854200	1.45233300
H	-0.66647000	2.20263800	0.12418700
H	-3.06918600	2.31228100	0.58559500
H	-5.25331900	1.19572500	0.77422400
H	-5.44977500	-1.24164700	0.35548900
H	-3.45894800	-2.55679100	-0.25133300
H	-1.03018800	-2.66484000	-0.72230800
H	1.15158300	-1.53467400	-0.90678000
C	1.81735900	2.53933100	-0.39102800

H 2.18951900 0.72154100 -1.46708400
H 1.17953700 3.00354500 -1.14277500
H 1.48160600 2.87265000 0.59367900
H 2.83889200 2.88641600 -0.53792600

(R)-31

0 1

C -2.97775500 0.09554600 0.18266100
O -3.12995600 -0.03668700 1.38216100
N -2.01520400 0.89093100 -0.35407800
C -3.82776900 -0.66694100 -0.82261200
C -5.28881600 -0.65606400 -0.39306200
C -3.28109900 -2.09510900 -0.90149000
C -0.99142200 1.55463100 0.44550900
C 0.29727100 0.75319700 0.39584500
C 1.47125900 1.24099700 -0.10428100
C 1.36198600 -1.37366500 0.85486100
C 2.64288900 0.44052000 -0.15006200
C 0.25444600 -0.58151100 0.88415100
C 2.58980400 -0.88878400 0.33472500
C 3.86436500 0.93222700 -0.66762800
C 4.97843900 0.14033400 -0.70146700
C 4.92482200 -1.18429800 -0.21765400
C 3.75761400 -1.68519000 0.28845500
C -0.85786200 3.00625000 0.01453300
H 1.53722600 2.25597100 -0.47745400
H 3.90197600 1.95027600 -1.03715200
H 5.90780100 0.52710100 -1.09897700
H 5.81328300 -1.80146000 -0.24855700
H 3.71035700 -2.70101600 0.66261100
H 1.32168500 -2.38733900 1.23590400
H -0.67917000 -0.95298300 1.29261200
H -1.37126000 1.51527000 1.46812500
H -0.55011300 3.08175200 -1.03093600
H -1.81761800 3.50850500 0.12433000
H -0.12024800 3.52648800 0.62511900
H -1.88026700 0.86650200 -1.35268600
H -3.73044600 -0.19333700 -1.80361800
H -5.68865100 0.35794200 -0.36572900
H -5.89053800 -1.24678900 -1.08468500
H -5.37958400 -1.08150300 0.60589600
H -3.37008600 -2.57526200 0.07402300
H -2.22968100 -2.10704900 -1.19481800
H -3.84764000 -2.67892500 -1.62764600

(R)-32

0 1

C -2.47067300 0.91379800 0.43558400
O -2.75279200 1.90369300 1.08369600
N -1.19830000 0.64137200 0.04670900

C -3.51592800 -0.08296800 0.02592800
C -5.55044400 -1.83287400 -0.70343600
C -4.83478500 0.35694700 -0.01876800
C -3.22265900 -1.40876100 -0.27993900
C -4.23867100 -2.28160100 -0.64189000
C -5.84757400 -0.51270200 -0.38936600
C -0.10143000 1.55710500 0.34378100
C 1.18593600 0.76001600 0.38262100
C 2.24593300 1.00923500 -0.44259200
C 2.40667200 -1.06139900 1.41639200
C 3.43284900 0.23390200 -0.37463300
C 1.28165700 -0.29872400 1.32562400
C 3.51702200 -0.81980000 0.56747300
C 4.53678300 0.48283600 -1.22401600
C 5.66853900 -0.27931200 -1.13974700
C 5.75174100 -1.32896300 -0.19983000
C 4.70041900 -1.59171300 0.63349100
C -0.10332000 2.74266000 -0.61096500
H 4.75875800 -2.39547500 1.35778500
H 6.65343000 -1.92456400 -0.14192200
H 6.50733300 -0.07995500 -1.79389500
H 2.20479700 1.81241700 -1.16800000
H 4.46933100 1.29023800 -1.94352600
H 2.47077800 -1.86183000 2.14398600
H 0.43762900 -0.48803700 1.97880600
H 0.68395700 3.45174100 -0.35321800
H 0.04270200 2.41452500 -1.64167200
H -1.03468700 -0.08079600 -0.63546600
H -1.06407900 3.24962600 -0.53833900
H -0.30236000 1.93291400 1.35039000
H -5.04241200 1.38541800 0.24531100
H -6.87093800 -0.16321800 -0.43005700
H -6.34184700 -2.51397400 -0.98843500
H -4.00647400 -3.31398000 -0.86823700
H -2.20786900 -1.78029600 -0.20432200

(R)-34

0 1

C -2.72302200 -0.58534100 0.19446000
O -3.21412900 0.36772300 0.76660500
N -1.41532500 -0.61601800 -0.16857800
C -3.53761900 -1.80934700 -0.15715600
C -0.50635300 0.47269200 0.17766300
C 0.91788800 -0.02842200 0.13213000
C 3.56158800 -0.92863300 0.02817200
C 1.73214100 0.03535500 1.25656200
C 1.44633400 -0.54598400 -1.04949300
C 2.75642100 -0.99785400 -1.10143900
C 3.04721900 -0.40853700 1.20648600
C -0.72776300 1.68367600 -0.73552700

C	0.10637800	2.88331100	-0.30952700	H	3.57153600	0.38340300	1.87382900
H	-3.94151300	-2.22807800	0.76356000	H	4.90888600	-0.48851600	1.10959500
H	-4.37779700	-1.49550200	-0.77463600	H	4.34453600	1.05159000	0.42914600
H	-2.96713000	-2.57271700	-0.68341200	H	4.02387000	-0.05274300	-1.82112100
H	-1.02797500	-1.46326000	-0.54777100	H	4.59987000	-1.58763900	-1.13855900
H	0.82950900	-0.58793000	-1.94088800	H	3.03891200	-1.51487800	-1.96908100
H	3.15226900	-1.39836100	-2.02584700				
H	4.58526400	-1.27711900	-0.01206700	(R)-36			
H	3.66882500	-0.34993300	2.09059300	0 1			
H	1.33130600	0.43844600	2.17899400	C	-0.85047300	-2.04093000	-0.57178400
H	-1.79011900	1.92749900	-0.70032500	O	-0.39624300	-3.13851600	-0.83025700
H	-0.48889100	1.39675300	-1.76321800	N	-0.07865200	-0.99756400	-0.19617300
H	-0.74582500	0.77760100	1.20003600	C	-2.35565300	-1.78420200	-0.66870100
H	1.17437100	2.66741000	-0.37059000	C	-2.82500700	-0.41574400	-0.26400300
H	-0.10022300	3.74604200	-0.94227300	C	-3.58838800	2.16078700	0.51339000
H	-0.12104400	3.16400600	0.72106700	C	-3.12298800	-0.13292700	1.06761900
				C	-2.91564200	0.61237800	-1.19944400
(R)-35				C	-3.29440000	1.89169600	-0.81593900
0 1				C	-3.50281800	1.14398900	1.45523500
C	1.89496800	0.33578800	-0.28901600	C	1.37226000	-1.11607800	-0.11080300
O	2.10683200	1.39192900	-0.85764000	C	1.99419900	0.25921400	-0.16379900
N	0.64685600	-0.02219500	0.09891200	C	3.17575600	2.79088000	-0.21994200
C	3.04618900	-0.63104300	0.02045000	C	2.96677700	0.56542900	-1.10801400
C	3.71916700	-0.96677400	-1.31384900	C	1.62221800	1.23723900	0.75723500
C	2.60938400	-1.91868500	0.71606700	C	2.20360600	2.49581800	0.72698200
C	4.03008400	0.12952200	0.91569300	C	3.55786900	1.82190800	-1.13581100
C	-0.50690000	0.82072400	-0.20056300	C	1.78352500	-1.88824600	1.14894000
C	-1.76570300	-0.01228100	-0.14543900	C	3.28166200	-2.15065800	1.20142600
C	-4.11037800	-1.52857800	-0.02402400	H	-2.62506200	-2.00049600	-1.70379200
C	-2.60062300	-0.11487600	-1.25169800	H	-2.82388500	-2.55649600	-0.05696900
C	-2.12260300	-0.67664900	1.02709300	H	-2.68472300	0.40592700	-2.23828400
C	-3.28297100	-1.43376100	1.08744200	H	-3.05453700	-0.92432800	1.80532000
C	-3.76787600	-0.86520400	-1.19287900	H	-3.73523500	1.34502000	2.49310600
C	-0.56443400	2.02670800	0.74401800	H	-3.88625300	3.15677100	0.81375700
C	-1.67314100	2.99879800	0.36726400	H	-3.36176500	2.67784600	-1.55672700
H	-1.49128700	-0.59389700	1.90548400	H	-0.50479700	-0.09506600	-0.05902900
H	-3.54601700	-1.94512000	2.00447800	H	1.70030300	-1.69326200	-0.97938400
H	-5.01820700	-2.11562100	0.02295000	H	1.23280900	-2.82971700	1.14737800
H	-4.40829100	-0.93290800	-2.06279900	H	1.46367200	-1.31842400	2.02580300
H	-2.33303900	0.39981700	-2.16688300	H	3.54271900	-2.74186900	2.07877600
H	0.40663500	2.52109400	0.69884700	H	3.60713600	-2.70412100	0.31797900
H	-1.54348000	3.35204500	-0.65792100	H	3.84788100	-1.21871300	1.24119600
H	-1.66742800	3.86966300	1.02222900	H	0.87414400	1.01200600	1.51032300
H	-0.70369500	1.66503400	1.76653800	H	1.90150200	3.24604400	1.44631400
H	-2.65548600	2.52882600	0.43845000	H	3.63276100	3.77153200	-0.24228200
H	-0.37189800	1.19927400	-1.21710600	H	4.31508400	2.04397400	-1.87663500
H	0.48323700	-0.93626200	0.48292200	H	3.26372100	-0.18885900	-1.82711300
H	1.92147500	-2.50241500	0.09957400				
H	3.48472300	-2.54289300	0.90174000	(S)-38			
H	2.14152300	-1.72005400	1.68308200	0 1			

C	-2.88301500	-0.25643000	-0.08703100	H	2.21047200	-1.86155800	-0.18377900
O	-3.23307400	0.50020300	-0.96938700	H	3.10146300	-1.46623800	1.29022900
N	-1.58128500	-0.38363700	0.28512200	H	4.09630200	-1.94231800	-1.69446900
C	-3.87121300	-1.12178400	0.66078900	H	5.10384900	-1.82801100	-0.24441700
C	-0.54032300	0.42762100	-0.30601800	H	5.37722100	-0.72763800	-1.59923500
C	-0.34478000	1.81209100	0.34545300	H	4.93105000	0.21356300	1.25695200
C	1.13608300	2.15032600	0.10210800	H	5.12927500	1.28346900	-0.13720700
C	1.78555500	0.78891000	0.04805300	H	3.72618500	1.45924300	0.93594700
C	2.52648000	-1.87462900	-0.15509200	H	-0.34516900	2.56765500	0.25762200
C	3.12065300	0.44344800	0.17782200	H	-0.55581600	1.58394400	-1.19766200
C	0.82928800	-0.19457700	-0.18525500	H	-2.70797600	2.67549000	-1.17895500
C	1.18654400	-1.52780900	-0.29298100	H	-0.83325400	0.68862200	1.67534500
C	3.48498000	-0.89551400	0.07839500	H	-2.76621400	2.69636000	0.57908300
H	-1.34524500	-0.95367800	1.08076300	H	-5.06693900	1.08110500	-1.01157100
H	-4.55984300	-0.47068800	1.19807700	H	-5.73190400	-1.28941000	-0.76106400
H	-4.45030600	-1.68689800	-0.06742800	H	-4.14747100	-2.94252700	0.14455500
H	-3.40062500	-1.80773400	1.36310500	H	-1.86127400	-2.24461700	0.81958600
H	0.43570000	-2.28640800	-0.48145700				
H	2.82536300	-2.91215500	-0.22927500	(S)-41			
H	4.52392900	-1.17881400	0.18759600	0 1			
H	3.87170000	1.20194800	0.36316000	C	-2.38556400	-0.61590900	0.08128900
H	1.26398900	2.66044600	-0.85707800	O	-2.44935000	-1.09747900	-1.03184500
H	1.55992900	2.79547000	0.87145500	N	-1.56989700	0.42594900	0.39025700
H	-0.52294100	1.70758600	1.41834000	C	-3.22064800	-1.15476600	1.22184300
H	-1.04025000	2.55112100	-0.04705000	C	-0.71564800	1.08835000	-0.58589500
H	-0.80932600	0.55372000	-1.35841200	C	0.74013700	0.59808500	-0.51488200
				C	2.86806500	0.42015500	0.84052200
(S)-39				C	2.28781300	-1.37860200	-0.81558800
0 1				C	2.95906000	-1.06911300	0.51975800
C	1.46108500	-0.18103200	0.93198000	C	0.83983300	-0.89577100	-0.82716300
O	1.60255100	0.63082000	1.82664700	C	1.41966900	0.90729800	0.82060000
N	0.26281900	-0.36834900	0.31434500	C	-0.84829300	2.59810600	-0.42714200
C	2.59977000	-1.03758100	0.42045200	H	-4.26723900	-1.12609300	0.92303100
C	3.62720100	-0.24325600	-0.41635300	H	-2.95069100	-2.19819200	1.37960400
C	2.91658300	0.51667000	-1.53729900	H	-3.09318500	-0.60479200	2.15287200
C	4.39620600	0.74168700	0.46466600	H	-1.58193100	0.78179700	1.33136900
C	4.60749600	-1.24688300	-1.02469500	H	-1.11307800	0.79237200	-1.55829000
C	-0.88164800	0.46475600	0.60626800	H	-1.86856700	2.91441000	-0.64270000
C	-0.94569500	1.78111400	-0.19571400	H	-0.60418800	2.91516600	0.58894100
C	-2.44605000	2.10828600	-0.28597100	H	-0.17259000	3.11558900	-1.10895200
C	-3.08787900	0.74273000	-0.24286900	H	0.26961500	-1.45213000	-0.07515200
C	-3.84392800	-1.90883500	0.04133600	H	0.36436900	-1.10647000	-1.78713700
C	-4.36685100	0.35823100	-0.61018600	H	1.28259200	1.14194400	-1.29978500
C	-2.19552400	-0.19563900	0.26647800	H	0.86639200	0.40578400	1.62402100
C	-2.56177000	-1.52212400	0.41721600	H	2.32729200	-2.44971800	-1.02263500
C	-4.73850700	-0.97485800	-0.46808300	H	2.84207400	-0.88104800	-1.61899800
H	0.21573800	-0.97068600	-0.49180700	H	4.00227200	-1.39119600	0.50831700
H	2.24389500	1.27742800	-1.13457200	H	1.39173900	1.97915400	1.02925200
H	3.64613400	1.01878700	-2.17555400	H	3.44216800	0.98202000	0.09582200
H	2.33135700	-0.16038000	-2.16596700	H	3.32098700	0.63040800	1.81160600

H 2.45950400 -1.63780400 1.31172300

(S)-42

O 1

C 1.86465600 0.22403500 0.27817100

O 1.91797300 0.08422100 1.48460500

N 0.89713300 0.95110200 -0.33815000

C 2.85318200 -0.46333200 -0.65470900

C 2.36365300 -1.89695000 -0.87929600

C 4.25009400 -0.44523700 -0.04996600

C -0.19991900 1.59450100 0.37071800

C -1.47582800 0.73501600 0.36906800

C -3.30966800 -0.35852700 -0.98817500

C -2.53002100 -1.42838100 1.14691500

C -3.07957100 -1.67697400 -0.25507200

C -1.25399500 -0.59234100 1.09624500

C -2.03506700 0.48347900 -1.03291500

H 0.92410200 1.02436000 -1.34199500

H 2.86200300 0.06204900 -1.61429100

H 4.61091700 0.57433200 0.08758900

H 4.23277400 -0.92900300 0.92611300

H 4.94976500 -0.97654800 -0.69627600

H 3.04464200 -2.43287800 -1.54144300

H 2.32266100 -2.42436700 0.07503900

H 1.36684300 -1.91542700 -1.32428800

C -0.41669700 2.99082200 -0.19891000

H 0.13825500 1.67673300 1.40519100

H -0.60941700 2.95766500 -1.27327500

H -1.27158600 3.47090200 0.27844900

H 0.46556000 3.60883100 -0.03432200

H -2.22775700 1.30397000 0.93211300

H -2.23784400 1.42771000 -1.54338600

H -1.28069800 -0.04960400 -1.62484900

H -3.67291800 -0.54242300 -2.00137600

H -4.09162400 0.20708700 -0.47004500

H -4.00682500 -2.25150500 -0.20767400

H -2.36019600 -2.28049700 -0.81975500

H -3.28563600 -0.90072200 1.73925300

H -2.33734400 -2.37561000 1.65418600

H -0.47536900 -1.15805900 0.57226300

H -0.86894300 -0.40515100 2.10054400

(S)-43

O 1

C 1.37888900 1.16721500 0.48375100

O 1.13179600 1.08802900 1.67372800

N 0.42911800 1.50398800 -0.42637300

C 2.75314600 0.87220400 -0.08017700

C 3.09746200 -0.63420600 -0.06833700

C 4.40629300 -0.81995500 -0.83690800

C 1.98758800 -1.43247800 -0.75435000

C 3.27901400 -1.13584300 1.36451300

C -0.96894900 1.67651300 -0.05411900

C -1.64567400 0.31303900 0.16175100

C -3.56990600 -0.94426700 1.18850100

C -2.38116400 -1.88064200 -0.82801000

C -3.71108500 -1.77696300 -0.08396700

C -1.81443500 -0.49349800 -1.12552800

C -2.98649500 0.43530600 0.88521200

C -1.64508600 2.56145200 -1.09106100

H 2.83021900 1.24567300 -1.10506300

H 3.48128200 1.41069500 0.52950800

H 1.81111700 -1.07162500 -1.77182700

H 1.04811700 -1.36164200 -0.20023300

H 2.26204200 -2.48736400 -0.81597800

H 2.37232800 -0.99554700 1.95112400

H 4.08627900 -0.59478400 1.86278400

H 3.53610700 -2.19750900 1.35633400

H 4.71126700 -1.86831800 -0.82356000

H 5.20812900 -0.22980900 -0.38778800

H 4.29939200 -0.51150200 -1.87951800

H 0.67081300 1.49478800 -1.40332900

H -0.96102900 2.18915700 0.91035400

H -1.17808400 3.54612800 -1.10961900

H -1.56729900 2.12827200 -2.09090400

H -2.70278100 2.68947800 -0.86456700

H -0.97224100 -0.24319800 0.82554400

H -0.85748700 -0.58062900 -1.64833100

H -1.66469500 -2.43524500 -0.21232900

H -2.50743200 -2.44550600 -1.75383600

H -2.50371600 0.03027300 -1.79749100

H -4.44996600 -1.30460000 -0.74073000

H -4.09138800 -2.77220600 0.15460600

H -2.90603400 -1.46414900 1.88686300

H -4.53683600 -0.84477900 1.68561600

H -3.69575800 0.98962400 0.26027900

H -2.85811300 1.00491600 1.80924600

(S)-44

O 1

C 0.36029400 -2.13883300 -0.72522100

O -0.21749000 -2.56857100 -1.70178800

N -0.26570000 -1.74549400 0.41185900

C 1.88384900 -1.99639500 -0.68213600

C 2.29042100 -0.60713200 -0.26377400

C 2.85109300 2.01206600 0.54061300

C 2.10571500 0.46080000 -1.14108100

C 2.77018900 -0.34460600 1.01567500

C 3.04700400 0.95679900 1.41845800

C 2.38460100 1.75913200 -0.74423300

C	-1.70678000	-1.57343400	0.52418200	H	2.33464600	-0.26522200	-1.66134600
C	-2.11809300	-0.11347400	0.25785900	H	0.39816600	-0.75403800	0.30403200
C	-1.88908000	2.31875300	0.91196600	H	1.00436600	1.69336200	-1.16599200
C	-2.33009000	1.70627800	-1.48526700	H	2.30138900	2.65040900	0.72069600
C	-1.64891100	2.69843300	-0.54648200	H	1.79709300	1.30458400	1.75737900
C	-1.87054800	0.27868300	-1.19964400	H	0.59402400	2.46311700	1.14814600
C	-1.42842800	0.88828200	1.18941400	H	-1.07274500	-2.32234500	-0.21807300
C	-2.17456100	-2.08884600	1.87936900	H	-2.53601200	-2.50333400	0.74290000
H	2.93108200	-1.16750100	1.70374900	H	-2.45178100	-1.11524100	-1.99563900
H	1.73211500	0.26523400	-2.14025400	H	-3.89893500	-1.31700300	-0.99684600
H	2.23632400	2.57731500	-1.43745200	H	-3.41393200	0.30042400	-1.54692000
H	3.06675100	3.02588100	0.85118900	H	-3.92884400	-0.51177900	1.39248500
H	3.42004600	1.14315000	2.41731000	H	-3.45598600	1.11071300	0.84638200
H	2.28576000	-2.73750000	0.01175800	H	-2.50943600	0.28190800	2.09037200
H	0.30242800	-1.29895000	1.11572500	H	-1.11799700	-1.75964800	1.46826100
H	2.24111600	-2.23392100	-1.68216300				
H	-1.67162000	-1.56939300	2.69744600	(R)-48			
H	-3.24835700	-1.93912500	1.99612000	0 1			
H	-1.95893000	-3.15263300	1.97419800	C	1.29440700	0.06292800	-0.15058100
H	-2.13632900	-2.19328500	-0.26437000	O	1.43520800	-0.41584400	-1.25761700
H	-3.19904100	-0.05707400	0.44295000	N	0.11789400	0.59073100	0.28104800
H	-2.36522100	-0.43094200	-1.86625100	C	2.41901700	0.09002400	0.87251100
H	-2.12566500	1.96457700	-2.52624500	C	3.78439000	-0.06644500	0.22459100
H	-3.41549000	1.77149600	-1.35103400	C	-1.09212800	0.62438600	-0.52759000
H	-2.00223000	3.71360000	-0.73891800	C	-2.05134700	-0.53032200	-0.18523800
H	-2.95810500	2.40321000	1.13563200	C	-1.38112400	-1.87959400	-0.42096600
H	-1.37055100	3.01281600	1.57667600	C	-2.59442900	-0.44229100	1.23800100
H	-1.61348400	0.63676100	2.23650800	C	-1.74212700	1.99666100	-0.40747200
H	-0.79749100	0.20237500	-1.40665100	H	-0.55760300	-2.02533200	0.28192400
H	-0.57027000	2.69055300	-0.74013300	H	-0.96769600	-1.94986000	-1.42710400
H	-0.34308100	0.84135100	1.02731300	H	-2.09312000	-2.69319400	-0.27458400
				H	-1.77830800	-0.48306600	1.96454500
(S)-46				H	-3.25329100	-1.28630100	1.44591500
0 1				H	-2.89251900	-0.43708400	-0.88061200
C	-1.11233900	0.53058900	-0.25462400	H	-2.68426500	2.02412200	-0.95618600
O	-1.39698000	1.65211100	-0.63639400	H	-3.16400600	0.47145300	1.41064000
N	0.17447900	0.13062000	-0.12076800	H	-1.95554300	2.24512700	0.63445500
C	-2.21495000	-0.48503500	0.07426300	H	0.08646100	0.99016400	1.20483900
C	-3.04748100	-0.66425200	-1.19921000	H	-1.08344200	2.76608200	-0.80932300
C	-1.69207700	-1.84147500	0.54217800	H	-0.75308600	0.47479900	-1.55389800
C	-3.08209500	0.14090100	1.17108000	H	2.36053300	1.01228400	1.45534900
C	1.27690400	1.05516700	-0.32391400	H	3.99048400	0.76475900	-0.44918600
C	2.50373100	0.24985100	-0.70667600	H	3.81907900	-0.98082900	-0.36421500
O	2.74984000	-0.69707300	0.30844400	H	2.23183200	-0.73187200	1.57033600
C	3.86802200	-1.50326300	0.03683600	H	4.56762100	-0.10170500	0.98116700
C	1.50916400	1.92366400	0.90745100				
H	3.97989200	-2.20217500	0.86299300	(R)-49			
H	4.77744700	-0.89803700	-0.04760200	0 1			
H	3.73360300	-2.06425100	-0.89505000	C	-0.20083500	-0.57382300	0.32515600
H	3.36753600	0.91703300	-0.82151200	O	-0.09819000	-1.78574300	0.36050800

N	0.84423800	0.27170400	0.50399000	H	-1.21947300	-1.29513500	-1.67587100
C	-1.51480600	0.07422100	0.07784500	H	-0.18487300	0.93769300	-1.32529900
C	-1.83547400	1.37436900	-0.20179700	H	-2.83984900	-0.70695700	-2.09170800
C	-3.22651200	1.56391200	-0.38699200	H	-3.62177200	1.89004800	-0.52334900
C	-3.92293000	0.39905000	-0.24439900	H	-2.13544200	2.81205700	-0.74108300
S	-2.90716300	-0.92152500	0.10371900	H	-2.55258200	1.52922200	-1.88051600
C	2.20215500	-0.18914000	0.76181700	H	-1.82925500	1.18405900	1.07921200
C	3.06383600	-0.17514800	-0.51378200	H	1.94921700	1.58869800	-1.04538500
C	2.46946100	-1.09210900	-1.57741400	H	2.56366000	1.77999500	0.60153100
C	3.26773500	1.23092800	-1.06983100	H	4.11908400	0.60157800	-1.69174100
C	2.80110000	0.62574100	1.90040000	H	4.70342600	0.76336700	-0.02969200
H	-3.68503100	2.51378000	-0.61859300	H	4.75478100	-0.80831400	-0.83592300
H	-1.11089900	2.17156900	-0.29662400	H	3.37422300	-0.25461700	1.89446200
H	-4.98794600	0.25537800	-0.33088800	H	3.48455600	-1.81868500	1.07042200
H	2.24249400	0.46183400	2.82150700	H	1.91091700	-1.17305500	1.56862500
H	2.78108100	1.69479100	1.67773600	H	2.65034800	-2.05698800	-1.32677700
H	3.84000600	0.34016200	2.06827200	H	1.95098600	-0.66511200	-2.15823000
H	0.65902900	1.25941300	0.55245900	H	1.07774700	-1.43595100	-0.82487700
H	4.04009700	-0.57486800	-0.21899700				
H	3.86703100	1.19553400	-1.98037500	(S)-52			
H	3.77736500	1.88845800	-0.36469700	O 1			
H	2.29686000	-2.09570700	-1.18828000	C	0.16469600	1.77013200	-0.12792300
H	3.13296100	-1.15884600	-2.44081100	O	0.94662400	2.63800000	-0.46092000
H	2.30712500	1.68242500	-1.33240100	N	0.53628400	0.61691800	0.47383100
H	1.50832500	-0.70494900	-1.92316800	C	-1.33678200	1.95629200	-0.36330300
H	2.09958500	-1.22856700	1.07734600	C	-2.18521300	0.72533000	-0.21482500
				C	-3.66721600	-1.62879600	0.08252700
(S)-51				C	-2.21972800	-0.22845000	-1.23177000
O 1				C	-2.90383300	0.48024400	0.95174600
C	0.62001600	0.98561400	0.54545200	C	-3.64153700	-0.68762900	1.10101000
O	0.44611600	0.96619400	1.74935900	C	-2.95382200	-1.39571800	-1.08677400
N	-0.40345000	0.88019800	-0.34379500	C	1.91984600	0.27417000	0.76534800
C	-1.80686300	0.83577700	0.04397300	C	2.49427500	-0.70938500	-0.28764400
C	-2.37028200	-0.60855700	0.04122100	C	2.40600400	-0.05744700	-1.66946700
C	-1.58147400	-1.44642900	1.04963100	C	3.96525700	-0.98867500	0.02851400
C	-3.83823800	-0.58247000	0.47357700	C	1.71662800	-2.02636000	-0.30522600
C	-2.25880900	-1.24861200	-1.34294500	C	2.00766400	-0.21246500	2.20790700
C	-2.57931200	1.82051200	-0.82791800	H	-1.42222500	2.37442500	-1.36666100
C	2.00463300	1.11663600	-0.06014800	H	-1.65698600	2.73625600	0.33013900
C	2.77084900	-0.21734800	-0.19163200	H	-1.66157600	-0.04967900	-2.14430300
C	2.06686600	-1.14559000	-1.18230200	H	-2.97185200	-2.12379300	-1.88747200
C	2.88927200	-0.90806500	1.16695300	H	-4.24245600	-2.53821700	0.19629800
C	4.16976200	0.10618500	-0.71924700	H	-4.19808200	-0.85958100	2.01324800
H	-4.19579800	-1.60045100	0.63854100	H	-2.88522500	1.21299900	1.75030600
H	-3.96106200	-0.02959400	1.40834600	H	3.03571600	-0.42551400	2.49516000
H	-4.47952100	-0.12698600	-0.28193000	H	1.62171600	0.55683700	2.87621300
H	-1.97628100	-2.46400200	1.08158600	H	1.41625100	-1.11787800	2.36019700
H	-1.64217200	-1.01504500	2.05001100	H	0.66075800	-1.86336200	-0.53639200
H	-2.63870900	-2.27165200	-1.31122200	H	2.12105600	-2.68509500	-1.07639300
H	-0.52545400	-1.50103000	0.78286800	H	1.78658300	-2.55518700	0.64694700

H	-0.18145700	-0.05084000	0.70900600
H	1.36896800	0.12292600	-1.95663500
H	2.85485900	-0.71046200	-2.42062300
H	2.92492400	0.90235900	-1.68536300
H	4.42113000	-1.55288800	-0.78711200
H	2.47597300	1.20899800	0.66914400
H	4.08333300	-1.57549400	0.94010900
H	4.52418100	-0.05669000	0.14401500

6. REFERENCES

- [1] M. Inaki, J. Liu, K. Matsuno, *Philosophical Transactions of the Royal Society B: Biological Sciences* **2016**, *371*, 20150403.
- [2] G. Lin, Y. Li, A. S. C. Chan, *Principles and Applications of Asymmetric Synthesis*, Wiley, **2001**.
- [3] R. Crabtree, *Acc Chem Res* **1979**, *12*, 331–337.
- [4] M. T. Reetz, *Angewandte Chemie International Edition* **2001**, *40*, 284–310.
- [5] K. W. Kuntz, M. L. Snapper, A. H. Hoveyda, *Curr Opin Chem Biol* **1999**, *3*, 313–319.
- [6] A. Soyemi, T. Szilvási, *Dalton Transactions* **2021**, *50*, 10325–10339.
- [7] T. A. Shear, F. Lin, L. N. Zakharov, D. W. Johnson, *Angewandte Chemie International Edition* **2020**, *59*, 1496–1500.
- [8] P. M. Murray, F. Bellany, L. Benhamou, D.-K. Bučar, A. B. Tabor, T. D. Sheppard, *Org Biomol Chem* **2016**, *14*, 2373–2384.
- [9] K. D. Shimizu, M. L. Snapper, A. H. Hoveyda, *Chemistry - A European Journal* **1998**, *4*, 1885–1889.
- [10] M. Shevlin, *ACS Med Chem Lett* **2017**, *8*, 601–607.
- [11] S. W. Krska, D. A. DiRocco, S. D. Dreher, M. Shevlin, *Acc Chem Res* **2017**, *50*, 2976–2985.
- [12] W. H. Brooks, W. C. Guida, K. G. Daniel, *Curr Top Med Chem* **2011**, *11*, 760–770.
- [13] D. Leung, S. O. Kang, E. V. Anslyn, *Chem Soc Rev* **2012**, *41*, 448–479.
- [14] J. R. Brandt, F. Salerno, M. J. Fuchter, *Nat Rev Chem* **2017**, *1*, 0045.
- [15] R. A. van Delden, B. L. Feringa, *Angewandte Chemie International Edition* **2001**, *40*, 3198–3200.
- [16] R. Eelkema, R. A. van Delden, B. L. Feringa, *Angewandte Chemie International Edition* **2004**, *43*, 5013–5016.
- [17] M. T. Reetz, M. H. Becker, K. M. Kühling, A. Holzwarth, *Angewandte Chemie International Edition* **1998**, *37*, 2647–2650.
- [18] N. Millot, P. Borman, M. S. Anson, I. B. Campbell, S. J. F. Macdonald, M. Mahmoudian, *Org Process Res Dev* **2002**, *6*, 463–470.
- [19] L. Yang, T. Wenzel, R. T. Williamson, M. Christensen, W. Schafer, C. J. Welch, *ACS Cent Sci* **2016**, *2*, 332–340.
- [20] B. Benedict, C. E. Lietz, T. J. Wenzel, *Tetrahedron* **2018**, *74*, 4846–4856.

- [21] F. Lanucara, S. W. Holman, C. J. Gray, C. E. Eyers, *Nat Chem* **2014**, *6*, 281–294.
- [22] M. Pitzer, M. Kunitski, A. S. Johnson, T. Jahnke, H. Sann, F. Sturm, L. Ph. H. Schmidt, H. Schmidt-Böcking, R. Dörner, J. Stohner, J. Kiedrowski, M. Reggelin, S. Marquardt, A. Schießer, R. Berger, M. S. Schöffler, *Science (1979)* **2013**, *341*, 1096–1100.
- [23] Á. Valentín-Pérez, P. Rosa, E. A. Hillard, M. Giorgi, *Chirality* **2022**, *34*, 163–181.
- [24] A. Hamberg, S. Lundgren, M. Penhoat, C. Moberg, K. Hult, *J Am Chem Soc* **2006**, *128*, 2234–2235.
- [25] F. Taran, C. Gauchet, B. Mohar, S. Meunier, A. Valleix, P. Y. Renard, C. Créminon, J. Grassi, A. Wagner, C. Mioskowski, *Angewandte Chemie International Edition* **2002**, *41*, 124–127.
- [26] C. J. Welch, *Chirality* **2009**, *21*, 114–118.
- [27] G. Gübitz, M. G. Schmid, *Mol Biotechnol* **2006**, *32*, 159–180.
- [28] A. Ozcelik, R. Pereira-Cameselle, N. Poklar Ulrih, A. G. Petrovic, J. L. Alonso-Gómez, *Sensors* **2020**, *20*, 974.
- [29] M. Quan, X. Y. Pang, W. Jiang, *Angewandte Chemie International Edition* **2022**, *61*, DOI 10.1002/anie.202201258.
- [30] T. Miyahara, H. Nakatsuji, H. Sugiyama, *J Phys Chem A* **2016**, *120*, 9008–9018.
- [31] A. J. Miles, R. W. Janes, B. A. Wallace, *Chem Soc Rev* **2021**, *50*, 8400–8413.
- [32] T. Šmidlehner, I. Piantanida, G. Pescitelli, *Beilstein Journal of Organic Chemistry* **2018**, *14*, 84–105.
- [33] T. Levi-Belenkova, A. O. Govorov, G. Markovich, *The Journal of Physical Chemistry C* **2016**, *120*, 12751–12756.
- [34] S. S. Andrews, J. Tretton, *J Chem Educ* **2020**, *97*, 4370–4376.
- [35] N. Berova, L. Di Bari, G. Pescitelli, *Chem Soc Rev* **2007**, *36*, 914.
- [36] C. Bohne, *Chem. Soc. Rev.* **2014**, *43*, 4037–4050.
- [37] G. Pescitelli, L. Di Bari, N. Berova, *Chem Soc Rev* **2011**, *40*, 4603.
- [38] L.-P. Yang, L. Zhang, M. Quan, J. S. Ward, Y.-L. Ma, H. Zhou, K. Rissanen, W. Jiang, *Nat Commun* **2020**, *11*, 2740.
- [39] C. Wolf, K. W. Bentley, *Chem Soc Rev* **2013**, *42*, 5408.
- [40] R. Berardozzi, E. Badetti, N. A. Carmo dos Santos, K. Wurst, G. Licini, G. Pescitelli, C. Zonta, L. Di Bari, *Chemical Communications* **2016**, *52*, 8428–8431.

- [41] R. Penasa, F. Begato, G. Licini, K. Wurst, S. Abbate, G. Longhi, C. Zonta, *Chemical Communications* **2023**, *59*, 6714–6717.
- [42] N. A. Carmo dos Santos, E. Badetti, G. Licini, S. Abbate, G. Longhi, C. Zonta, *Chirality* **2018**, *30*, 65–73.
- [43] S. Superchi, R. Bisaccia, D. Casarini, A. Laurita, C. Rosini, *J Am Chem Soc* **2006**, *128*, 6893–6902.
- [44] M. W. Ghosn, C. Wolf, *J Am Chem Soc* **2009**, *131*, 16360–16361.
- [45] M. W. Ghosn, C. Wolf, *Tetrahedron* **2010**, *66*, 3989–3994.
- [46] J. Ściebura, P. Skowronek, J. Gawronski, *Angewandte Chemie International Edition* **2009**, *48*, 7069–7072.
- [47] J. Ściebura, J. Gawroński, *Chemistry – A European Journal* **2011**, *17*, 13138–13141.
- [48] X. Huang, K. Nakanishi, N. Berova, *Chirality* **2000**, *12*, 237–255.
- [49] X. Huang, B. H. Rickman, B. Borhan, N. Berova, K. Nakanishi, *J Am Chem Soc* **1998**, *120*, 6185–6186.
- [50] X. Huang, B. Borhan, B. H. Rickman, K. Nakanishi, N. Berova, *Chemistry - A European Journal* **2000**, *6*, 216–224.
- [51] L. A. Joyce, M. S. Maynor, J. M. Dagna, G. M. da Cruz, V. M. Lynch, J. W. Canary, E. V. Anslyn, *J Am Chem Soc* **2011**, *133*, 13746–13752.
- [52] L. A. Joyce, J. W. Canary, E. V. Anslyn, *Chemistry – A European Journal* **2012**, *18*, 8064–8069.
- [53] P. Zardi, K. Wurst, G. Licini, C. Zonta, *J Am Chem Soc* **2017**, *139*, 15616–15619.
- [54] W. L. Williams, L. Zeng, T. Gensch, M. S. Sigman, A. G. Doyle, E. V. Anslyn, *ACS Cent Sci* **2021**, *7*, 1622–1637.
- [55] M. S. Sigman, K. C. Harper, E. N. Bess, A. Milo, *Acc Chem Res* **2016**, *49*, 1292–1301.
- [56] M. J. Frisch, G. W. Trucks, H. B. Schlegel, G. E. Scuseria, M. A. Robb, J. R. Cheeseman, G. Scalmani, V. Barone, G. A. Petersson, H. Nakatsuji, X. Li, M. Caricato, A. V. Marenich, J. Bloino, B. G. Janesko, R. Gomperts, B. Mennucci, H. P. Hratchian, J. V. Ortiz, A. F. Izmaylov, J. L. Sonnenberg, D. Williams-Young, F. Ding, F. Lipparini, F. Egidi, J. Goings, B. Peng, A. Petrone, T. Henderson, D. Ranasinghe, V. G. Zakrzewski, J. Gao, N. Rega, G. Zheng, W. Liang, M. Hada, M. Ehara, K. Toyota, R. Fukuda, J. Hasegawa, M. Ishida, T. Nakajima, Y. Honda, O. Kitao, H. Nakai, T. Vreven, K. Throssell, J. A. Montgomery, J. E. Peralta, F. Ogliaro, M. J. Bearpark, J. J. Heyd, E. N. Brothers, K. N. Kudin, V. N. Staroverov, T. A. Keith, R. Kobayashi, J. Normand, K. Raghavachari, A. P. Rendell, J. C. Burant, S. S. Iyengar, J. Tomasi, M. Cossi, J.

- M. Millam, M. Klene, C. Adamo, R. Cammi, J. W. Ochterski, R. L. Martin, K. Morokuma, O. Farkas, J. B. Foresman, D. J. Fox, **Gaussian 16, Revision B.01**.
- [57] E. D. Glendening, A. E. Reed, J. E. Carpenter, F. Weinhold, **NBO Version 3.1**.
- [58] C. B. Santiago, J.-Y. Guo, M. S. Sigman, *Chem Sci* **2018**, *9*, 2398–2412.
- [59] A. C. Hillier, W. J. Sommer, B. S. Yong, J. L. Petersen, L. Cavallo, S. P. Nolan, *Organometallics* **2003**, *22*, 4322–4326.
- [60] A. V. Brethomé, S. P. Fletcher, R. S. Paton, *ACS Catal* **2019**, *9*, 2313–2323.
- [61] L. Falivene, Z. Cao, A. Petta, L. Serra, A. Poater, R. Oliva, V. Scarano, L. Cavallo, *Nat Chem* **2019**, *11*, 872–879.
- [62] Roy D. Dennington II, T. A. K., J. M. M., **GaussView 6.0.16**.
- [63] T. Nakamura, K. Tateishi, S. Tsukagoshi, S. Hashimoto, S. Watanabe, V. A. Soloshonok, J. L. Aceña, O. Kitagawa, *Tetrahedron* **2012**, *68*, 4013–4017.
- [64] A. Wzorek, A. Sato, J. Drabowicz, V. A. Soloshonok, K. D. Klika, *Helv Chim Acta* **2015**, *98*, 1147–1159.
- [65] T. Jerphagnon, A. J. A. Gayet, F. Berthiol, V. Ritleng, N. Mršić, A. Meetsma, M. Pfeffer, A. J. Minnaard, B. L. Feringa, J. G. de Vries, *Chemistry – A European Journal* **2009**, *15*, 12780–12790.

7. ACKNOWLEDGEMENTS

Ringrazio il mio relatore, il Prof. Cristiano Zonta, per avermi affidato questo progetto e guidato in questo percorso di tesi.

Ringrazio il mio controrelatore, la Prof.ssa Elisabetta Collini, per i preziosi consigli datomi durante gli incontri.

Ringrazio il Dott. Manuel Orlandi, per avermi seguito e aiutato nello sviluppo del modello multidimensionale.

Ringrazio la Prof.ssa Giulia Licini, per la professionalità e i consigli sempre utili.

Ringrazio Roberto Penasa, il quale mi ha affiancato per tutta la durata di questo percorso di tesi, aiutandomi e insegnandomi la vita in laboratorio.

Ringrazio tutti i post-doc, dottorandi e studenti del laboratorio, per aver condiviso con me questo percorso di crescita scientifica e personale.

Ringrazio i ragazzi del Collegio San Francesco, gli amici e tutti coloro che hanno avuto un ruolo importante in questo percorso.

Un grazie particolare alla mia compagna di corso Elisa, degna “compagna di merende”, per aver condiviso questo percorso universitario composto di tante soddisfazioni.

Infine, un enorme ringraziamento ai miei genitori Silvana e Silvano, per avermi sempre supportato e sopportato durante questo lungo percorso. Grazie per avermi sempre incoraggiato a inseguire ciò che mi appassiona, sperando di poterlo fare per tutta la vita.

Voglio aggiungere un ultimo ringraziamento ai miei nonni, i quali purtroppo non ci sono più, ma sono convinto che sarebbero i primi a festeggiare questo traguardo.